Alma Mater Studiorum – Università di Bologna

DOTTORATO DI RICERCA IN

CHIMICA

Ciclo XXXII

Settore Concorsuale: 03/C2

Settore Scientifico Disciplinare: CHIM/04

Catalytic upgrading of carboxylic acids and esters to bio fuels and bio chemicals

Presentata da: Jacopo De Maron

Coordinatore Dottorato   **Supervisore**

Prof.ssa Domenica Tonelli   **Prof. Fabrizio Cavani**

Esame finale anno 2020

Key words

Propionic Acid (PA)
Ketonization
3-Pentanone (3-P)
Methyl Propionate (MP)
Hydroxy-methylation
Methanol (MeOH)
Methyl Methacrylate (MMA)
Gallium Oxide (Ga$_2$O$_3$)
Heterogeneous Catalyst
Gas-phase

Abstract

The research activity was focused on the transformation of methyl propionate (MP) into methyl methacrylate (MMA), avoiding the use of formaldehyde (FAL) thanks to a one-pot strategy involving *in situ* methanol (MeOH) dehydrogenation over the same catalytic bed were the hydroxy-methylation/dehydration of MP with FAL occurs. The relevance of such research line is related to the availability of cheap renewable bio-glycerol from biodiesel production, from which MP can be obtained via a series of simple catalytic reactions. Moreover, the conventional MMA synthesis (Lucite process) suffers from safety issues related to the direct use of carcinogenic FAL and depends on non-renewable MP. During preliminary studies, ketonization of carboxylic acids and esters has been recognized as a detrimental reaction which hinders the selective synthesis of MMA at low temperature, together with H-transfer hydrogenation with FAL or MeOH as the H-donor at higher temperatures. Therefore, ketonization of propionic acid (PA) and MP was investigated over several catalysts (metal oxides and metal phosphates), to obtain a better understanding of the structure-activity relationship governing the reaction and to design a catalyst for MMA synthesis capable to promote the desired reaction while minimizing ketonization and H-transfer. However, ketonization possesses scientific and industrial value itself and represents a strategy for the upgrade of bio oils from fast pyrolysis of lignocellulosic materials, a robust and versatile technology capable to transform the most abundant biomass into liquid biofuels. The catalysts screening showed that ZrO_2 and La_2O_3 are the best catalysts, while MgO possesses low ketonization activity, but still, H-transfer parasitic hydrogenation of MMA reduces its yield over all catalysts. Such study resulted in the design of Mg/Ga mixed oxides that showed enhanced dehydrogenating activity towards MeOH at low temperatures. It was found that the introduction of Ga not only minimize ketonization, but also modulates catalyst basicity reducing H-transfer hydrogenations.

Summary

Nomenclature

1,2-PDO = **1,2-P**ropane**dio**l

2MP = **2-M**ethyl **P**ropanol

2-B = **2-B**utanone

3-P = **3-P**entanone

AA = **A**cetic **A**cid

AcCN = Acetonitrile

ACH = **A**cetone **C**yano**h**ydrin

AFEX = **A**mmonia **F**iber **Ex**plosion

ATR FT-IR = **A**ttenuated **T**otal **R**eflectance **F**ourier **T**ransform **I**nfrared **S**pectroscopy

BA = **B**enzoic **A**cid

CCA = **C**yclopropane **C**arboxylic **A**cid

CH₄ = Methane

CO₂ = Carbon Dioxide

CCS = **C**arbon Dioxide **C**apture and **S**torage

DM-3Pa = 2,4-**Dim**ethyl-**3-P**ent**a**none

DM-3Pe = 2,4-**Dim**ethyl-**3-P**ent**e**none

DME = **Dim**ethyl **e**ther

EtOH = Ethanol

FAL = **F**orm**al**dehyde

GLY = **Gl**y**cerol

GTE = **G**lycerol to **E**thylene **G**lycol

H₂ = Hydrogen

HDO = **H**ydro**deo**xygenation

IB = **I**so**b**utylene

IBA = **I**so**b**utyric **A**cid

IBAL =**I**so**b**utyr**al**dehyde

IBIB = **I**so**b**utyl **I**so**b**utyrate

M-3Pa = 2-**m**ethyl-**3-P**ent**a**none

M-3Pe = 2-**m**ethyl-**3-P**ent**e**none

MAA = **M**eth**a**crylic **A**cid

MAL = **M**eth**a**cro**l**ein

MeOH = *Methanol*

Mg/Ga/O = *Magnesium Gallium Mixed Oxides*

MIB = **M**ethyl **I**so**b**utyrate

MOs = **M**etal **O**xides

MMA = **M**ethyl **M**eth**a**crylate

MP = **M**ethyl **P**ropionate

MPOs = *Metal Phosphates*

NH$_3$ = *Ammonia*

PA = **P**ropionic **A**cid

PAL =**P**ropion**al**dehyde

PAN = **P**ropionic **An**hydride

PP = **P**ropyl **p**ropionate

PrOH = *Propanol*

SEM-EDS = **S**canning **E**lectron **M**icroscopy - **E**nergy **D**ispersive X-Ray **S**pectrometry

TGA = **T**hermo**g**ravimetric **A**nalysis

TMMA = **T**ri**m**ethyl **A**cetic **A**cid

TPD = **T**emperature **P**rogrammed **D**esorption

W/F = *Time Factor*

X = *Conversion*

XPS = **X**-Ray **P**hotoelectron **S**pectroscopy

XRD = **X**-**R**ay **D**iffraction

Y = *Yield*

YS = *Sum of Yields*

YS/X = *Molar Balance*

Zr/P/O = *Zirconium Phosphate*

Acknowledgements

1 General introduction

1.1 Global warming and climate change

During the twentieth century, humanity experienced a demographic growth unprecedented in history. The main reason behind this exponential growth in population lies in the development of several industrial processes, in particular the Haber-Bosch process for ammonia (NH_3) production in 1913 [1]. The availability of this highly reactive form of fixed nitrogen boosted the production of fertilizer on industrial scale, dramatically increasing global agricultural productivity and allowing to sustain more people around the globe (Figure 1). It is estimated that by 2008 nitrogen fertilizers were responsible for feeding about 48 % of the world's population [2]. NH_3 is synthesized from a mixture of nitrogen (N_2) and hydrogen (H_2) in a 1:3 molar ratio, which are abundantly available in the form of air and water. However, in order to obtain pure H_2 from water, a reducing carbon medium (coal, naphtha, natural gas) is required (Steam Reforming process); N_2 can be obtained by liquid air rectification or reacting the oxygen (O_2) in air with coal (Coal Gasification Process). For these reasons, fossil resources are usually regarded as the only raw material for NH_3 synthesis due to the abundance of water and air. Fossil energy is also required to operate plants (liquid air rectification [3], coal gasification [4], steam reforming [5] and NH_3 synthesis [6] are highly energy-demanding processes). A large-scale NH_3 production would not be possible without oil, natural gas and coal: as a matter of fact, half the world population "feeds on fossil resources".
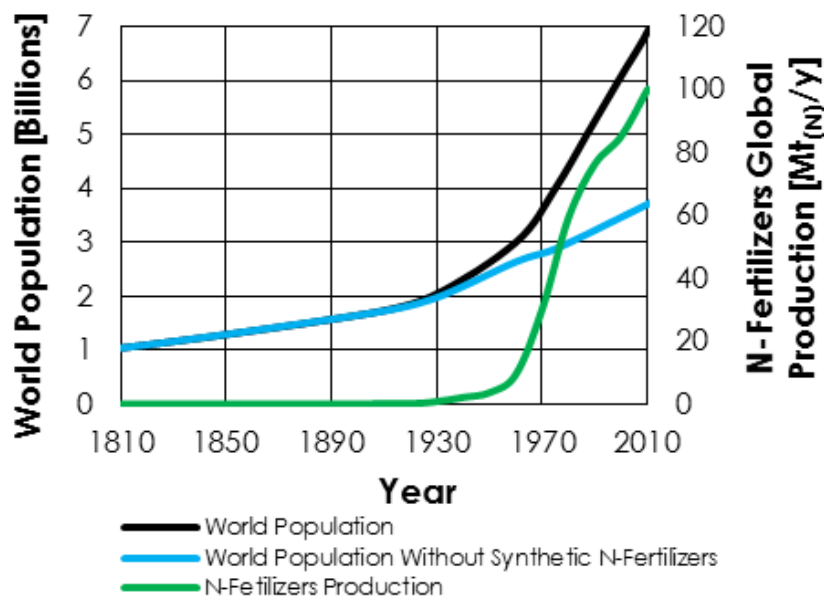
Figure 1: world population with and without synthetic N-fertilizers [2] and global production of synthetic N-fertilizers [7] plotted in the period 1810-2010.

Human activities have always produced local effects in the surrounding environment; however, during the twentieth century these effects have grown up to global scale due to demoGraphic, economic and industrial growth of most countries and started endangering the environment. Consequently, between the 60s and the 70s of the twentieth century more and more nations began to realize the environmental impact of their activities and later started to join their effort in order to overcome global environmental issues. One of the most

General Introduction

relevant achievement in this sense is the reduction of the ozone layer depletion that followed the ratification of the Montreal Protocol in 1987 and the ban on chlorofluorocarbons (CFCs). Recent studies demonstrate that the ozone layer is slowly regenerating and predict that it will return to pre-1980 levels between 2050 and 2070 [8]. However, at present time the most urgent environmental issue to be solved is the global warming caused by the ever-growing anthropogenic emissions of greenhouse gases (GHGs), namely carbon dioxide (CO_2), methane (CH_4) and dinitrogen monoxide (N_2O), which have been recognized as the main responsible for climate change.
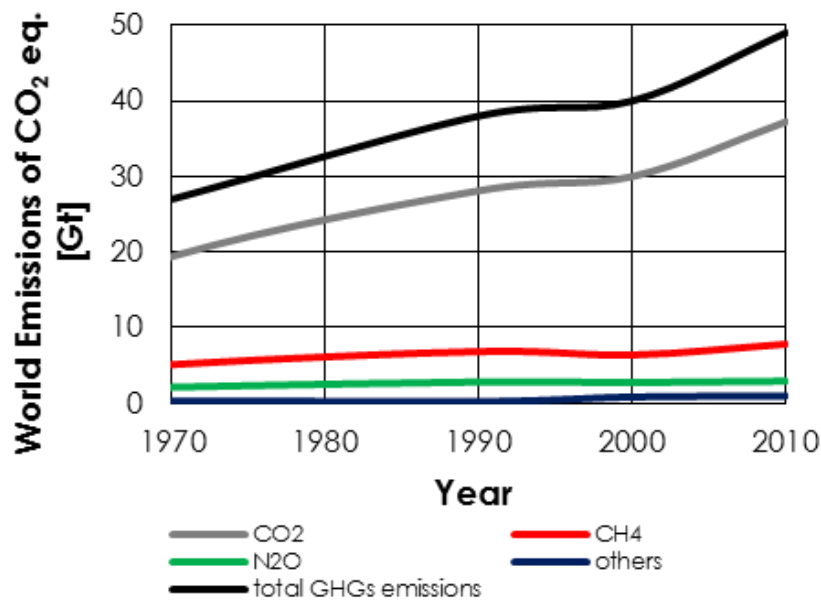
Figure 2: global emissions of greenhouse gases (GHGs) plotted in the period 1970-2010 [9].

According to IPCC (Intergovernmental panel on Climate Change) [10], the atmospheric concentration of GHGs exceeded the highest concentration recorded in ice cores in the past 800 000 years and CO_2, CH_4 and N_2O concentration have increased by 40 %, 150 % and 20 % respectively since pre-industrial times. The consequences of such high levels of GHGs in atmosphere includes:

1. Earth's mean surface warming: estimated between 0.5 °C and 1.3 °C between 1951 and 2010. The decades from 1983 to 2012 has been successively warmer than any preceding decade since 1850.

2. Ocean warming and acidification: seas stored more than 90% of the energy accumulated between 1971 and 2010 in the climate system. Over the period 1901 to 2010, global mean sea level rose by 0.19 meters and ocean has absorbed about 30 % of anthropogenic emitted CO_2 causing ocean acidification.

3. Ice melting: over the last two decades, the Greenland and Antarctic ice sheets have been losing mass, glaciers have continued to shrink worldwide, and Arctic sea ice and Northern Hemisphere spring snow cover have continued to decrease in extent.

4. Extreme weather events such as heavy precipitations, floods and droughts on regional scale.

Most aspects of climate change will persist for many centuries due to the climate system inertia, even if GHGs emissions will be nullified. However, this scenario would very likely imply dramatic social consequences, first of all, hunger for half of the world population.

1.2 The role of chemical industry

Industry direct contribution to global GHGs emissions (Figure 3, left) was estimated in 10.3 Gt of equivalent CO_2 in 2010. This value represented the 21 % of the total GHGs emission and is lower compared to the contribution related to energy production (25 %) and agricultural, forestry and other land usage (AFOLU, 24 %). However, when indirect emissions (Figure 3, right) related to electricity and heat generation are considered into the calculation, the cumulative contribution of industrial activities (direct + indirect) to GHGs emissions becomes 15.7 Gt of equivalent CO_2, which represent the 32.1 % of the total and makes it the major contributor to GHGs emissions, followed by AFOLU (24.7 %), buildings (18.3 %), and transport (14.2 %).

Total GHGs Emissions by Economic Sector (2010)

Industry 21 %
Electricity and Heat Production 25 %
Other Energy 9.6 %
AFOLU 24 %
Buildings 6.4 %
Transport 14 %

49 Gt

Indirect (Electricity and Heat) GHGs Emissions by Economic Sector (2010)

Transport 1.2 %
Industry 43 %
Energy 5.5 %
AFOLU 3.4 %
Buildings 46.9 %

12.3 Gt
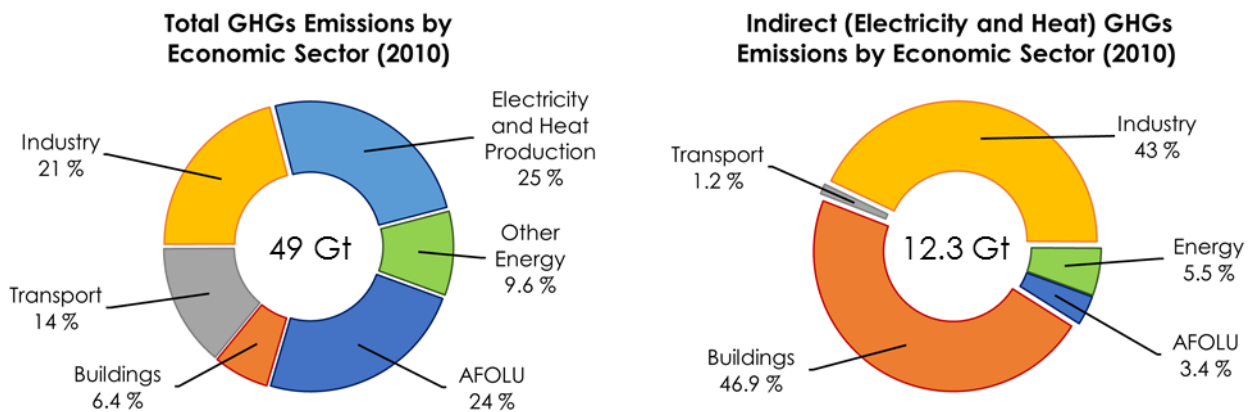
Figure 3: contributions to global GHGs emissions by economic sector (left); indirect contribution to global GHGs emissions related to energy production by economic sector (right).

The chemical industry share of GHGs direct emissions (Figure 4) was estimated in 1.5 Gt of equivalent CO_2, which represent only the 9.8 % of the total. However, this estimate does not consider the contribution of energy production, solid waste disposal and wastewater treatment for chemical industry.

Industrial GHGs Emissions by Source (2010)

Other 24.5 %
Indirect: Energy Production 34.3 %
Solid Waste 4.3 %
Wastewater 5 %
Chemicals 9.8 %
Metals 14.4 %
Cement 8.5 %

15.7 Gt
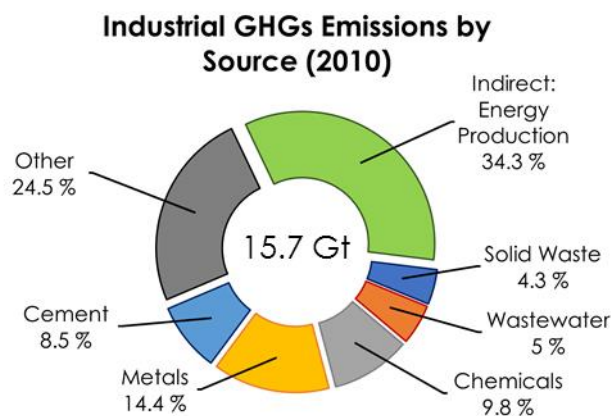
Figure 4: contributions to Industry GHGs emission by source. The contribution of chemical industries represents about 10 % of the total.

Because of the impact that chemical production has on human health and environmental pollution, chemical industries must meet strict legal requirements in terms of GHGs and pollutants emissions limits, plants safety and quality control. Moreover, economic consideration indicates that designing products and processes for energy efficiency, waste

prevention and severe limitation of hazardous substances often result in lower operative costs, fines prevention and higher profits. Therefore, over the course of the last two decade, an approach aimed at the design of intrinsically safer and more efficient processes, at limiting the production of pollutant and toxic by-products and at increasing energetic efficiency has been proposed and adopted. Such approach, known as *Green Chemistry*, has imposed itself as the high road of chemical research in both industries and academia. As a result, several noteworthy improvements have been achieved in key research areas such as the design of new and more selective catalysts, the progressive substitution of highly toxic/harmful/polluting reagents and solvents with safer alternatives and the exponential increase in publications and patents regarding the chemical valorization of platform molecules derived from biomass. Paul Anastas and John Warner systematically organized the fundamental concepts that constitutes the Green Chemistry pillars in Twelve Principles in 1998 [11]. Each of them focuses on a single aspect of sustainability and helps to compare qualitatively different compounds or processes. Quantitative comparison can be carried out using the mathematical parameters that constitute *Green Metrics* [12]; however, in order to properly evaluate the sustainability and environmental impact of a product, much more complex complete life-cycle assessment tools should be used. The twelve principles of Green Chemistry are reported below as they can be found on the American Chemical Society website.

1   Waste Prevention: it is better to prevent waste than to treat or clean up waste after it has been created (E = environmental factor, PMI = process mass intensity).

2   Atom Economy: synthetic methods should be designed to maximize the incorporation of all materials used in the process into the final product (AE = atom economy, CE = carbon efficiency, RME = reaction mass efficiency)

3   Less Hazardous Chemical Syntheses: wherever practicable, synthetic methods should be designed to use and generate substances that possess little or no toxicity to human health and the environment.

4   Designing Safer Chemicals: chemical products should be designed to preserve their desired function while minimizing their toxicity (LD50 = lethal dose in 50 % of cases)

5   Safer Solvents and Auxiliaries: the use of auxiliary substances (e.g., solvents, separation agents, etc.) should be made unnecessary wherever possible and innocuous when used (S^{-1} = mass intensity).

6   Design for Energy Efficiency: energy requirements of chemical processes should be recognized for their environmental and economic impacts and should be minimized. If possible, synthetic methods should be conducted at ambient temperature and pressure (EE = energy efficiency, GGE = GHGs emission)

7   Use of Renewable Feedstocks: a raw material or feedstock should be renewable rather than depleting whenever technically and economically practicable.

8   Reduce Derivatives: unnecessary derivatization (use of blocking groups, protection/ deprotection, temporary modification of physical/chemical processes) should be minimized or avoided if possible, because such steps require additional reagents and can generate waste (S^{-1} = mass intensity, E = environmental factor)

9   Catalysts (vs Stoichiometric): catalytic reagents (as selective as possible) are superior to stoichiometric reagents.

10   Design for Degradation: chemical products should be designed so that at the end of their function they break down into innocuous degradation products and do not persist in the environment (half-life in soil, water, air).

11   Real-time analysis for Pollution Prevention: analytical methodologies need to be further developed to allow for real-time, in-process monitoring and control prior to the formation of hazardous substances.

12   Inherently Safer Chemistry for Accident Prevention: substances and the form of a substance used in a chemical process should be chosen to minimize the potential for chemical accidents, including releases, explosions, and fires.

Even though these guidelines were developed with the aim of increase the sustainability of chemical processes years before the climate change was recognized as a major issue, they represent a most valuable set of tools when designing a chemical product or process with the aim of mitigation. For example, being able to develop a process that respects the principles of Waste Prevention (1), Atom Economy (2), Safer Solvents and Auxiliaries (5), Design for Energy Efficiency (6) and Reduce Derivatives (8) would lead to lower emissions for waste disposal, for electricity/heat generation and for work up operations such as solvent recycling and distillations. When these principles are respected together with the Use of Renewable Feedstock (7), even higher reduction of GHGs emission can be achieved. Often, significant reduction in terms of waste production and energy consumption has been achieved substituting complex multi-step and reagent-intensive syntheses with alternative simpler synthetic pathways thanks to the development of a selective catalyst (9).

1.3 Strategies aimed at mitigation

Climate change mitigation consist of actions aimed at reducing the extent and rate of climate change. Since anthropogenic GHGs emission are the main responsible of global warming and climate change, these actions are aimed in the end to avoid or at least reduce GHGs emissions by several means, and three main strategies can be distinguished:

1. Energy technologies and chemical processes that do not produce GHGs emission at all because they are not based on fossil resources: clean H_2 production with electrocatalyst or photocatalyst, hydroelectric energy, solar energy, wind energy, marine energy, geothermal energy, nuclear energy.

2. Technologies for CO_2 sequestration: it is the only strategy capable to result in negative net emission of CO_2 and therefore the only one that might help to reduce the GHGs in the atmosphere to preindustrial levels. It is also the only strategy capable (in principle) to reduce the net emission of GHGs to zero during the transition period required for a complete shift from fossil energy to renewable energy on a global scale. In this regard, the most promising strategies are the carbon dioxide (CO_2) capture and storage (CCS) technologies and the catalytic valorization of CO_2 as feedstock.

3. Energy technologies and chemical processes based on biomass, which produce a net GHGs emission equal or near to zero: the amount of CO_2 released from biofuels and bio-based chemicals combustion is nearly equal to the one sequestered from the atmosphere by the biological processes for biomass growth. According to the

IPCC, bioenergy can play a critical role for mitigation, and combining bioenergy with CCS offers the prospects of energy supply with large-scale net negative emissions [9].

Over the past two decades, catalysis played a key role in the development of technologies inspired by these three strategies and will maintain its relevance in their future developments.

1.4 Catalysis for biomass valorization

1.4.1 Advantages of biomass as feedstock

Biomass is defined as the biodegradable fraction of products, waste and residues of biological origin from agriculture (including plant and animal substances), from forestry and from related industries, including fisheries and aquaculture, as well as the biodegradable part of industrial and urban waste. The global live biomass on land was estimated in 560 Gt [13], while the global net primary production of biomass (NPP), which represent the amount of CO_2 fixated by the biosphere in one year, was estimated in 1998 in 105 Gt/y of carbon [14, 15], with roughly equal contributions from land and oceans. This makes about 50 Gt/y of biomass on land, 9 Gt of which are harvested every year for food, livestock, heating and other uses [16]. For comparison, the world consumption of fossil fuels is about 10 Gt/y. As briefly described in Chapter 1.1.3, the use of biomass as feedstock for chemicals and energy production has advantages over the use of fossil fuels because theoretically the amount of CO_2 released from biofuels combustion and bio-based chemicals production and incineration at the end of their life is nearly equal to the one sequestered from the atmosphere by the biological processes for biomass growth. In other words, the use of biomass as feedstock would help mitigate climate change establishing a closed carbon cycle that could, in principle, allow producing the same chemical or fuel an indefinite number of times without adding any CO_2 to the atmosphere. Figure 5 depicts two simplified chemical processes: the former is based on fossil-feedstock and fossil-energy, the latter uses biomass feedstock and is fueled by renewable bioenergy.
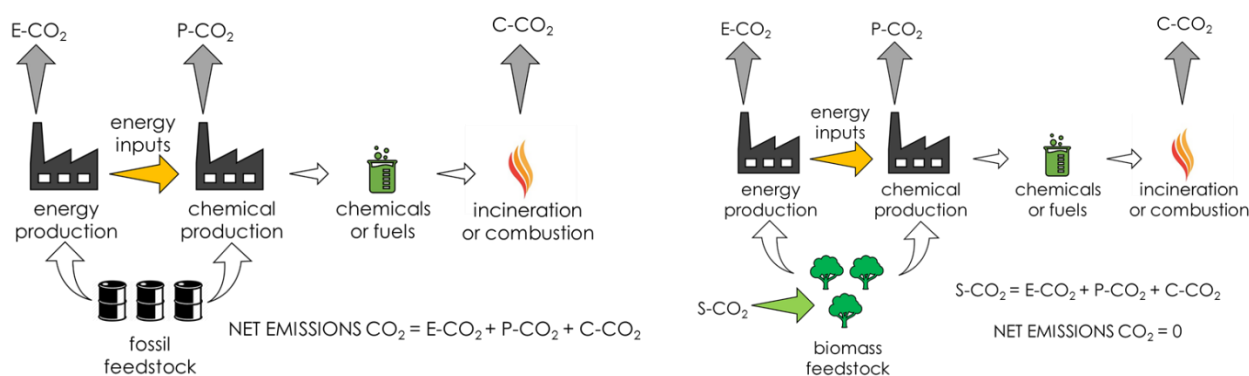
Figure 5: simplified chemical processes based on fossil-feedstock and fossil-energy (left); based on biomass feedstock and fueled by renewable energy (right).

Three positive contribution to CO_2 emissions can distinguished in both case: 1) the emission deriving from the production of the energy (heat or refrigeration and electricity for liquid/gas pumping, mixing and work up operations) required to carry out the process (E-CO_2); 2) the emissions related to the process itself (e.g. if reactions of decarboxylation or unselective oxidation occur) (P-CO_2); 3) the emissions deriving from fuels combustion or chemicals incineration at the end of their life (C-CO_2). The only negative contribution to CO_2 emission is the amount of CO_2 sequestered from the atmosphere during the growth of

the biomass (S-CO$_2$). For the fossil-based process, the S-CO$_2$ contribution is equal to zero and this result in positive emissions (NET EMISSIONS = E-CO$_2$ + P-CO$_2$ + C-CO$_2$). For the biomass-based process instead, the S-CO$_2$ contribution equals the sum of the other three contribution and the net emissions are nearly equal to zero [17]. Moreover, if a process like the one just described were coupled to a CCS unit or if CO$_2$ were used as reactant, it would result in negative net emission. However, a beneficial effect in terms of total net emissions may be achieved in particular cases also with a "mixed configuration", where biomass feedstock is used to produce the energy required to process fossil raw materials, or in the case fossil fuels provides the energy required to transform biomass raw materials into chemicals or fuels (Figure 6).
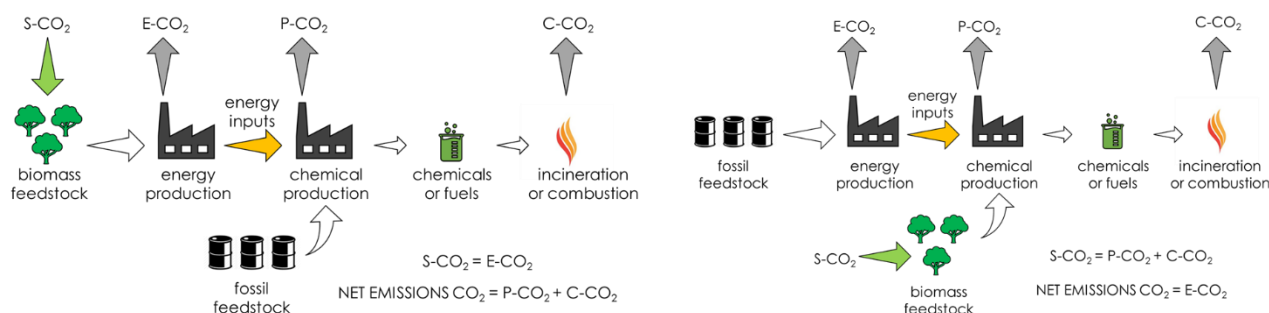
Figure 6: simplified chemical processes with "mixed configuration": fossil feedstock and renewable energy (left); renewable feedstock and fossil energy (right).

When evaluating the suitability of biomasses to produce biochemicals or biofuels, a fundamental distinction must be made between edible and non-edible products. 1st generation biofuels such as bio ethanol (EtOH) from the fermentation of sugars (sugarcane, beetroots, wheat or corn) and biodiesel from the transesterification of edible fats and oils are now considered unsustainable because of the impact that large monoculture has on biodiversity and the potential stress that their production places on food commodities [18]. As an example, there is the concrete risk of an increase of the price of these edible products during energy crises. Moreover, these two biofuels have been criticized for competing for land with food crops, directly because edible products would be destined for energy rather than food, and indirectly because land needed for food production would be diverted to energy crops. Finally, it is worth noticing that producing biochemicals and biofuels from non-edible products would be detrimental as well if they compete indirectly for land with food crops. Therefore, at present time the most suitable biomasses to produce biochemical and 2nd generation biofuels are considered the non-edible ones that do not compete for land with edible crops:

1. Lignocellulosic materials (wood, weeds).

2. Non-edible products that grows in land not suitable for food-crops.

3. Wastes from paper, wood and food industry, from agriculture and urban solid waste.

Finally, algae and CO$_2$ are usually addressed as feed for the 3rd generation biofuels [19].

1.4.2 Integrated Biorefinery

In comparison to relatively composition-constant oils processed by conventional refineries, biomass varies greatly from species to species and from season to season; the biomass supply is in most cases intermittent because harvesting is not possible throughout the entire year. Therefore, a mandatory requirement for biomass transformation is flexibility [20]: biomass-processing sites, "biorefineries", should be able to cope with muTable feedstock composition and manufacture products in a seasonal timeframe; alternatively, biomass

have to be stabilized prior to long-term storage in order to ensure continuous operations. Another requirement for biorefineries is a high degree of integration between different processes in order to maximize circularity and close as much as possible the carbon cycle in the production site. When the waste of a process become feed for another one the environmental impact of the former process is reduced and the latter benefits from the continuous supply of a cheap raw material. Moreover, the spectrum of value-added products of the biorefinery chain is expanded and a better exploitation of the biomass is achieved. The same considerations apply to energy: the establishment of a closed energy cycle would maximize energy efficiency and reduce both environmental impact and production costs. Finally, as described in the previous Chapter, biorefinery sites that generate heat and electricity by their own from biomasses, would achieve near zero net CO_2 emissions. These features make integrated biorefinery a mixed feedstock source of chemicals, energy, fuels and materials. Two main process option to bioproducts can be distinguished [21]:

1. Via platform molecules: this strategy involves the controlled degradation of natural polymers to obtain specific molecules (platform molecules) with high selectivity, thanks to catalytic or enzymatic processes. In order to achieve high selectivity a pretreatment step is usually required to separate the biomass in its constituents: this way, every fraction is then further transformed with tailor-made treatments maximizing selectivity. Platform molecules are the renewable counterpart of fossil building blocks and can be further converted into a broad spectrum of added value bioproducts by means of catalytic chemical reactions or fermentations.

2. Via degraded molecules: this strategy is based on the concept of breaking down the biomass to smaller building block and involves the less controlled thermochemical degradation of natural polymers into a broad range of molecules. This approach is applicable to any kind of biomass without fractions separation but is also much less selective and yields mixtures of products that are difficult to separate. For this reason, it is usually performed in order to obtain fuels, where a high selectivity is less important.

Finally, it is worth noticing that the development of processes capable to transform platform molecules into the traditional building blocks obtained from fossil fuels would allow to use all the conventional catalytic processes already applied to that building block to enlarge the spectrum of bioproducts obtainable from biomasses [20]. Despite the undisputed advantages from the environmental point of view, the major obstacle that the bio-refinery must be able to overcome is represented by economic sustainability: the real challenge to its diffusion is in fact represented by the economy, competitiveness and greater degree of optimization of the processes based on fossil raw materials. Ultimately, biorefinery would develop and diffuse worldwide only if its product will become cheaper than fossil-based products.

2 Aim of the work

The research work presented and discussed in this Thesis is inspired by the principles of green chemistry that advocate the development of safer and more sustainable processes in respect to conventional ones, thanks to the development of new catalysts capable to valorize renewable raw materials. The main aim of this work was to achieve the catalytic transformation of methyl propionate (MP), obtainable from renewable glycerol (GLY), into valuable bio-based methyl methacrylate (MMA), avoiding the direct use of formaldehyde (FAL) thanks to a one-pot strategy which involves *in situ* methanol (MeOH) dehydrogenation. The relevance of such research line is related to the large availability of cheap renewable bio-based GLY from bio diesel production, which is expected to grow steadily in the future, and to the safety/toxicity issues related to the direct use of FAL as reactant in the conventional MMA synthesis (Lucite process), which depends on non-renewable MP. As a preliminary study, the catalytic ketonization of carboxylic acids and esters was investigated too over several metal oxides and metal phosphates, in order to obtain a better understanding of the structure-activity relationship governing the reaction. In fact, ketonization is most likely to be a detrimental parasitic reaction during MMA synthesis. However, the investigation of the ketonization of carboxylic acids and ester possess scientific and industrial value itself and is currently under investigation by several research groups as a strategy for the upgrading of the bio oil obtained from the fast pyrolysis of lignocellulosic materials, which represent a robust and versatile technology virtually capable to transform one of the most abundant kind of biomass into liquid bio fuels.

In particular, the main goals of this work were:

1. To investigate the gas-phase catalytic ketonization of some model compounds for carboxylic acids usually found in bio oils, namely PA to 3-pentanone (3-P) and AA to acetone, over several catalytic systems possessing different surface acidity and basicity features. La, Al, Zr and Si oxides (MOs) and La, Al and Zr phosphates (MPOs) were investigated in order to assess how the target reaction is influenced by such features.

2. To investigate the gas-phase catalytic ketonization of the model compound MP in the presence of another compound usually found in bio oils, MeOH, in order to investigate the reaction scheme arising from the competition between several reaction pathways:

    *   Homo-ketonization of MP.
    *   Dehydrogenation of MeOH to FAL.
    *   Hydroxy-methylation and dehydration of MP with FAL
    *   H-transfer hydrogenation with MeOH as H-donor of unsaturated compounds.

3. To achieve the synthesis of valuable MMA from MP and MeOH, both obtainable from renewable resources, thanks to the conclusions drawn at the end of the previous work, through the design of a catalyst capable to favor the desired reaction pathways of MeOH dehydrogenation and MP hydroxy-methylation/dehydration with FAL among the others (e.g. minimizing ketonization and H-transfer parasitic reactions).

3 General operative procedures

3.1 Gas-phase continuous-flow reactor and typical catalytic test

3.1.1 Gas-phase continuous-flow reactor

Figure 7 depicts the bench-scale reactor used to carry out all the catalytic tests.
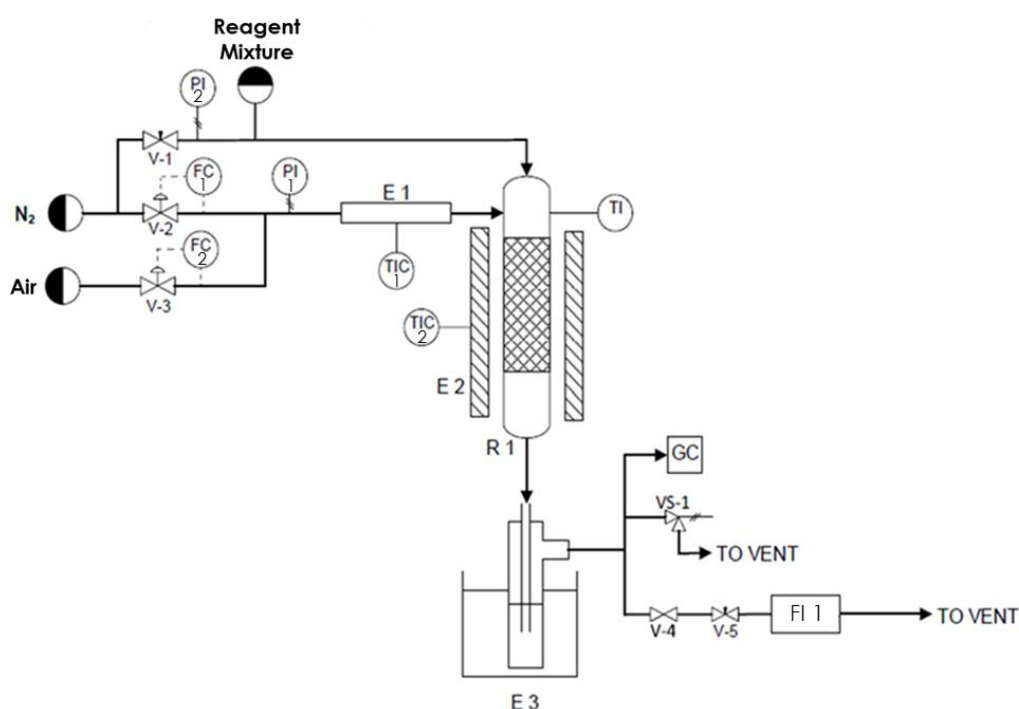
Figure 7: gas-phase rig P&ID.

The rig can be divided into three zones: a feeding zone, a reaction zone and a sampling zone. Several devices able to set and control both the carrier gas and the liquid reagents mixture flow constitute the feeding zone:

- FC1 is a Brooks "mass flow controller 5850 E series" mass flow meter that regulates the flux of carrier (N_2) through the carrier feeding pipe (diameter = 1/8 inch).

- FC2 is a Brooks "mass flow controller 5850 E series" mass flow meter that regulates an optional flux of air through the carrier feeding pipe.

- E1 is a heating band coiled around the carrier feeding pipe. It is used to maintain the feeding pipe at 210 °C, in order to heat the carrier before it enters the reactor.

- TIC1 is the thermocouple that controls the heating band E1.

- PI1 is a pressure gauge used to detect any increase in pressure within the rig. It is also used to verify the absence of leakages before every catalytic test.

- V-1 is a needle valve that is regulated to send a small flux of carrier (8-12 mL/min) through the regent mixture feeding pipe (diameter = 1/16 inch). Such pipe delivers the reagent mixture 5 cm above the catalytic bed.

- The input flow rate of the reagent mixture is fed to the reagent mixture feeding pipe by means of a syringe secured to a high precision infusion pump Kd Scientific 100. The syringe needle enters in the reagent mixture feeding pipe piercing a gastight septum.

- PI2 is a pressure gauge use to detect any increase in the pressure within the reagent mixture feeding pipe, which may be subject to clogging due to its small diameter.

- FI 1 is a bubble flow meter, in order to further control the pre-set flow of N_2 from the mass flow meter FC1, to ensure that it matches the flow delivered. Such flow is given by the sum of the one delivered through the carrier feeding pipe and the one from reagent mixture feeding pipe.

A conventional fixed bed down-flow quartz reactor (internal diameter = 11 mm) and the gear required to reach and control the reaction temperature constitutes the reaction zone:

- E2 is a Lenton thermal designs tubular furnace.

- TIC2 is a thermocouple positioned inside the furnace but outside the reactor, which controls the temperature of E2.

- TI is a thermocouple that measures the temperature of the catalytic bed, which can differ from E2 set point. Its end is immersed in the catalytic bed and is protected by a quartz sheath that enters in the reactor through the same gastight septum where enters the reagent mixture feeding pipe.

The catalyst is packed in the reactor over a porous sintered glass septum in the form of pellets with granulometry between 30 and 60 mesh so that it is entirely inside the isothermal zone of the furnace. A cold trap and a system of valves and pipes connected to the vent and the gas chromatograph constitutes the sampling zone.

- E3 is the cold trap, thermostated at 0 °C thanks to an ice bath and constituted by two or three glass devices in series that allows the reactor outgoing flow to bubble through a solvent which absorb the condensable products. Periodically the solvent is recovered and analyzed by GC-FID. Non-condensable products and the carrier constitute the cold trap outgoing flow, which is sent to the gas chromatograph for online GC-TCD analysis of permanent gases.

- V4 is a two-way valve used to perform leakages tests and is always open during catalytic tests.

- V5 is a needle valve that ensures the constant pressure of the gaseous flow exiting from the cold trap.

3.1.2 Catalytic tests procedure

The reactor, bubbling devices, and feeding syringe were thoroughly washed and dried prior to every catalytic test. The catalyst is introduced inside the reactor in the form of pellets with granulometry between 30-60 mesh. The reactor is put inside the tubular furnace and connected to the carrier feeding pipe, the reagent mixture feeding pipe and the vent pipe. The absence of leakages is verified prior to every catalytic test: the V4 is closed while flowing carrier until the rig is slightly pressurized (1.5 bar); it is considered gastight if the pressure within does not drop after 2 minutes. The overpressure is removed, the carrier feeding pipe and the head of the reactor are coiled with the heating band E1 and an insulating ceramic band; the tail of the reactor is coiled in insulating ceramic band too and the leakage test is repeated. 8-12 mL/min of carrier are sent through the reagent mixture feeding pipe regulating V1 and checked with the bubble flow meter FI 1. A flux of carrier is sent through

General operative procedures

the carrier feeding pipe too, and the total flux is checked one last time by means of the bubble flow meter FI 1. Both flux measurements are carried out at room temperature. Once the desired carrier flux is achieved, the bubbling devices filled with solvent are connected to the tail of the reactor and the vent line and immersed in the ice bath E3. The carrier feeding pipe and the reactor are slowly heated up with E1 and E2 to 210 °C and reaction temperature respectively under carrier flow. Once the rig is ready, the reagent mixture is prepared (weighting the reagents in the desired ratio with an analytical balance) and charged inside the feeding syringe, which is secured to the precision pump. The pump is turned on until a steady flux of the reagent mixture is reached. Then the syringe is removed from the pump, weighted ($m^i_{SYRINGE}$), connected to the reagent mixture feeding pipe by piercing the gastight septum and secured again to the pump. The catalytic test starts when the pump is turned on again and is carried out for at least 6 hours ($t_{REACTION}$), collecting the condensable products every 60-120 minutes ($t_{SAMPLING}$). The total reaction time and the sampling times are measured with a chronometer. Non-condensable products collection is carried out thanks to an online system of valves and loops by means of GC-TCD; such system will be described in the next Chapter. Liquid products collection involves:

1. Disconnection of the sampling devices from the tail of the reactor and their removal from E3.

2. Washing the inner part of the reactor tail with the same solvent used for the sampling, in order to collect the heavy products which might have condensed below the catalytic bed inside a 100 mL flask.

3. Connection of another set of sampling devices filled with fresh solvent to the tail of the reactor and their immersion in the ice bath E3.

4. Transfer of the content of the first set of sampling devices into the same flask used to collect the solvent used for the reactor tail washing.

5. Rinsing with solvent all the parts of the sampling devices collecting the solvent in the 100 mL flask.

The pump kept running during these operations and operations 1, 2 and 3 are carried out quickly (1-2 minutes between previous sampling devices disconnection and next sampling devices reconnection). This procedure allows recovering completely all condensable products and ensures that a steady state is maintained within the reactor, with no transients due to pump stop and restart. As a result, about 100 mL of diluted reaction mixture is collected inside the flask. The flask is weighted (m^i_{FLASK}) and then about four grams of internal standard solution (IS = dodecane, in the same solvent used for sampling) is added with a Pasteur pipette. Then the flask is weighted again (m^f_{FLASK}) and the sample is ready for the GC-FID analysis, which will be described in the next Chapter. At the end of the catalytic test the pump is turned off and the feeding syringe is removed from the pump and weighted again ($m^f_{SYRINGE}$), while the carrier flow is left flowing through the sampling device for 15 minutes prior to collect the last sample. This way the reactants and product inside the reactor and lines in the moment the pump is turned off have enough time to reach the sampling device. The IS solution is prepared by weighting an empty 25 mL volumetric flask ($m^e_{V. FLASK}$), transferring 0.15 g of dodecane into it, bring to volume with the solvent used for sampling and weighting the full volumetric flask ($m^f_{V. FLASK}$). The IS concentration is expressed in terms of moles per gram of solution. The equations used to calculate the mass flow of the reagent mixture, the mass of reagent mixture in each accumulation, the concentration in moles per gram of IS and the moles of IS added to each sample are reported below.

$$\dot{m}_{\text{ REAGENT MIXTURE}} = \frac{\left(m^i_{SYRINGE} - m^f_{SYRINGE}\right)}{t_{\text{ REACTION}}} = [g/min]$$

$$m_{\text{ REAGENT MIXTURE SAMPLING } i} = (\dot{m}_{\text{ REAGENT MIXTURE}}) \cdot (t_{SAMPLING \, i}) = [g]$$

$$C_{IS} = \frac{n_{IS}}{\left(m^f_{V.FLASK} - m^e_{V. \, FLASK}\right)} = \left[\frac{mol}{g}\right]$$

$$n_{IS \, ADDED \, TO \, SAMPLE} = \left(m^f_{FLASK} - m^i_{FLASK}\right) \cdot C_{IS} = [mol]$$

The mass flow of the reagent mixture and the volumetric total flow of carrier at room temperature are converted into molar flows. Their sum is converted again into a volumetric flow at reaction temperature to calculate the "residence time" W/F:

$$\frac{W}{F} = \frac{m_{CATALYST \, PELLETS}}{\dot{V}^{GAS}_{TOT}(reaction \, temperature)} \cdot 60 = [s * \frac{g}{mL}]$$

3.2 Compounds analysis and quantification

3.2.1 Gas-chromatograph

The compounds of interest were analyzed and quantified using a gas-chromatograph Hewlett Packard 5890 Series II GC instrument equipped with FID and TCD detector and three capillary columns with Argon as carrier:

1. Agilent J&W DB-1701 capillary column (25m x 530 µm x 1.05 µm), connected to a flame ionization detector (FID) and used to elute and quantify the condensed products.

2. Agilent CP-Molsieve 5A capillary column (25m x 530 µm x 50 µm), connected to a thermal conductivity detector (TCD) detector and used to elute and quantify H_2, O_2 and N_2.

3. Agilent CP-SilicaPLOT capillary column (30m x 530 µm x 6 µm), connected to the TCD and used to elute and quantify CO, CO_2, CH_4, ethylene, propylene and propane.

The gas chromatograph schematic is depicted in Figure 8:
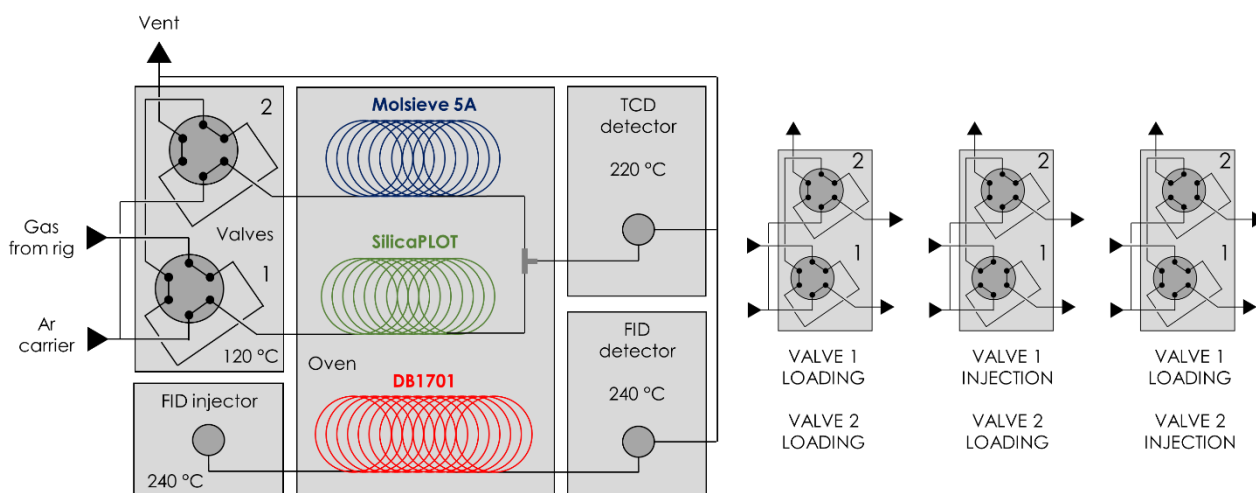
Figure 8: GC Hewlett Packard 5890 Series II used to perform the analysis.

3.2.2 FID calibration and analysis

The response factor f for the GC-FID was calibrated for each compound of interest in an appropriate range of concentrations with the internal standard method, using dodecane as the IS and the following equation:

$$\frac{A_i}{A_{SI}} = \frac{mol_i}{mol_{SI}} * f$$

The most concentrated standard solution was prepared so that its concentration was slightly higher to the one inside the accumulation in the case of conversion equal to 0 % for reactants and in the case of yield equal to 100 % for products. The less concentrated standard solution was prepared so that its concentration was equal to the one inside the accumulation in the case of 99 % conversion for reactants and yield equal to 1 % for products. Three other standard solutions with intermediate concentrations between these two extremes were prepared too. The temperature ramp used for GC-FID calibration and reaction mixtures analysis is depicted in Figure 9:
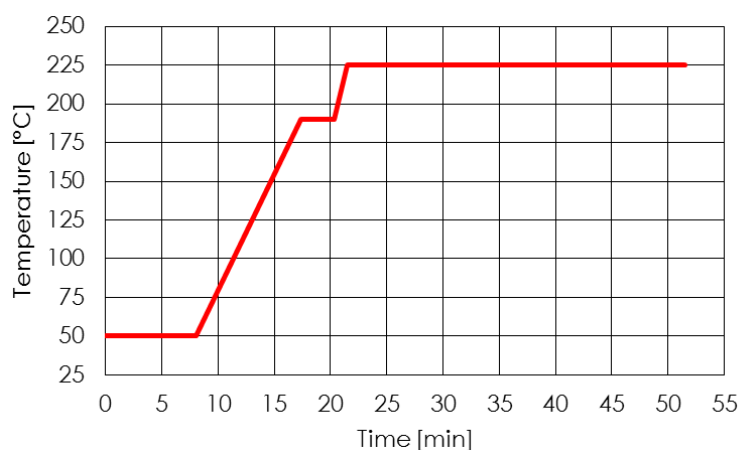
Figure 9: temperature ramp used for GC-FID analyses.

The initial temperature in the oven was 50 °C and was kept for 8 minutes. Then the temperature was risen to 190 °C with a heating rate of 15 °C/min and was kept constant for 3 minutes. Finally, the temperature was risen to 225 °C with heating rate equal to 30 °C/min and was kept constant for 30 minutes.

3.2.3 TCD calibration and analysis

The response factor f for the GC-TCD was calibrated for each gas of interest in an appropriate range of molar fractions mixing the N_2 carrier inside the gas-phase plant with a mixture of gas (CO, CO_2, CH_4, H_2 and ethylene) from another cylinder. The following equation was used to calculate f:

$$A_i = x_i * f$$

The highest molar fraction was obtained flowing the pure mixture; then, lower molar fractions were obtained diluting the mixture with the N_2 carrier. The two capillary columns were connected to the TCD by means of a T union and a short piece of empty (i.e. with no stationary phase) capillary column. Therefore, the injection in the two columns was carried out at different times:

- t = 0 min: the six-way valve 1 (Figure 10) injects the gas mixture from the rig contained in the first loop in the SilicaPLOT.

- t = 1 min: the six-way valve 1 come back in loading position.
- t = 2 min: the six-way valve 2 injects the gas mixture from the rig contained in the second loop in the Molsieve 5A.
- t = 3 min: the six-way valve 2 come back in loading position.

The temperature ramp used for GC-TCD calibration and reaction mixtures analysis is depicted in the following Figure:
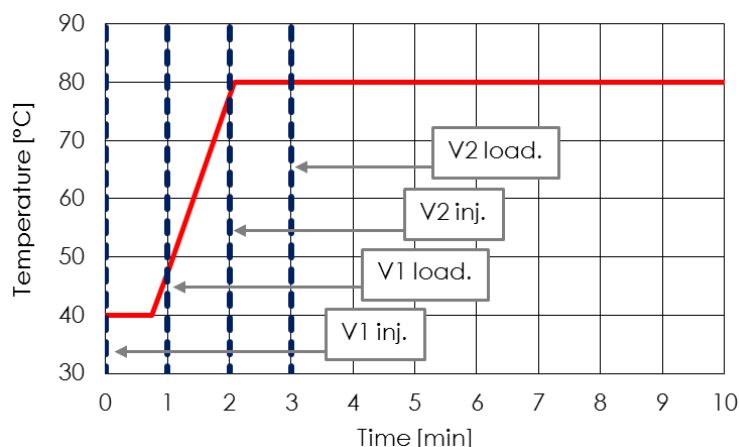
Figure 10: temperature ramp used for GC-TCD analyses.

3.2.4 GC-MS: unknown products identification

Unknown products were identified by means of GC-MS; then, pure reference reagents were purchased and injected in the GC-FID in order to further confirm the identification, checking the retention time match in two different gas chromatographs equipped with different columns. The GC-MS used was an Agilent Technologies 6890 GC coupled with a mass spectrometer Agilent Technologies 5973 and equipped with an Agilent HP5 capillary column (30m x 250 μm x 1.05 μm). In this case, the GC carrier was Helium; the injector temperature and temperature ramp were the same as those used for products analysis.

3.2.5 Equations and results expression

Usually, when the stoichiometric coefficients linking reagents and products were known, conversion (X), yields (Y), sum of yields (YS) and molar balance (YS/X) in respect to reactant R were calculated as follows:

$$X_R \ [\%] = \frac{\left(mol_R^{IN} - mol_R^{OUT}\right)}{mol_R^{IN}} \cdot 100$$

$$Y_{Pi} \ [\%] = \frac{\nu \cdot mol_{Pi}^{OUT}}{mol_R^{IN}} \cdot 100$$

$$YS \ [\%] = \sum_i Y_{Pi}$$

$$molar \ balance \ [\%] = \frac{YS \ [\%]}{X \ [\%]} \cdot 100 = \frac{\sum_i \nu \cdot mol_{Pi}^{OUT}}{\left(mol_R^{IN} - mol_R^{OUT}\right)} \cdot 100$$

Where:

- mol $_R^{IN}$ = moles of reagent entering the reactor.
- mol $_R^{OUT}$ = moles of reagent exiting the reactor.
- mol $_{Pi}^{OUT}$ = moles of product i exiting the reactor.
- ν = stoichiometric coefficient (ratio between ν reagent and ν product in the stoichiometry of the reaction).

It is worth noticing that when these equation are used to calculate the yield of the products of reactions of the type A → B + C, only the yield of one of the two product is used to calculate YS. As an example, in the case of ketonization the stoichiometry is 2 A → B + C +D (where A=acid, B=ketone, C=H_2O and D=CO_2); in this case ν = 2 for A, B and C, but only the yield of the ketone B has been taken into consideration for the calculation of YS.

3.3 Catalysts Synthesis and Characterization

3.3.1 Catalysts Synthesis

Catalysts have been synthesized adapting precipitation and co-precipitations techniques from the literature.
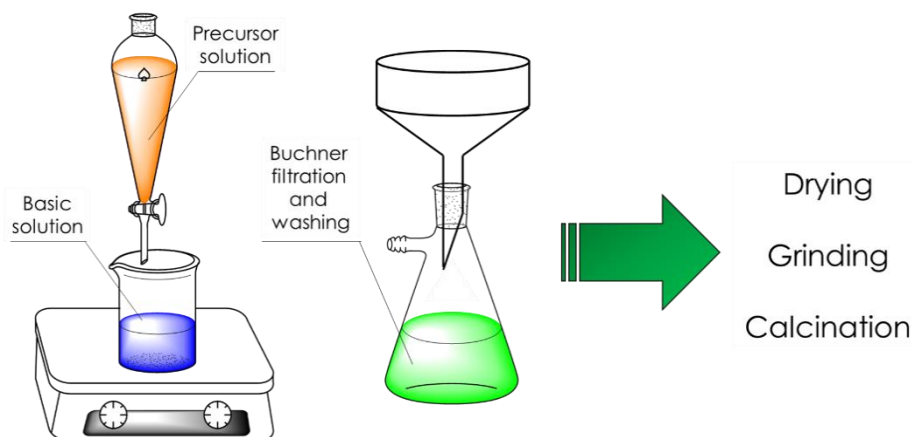
Figure 11: catalysts synthesis by precipitation and co-precipitation.

The former technique, in the case of metal oxide catalysts, involves the preparation of a metal cation precursor solution as the first step; the metal cation precursor should be readily soluble in deionized water and its counter ion should be easily removed from the precipitated solid either by washing or upon calcination. Nitrates and oxy-nitrates are suitable precursor and are usually preferred; however, when the required metal nitrates were unavailable, chlorides and oxy-chlorides have been also used. In co-precipitation technique, this solution contains two metal precursors, and their molar ratio is equal to the one desired in the final catalyst. The second step involves the preparation of a basic solution dissolving an alkali (usually Sodium) hydroxide or carbonate in water; aqueous ammonium hydroxide is a suitable base too. Again, the counter cation should be easily removed either by washing (Na^+) the precipitate or upon calcination (NH_4^+). The metal cation solution is transferred in a separating funnel and slowly added dropwise to the basic solution under vigorous stirring. During this operation, the pH is decreased due to the acidity of the metal precursor solution, therefore it is maintained constant and equal to the optimal value

adding a basic solution. After completing the addition of the metal cation/cations, the resulting insoluble hydroxide suspension is let aging for a one hour under vigorous stirring, then is filtered over a Buchner funnel and thoroughly washed with deionized water. Finally, the wet hydroxide is dried in an oven, grinded in powder and calcined. Calcination temperature should be at least 50 °C higher than the highest reaction temperature at which the catalyst is subjected during catalytic tests. If not, it could be unstable under reaction condition and change, making the fresh catalyst characterization non-representative of the real catalyst. The co-precipitation technique used for the preparation of MPOs is slightly different: in this particular case, a phosphoric acid or ammonium phosphate solution is mixed with an acidic metal precursor solution; both components of the final mixture are acidic, therefore after mixing a base is added until neutral or slightly basic pH is obtained. High pH value lead to the formation of metal hydroxides, which contaminates the final phosphate catalyst with segregated oxides.

3.3.2 X-Ray spectroscopies

X-ray diffraction was used to determine the crystal structure of catalysts, their phase purity and to estimate their degree of crystallinity. Powder patterns of catalysts were recorded with Cu Kα radiation (λ = 1.54178 Å, Ni-filtered) on a Philips X'Pert diffractometer with the Bragg Brentano design, equipped with a pulse height analyzer and a secondary curved Graphite-crystal monochromator. Catalyst powders were charged on plane specimen holders. The analysis of the phases present in the patterns was performed using the Bragg's Law:

$$n\lambda = 2dsen\theta$$

in order to calculate the crystalline d values and compare them with those reported in the literature and collected in the ICSD (International Crystal Structures Database).

X-ray photoelectron spectra (XPS-ESCA) was used to semi-quantify the surface elemental composition and investigate the carbon deposition and surface reduction of catalysts before and after reaction. Spectra were recorded with a PHI VersaProbe II Scanning XPS Microprobe with scanning monochromatic X-ray Al Kα radiation as the excitation source (200 micrometer area analyzed, 52.8 W, 15kV, 1,486.6 eV), and a charge neutralizer. The pressure in analysis chamber was maintained lower than 2.0 x 10^{-6} Pa. High-resolution spectra were recorded at a given take-off angle of 45° by a multi-channel hemispherical electron analyzer operating in the constant pass energy mode at 29.35 eV. Energy scale was calibrated using Cu $2p_{3/2}$, Ag $3d_{5/2}$, and Au $4f_{7/2}$ photoelectron lines at 932.659, 368.2, and 83.95 eV, respectively.

Energy Dispersive X-ray spectroscopy was used to assess the elemental composition of catalyst. Spectra (SEM-EDS) were recorded with a Zeiss EP EVO 50 scanning electron microscope equipped with an EDX probe Oxford Instruments INCA ENERGY 350. General conditions of the analysis were EHT 20 KeV, high vacuum (10^{-6} Pa) or variable vacuum between 60 – 100 Pa. The EDX probe used a Mn Kα radiation with 133 eV of resolution.

3.3.3 N$_2$ Adsorption/desorption isotherms (BET)

N$_2$ multipoint adsorption/desorption isotherms at 77 K were collected with Micromeritics ASAP 2020 instrument in order to measure specific surface area of

catalyst pellets using the BET (Brunauer-Emmett-Teller) model. Typically, 0.1 grams of sample were outgassed at 250 °C before N_2 adsorption.

3.3.4 Temperature Programmed Desorption (TPD)

The total acidity and the total basicity of catalysts were measured by means of temperature programmed desorption of NH_3 and CO_2 using a Micromeritics Autochem II 2920 instrument. The effluents were analyzed by means of an online Cirrus 2 quadrupole mass spectrometer recording the intensity of the following ion current signals: NH_3 (m/z=17), H_2O (m/z=18), CO_2 (m/z=44). Typically, 0.2 grams of catalyst pellets were charged in a quartz tube and heated up to calcination temperature in He flow (30 mL/min) with heating rate of 10°C/min. Final temperature was kept for 60 minutes in order to clean catalyst surface from adsorbed water and carbonates. The successful surface cleaning was verified following the evolution of H_2O and CO_2 with the mass spectrometer. After cooling to probe adsorption temperature, NH_3 and CO_2 chemisorptions were conducted at 100°C for 20 minutes flowing 10% NH_3/He (30 mL/min) and 40°C for 60 minutes flowing 10% CO_2/He (30 mL/min) respectively.
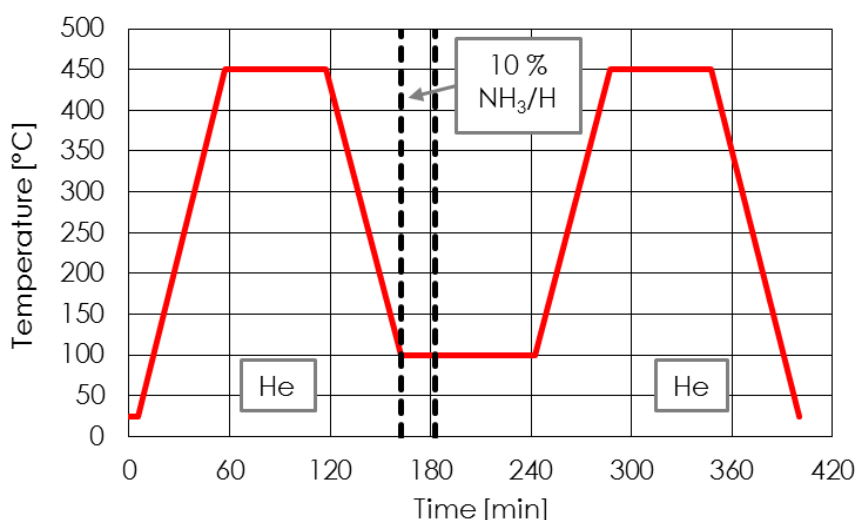
Figure 12: example of temperature ramp for NH_3-TPD analysis for a catalyst with calcination temperature = 450 °C.
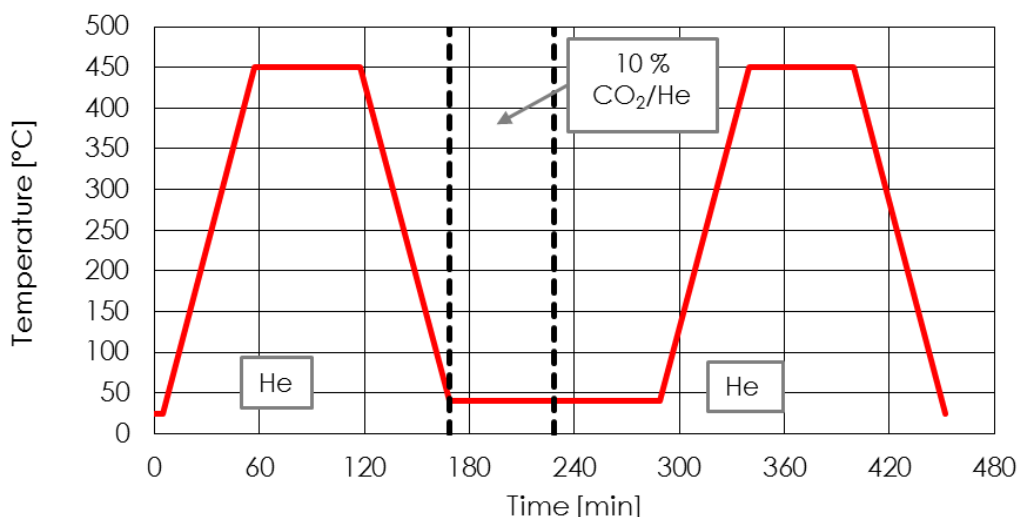
Figure 13: example of temperature ramp for CO_2-TPD analysis for a catalyst with calcination temperature = 450 °C.

In order to remove the weakly physisorbed probe molecules, before desorption samples were flown with pure He (30 mL/min) for 60 minutes at adsorption temperature. Finally, temperature programmed desorption was conducted in the same way of the sample surface cleaning.

3.3.5 Attenuated total reflectance (ATR)

IR spectra were collected with a Bruker Alpha spectrometer, equipped with a diamond plate-ATR device. Spectra were registered from 4000 to 400 cm^{-1} with resolution of 1 cm^{-1}.

3.3.6 Thermogravimetric analysis (TGA)

TGA analyses were performed with a SDTQ 600 instrument, typically on 15 milligrams of sample charged into an alumina pan. Depending on the kind of information needed, three different thermal treatments were employed.

1. To determine the water content on the surface of fresh catalysts or precursors, the samples were heated up to 550-900°C with heating rate of 10°C/min in 100 mL/min of N_2 and the final temperature was kept for 1 hour.

2. To investigate the transformations occurring during catalyst precursors calcination, the samples were heated up to 550-900°C with heating rate of 10°C/min in 100 mL/min of air and the final temperature was kept for 1 hour.

To measure the mass of carbon deposited on catalyst surface after reaction, the samples were heated up to 550-900°C with heating rate of 10°C/min in 100 mL/min of N_2; the final temperature was kept for 1 hour to desorb volatiles and volatile carbonaceous matter. Then, the gaseous flow was switched from N_2 to air for 1 hour in order to burn all the residual carbon on catalyst surface.

4 Carboxylic acids ketonization

4.1 Introduction and aim of this Chapter

4.1.1 Lignocellulosic materials

Lignocellulosic materials are the most abundant kind of biomass on land and can be classified in virgin biomass, waste biomass, and dedicated crops. Virgin lignocellulose includes all naturally occurring terrestrial plants (trees, bushes and grass). Waste lignocellulose is produced as a low value byproduct of various industrial sectors (agriculture, forestry and paper industry). Dedicated crops consist in fast-growing plants (poplars, eucalypti, elephant grass) that provide high yields of biomass and can be harvested multiple times each year. Dry lignocellulosic materials (Figure 14) are mainly composed by three natural macromolecules: cellulose, hemicellulose and lignin [22].
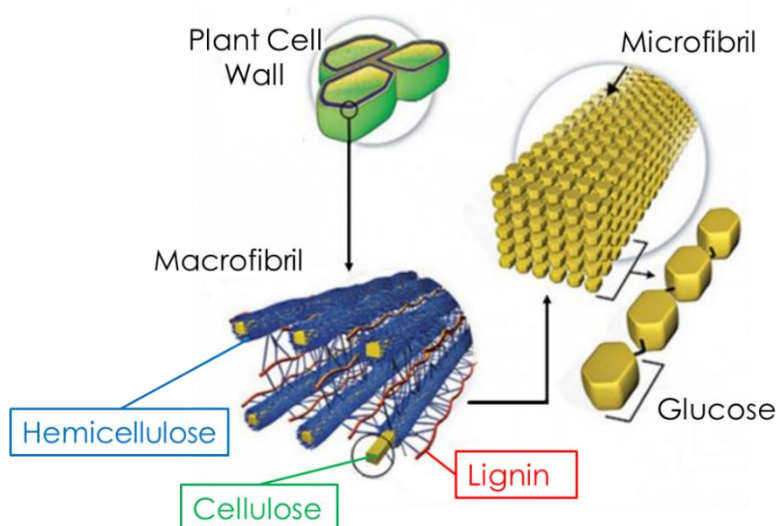
Figure 14: lignocellulose structure

Cellulose (Figure 15) is the main constituent of lignocellulosic materials by weight (38-50 % in woods [23]) and the world's largest raw material resource obtainable from biomass. It is a polysaccharide consisting of 7000 – 15 000 linearly connected β (1→4) linked D-glucose units. In order to achieve optimal glucosidic bond angles, alternating glucose units are rotated by 180 degree along the axis of the polymer chain and unlike starch, no coiling nor branching are present, but chains adopt a rigid rod-like conformation. Due to the abundance of hydroxy groups in the repeating unit, cellulose forms extensive networks of intra and intermolecular H_2 bonds that holds the chains firmly together forming microfibrils with high tensile strength [24]. Hemicellulose is a collective term to address a family of polysaccharides which constitute about 23-32 % by weight of lignocellulosic biomass [23] and represent the second most abundant raw material in natures. Unlike cellulose, it is a heteropolysaccharide and may contain several different sugars (Figure 16): pentoses (xylose, arabinose), hexoses (glucose, galactose, mannose), deoxyhexoses (rhamnose, fucose) and hexuronic acids (glucuronic acid, galacturonic acid) [25]. Its molecular weight is much lower than the one of cellulose (500 – 3000 monomer units) and unlike cellulose it is amorphous. The polymers that constitutes hemicellulose vary in composition and structure

from species to species but can be grouped into several families [26]. They take their name from the most common repeating units: xylans (xylanose in the backbone), glucomannans (glucose and mannose in the backbone), galactans (galactose in the backbone), glucans (glucose in the backbone) and Xyloglucans (glucose in the backbone and xylose in the lateral chains). All the other sugars and hexuronic acids are found in the side chains [26].

β-D-glucopyranose

Poly-β(1→4)-D-glucopyranose

7000-15000

Hydrogen bonding in cellulose
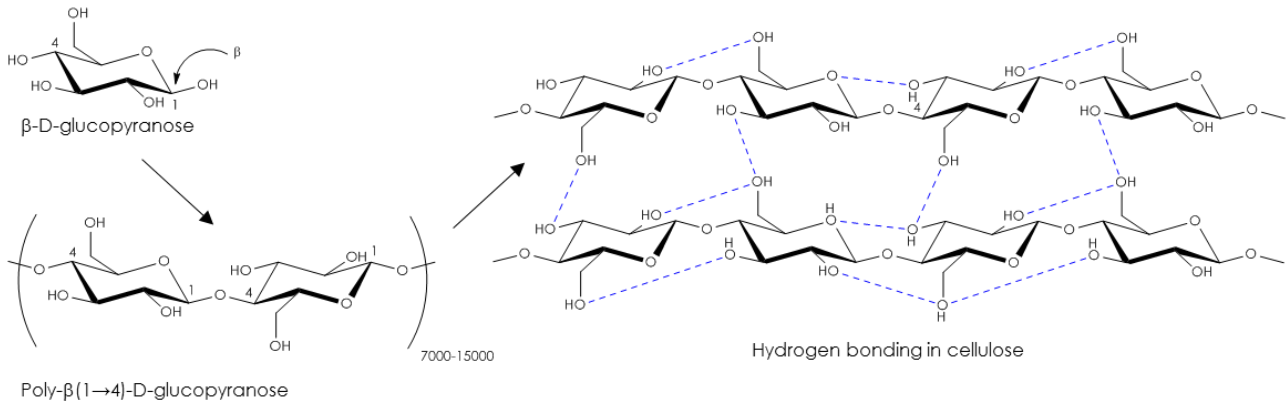
Figure 15: cellulose chemical structure.

β-D-glucopyranose   β-D-galactopyranose   β-D-mannopyranose   β-D-xylopyranose

α-L-arabinofuranose

β-D-glucoronic acid   β-D-galacturonic acid   α-L-fucopyranose   α-L-rhamnopyranose
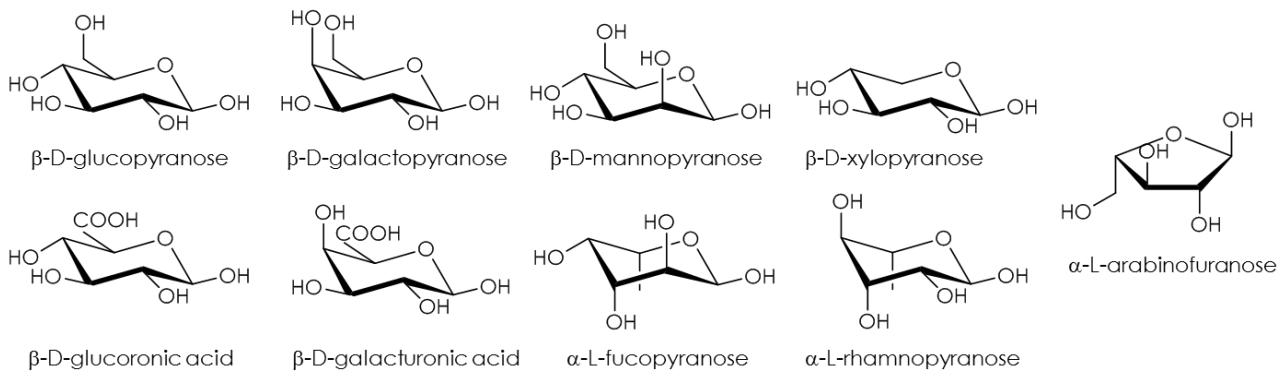
Figure 16: sugars obtainable from hemicellulose.

Lignin is a three-dimensional amorphous cross-linked phenolic polymer that lend rigidity and mechanical strength to cell plants walls [27]. It generally represents 15-30 % by weight of lignocellulosic materials, but its content can be higher in the most though part of plants (e.g. nutshell and tree trunks). Lignin biosynthesis mainly occur via the oxidative coupling of three monomers, called monolignols: para-coumaryl alcohol, coniferyl alcohol and synapyl alcohol.

RO_4 R_β R_1 R_5
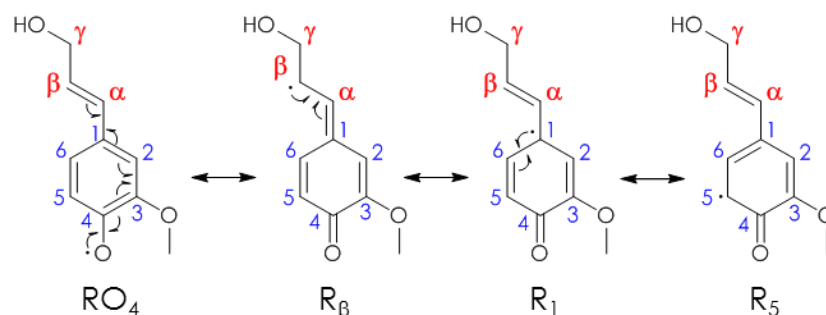
Figure 17: monolignol radical delocalization; from left to right: phenolic oxygen radical, β-position radical, position 1 radical, position 5 radical.

The polymerization mechanism involves the formation of monolignols radicals (Figure 17) thanks to a specific enzyme: as a result of the delocalization of the radical electron, different chemical bonds, including ether and carbon–carbon bonds, can be formed between

monolignol units and the growing lignin polymer. Although the formation of the radicals is catalyzed by an enzyme, only chemistry controls the following polymerization, and lignin has no regular structure, unlike cellulose. The β-O-4 bond between monolignols is the dominant one, consisting of more than half of the linkage structures of lignin; however, other kind of linkages such as α-O-4, β-5, β-β, 5-5, 4-O-5, α-5 and α-β are formed to a certain extent (Figure 18). Once polymerized, the three monolignols result in p-hydroxyphenyl, guaiacyl, and syringyl residues respectively [27].
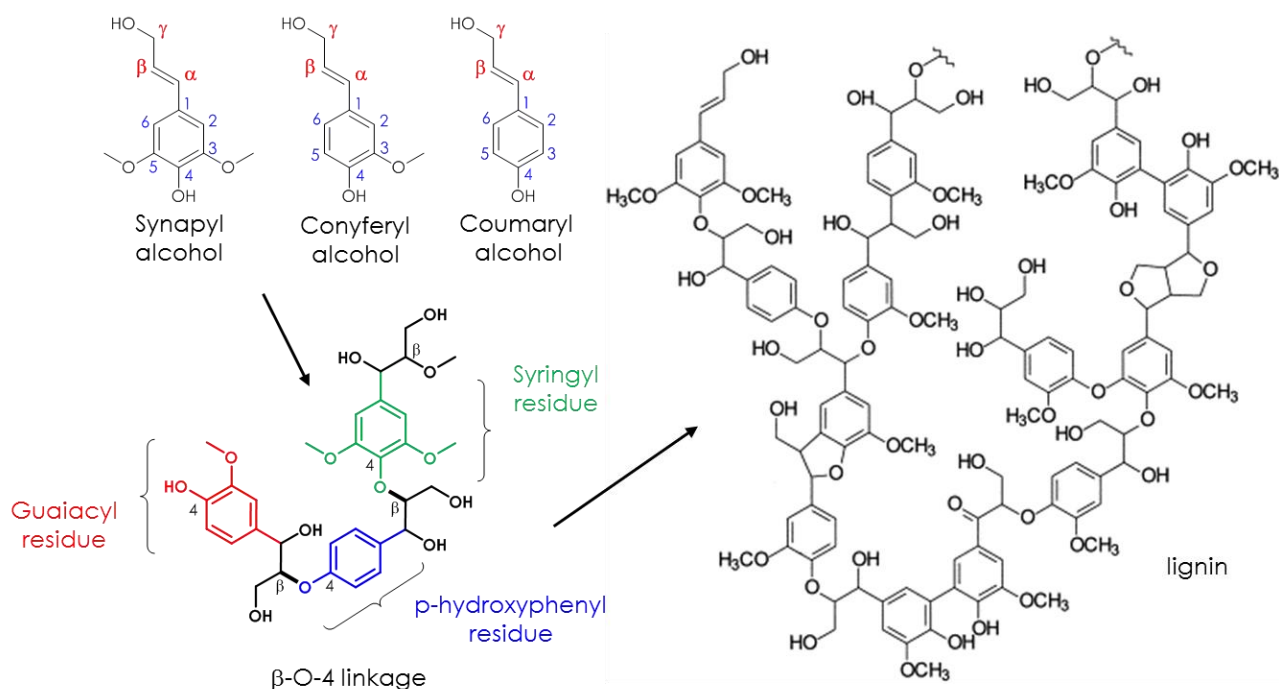
Figure 18: lignin chemical structure.

These three polymers are closely associated together (Figure 14) to form the walls of plant cells [24] and their relative amount varies from plant to plant and from part to part of the same plant. Cellulose chains are closely packed together by means of hydrogen bonding, forming microfibrils containing both hydrophobic crystalline regions and more reactive and hydrophilic amorphous regions. Hemicellulose is bonded to cellulose by means of inter-polymer linkages forming a soft matrix that surrounds every microfibril. Lignin is covalently bonded to hemicellulose and fills the spaces between different microfibrils, forming a rigid three-dimensional support for hemicellulose. This way, lignin together with hemicellulose form a matrix that acts like a glue holding several microfibrils together and forming macrofibrils [27]. Plant cell walls are formed by the association of macrofibrils. Lignin also provides a barrier against pathogens and a hydrophobic surface for plant vasculature. The chemical and mechanical resistance of lignocellulose arise from the close association of these three polymers, which results in a natural composite material. This composite structure, together with cellulose crystallinity, prevents the diffusion of reagents and enzymes, resulting in insolubility and scarce reactivity toward chemicals. Mechanical properties too (elasticity, toughness, tensile strength) are the result of the hierarchical structure of lignocellulose.

4.1.2 Thermochemical degradation of lignocellulose

4.1.2.1 Thermovalorization

Thermovalorization of lignocellulosic biomass consists in its total combustion to produce steam that runs a turbine for electricity production. Lignocellulosic biomass can also be co-fired in coal-based power plants in order to reduce CO_2 emissions. Suitable biomasses for energy production are lignocellulosic materials such as wood waste, agricultural waste, dedicated energy crops (short rotation wood crops and herbaceous crops) and urban solid wastes. The main hurdles [28] linked to the use of biomasses for energy production are listed below:

1. Biomass grows on large surfaces, therefore the costs related to harvesting and transportation to the power plant site result in higher expenses for energy production, which become difficult to scale up.

2. Biomass contains moisture and possess a lower energy density in respect to coal; moreover, especially in pulverized firing systems, size reduction of biomass material is much more demanding than for coal due to its fibrous and more tenacious structure.

For these reasons a pretreatment step known as torrefaction, which consists of a mild pyrolysis carried out at 200-300 °C and atmospheric pressure in the absence of O_2 [29] is usually beneficial. During torrefaction of lignocellulosic materials, moisture is removed, and the most reactive hemicellulose fraction is degraded to volatiles, while the cellulose and lignin fraction are mostly unaffected. The volatile fraction can be recycled to fuel the torrefaction process itself and make it autothermal, or at least reduce the energy consumption required to heat up the biomass. As a result of the torrefaction process, the starting biomass loses roughly 30 % of its weight and only 10 % of its energy [30], and becomes a torrefied biomass with enhanced energy density. Moreover, the degradation of hemicellulose results in the loss of the tenacious structure of lignocellulose, which makes easier the following process of densification through pelletization. Finally, torrefaction reduces the hydrophilicity of biomass leading to long-term stability and very limited moisture uptake and represents a general pretreatment method capable to enhance the feature of biomass destined not only to thermovalorization, but also gasification and pyrolysis.

4.1.2.2 Gasification

Thermochemical gasification consists in the partial oxidation of carbonaceous feedstocks in order to obtain a syngas containing CO and H_2. Conventional gasification plants [4] utilize coal as feedstock to produce a syngas that can be used for H_2 production (water gas shift reaction [5]), liquid hydrocarbon fuels production (Fischer-Tropsch process) or MeOH synthesis (Scheme 1).

Water-gas shift reaction	Fischer-Tropsch Process	Methanol synthesis
$CO + H_2O \longrightarrow CO_2 + H_2$	$(2n+1) \, H_2 + n \, CO \longrightarrow C_nH_{2n+2} + n \, H_2O$	$CO + 2 \, H_2 \longrightarrow CH_3OH$
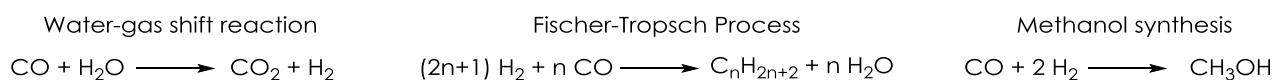
Scheme 1: reactions involved in H_2 production (water gas shift reaction), Fischer-Tropsch process and MeOH synthesis from syngas

As in the case of thermovalorization, gasification of biomasses could reduce the environmental impact of gasification by either completely switching the feedstock from coal or fossil hydrocarbons to lignocellulosic materials or by co-firing renewable feedstock in present coal-based power stations. The overall reaction is exothermic and requires an O_2-deficient atmosphere and high temperatures comprised between 650 and 900 °C; the

oxidant can be air, pure O_2, steam or a mixture of these depending on the final utilization of the syngas. As an example, O_2 may be preferred to air in order to avoid the presence of nitrogen in the final syngas for MeOH synthesis, and steam may be added if the goal is the production of H_2. In general, gasification occurs in sequential steps:

1. Dehydration and drying (endothermic): when the feed (coal or biomass) is heated up to 100 °C moisture is released, and the resulting steam is mixed into the gas flow and can be involve in subsequent chemical reaction such as water-gas shift reactions. In order to reduce the energy inputs required to heat up the feed, biomass should be dried prior to gasification; moreover, it must be densified and shaped in pellets or powders to be fed in moving bed and fluid bed reactors respectively. Therefore, as well as thermovalorization, gasification benefits from the use of torrefied biomass.

2. Pyrolysis (endothermic): around 200-300 °C volatile organic products can be desorbed from coal and biomass leaving behind a solid char.

3. Total combustion (exothermic): the oxidant atmosphere reacts with char and pyrolysis products above 300 °C to yield steam and CO_2, together with small amounts of CO. This step provides the heat required to push forward the subsequent reaction of gasification.

4. Gasification (endothermic): it consists in reactions between the char and the steam and CO_2 produced by the previous step of total combustion. The gasification process produces H_2 and CO.

5. Water-gas shift reaction (exothermic): the excess steam in the gaseous flow can lead to the conversion of CO into CO_2 and H_2; this reaction, at the temperatures in a gasifier, balance the concentration of CO, CO_2, H_2 and H_2O.

Reaction involved in gasification of both coal and biochar are depicted in Scheme 2:

$$C_nH_m + (n+m/4)\,O_2 \longrightarrow n\,CO_2 + m\,H_2O$$
$$C + O_2 \longrightarrow CO_2$$

Total combustion of pyrolysis products and coal/biochar

$$C + CO_2 \longrightarrow 2\,CO$$
$$C + H_2O \longrightarrow H_2 + CO$$

gasification of coal/biochar

$$CO + H_2O \longrightarrow CO_2 + H_2$$

Water-gas shift reaction
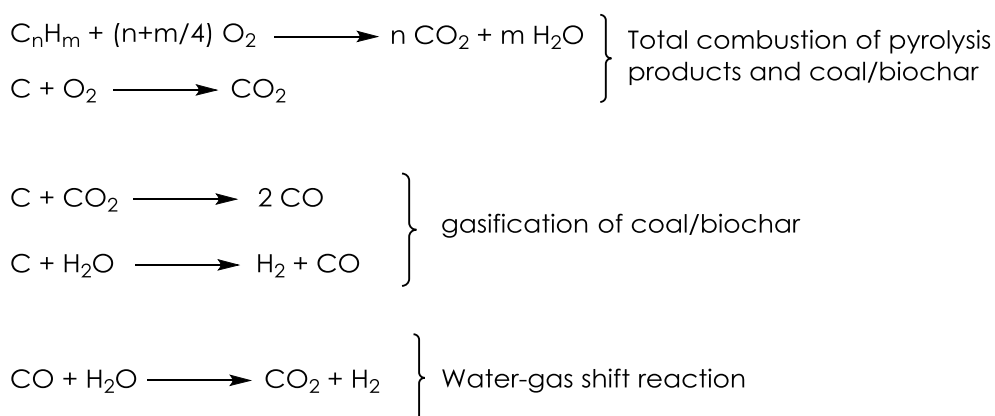
Scheme 2: reactions involved in coal or biochar gasification.

4.1.2.3 Pyrolysis

The process of charcoal burning, which consists of wood combustion in an O_2-poor atmosphere to obtain a solid fuel with higher energy density (synthetic coal), has been known to mankind and used for thousands of years. Pyrolysis can be seen as an evolution of charcoal burning and consists in the thermal degradation of lignocellulose in the complete absence of O_2 at temperatures roughly intermediate between torrefaction and gasification [31, 32]. This kind of treatment results in the evolution of a mixture of permanent gases and condensable products and leaves behind a solid residue. The solid residue, char, is a bio coal possessing higher energy density in respect to lignocellulose and can be used

as near-zero net emission fuel in coal-fired power stations or gasification plants or applied to soil as amendment [32]. The permanent gases represent the less valuable fraction of obtainable products and are usually burnt to produce the heat required for the endothermic process of pyrolysis [32]. The condensable products, bio oils, are separated from permanent gases by means of condensation. In recent years, several efforts have been made in order to develop the pyrolysis of lignocellulose and maximize the yield in bio oil, which represents the most valuable fraction of pyrolysis products [31]. Due to the abundance of available lignocellulosic materials, bio oil represents a favorable starting material for biofuels and biochemicals production. In particular, the pyrolysis of the lignin fraction of lignocellulose represents the most promising strategy for the sustainable production of aromatic biochemicals. The relative amounts of gas, bio oil and char strongly depend on the operative condition adopted. The conventional pyrolysis (slow pyrolysis) is aimed at the production of char and is carried out at 600 °C on massive chunks of wood and long vapor residence time (5 to 30 minutes). In these conditions, heat transfer and heating rate are slow, and the gas and vapors continue to react with each other while the solid char and any liquid are formed. Fast and flash pyrolysis are aimed at maximizing the yield in the condensable products that constitutes bio oil. They are carried out on finely grinded particles of lignocellulose in order to enhance the heat transfer and achieve very high heating rates (1000 and even 10000 °C/s have been claimed), at temperature between 500 and 650 °C. In order to avoid as much as possible the degradation of condensable products, very short residence times, usually less than 2 seconds, and immediate cooling and condensation of bio oil are required. Such high heating rates can be obtained in fluid bed reactor where the heat transfer is provided by particles of sand; such systems allow obtaining bio oil yields around 70-80 % and 10-15 % of gases and char respectively [31]. The gases and char are usually separated and burnt to produce heat. A Scheme of a fast pyrolysis plant is reported in Figure 19.
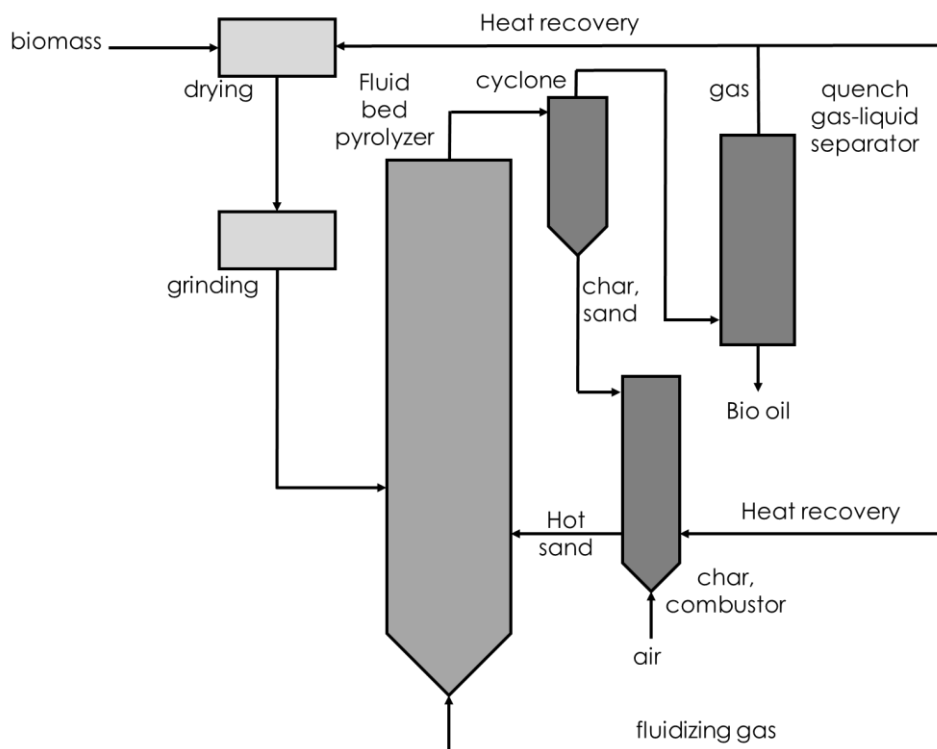
Figure 19: schematic representation of the fast pyrolysis process.

The pyrolysis process is very complex and occurs in sequential steps. At first moisture is removed from lignocellulose between 50 and 100 °C (primarily dry); between 120 and 200 °C a reactive drying process (deep drying) start to change the biomass chemical structure

Carboxylic acids ketonization

and water, small oxygenated molecules and permanent gases are released [33]. The hemicellulose fraction (the less stable at high temperatures) decomposes completely between 200 and 350 °C; this phase is called destructive drying and is equivalent to the torrefaction pretreatment. The pyrolysis of cellulose and lignin instead becomes fast above 350 °C. Every fraction of lignocellulose give rise to specific chemical reactions during pyrolysis; the temperature needed for these reactions to occur may vary from biomass to biomass depending on the degree of polymerization of the three polymeric constituents, degree of reticulation of lignin and degree of crystallinity of cellulose. As briefly explained before, also operative conditions have a strong impact on product distribution. However, the pyrolysis of biomass is frequently considered as the superimposition of three primary mechanism [34]:

1. Char formation consists in the conversion of biomass in a solid residue via intra- and intermolecular rearrangement reactions that forms benzenes rings, which then combine themselves in a polycyclic structure. These reactions are generally accompanied by the release of water, small oxygenates and permanent gases, and leave behind a solid with a higher degree of reticulation and thermal stability.

2. Depolymerization consists of the cleavage of the bonds between the monomeric units of the natural polymers. The process results in a progressive reduction of the degree of polymerization until volatile fragments are formed. These fragments (small oligomers and monomers) are generally recovered in the liquid fraction.

3. Fragmentation consists in the cleavage of chemical bond in the polymer within the monomeric units, which results in the formation of small condensable oxygenated molecules, recovered in the liquid fraction, and permanent gases which will constitutes the gaseous fraction.

Desorbed molecules produced by depolymerization and fragmentation (primary mechanisms) are not stable in reaction condition and they will react further via cracking (decomposition in lower molecular weight molecules) or recombination (coupling to form higher molecular weight molecules): these mechanisms are denoted as secondary mechanisms.

4.1.3 Bio oil

Fast pyrolysis bio oil obtained from lignocellulose is a very complex liquid mixture, which can contain more than 300 different compounds [35]:

- Water.

- Aromatics: bezenes, phenols, benzoic acids, guaiacols, catechols, syringols and vanillins from lignin depolymerization).

- Small oxygenated molecules: carboxylic acids, esters, aldehydes, hydroxy aldehydes, ketones, hydroxy ketones and alcohols formed via cellulose and hemicellulose fragmentation.

- Sugars: levoglucosan and glucose from cellulose depolymerization, hexoses and pentoses from hemicellulose depolymerization.

- Furans: furfural, furfuryl alcohol, furoic acid, hydroxymethyl furfural etc. formed by dehydration of sugars from both cellulose and hemicellulose.

- Oligomeric species with molecular weight ranging from hundreds to thousands of grams per mole, deriving mainly from lignin and (at a minor extent) from cellulose.

The relative amounts of these compounds mainly depend on the original biomass composition and the operative condition of pyrolysis. As an example, a higher fraction of aromatics is obtainable from high-lignin lignocellulose or from the pyrolysis of Kraft lignin. A higher fraction of furans, sugars and small oxygenated molecules is obtainable from low lignin lignocellulose or via pyrolysis of pure cellulose. Bio oils actually consists of metastable microemulsions [36] containing char particles, liquid droplets, waxy materials and micelles formed by heavy compounds in a continuous phase consisting of water, hydrophilic organic compounds and salts. Usually bio oils have an oxygen content around 35-50 % by weight and water is the main component (up to 30 % by weight) followed by hydroxyacetaldehyde (10 %), formic acid (5 %) and acetic acid (AA, 3 %). Bio oils, as recovered, do not mix with fossil fuels due to their strong hydrophilicity and possess a lower heating power due to the presence of highly oxygenates compounds and water: typical higher heating value for bio oil is 17 MJ/Kg against 40 MJ/Kg of heavy fuel oil [36]. It is worth noticing, however, that a significant difference in density exists between these two liquids (1.2 Kg/L and 0.94 Kg/L respectively). The presence of carboxylic acids results in pH values around 2.5 which, together with suspended char and metal cations, makes bio oil non suitable for the direct use as fuel [37]. Moreover, bio oil ages after it is first recovered, and some phase separation may occur. This instability is believed to result from a breakdown in the stabilized micro emulsion and to chemical reactions proceed after the condensation of the bio oil. As an example, the presence of acids can lead to esters hydrolysis and a rise in the pH and water content; reactive molecules such as aldehydes can undergo several acid catalyzed reactions too. In order to transform bio oil into a usable biofuel, upgrading processes are needed to remove acidity, water, char particulate and salts; moreover, the oxygen content must be reduced to further enhance its calorific power.

4.1.3.1 Bio-oil upgrading

Bio oil upgrading is aimed at enhancing the fuel properties of bio oils by means of:

1. Water, salts and particulate removal. Water reduces significantly the calorific power of bio oils due to its high latent heat of vaporization. Salts and particulate must be removed prior to use in engines or further upgrading to avoid erosion and catalyst deactivation/poisoning respectively.

2. Oxygen, nitrogen and sulfur removal. Bio oils usually contain less sulfur in respect to fossil oils, but the oxygen content is much higher. Oxygen removal increases the heating power of bio oils while reducing its density and viscosity.

3. Acidity removal: the presence of acids leads to corrosion issues and instability during room temperature handling and storage because the occurrence of acid catalyzed reactions results in changes in composition, viscosity, density and water content; moreover, phase separation may occur.

4. Small oxygenated molecules coupling to produce higher molecular weight molecules.

5. Oligomers cracking to reduce their degree of polymerization and molecular weight.

Several solutions have been proposed in order to overcome these problems. Each strategy have advantages and drawbacks, therefore a well-designed multistep upgrading process is required in order to maximize bio oil fuel performances, avoid unnecessary waste of chemical reagents and solvents, reduce the loss of carbon due to the formation of light compounds (permanent gases) during chemical upgrading and reduce the energy intensity of the overall process of bio oil refinement. The fast pyrolysis of very fine lignocellulosic particles is achieved with extremely high heating rates, which results in the

Carboxylic acids ketonization

explosive vaporization of water and other small molecules that shreds the feed particles aiding heat transfers. However, during the process non-volatile heavy oligomers and char particles are "blown apart" forming aerosols [36], which ultimately are recovered together with bio oil. The separation of these particles can be achieved with cyclonic separator or hot filters prior to bio oil condensation (hot vapor filtration); alternatively, liquid phase microfiltration of cool bio oil may be used. Kang et [38] al reported a 0.01 weight % of residual solids in bio oil when a cyclonic separator coupled with a hot filter constituted of three cylindrical ceramic filters is used. This value is ten time lower than the typical value of 0.1 % and very similar to the one of mineral oil. Moreover, this method reduced also the alkaline and alkaline earth ions (Na, K, Mg, Ca) concentration to 1-10 ppm. The cyclonic separator captured particles in the range 10-450 μm, while the hot filter captured particles around 10 μm and smaller. Membrane microfiltration is a suitable technique to remove particles smaller than 10 μm: Javaid et al [39] investigated the microfiltration of liquid bio oil in the cross-flow mode at 40 °C using Membralox TI 70 tubular ceramic membranes of nominal pore sizes 0.5 and 0.8 μm, reporting a reduction in the ashes content of 40 % by weight. The simplest strategies to enhance the calorific power of bio oils are the solvent addition and the emulsionation with a hydrocarbon fuel. The addition of polar solvents such as MeOH, EtOH, and furfural has been used for many years to homogenize and to reduce viscosity of biomass oils. The immediate effects of polar solvents addition are an increase in the overall heating value attributable to the higher heating value of the solvent added and a decrease in viscosity due to physical dilution of the bio oil. In recent years, several studies reported that the reaction between a solvent such as MeOH or EtOH with bio oils in the presence of a catalyst in reactive distillation systems is capable to enhance the heating value of the resulting refined bio oil. The reactions involved in the process are esterification of carboxylic acids and acetalization of aldehydes (Scheme 3). Thus, in addition to the decrease in viscosity and in the aging rate, they also lead to other desirable changes, such as reduced acidity, improved volatility and heating value, and better miscibility with diesel fuels.
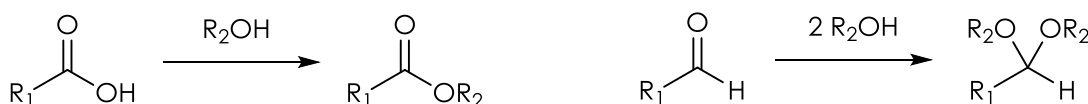
Scheme 3: esterification of carboxylic acids (left) and acetalization of aldehydes (right).

Both acid [40] and basic [41] heterogeneous solid catalysts were found to be active in the previously described reactions. Bio oils are not miscible with hydrocarbon fuels, but with the aid of a surfactant such as octanol [42], they can form stable emulsions with diesel oil up to 30 % by weight, which can be readily used in diesel engines and boilers. This solution provides a short-term approach to the use of bio-oil and the emulsions showed promising ignition characteristics, but heating value, water content, density, pH value, or ash content do not change. In order to enhance these features, more complex chemical processes and severe reaction conditions are needed. The most investigated process for bio oil upgrading takes inspiration by the well-established technologies of crude oil hydrodesulphurization (HDS), where the sulfur heteroatom is removed by means of hydrogenation to produce H_2S. Therefore, bio oil hydrogenation with the aim of oxygen removal is usually denoted as hydrodeoxygenation (HDO). Another process for bio oil valorization is the hydrocracking, which instead take inspiration from the fluid catalytic cracking (FCC) of heavy oil. Bio oil HDO has been investigated in continuous reactors between 80 and 300 bar of H_2 pressure and 300-400 °C of temperature with HDS catalysts (Co-MoS_2/Al_2O_3 [43], Ni-MoS_2/Al_2O_3 [44]) and supported noble metals catalysts (Pd/C [45], Pt/Al_2O_3/SiO_2 [44], Ru/C [46]). Bio oils hydrocracking has been investigated in continuous reactors at atmospheric pressure and temperature between 330 and 380 °C, over zeolitic catalysts (H-mordenite and H-β [47], SAPO-5 [48]). Both processes involve multiple transformations and a complex reaction

network due to the high diversity of compounds in the feed and the severe conditions employed. Among the reaction involved, there are decarboxylation of acids (Scheme 4c), decarbonylation of aldehydes (Scheme 4f), HDO of alcohols and phenols (Scheme 4a and 4b respectively), hydrogenation of double bonds (Scheme 4d), cracking (Scheme 4e) and hydrocracking of hydrocarbons and coke formation [49].
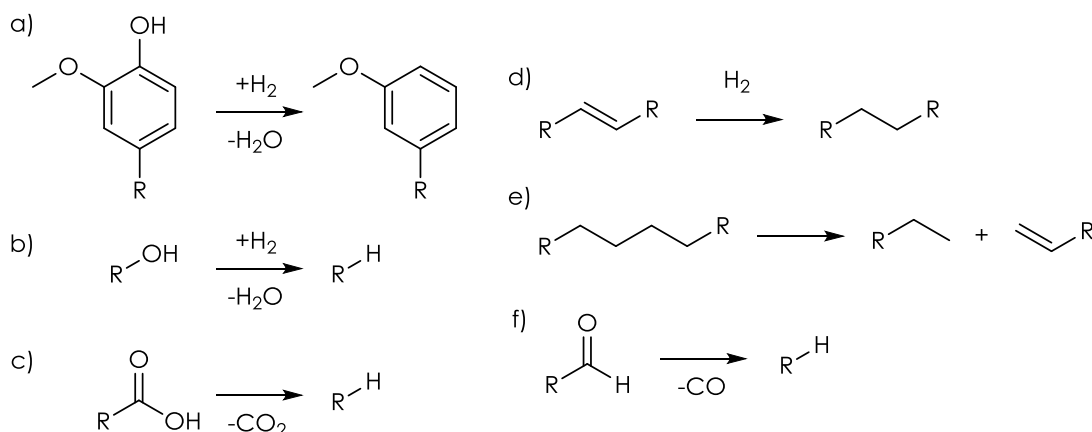
Scheme 4: reactions involved in HDO and hydrocracking of bio oil; a) HDO of phenolics, b) HDO of alcohols, c) decarboxylation of carboxylic acids, d) hydrogenation of double bonds, e) cracking, f) decarbonylation of aldehydes.

Cracking reactions can be considered side-reactions during HDO while are predominant during hydrocracking. In respect to the upgrading strategies of solvent addition and emulsionation these two solutions afford several advantages:

1. The oxygen content is reduced, new C-H bond are formed, and water content is increased because it is the side product of hydrogenation. The resulting refined bio oil possess a lower viscosity and higher calorific power and its hydrophilic character is so reduced that some authors [46] reported the segregation of an organic phase which separates on top of an aqueous phase. The lighter phase is considerably less rich in oxygen in respect to the staring bio oil, while water and oxygenated compounds concentrates in the aqueous phase.

2. Sulfur and nitrogen are hydrogenated to H_2S and NH_3 respectively and are removed from the organic phase by dissolution in the aqueous phase.

3. Acidity is reduced due to the occurrence of decarboxylation and decarbonylation of acids and aldehydes respectively. These reactions contribute to reduce the overall oxygen content.

On the other hand, both HDO and hydrocracking suffer from at least two main drawbacks:

1. Cracking and HDO of light oxygenated molecules lead to the formation of permanent gases, resulting in a significant waste of renewable carbon.

2. H_2 consumption is massive, and its cost represent the main hurdle to HDO process scale up, as opposed to HDS for desulfurization of conventional oil, where the sulfur content is much lower.

In general, HDO process is too hydrogen-demanding and do not valorize the lighter oxygenated compounds which constitutes the major components of bio oil. For these reasons, in recent years a new promising upgrading strategy has been proposed. It plans to valorize the light oxygenated compounds in the bio oil (acids, aldehydes, ketones and alcohols) creating new C-C bonds and reducing the oxygen content and the acidity without the aid of expensive H_2. These results can be achieved by means of catalytically controlled reactions such as dehydration, aldol condensation, and ketonization, and would

allow exploiting the HDO process as the last step of the bio oil upgrading chain, reducing the H_2 consumption and the production of permanent gases.

4.1.3.2 Catalysis for oxygen removal: aldol condensation

The catalytic coupling of small oxygenates can be performed either in the gas-phase, after aerosols removal by cyclonic and hot filtration and prior to bio oil condensation, or in the liquid phase after bio oil condensation and thermal quench. The gas phase catalytic upgrading of bio oil will require robust catalyst to avoid deactivation/poisoning due to the residual char and inorganic salts suspended in the gas feed in the form of aerosols. Microfiltration of liquid bio oil would ensure a more efficient removal of particles with dimensions < 10 μm, but the re-vaporization of bio oil would be energy demanding and could lead to decomposition of reactive molecules. Therefore, both gas phase and liquid phase catalytic upgrade of bio oils are currently under investigation. Aldehydes are highly reactive and toxic molecules and one of the main responsible for bio oil instability. The homo-aldol condensation between aldehydes reduces the oxygen content by 50 % in respect to the starting material and retain 100 % of the precious renewable carbon. Moreover, the spectrum of obtainable products is not limited at the dimer, but also trimers and oligomers may be obtained, which makes aldol condensation the most powerful tool to build longer carbon chains up too gasoline and diesel level. The coupling of aldehydes by means of aldol condensation [50] is depicted in Scheme 5:
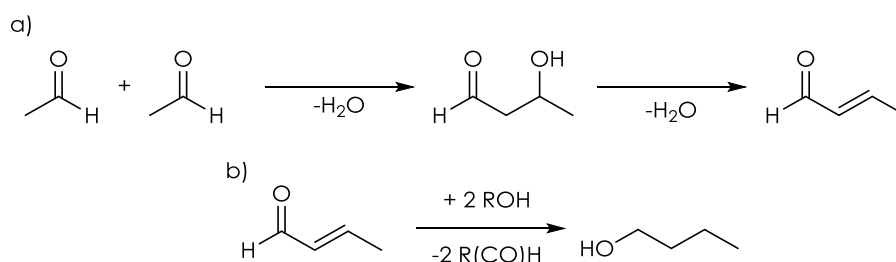
Scheme 5: homo-aldol condensation of a) acetaldehyde, b) H-transfer hydrogenation of α,β-unsaturated aldehyde to BuOH.

In the presence of a suitable catalyst, primary alcohols with three or more carbon atoms (e.g. propanol (PrOH) and 1-butanol (BuOH)) can react to produce branched alcohols of higher molecular weight. This reaction is known as Guerbet reaction [51] and is heterogeneously catalyzed by cheap materials such as MgO, Mg/Al/O mixed oxides, hydrotalcites and hydroxyapatites [52]. Its mechanism involves 1) the dehydrogenation of the alcohols to the respective aldehydes, 2) aldehydes coupling by means of aldol condensation and 3) H-transfer hydrogenation of the resulting dimer with the alcohol acting as H-donor. The reaction is nowadays under intensive investigation in order to valorize bio-EtOH to higher alcohols, particularly BuOH. This is the only case in which the Guerbet reaction leads also to the formation of a linear alcohol. Aldol condensation is catalyzed by both acidic and basic catalysts and require the presence in the reactant of at least one α-hydrogen; α-hydrogens are the hydrogens bonded to the carbon atom in the α position relative to a carbonyl group. This hydrogen displays relatively higher acidity in comparison to other alkyl hydrogens. For instance, while the pKa values for alkyl C-H bond dissociation is about 40-50, those for the α-hydrogen atoms are usually in the range of 19-20 [53]. The acid and base catalyzed mechanism of aldol condensation for acetaldehyde is depicted in Scheme 6.
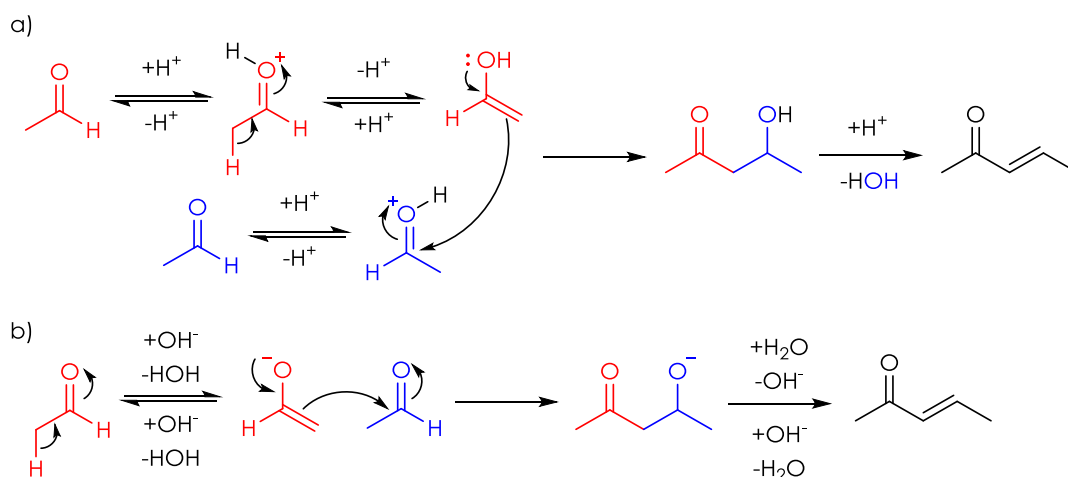
Scheme 6: a) acid catalyzed and b) base catalyzed mechanisms of aldol condensation in aqueous medium.

Once the dehydrated dimer is formed, another aldol condensation or Michael addition reactions may occur too [50], leading to the formation of molecules that retain all the carbon, as depicted in Scheme 7a and 7b. Both aldol condensation and Michael addition can occur between the same aldehyde or between different aldehydes (cross-aldol condensation and cross-Michael addition). It is worth noticing that when fuels synthesis is concerned, a high selectivity toward a certain product is not required: indeed, a high selectivity toward a certain class or group of product is instead desired, e.g. molecules with long carbon chains, low oxygen content, low aldehydes and acidic functionalities and high concentration of branching.
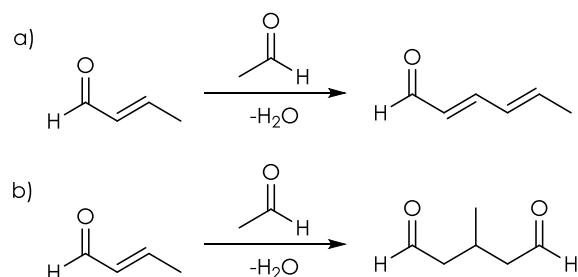
Scheme 7: a) acetaldehyde dimer aldol condensation with acetaldehyde; b) Michael addition of acetaldehyde to acetaldehyde dimer.

Therefore, the well-known low selectivity of aldolic reaction towards a single specific product is not an issue until bio oil upgrading is aimed at fuel production. Ketones can be coupled too by aldol condensation with other ketones: this reaction has the advantage to produce more branched chains in respect to the coupling of aldehydes, which leads to fuels with high energy density; moreover, cyclization of trimers may occur producing cyclic molecules (Scheme 8), which further enhances the octane number [50]:
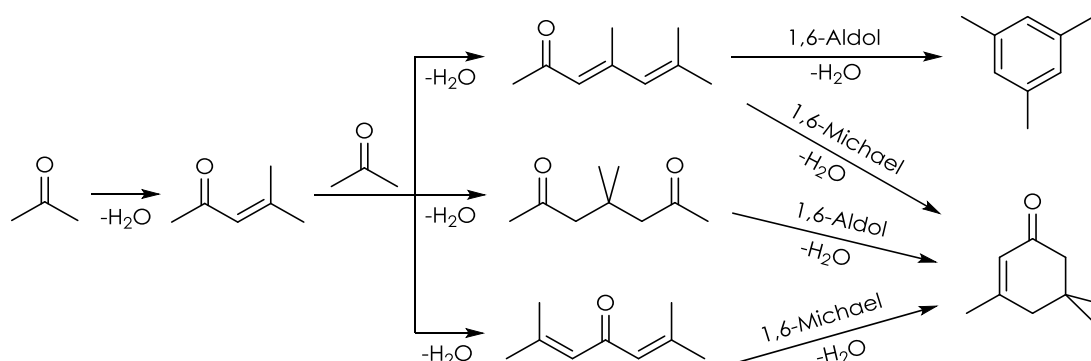
Scheme 8: homo-aldol condensation of acetone.

Carboxylic acids ketonization

The usefulness of aldol condensation is not limited to the coupling of small oxygenated molecules because aldol-type reactions may also occur between furfural-like compounds and ketones [54] or aldehydes: in this case, since furfural do not possess the α-hydrogen required by the aldolic reaction, it must be provided by a ketone or an aldehyde (Scheme 9).
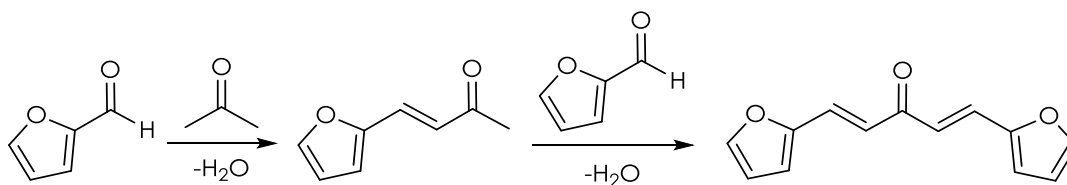
Scheme 9: aldol condensation between furfural and acetone.

Finally, aldehydes may also participate with phenolics deriving from lignin and furanics deriving from cellulose and hemicellulose to electrophilic aromatic substitutions (hydroxy-methylation/dehydration) [55, 56] (Scheme 10):
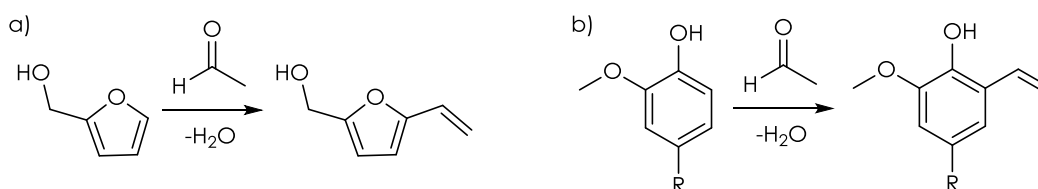
Scheme 10: hydroxy-methylation/dehydration of a) furanics; b) phenolics.

4.1.3.3 Catalysis for oxygen removal: ketonization

Carboxylic acids and esters contain the larger amount of oxygen among the light molecules found in bio oils. Carboxylic acids are also one of the major contributors to undesired features of bio oil such as high viscosity, presence of dissolved inorganic cations with carboxylate anions as counter ions and acidity: the latter feature lead to corrosion and aging of the bio oil due to esters hydrolysis. Two carboxylic acids can be coupled through the reaction of ketonization [53], which produces a ketone and reduces the oxygen content thanks to the evolution of water and CO_2 as co products, as depicted in Scheme 11:
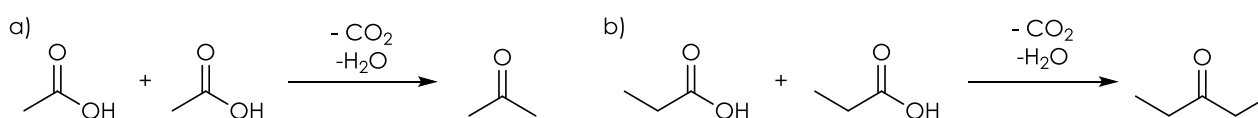
Scheme 11: homo- ketonization: a) acetic acid to acetone; b) propionic acid to 3-pentanone.

Ketonization completely removes the acidity from bio oil creating new C-C bonds; the oxygen content in the final products is always reduced by 75 % in respect to reactants, while the carbon retained in the products depends on the length of the carbon chain in the starting acid, and is 75 % and 83 % for AA and propionic acid (PA) respectively. This reaction is one of the most powerful tools to reduce simultaneously both the oxygen content and the acidity in the bio oil. Cross ketonization between acids with different chain length may also occurs. In conclusion, aldolic reactions, ketonization and electrophilic aromatic substitutions represent a powerful tool to reduce the oxygen content, create new C-C bonds, remove reactive or acidic functionalities and increase the branching of the components of bio oil prior to further upgrading by means of HDO (Scheme 12).
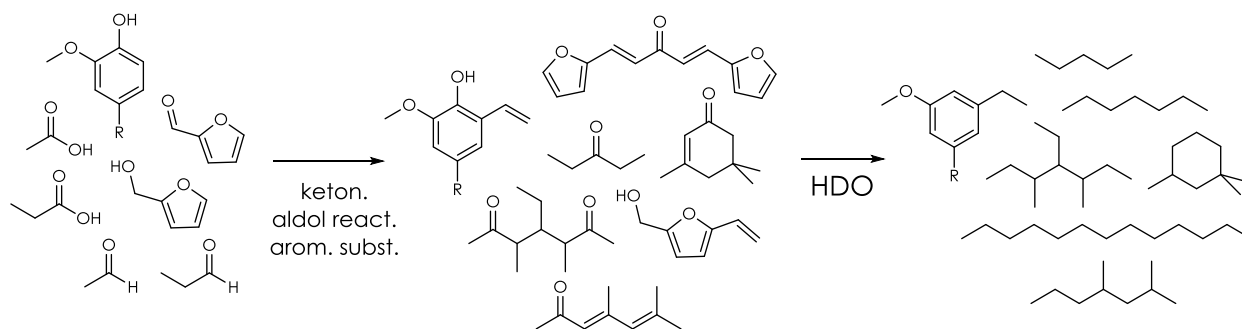
Scheme 12: overall bio oil upgrading.

Since ketonization eventually produces the greenhouse gas CO_2, it may be argued that its use for bio oils upgrading may not be sustainable. Such objection loses its significance considering that this reaction is meant to upgrade a renewable feedstock, therefore the net emission related to the ketonization itself (without considering the energy inputs of the process, which may derive from fossil energy) will be near to zero. Moreover, ketonization for bio oil upgrading is meant to produce a biofuel, which would eventually be burned in an engine producing CO_2 (with near-to-zero net emission). Finally, another aim of the development of an upgrading process for bio oils based on ketonization is a significative reduction of H_2 consumption during the final hydrodeoxygenation (HDO) process: in fact, such process requires large amounts of H_2 and at present days it is economically viable only using cheap H_2 from fossil resources.

4.1.4 Ketonization

4.1.4.1 Bulk ketonization

The first examples of ketonization was reported in 1858 by the French chemist Charles Friedel, which synthesized acetone via distillative pyrolysis of calcium acetate [57], and until World War I this reaction was the premier commercial method for its production [58]. In 1856 however, two year before Friedel, the Italian chemist Raffaele Piria reported the reaction between calcium acetate and calcium formate to produce acetic aldehyde [59].
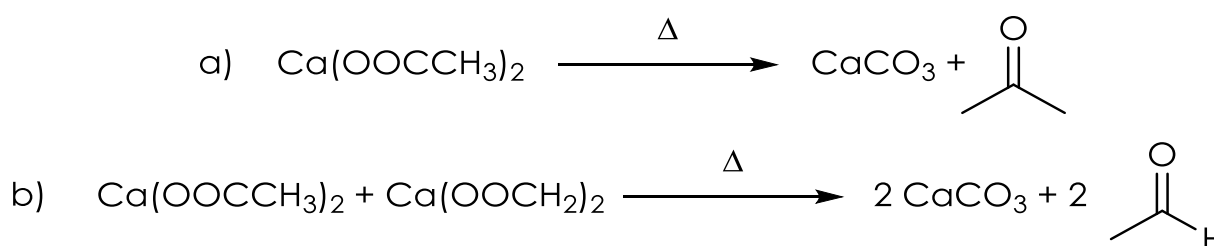
Scheme 13: a) Friedel synthesis of acetone (1858); b) Piria synthesis of acetaldehyde (1856).

When a monocarboxylic acid reacts with itself, the reaction is called homo-ketonization and produces a symmetric ketone (this reaction is depicted in Scheme 11, Chapter 4.1.3.3). On the other hand, when two or more different mono-carboxylic acids reacts between each other, both homo-ketonization and cross-ketonization may occur, leading to a reaction mixture containing both symmetric and asymmetric ketones (Scheme 14a). Finally, when dicarboxylic acids possessing a carbon chain long enough (e.g. 4, 5 or more carbon atoms between the two carboxylic functionalities), undergo ketonization, the product is a cyclic ketone [60] (Scheme 14b).

Carboxylic acids ketonization
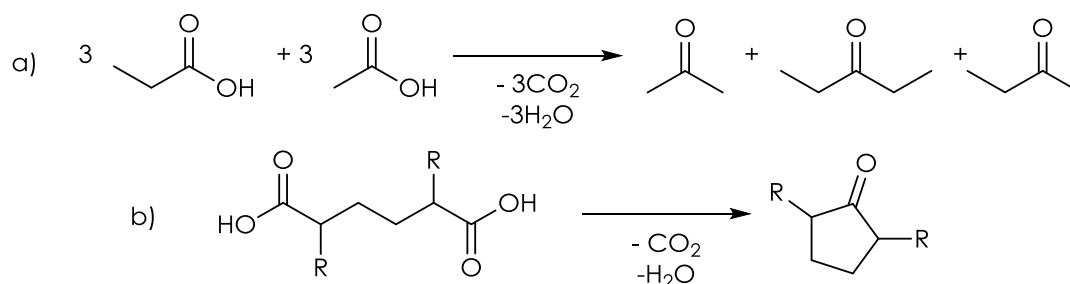
Scheme 14: a) cross-ketonization of PA and AA; b) ketonization of a generic dicarboxylic acid with 4 carbon atoms between the carboxylic functionalities.

Two entirely different mechanisms can lead to the formation of ketones from carboxylic acids. Oxides with low lattice energies or very high basicity, namely alkali, alkali earth [61] and rare earth oxides [62] (e.g. Bi_2O_3, MgO, CaO, BaO, SrO, CdO, La_2O_3, Pr_6O_{11} and Nd_2O_3) interact strongly with carboxylic acids forming bulk carboxylate salts, which decompose upon thermal treatment producing ketones, water and CO_2. In the case of alkali oxides, the reaction is bimolecular and occur in the liquid phase, where the mobility of reacting species is higher. Scheme 15 depicts the so called "bulk ketonization" of such kind of oxides. The tree reaction steps of 1) carboxylate salt formation from carboxylic acid and metal oxide, 2) decomposition of the carboxylate salt into metal carbonate or oxycarbonate and ketone and 3) decarboxylation of the carbonate or oxycarbonate to regenerate the oxide, has been found to require different temperatures. Pestman et al [63] investigated the catalytic behavior of Bi_2O_3, PbO, MgO and ZnO in respect to a mixture of H_2 and AA in a continuous-flow system varying reaction temperature from room temperature to 450 °C (heating rate = 7 °C/min). A drop in the concentration of AA in the outgoing flow below 200 °C was clear, but the only product desorbing at this temperature was water; moreover, when the reaction was carried out below 200 °C at constant temperature, the only product was water and a metal acetate. CO_2 and acetone appeared raising temperature up to 250-300 °C, leaving behind a metal carbonate.
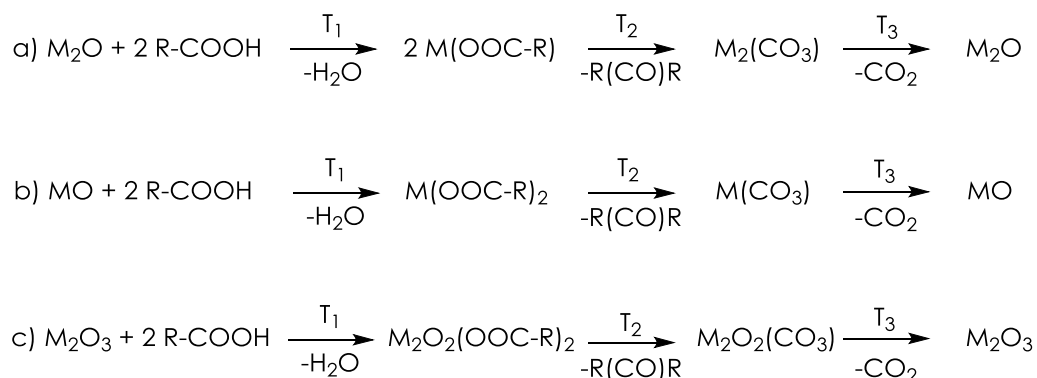
Scheme 15: bulk ketonization mechanism for a) alkali oxides; b) alkali earth oxides; c) rare earth oxides.

Hites et al [64] investigated the thermal decomposition of Calcium decanoate salts (Scheme 16) and proposed a radical-like mechanism involving the formation of an alkyl and an acyl radical fragment:
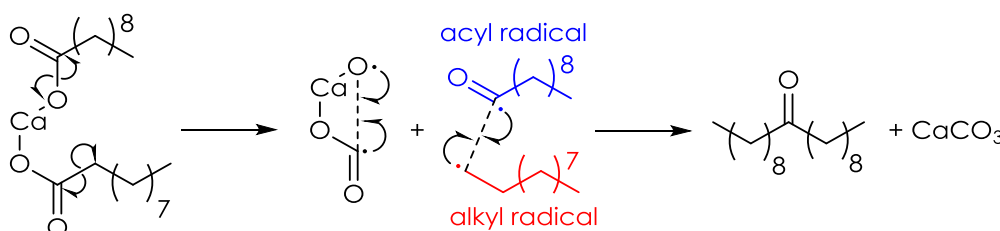
Scheme 16: radical-like mechanism of the bulk ketonization of Calcium decanoate.

Sakata et al [65] proposed the same mechanism to explain the formation of diphenylketone when they fed benzoic acid (BA) and H_2 over MgO in the attempt to produce benzaldehyde. In spite of their efforts, these authors obtained a 65 % selectivity in diphenylketone; moreover, they were also able to observe the liquefaction of the catalyst above the melting temperature of magnesium benzoate, further demonstrating the formation of a bulk carboxylate salt as the first step of the reaction.

4.1.4.2 Surface Ketonization

4.1.4.2.1 α-hydrogen abstraction from carboxylates

Not all ketonization catalysts reacts with carboxylic acids to produce bulk carboxylates: over oxides with high lattice energies such as TiO_2 [66], CeO_2 [67], ZrO_2 [68], Al_2O_3 and Mn_3O_4, the reaction proceeds via a completely different pathway, which is confined to the catalyst surface. As an example, when Pestman at al [63] submitted Al_2O_3 and Mn_3O_4 to the variable temperature experiment mentioned in Chapter 4.1.4.1, they found that the drop in AA concentration was contemporary to water, acetone and CO_2 desorption; moreover, no change in catalysts chemical composition was detectable after reaction. Besides the bulk reaction between the acid and the catalysts, another major difference exists between bulk and surface ketonization. In fact, when the reaction is confined on catalyst surface, not all carboxylic acids undergo ketonization: several authors [60] pointed out the fact that only carboxylic acids possessing at least one acidic α-hydrogen can undergo homo-ketonization. As explained in Chapter 4.1.3.2, α-hydrogens are the hydrogens bonded to the carbon atom in the α position relative to a carbonyl group. Pivalic acid (trimethylacetic acid, TMAA) [63] and BA have been found to be completely unreactive over these catalysts where ketonization is confined to the surface. These acids [67, 69], however, participate to cross-ketonization with carboxylic acids possessing α-hydrogens such as PA; therefore, it is mandatory that *at least one of the two reacting acid* possesses acidic α-hydrogens for surface ketonization to occur (Scheme 17).
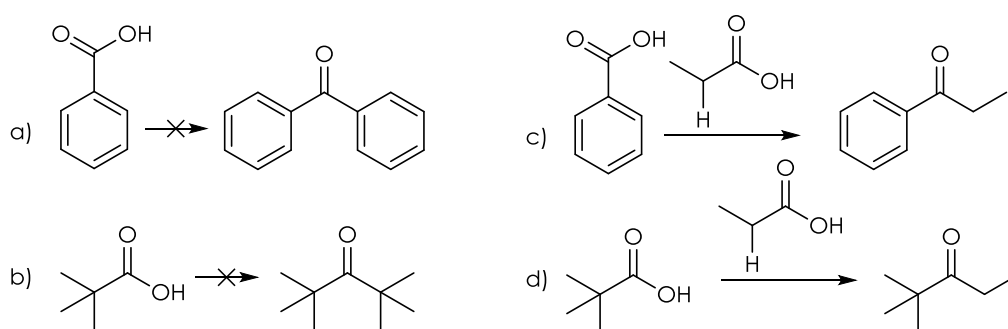
Scheme 17: role of α-hydrogen in surface ketonization: a)homo-ketonization of BA; b) homo-ketonization of TMAA; c) cross ketonization of benzoic and PA; d) cross-ketonization of TMAA and PA.

Surface ketonization reaction rate over the same catalyst has been demonstrated to be dependent on the number of acidic α-protons [68] (acetic > propionic > isobutyric > pivalic) and the number of substituents on the β-carbon [67, 70] (acetic > propanoic > butyric > 3-methyl butyric > 3,3-dimethyl butyric), as depicted in the Figure 20. The crucial role of α-hydrogens was corroborated by means of isotopic labelling experiments [63, 71, 72]: when non deuterated AA was fed over deuterated catalysts surfaces, deuterium was found bonded to a significant fraction of the α-carbons of both the resulting acetone and unreacted AA. When acetone was fed directly over these surfaces, instead, no α–H/α–D exchange between the reactant and the catalyst surface was detected. The nature of the species resulting from this α-hydrogen abstraction is still object of debate. Of course, α-

Carboxylic acids ketonization

hydrogens are not the most acidic protons in carboxylic acids, which readily dissociates on oxides surfaces forming carboxylate ions and surface hydroxy groups; this interaction can be seen as the abstraction of the carboxylic proton from a lattice oxygen.
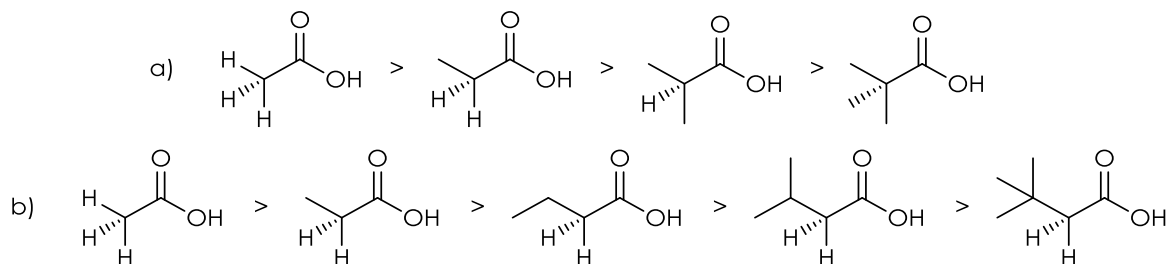
Figure 20: ketonization reaction rate grows with a) the number of acidic α-protons and decrease with b) the steric hindrance of the substituent in the α-carbon in acids with the same number of α-protons.

Several mode of adsorption of such carboxylate ions are possible [53] (monodentate, bridging bidentate and chelating bidentate) depending on both the acid and the catalyst features (e.g. acid and M-O bond length, metal cation radius and coordination number, metal oxide polymorph, metal oxide reticular plane and presence of defects). The higher acidity of carboxylic protons implies that the α-protons abstraction must occur from carboxylate species that are already negatively charged. Ignatchenko [73] calculated the energy barrier for α-hydrogen abstraction from the carboxylates anions resulting from acetic, propionic and isobutyric acid (IBA) on the (111) plane of monoclinic ZrO_2, using periodic DFT calculations. It was found that the α-hydrogen is easily abstracted and that the energy barrier to produce the dianion species appears to be 120-159 kJ/mol depending on acid branching. In another theoretical DFT study over the same catalyst [74], the reaction pathway involving a α-hydrogen abstraction step was compared to a concerted mechanism that does not involve α-hydrogen abstraction. The calculations indicated that the former mechanism is kinetically favorable with a much lower activation energy, mainly due to the formation of a reactive nucleophilic center that can easily couple with another adsorbed molecule. Scheme 18 (next page) depicts the three absorption modes of carboxylates in the particular case of PA and all the theoretically possible species resulting from the abstraction of a α-proton from such species (ionic bonds in this particular case are depicted as dotted line and the charge is drawn explicitly). Among the various adsorption modes, the bridging bidentate is considered the most stable [53]. Pei et al [75] investigated AA chemisorption on TiO_2 by means of FT-IR and found that it leads to the formation of acetates in both monodentate and bridging bidentate configuration at room temperature. Upon heating to 100-300 °C, the bands of the less tightly bonded monodentate disappeared leaving only bidentate acetates. In another study [76], it was found that on a TiO_2 single crystal two monodentate carboxylates (acetates and propionates) are chemisorbed on the same metal cation on the (114) plane and react to produce ketones upon heating. On the contrary, on the (011) plane, where metal cations bond only one carboxylate, ketene formation was favored. These results suggest that carboxylates can bound in different ways to oxides surface during ketonization. It is possible that the first species formed is the most stable bridging bidentate that then during the catalytic cycle undergoes a transformation to the less restricted monodentate mode of adsorption, which leads to a lower energy barrier for ketonization. Hasan et al [77] and Stubenrauch et al [78] investigated AA chemisorption on CeO_2 surface by FT-IR and TPD-HREELS respectively and found that it is essentially similar to its adsorption on TiO_2. AA adsorption occurs via the formation of acetate anions and surface hydroxyl groups also over MgO [79], but only with monodentate configuration [80]. Tong et al [81] investigated the interaction between AA and PA with $α-Al_2O_3$ and found that also in this case it occurs via surface the formation of surface carboxylates; DFT calculations by the same authors predicted a bridging bidentate configuration. Young [82], investigating the adsorption of AA, acetyl chloride and acetic
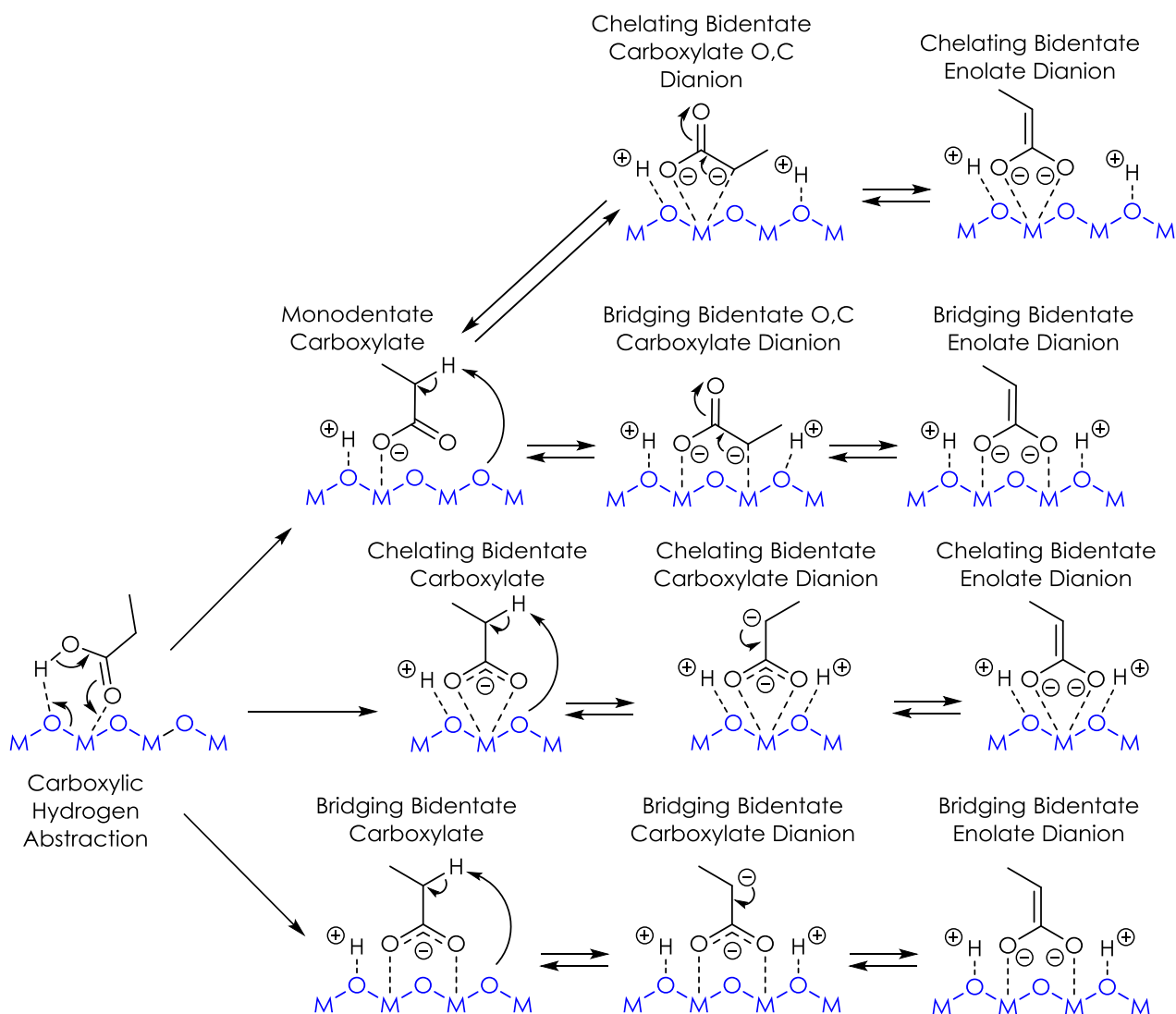
Scheme 18: Carboxylate ions modes of adsorption adapted from [83] and possible species resulting from the abstraction of a α-proton from such carboxylates.
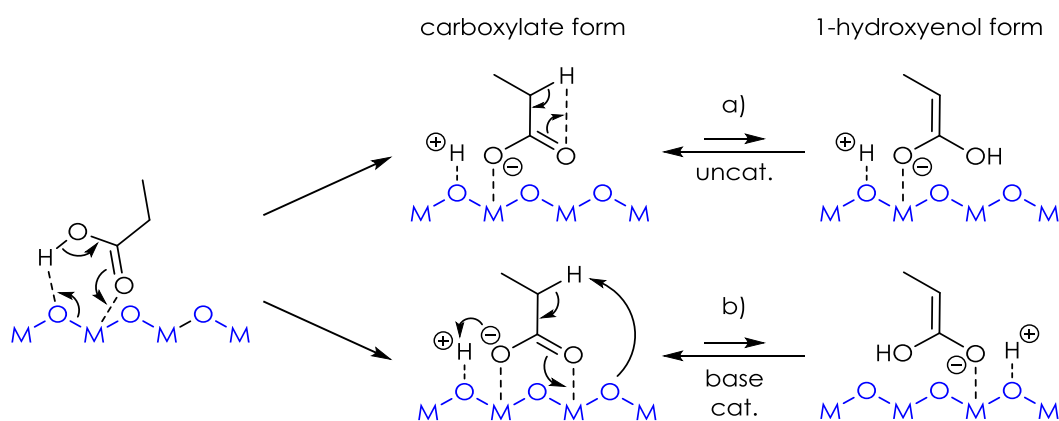
Scheme 19: α-hydrogen participation via 1-hydroxyenol intermediate: a) uncatalyzed mechanism [84]; b) basic catalyzed mechanism.

anhydride over SiO_2 by means of FT-IR, found that bands relative to the acetyl group were present in all case, and concluded that AA chemisorption may occur via condensation with silanol groups followed by evolution of water. To sum up, adsorption of carboxylates occurs in similar ways on different oxides and, upon heating, ketonization occurs only on certain planes, while the others lead to the formation of ketenes. An alternative route, which

do not require the formation of a dianion intermediate, postulates that a keto-enol tautomerization of the chemisorbed carboxylates may occur [84], leading to the formation of 1-hydroxy enolate ion. This route does not require the direct abstraction of the α-hydrogen from a negatively charged carboxylate ion by a basic site and one might expect that, being the enolate species more electronically stable than the dianion, this route is energetically more favorable. It is possible however to imagine a second route for the 1-hydroxyenolate ion formation: in this case, the participation of a basic site in the direct abstraction of the α-proton could help and speed up the interconversion between the carboxylate and 1-hydroxyenol, as depicted in Scheme 19. At the best of our knowledge, however, theoretical calculations comparing these three routes (dianion intermediate (1), uncatalyzed (2) and base catalyzed (3) keto-enol tautomerism of adsorbed carboxylates) have not been attempted yet.

4.1.4.2.2 Coupling mechanisms

Several surface mechanisms have been proposed to explain role of α-hydrogen. Gonzales et al [72], investigated the ketonization of AA combined with FT-IR analysis over TiO_2 and proposed that a carboxylate anion could dehydrate to produce a surface ketene, which then reacts with another carboxylate anion leading to CO_2 and a ketone. They arrived to this conclusion on the basis of some similarities between the bands of species adsorbed on TiO_2 and those of vapor phase ketene (3005 and 1730 cm^{-1}) and by means of isotopic labelling experiments with deuterium, which clearly showed the exchange of the α-hydrogens of AA. The most solid argument in favor of this mechanism is the fact that the formation of ketene requires the presence, in one of the reacting acids, of at least one α-hydrogen. Moreover, the formation of the ketene by dehydration explains the formation of water and the coupling of the ketene with the alkyl fragment another carboxylate result in the evolution of CO_2.
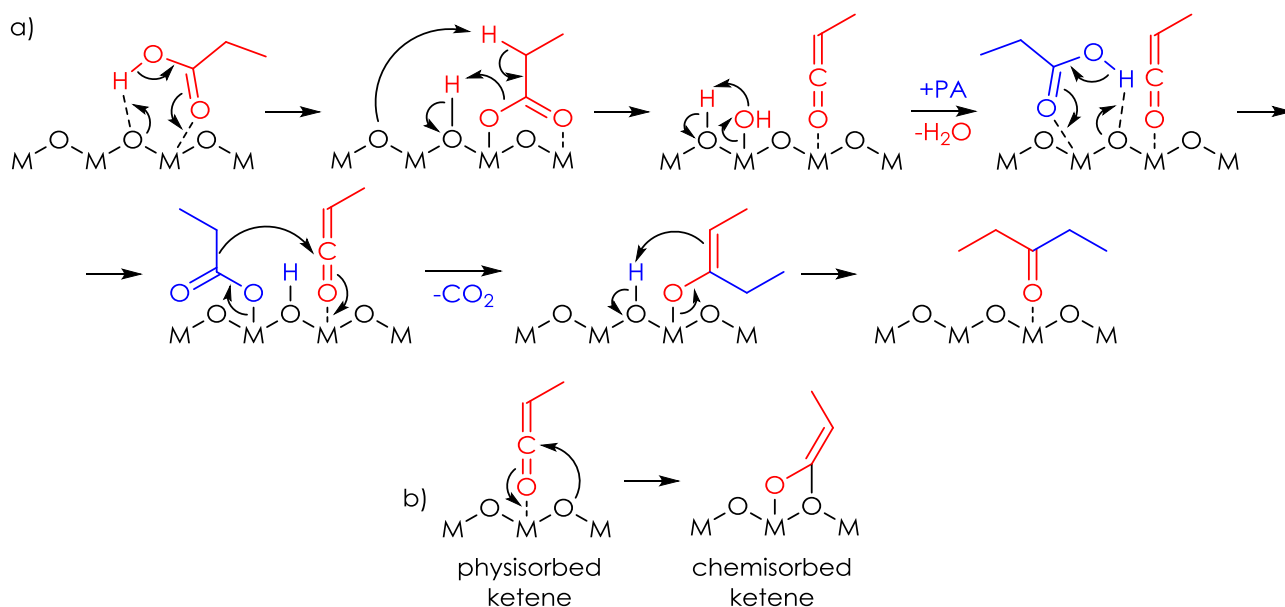
Scheme 20: a) possible surface mechanism of PA surface ketonization via ketene. This mechanism postulates that the carbonyl carbon atom of the resulting ketone derives from the acid that lost its α-hydrogen and dehydrated to ketene, while CO_2 derives from the acid that did not lose its α-hydrogen. b) Physisorbed and chemisorbed ketenes.

Hendren et al [85] arrived at the same conclusion investigating the coupling between AA and cyclopropane carboxylic acid (CCA) over CeO_2 by means of isotopic labelling experiments. They found that CCA do not exchange α-hydrogens and that when CH_3^{13}COOH was coupled with CCA most of the carbonyl carbon in the resulting ketone

derived from CCA. However, the latter result is in contrast with the mechanism via ketene, which postulates that the carbonyl carbon atom in the resulting ketone must derive from the acid that exchange α-protons and dehydrates to produce the ketene. Scheme 20a attempts to depict a possible surface mechanism for surface ketonization via ketene on a generic metal oxide. In this Scheme: 1) solid lines represents chemical bonds (both ionic and covalent) and dotted lines represents weaker electrostatic interactions. 2) To simplify drawings, chemisorbed carboxylates ions are always depicted in monodentate conformation, but, depending on the catalyst, this could not be the exact mode of adsorption. 3) The dehydration of the carboxylate ion (in red in the drawing) to produce the ketene is depicted as a concerted mechanism, but the exact mechanism could involve a 1-hydroxyenol or a dianion intermediate and depending on the catalyst also these intermediates could not be chemisorbed in monodentate configuration. Finally, the drawing shows a physisorbed ketene, but, most likely, it would be chemisorbed as an enolate anion, formed when a lattice oxygen attacks the carbonyl carbon of the physisorbed ketene (Scheme 20b). Several authors provided convincing evidence that seems to demonstrate that the ketene may be a parallel side product rather than being the intermediate. The strongest argument was offered by Pestman et al [63], which investigated the cross-ketonization of AA and TMAA over TiO_2 using labeled $CH_3{}^{13}COOH$ and unlabeled TMMA. TMMA do not possess α-hydrogens and cannot form a ketene, therefore the ketene must form from AA and if the ketene mechanism is actually preferred, all the resulting 2,2-dimethyl-3-butanone (pinacoline) should contain ^{13}C-labeled carbonyls, while all the CO_2 should be unlabeled. Their results clearly showed that the outcome was exactly the opposite, therefore the ketene could be formed and be in equilibrium with other adsorbed species, but it is unlikely to be the intermediate for surface ketonization. Martinez et al [86] investigated the ketonization of AA over TiO_2 supported on a SiO_2 monolith at low contact time to preserve the highly reactive ketene. If a ketene was the intermediate in AA ketonization, a decrease in its selectivity should be expected at higher AA conversion, together with a contemporary growth in acetone selectivity. However, they found that the selectivity in acetone and ketene did not change significantly raising AA conversion from 3 to 100 %. Their results demonstrated that both ketenes and ketones are formed over TiO_2 by parallel, rather than consecutive reactions, and that ketene is likely to be formed when acetate species are isolated from each other. If ketene is not the intermediate in carboxylic acid ketonization, the abstraction of an α-hydrogen must result in a different species capable to condense with a carboxylate ion releasing water; moreover, this coupling must result in the formation of an intermediate capable to decompose producing a ketone and CO_2. β-keto acids (3-oxocarboxylic acids) fulfill these requirements. The decarboxylation of β-keto acids occurs easily upon mild thermal treatment and involves the redistribution of six electrons in a six-membered cyclic transition state to produce CO_2 and an enol that rapidly tautomerize into the corresponding ketone. Several studies supported the path involving a β-keto acid as the intermediate in ketonization, even though this intermediate has never been detected: its rapid decomposition makes its detection practically impossible. Scheme 21 (next page) attempts to depict the surface mechanism via β-keto-acid on a generic metal oxide, under the assumption that the abstraction of the α-protons is catalyzed by a basic site and results in the formation of the 1-hydroxy enolate intermediate (instead of a dianion); of course this could not be the preferred pathway over some catalysts. As mentioned in the previous Chapter, Pulido et al [74] in their computational work over ZrO_2 found that the β-keto acid pathway is energetically favored in respect to the concerted mechanism that do not involve the abstraction of the α-hydrogen and the formation of the β-keto acid. However, it is worth noticing that in the mechanism proposed by these authors the two reacting species which forms the β-keto acid are an enolate dianion and an acylium ion. Even though acylium species have been detected over zeolites, on reducible

Carboxylic acids ketonization

oxides, it is hard to differentiate between acyl and a carboxylate since an acyl can be converted to a carboxylate by nucleophilic addition of lattice oxygen [53] (Scheme 22).
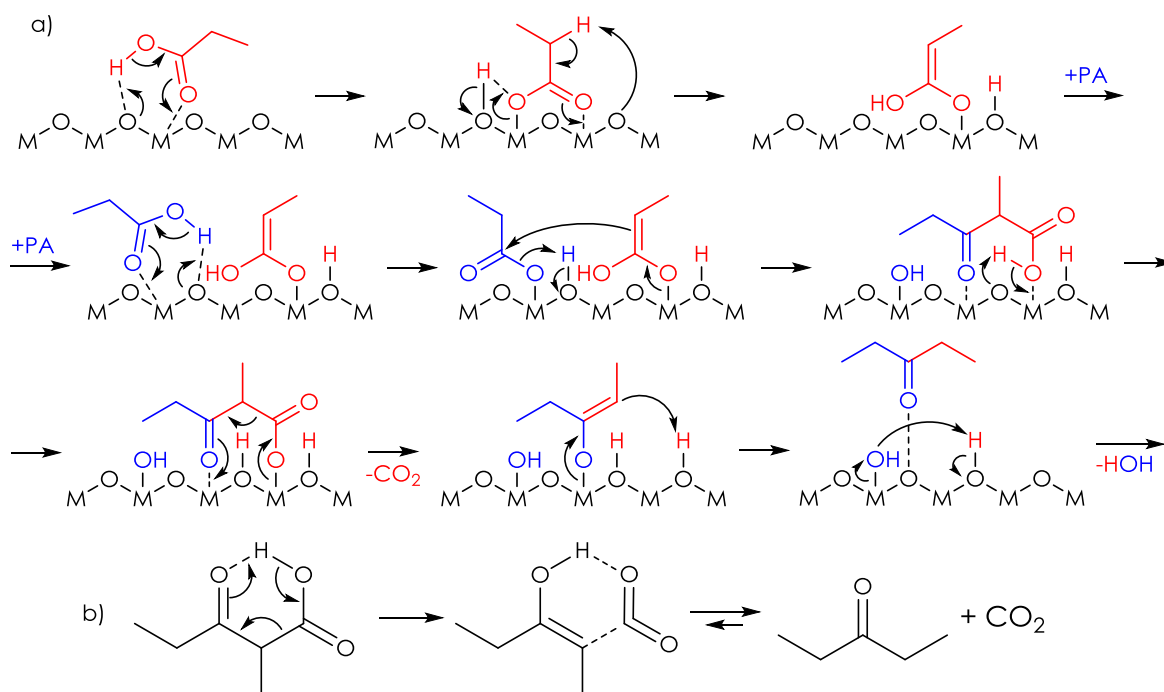
Scheme 21: a) possible surface mechanism of PA surface ketonization via β-keto acid. This mechanism postulates that the carbonyl carbon atom of the resulting ketone derives from the acid that did not lose its α-hydrogen, while CO_2 derives from the acid that lost its α-hydrogen. b) Uncatalyzed thermal decomposition of β-keto acid via redistribution of six electrons in a six-membered cyclic transition state.
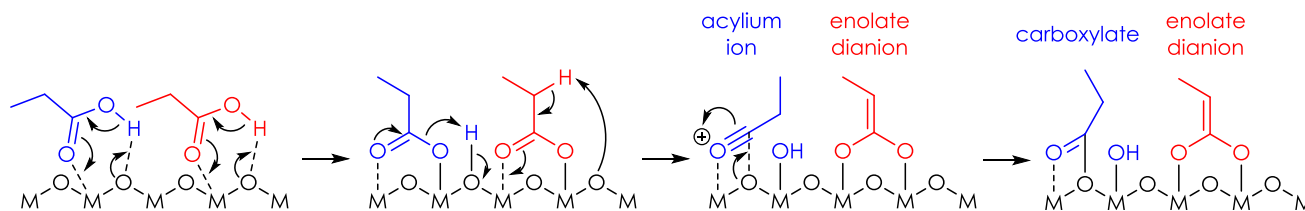
Scheme 22: formation of an acylium ion and an enolate dianion as proposed in [74], followed by conversion of the acylium ion into a carboxylate via nucleophilic addition of lattice oxygen.

Two other entirely different mechanism have been proposed; the former involves the formation of an anhydride as the reaction intermediate [53].
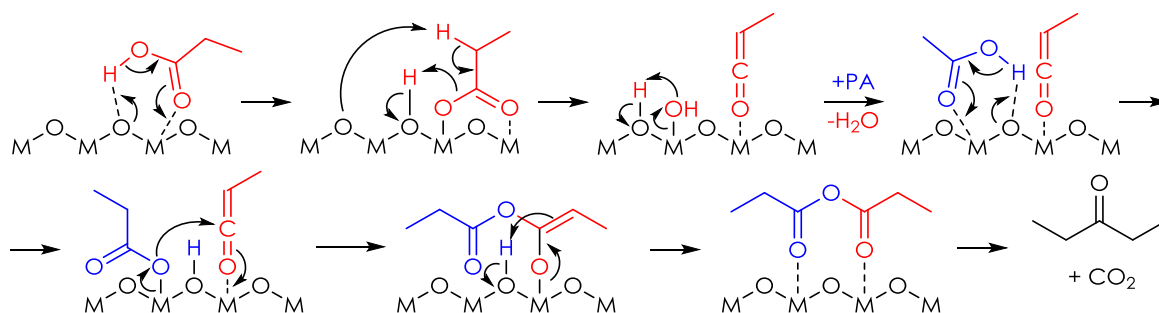
Scheme 23: surface ketonization of PA via propionic anhydride.

An anhydride is formed when a carboxylate anion couples with ketene without decarboxylation: in other word, is one of the oxygens of the carboxylate anion that attack the electrophilic center of the ketene, as depicted in Scheme 23. However, it is unclear how a ketone might form by decarboxylation of the anhydride and why such intermediate

45

should not be hydrolyzed back to the acid reacting with the water produced by carboxylates dehydration to ketenes. The latter mechanism was proposed by Pestman et al [63] while studying the ketonization of AA. It postulates that the real intermediate is a dianion that interacts with catalyst surface with a negatively charged α-carbon and a bidentate carboxylate group. Such intermediate adsorbs parallel to catalyst surface and is in equilibrium with ketene; the cleavage of the C-C bond between the carboxylic carbon and the α-carbon result in the formation of a reactive methylene species (in the case of AA) which then reacts with another chemisorbed carboxylate, as depicted in Scheme 24:
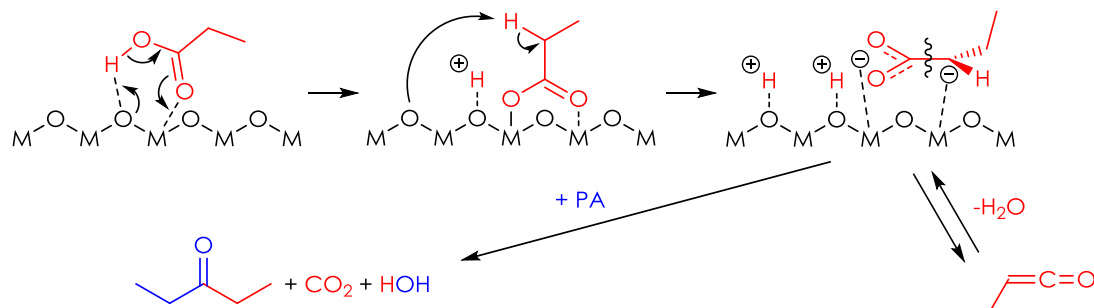
Scheme 24: surface ketonization of PA via a dianion chemisorbed in parallel to catalyst surface; adapted from the one proposed by Pestman et al [63] for AA.

A valid argument against this mechanism was proposed by Nagashima et al [67]. They argue that the water in the reaction environment should be able to react with such methylene (or alkylene) species, forming MeOH (or other alcohols) in significant amounts.

4.1.4.2.3 Activity, acid-base and redox properties

Basic, acidic and amphoteric oxide catalysts have been thoroughly investigated for ketonization, with different carboxylic acids and under various reaction conditions. Glinsky et al [87] studied PA ketonization over oxides of 27 elements (Ag, Bi, Cd, Cu, In, Pb, Re, Si, Cr, Mg, Zn, Ca, Ga, Sr, Ba, Al, Eu, Nd, V, Co, Fe, La, Mn, Zr, Ce, Th and U) supported on SiO_2, Al_2O_3 and TiO_2. They found that most MOs catalyze ketonization, but the five most active oxides are those displaying the strongest amphoteric character (U > Th > Ce > Zr > Mn). No synergistic effects were noted for supported catalyst. The change in activity with different supports depends on the contribution to ketonization of the support itself: results showed that SiO_2 is barely active (X PA < 10 %), while Al_2O_3 and TiO_2 are fairly active (X PA = 50 and 40 % respectively).

catalyst	X PA (SiO_2)	X PA (Al_2O_3)
U	> 95	> 95
Th	> 95	> 95
Ce	> 90	> 95
Zr	> 80	> 95
Mn	> 60	> 95
La	> 55	> 95

Table 1: activity of supported catalyst; PA/N_2 feed composition [mol %] = 10/90; residence time t = 0.32 s; T = 450 °C.

Even though all ketonization mechanisms proposed in the literature in principle require only the abstraction of a α-proton by a surface basic site, Glinsky et al found that strong basic oxides possessing negligible Lewis acidity such as MgO, CaO and SrO are less active than amphoteric oxides. On the other hand, a strong Lewis acid such as Al_2O_3, which possess only a very weak basicity, resulted more active for PA ketonization than MgO [87]. These results indicate the occurrence of a synergistic effect between Lewis acid sites and Brønsted

basic sites on amphoteric oxides and that surface M^{n+}-O^{2-} acid-base pairs play a crucial role towards ketonization activity. It is likely that the interaction between the carboxylic oxygens of the acid and the metal cations of amphoteric oxides enhances the acidity of both the carboxylic and the α-hydrogen, allowing an easier abstraction by basic sites of moderate strength. The participation of acid-base pairs in ketonization has been demonstrated by several means. Kuriacose et al [88] investigated the effect of the presence of AA on the dehydration and dehydrogenation of selected alcohols over Cr_2O_3. Tert-Butyl alcohol can undergo only dehydration to isobutene on acidic sites, while benzyl alcohol can undergo only dehydrogenation to benzaldehyde on basic sites. They found that AA inhibits both reactions, but when they investigated AA ketonization in the presence of these two alcohols, they found that only benzyl alcohol strongly inhibits ketonization occupying basic sites. These results suggest that both acidic and basic sites are involved in ketonization of AA and evidence the importance of the abstraction of a α-hydrogen by a basic site. The activity towards ketonization do not depend only on the strength of acid-base pairs, but also on the exposure of defective reticular planes and on presence of coordination vacancies: in fact, coordinatively unsaturated metal cations and anionic vacancies strongly bond oxygenate compounds even if the metal cation is weakly acidic [53]. Since CO_2 and acetone have affinity for surface base and acid sites, they act as inhibitors of the ketonization reaction as they compete with acid molecules for the coordination sites. Rajadurai et al [89] demonstrated the inhibiting effect of acetone on AA ketonization over a Zn/Cr/Fe/O mixed oxide. Gaertner et al [90] investigated hexanoic acid ketonization over Ce/Zr/O and reported that CO_2 co-feeding reduced the conversion to a third of the initial value; moreover, conversion did not turn back to the initial value after stopping CO_2 co-feeding. They deduced that an irreversible loss of active sites (oxygen vacancies or coordinatively unsaturated cations) occurred due to the formation of surface carbonates over highly basic CeO_2. This last result clearly indicate that oxygen vacancies play an important role in ketonization activity: Ceria-Zirconia show high activity for ketonization and is well known for its oxygen mobility and redox properties [91], being capable to store oxygen in its lattice in oxygen-rich streams and releasing it in oxygen-poor streams, according to the equation: $CeZrO_2 \rightarrow CeZrO_{2-x} + xO$. Another argument in favor of the role of oxygen vacancies in as active sites for ketonization is the fact that several of the most active catalyst individuated by Glinsky et al [87], namely CeO_2, ZrO_2 and TiO_2, are able to form oxygen vacancies and exposed surface cations with a high degree of unsaturation. As an example, Pham et al [70, 84] demonstrated that a pre-reduced Ru/TiO_2 catalyst is much more active towards ketonization than pure TiO_2. The superior catalytic activity was ascribed to the formation of unsaturated Ti^{3+} and anionic vacancies promoted by the presence of Ru upon reduction with hydrogen, and not to the presence of Ru itself, which do not catalyze ketonization.

4.1.5 Aim of this Chapter

The aim of the work presented in this Chapter was to perform a catalyst screening for the homo-ketonization of PA in order to obtain a better understanding of how surface acidic/basic properties of catalysts influence the reaction outcome, and which catalytic sites (basic, acidic or both) are mandatory for ketonization to occur. Such work is motivated by the scientific and industrial relevance of ketonization as a strategy for bio oil upgrading and by the fact that ketonization is a major side reaction during the MMA synthesis from MP, which will be discussed in Chapter 6. Several catalysts have been investigated:

- $AlPO_4$, Zr/P/O and $LaPO_4$ have been chosen because they are purely acidic in nature and do not possess any basic character.

- γ-Al_2O_3 was chosen due to its amphoteric character strongly shifted toward Lewis acidity.

- ZrO_2 was chosen due to its balanced amphoteric character and because is generally considered one of the best ketonization catalyst.

- La_2O_3 was chosen due to its very strong basic character and because it is considered a good ketonization catalyst too.

- SiO_2 was chosen because it is the only catalyst among the ones investigated which do not possess Lewis acidity nor basicity, but only a weak Brønsted acidity.

Homo-ketonization of AA and cross-ketonization of AA/PA mixtures has also been investigated, over the $AlPO_4$ catalyst.

4.2 Experimental

4.2.1 Catalysts Synthesis and characterization

4.2.1.1 Commercial Catalysts

γ-Al_2O_3 (SASOL Puralox SCFa140, 98 %) and SiO_2 (GRACE 360, 98 %) were commercial reference materials and were calcined prior to use in static air, with a temperature ramp of 5°C/min until 600°C and maintained at this temperature for 3 hours.

4.2.1.2 Metal phosphates

Aluminum, Zirconium and Lanthanum phosphate (respectively $AlPO_4$, Zr/P/O and $LaPO_4$) were synthesized by means of co-precipitation adapting the methods reported in literature. Each metal precursor (99 % $AlCl_3$, 99.9 % $La(NO_3)_3$*$6H_2O$ and 98 % $ZrOCl_2$*$8H_2O$) was dissolved in 300 mL of deionized water in order to obtain a 1 mol/L solution. Then, 300 mL of H_3PO_4 (1 mol/L) were added under continuous stirring to the metal precursor solution and the pH was risen from 1-1.5 to 7.0 adding aqueous NH_4OH (28 % wt) in order to promote metal phosphates (MPOs) precipitation. Precipitates were aged for 3-4 hours under stirring, filtered over a Buchner funnel and washed with 2 L of distilled water to remove adsorbed ions. Finally, the resulting wet solid was dried at 120°C overnight and calcined at 550°C for 3 hours in static air and with heating rate of 5 °C/min.

4.2.1.3 Metal oxides

Zirconium and Lanthanum oxide (ZrO_2 and La_2O_3) were synthesized by means of co-precipitation. Each metal precursor (99.9 % $La(NO_3)_3$*$6H_2O$ and 98 % $ZrOCl_2$*$8H_2O$) was dissolved in deionized water in order to obtain a 0.5 mol/L solution (60 mL for La and 70 mL for Zr) and slowly added dropwise to aqueous NH_4OH (2 mol/L, 300 mL for La and 400 mL for Zr) under vigorous stirring. The pH of the basic solution was maintained constant and equal to 11.5 during the dropwise addition of the acidic cationic solution adding aqueous NH_4OH (28 % wt). Precipitates were aged for 1-2 hours under stirring, filtered over a Buchner funnel and washed with 2 L of distilled water for each 3 g of hydroxide obtained to remove adsorbed ions. Finally, the resulting wet solid was dried at 120°C overnight and calcined at 550°C (Zr) or 750 °C (La) for 3 hours in static air and with heating rate of 5 °C/min.

4.2.1.4 Catalysts Characterization

Catalysts crystal structure was determined by means of XRD of their powders; commercial SiO_2 had been found to be completely amorphous (Figure 21, left side), while commercial Al_2O_3 is a poorly crystalline γ-form, due to the intrinsic defectivity of its spinel structure (Figure 21, right side). Both patterns show broad and weak peaks: in these cases, the contribution of fluorescence at small 2θ angle becomes important. Crystal phases were identified after baseline correction; however, the baseline was not subtracted in order to show the actual XRD spectra.
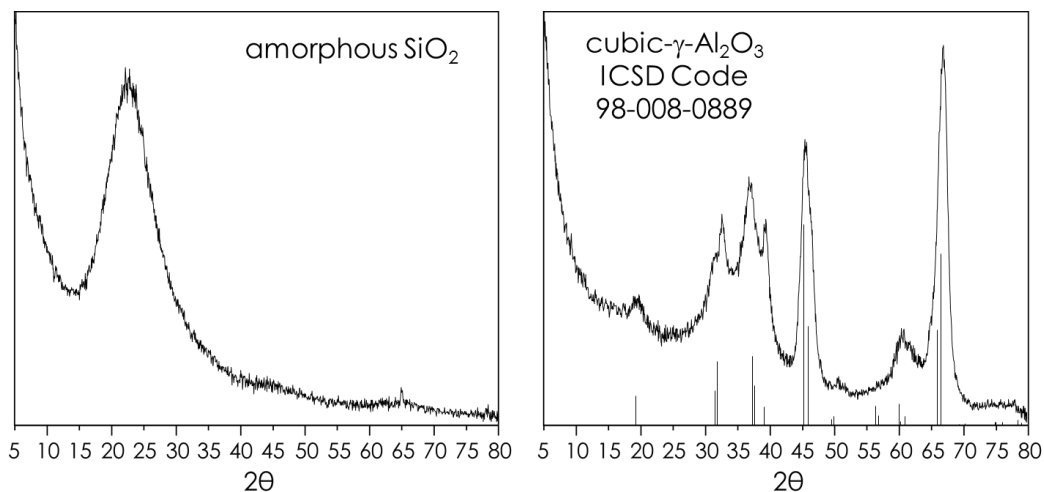
Figure 21: XRD powder patterns of SiO_2 (left side) and γ-Al_2O_3 (right side).

$AlPO_4$ (Figure 22, left side) is amorphous and its XRD pattern is similar to that of SiO_2 due to the similarity between their disordered structures. Amorphous SiO_2 consists of neutral SiO_4 tetrahedra sharing corners with each other, while $AlPO_4$ consist of negatively charged AlO_4 tetrahedra sharing corners with positively charged PO_4 tetrahedra. Being the ionic radii of Al^{3+} and P^{5+} respectively higher and lower than the one of Si^{4+}, the Si-O-Si and the Al-O-P distance in these two materials happens to be very similar. $LaPO_4$ is poorly crystalline and consists in a pure monoclinic monazite phase (Figure 22, right side); it is however the most crystalline material among the three MPOs. Zr/P/O is mainly amorphous (Figure 23).
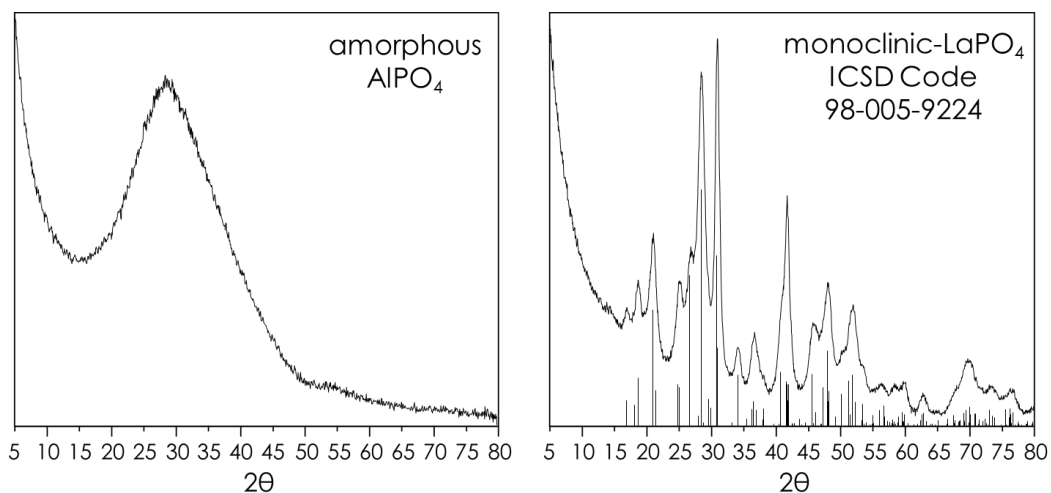
Figure 22: XRD powder patterns of $AlPO_4$ (left side) and $LaPO_4$ (right side).
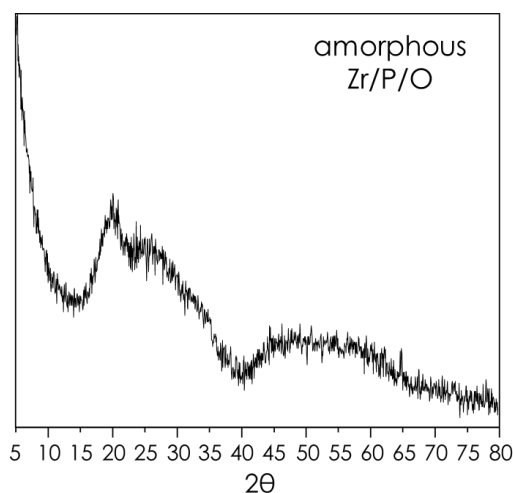
Figure 23: XRD powder pattern of Zr/P/O.

ZrO_2 (Figure 24, left side) possess the typical XRD pattern of the monoclinic phase; La_2O_3 (Figure 24, right side) consists of a pure hexagonal and highly crystalline phase, probably due to the high calcination temperature of 750 °C required to decompose all the lanthanum carbonates formed during the synthesis, due to CO_2 absorption in the basic solution.
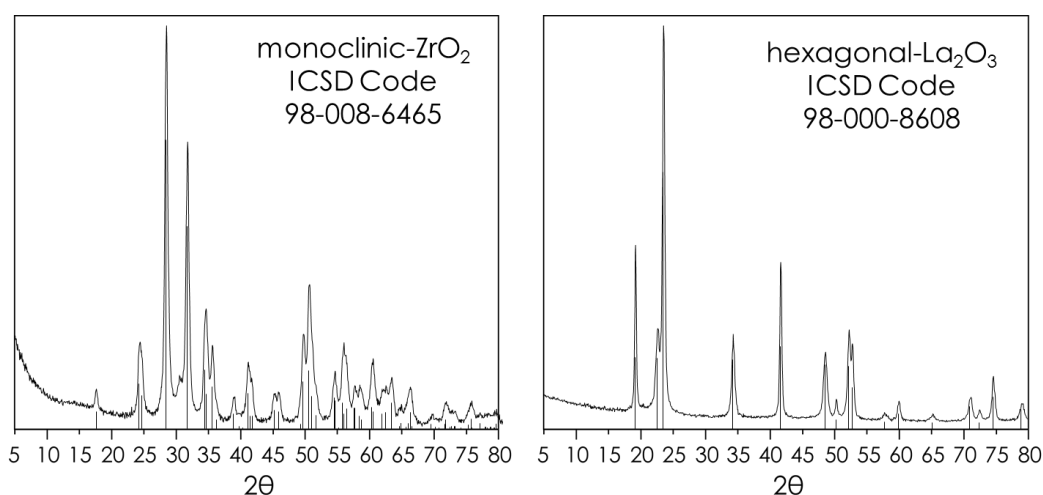
Figure 24: XRD powder patterns of ZrO_2 (left side) and La_2O_3 (right side).

The multipoint adsorption/desorption isotherms of N_2 for the different samples were acquired with a porosimeter and specific surface area (SSA) and mean pore diameter have been calculated using the BET equation. The results are reported in Table 2.

catalyst	SSA [m²/g]	Mean Pore Diameter [nm]	M/P/O atomic ratio
$AlPO_4$	126	10	1/1/4
Zr/P/O	49	4	1/1,5/5.7
$LaPO_4$	85	5	1,1/1/4.2
γ-Al_2O_3	159	9	1/0/1.5
SiO_2	544	6	1/0/2
ZrO_2	36	11	1/0/2
La_2O_3	26	21	1/0/1.5

Table 2: catalysts specific surface area, mean pore diameter (porosimetry) and M/P/O atomic ratio (XRF).

The atomic ratio between the different elements in the various samples measured by means of XRF is reported in the same Table. Interestingly, except for Zr/P/O and $LaPO_4$, the M/P/O and M/O ratio is equal to the stoichiometric value in all catalyst. The theoretical M/P/O ratio

Carboxylic acids ketonization

in $Zr_3(PO_4)_4$ is 1/1.33/5.33, while our Zr/P/O material is characterized by a M/P/O equal to 1/1.5/5.7, which means that phosphorus and oxygen are in excess in respect to Zr, probably in the form of HPO_4^{2-}. In $LaPO_4$ instead, La and O are in slight excess in respect to P (La/P/O of 1.1/1/4.2), which means that La_2O_3 could have partially segregated; however, no La_2O_3 reflexes were found in $LaPO_4$ XRD pattern.
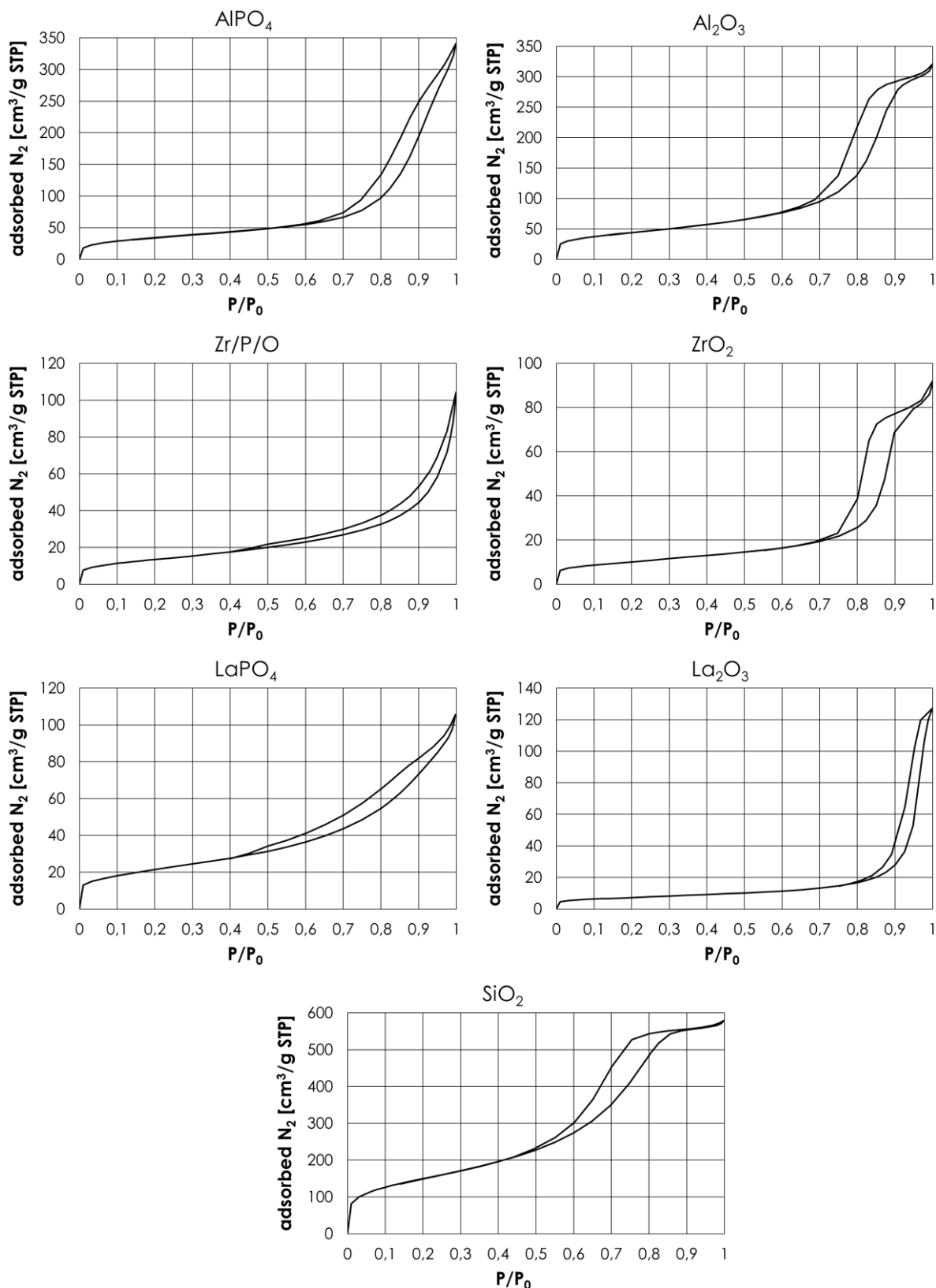
Figure 25: N2 adsorption/desorption isotherms of phosphates and oxides of Al, Zr and La and SiO2.

N_2 multipoint adsorption/desorption isotherms at 77 K are shown in Figure 25: all catalysts display the hysteresis loop typical of mesoporous materials and a type IV adsorption isotherm. Metal oxides consists of an ordered three-dimensional array of O^{2-} anion and M^{n+} cation; the former is a strong base, while the latter act as Lewis acid. The acid-base properties of oxides are related to the ionic character of the M-O bond, which can be estimated from the difference in electronegativity between oxygen and the metal.

$$Ionicity \% = \left\{ 1 - e^{\left[-0.25 \cdot (\chi_O - \chi_M)^2 \right]} \right\} \cdot 100$$

$\chi_O = Pauling\ electronegativity\ of\ oxygen$

$\chi_M = Pauling\ electronegativity\ of\ metal$

element	χ	bond	Ionicity %
P	2.19	P-O	32.3
Si	1.90	Si-O	44.7
Al	1.61	Al-O	56.7
Zr	1.33	Zr-O	67.1
La	1.10	La-O	74.6
O	3.44	/	/

Table 3: electronegativity and empirical equation for the calculation of the percentage of the ionic character of a bond proposed by Linus Pauling.

Electronegative metal cations attract a significant part of the electronic density of O^{2-} anions, reducing their nucleophile/basic character. In SiO_2, the difference in electronegativity between Si and O is so small that the Si-O bond possess a very low ionic character and O^{2-} is so electron poor that displays no basicity at all. In γ-Al_2O_3 the difference in electronegativity between O and Al is higher than in the case of SiO_2 and the higher ionic character of the Al-O bond makes O^{2-} anions less electron poor, therefore they display a little nucleophilic/basic character. Even if γ-Al_2O_3 possess a strong Lewis acidic character, it is an amphoteric oxide and water adsorption on its surface produces surface hydroxyls that act as Brønsted acidic sites. As a proof, Al is known to be dissolved by both acids and bases. These considerations are reflected by the results of TPD characterization.
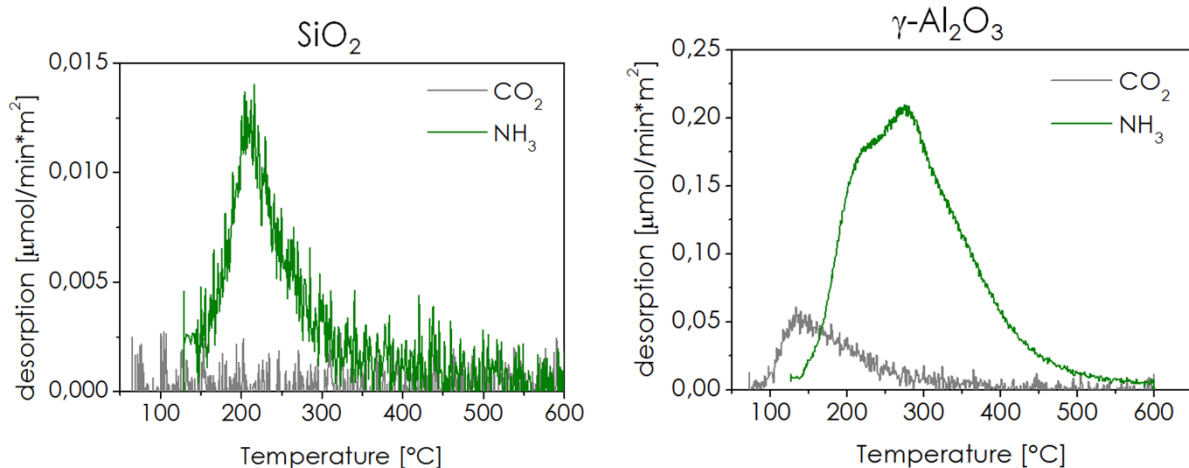
Figure 26: CO_2 and NH_3 temperature programmed desorption profiles of SiO_2 (left side) and γ-Al_2O_3 (right side),

SiO_2 (Figure 26, left side) adsorbs small amounts of NH_3 due to the weak Brønsted acidity of its pending silanol groups (Si-OH) and do not possess any basicity, leading to flat CO_2-TPD profile with no CO_2 desorption. NH_3-TPD profile for γ-Al_2O_3 (Figure 26, right side) shows a broad desorption band in the temperature range 150-600 °C, which indicates the presence of weak, medium-strength and strong acidic sites. The maximum of desorption is located at 275 °C, with a significant shoulder around 220 °C; NH_3, however, keep desorbing in small amounts up to 600 °C and a very small shoulder can be seen at around 350 °C. Therefore, medium-strength acidic sites (275 °C) are predominant in respect to weakly acidic sites

Carboxylic acids ketonization

(100-220 °C) and strong basic sites (350-600 °C). The slightly amphoteric character of γ-Al$_2$O$_3$ is confirmed by the small amount of CO_2 desorbed from weak basic sites around 135 °C. On the other hand, Zr and La, being less electronegative than Al and Si, and the ionic character of their bond with O is higher. This fact allows the presence more electron rich O^{2-} anions in ZrO_2 and La_2O_3 lattice, which display higher nucleophile/basic character. ZrO_2 is a well-known amphoteric material thanks to the Lewis acidity of Zr^{4+} cations; moreover, as mentioned in Chapter 4.1.4.2.3, ZrO_2 is capable to form oxygen vacancies and exposed surface cations with a high degree of unsaturation, which behave as strong Lewis acidic sites. Again, CO_2 and NH_3-TPD evidence a correlation between electronegativity of the metals, ionic character of the M-O bond and acid/base properties.
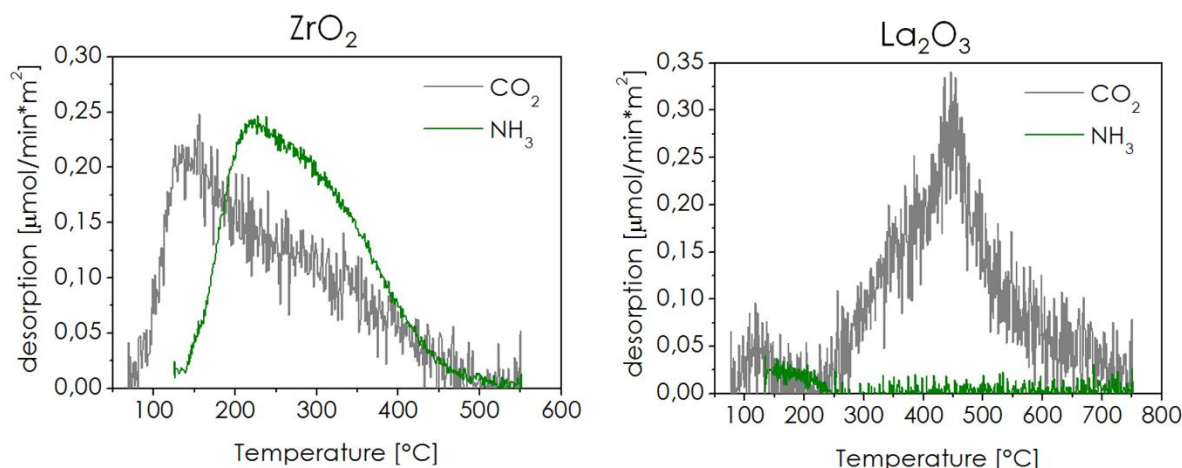
Figure 27: CO_2 and NH_3 temperature programmed desorption profiles of ZrO_2 (left side) and La_2O_3 (right side).

ZrO_2 (Figure 27, left side) desorbed CO_2 in a broad temperature range (100-450 °C) indicating the presence of weak, medium-strength and strong basic sites. The maximum of adsorption is 135 °C, meaning that weak basic sites are predominant; the density of medium-strength and strong basic sites is lower (shoulders at about 250 and 350 °C). ZrO_2 desorbed also significant amount of NH_3 in the temperature range 150-500 °C with a maximum at 220 °C, indicating the presence of weak, medium-strength and strong acidic sites, the formers being predominant. Therefore, TPD characterization confirmed the amphoteric nature of ZrO_2. La_2O_3 is the oxide characterized by the strongest ionic character and is expected to be the most basic oxide among those investigated. In fact, lanthanides are known to possess an intermediate basicity between alkali-earth metals and transition metals. Finally, the very high calcination temperature of 750 °C required to decompose Lanthanum carbonates formed during the synthesis due to CO_2 absorption in the basic solution is a clear indication of its basicity. TPD-CO_2 desorption profile for La_2O_3 (Figure 27, right side) confirms these considerations and show two maxima: the former (120 °C) indicate the presence of a very small amount of weak basic sites, while the latter (445 °C) indicates that very strong basic sites are predominant on this catalyst; moreover, CO_2 keep desorbing up to 700 °C. NH_3-TPD profile for this catalyst is characterized by a very small desorption which stops completely at 250 °C. To sum up, CO_2 and NH_3-TPD characterization showed that γ-Al$_2$O$_3$ display a slightly amphoteric character, ZrO_2 display a strong amphoteric character and La_2O_3 is highly basic. The strength and density of the strongest acidic sites grows in the order $La_2O_3 < SiO_2 << ZrO_2 < \gamma$-Al$_2O_3$, but the total acidity do not strictly follow this order: in fact, ZrO_2 desorbed more NH_3 than γ-Al$_2$O$_3$ (see Table 4). The strength of basic sites and the total basicity of these oxides instead strictly follow the order of the increasing percentage of ionic character of the M-O bond and decreasing electronegativity of the metal: $SiO_2 << \gamma$-Al$_2$O$_3 < ZrO_2 < La_2O_3$. TPD profiles of MPOs are reported in Figure 28: the acid-base properties of these materials are much more homogeneous than the ones of oxides; therefore, CO_2-TPD and NH_3-TPD have been reported in the same Graphs for all the three phosphates. CO_2-TPD clearly indicates that phosphates of Al, Zr and La do not possess any

basicity. In order to explain this behavior, the low ionic character of the P-O bond (32.3 %, much lower than the 44.7 % of the Si-O bond) must be taken into consideration. Oxygens in PO_4^{3-} tetrahedra do not possess nucleophilic/basic character because they share their electrons with the highly electronegative P^{5+} ion, which possess very strong Lewis acidity. This cation is so electrophilic that the anhydride P_2O_5 reacts violently with water to produce orthophosphoric acid. However, the oxygens in H_3PO_4 are still so electron poor that they are more stable when negatively charged: for this reason, H_3PO_4 is a strong mineral acid and release its protons in aqueous solutions forming solvated $H_2PO_4^-$, HPO_4^{2-} and PO_4^{3-} ions. In comparison with MOs, the effect of the introduction of phosphorus ions consists in the total suppression of O^{2-} nucleophilicity/basicity.
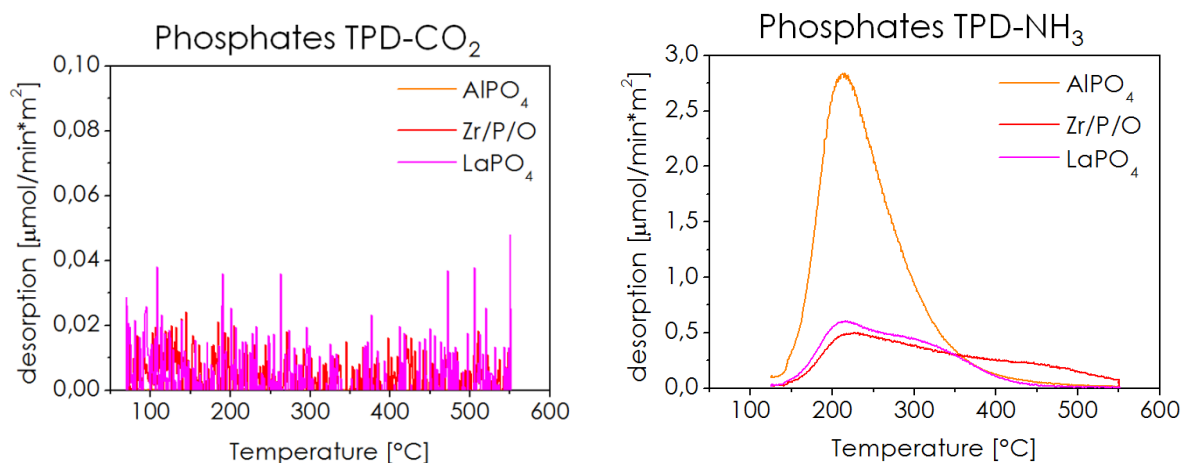
Figure 28: CO_2 (left side) and NH_3 (right side) temperature programmed desorption profiles of MPOs.

The introduction of phosphorus has, however, also a significant effect on the acidity of MPOs in respect to the relative oxides. Two reasons can be given for that: 1) pending PO_4 tetrahedra saturate their excess negative charge with H^+ ions, therefore Brønsted acidic sites (P-OH), much stronger than silanol groups (Si-OH), are present. 2) Metal cations are Lewis acids and attract electronic density from their counter ions. Being oxygen in the form of O^{2-} anion (in MOs) more electron rich than oxygen in the form of PO_4^{3-} (in MPOs), the same metal cation in MPOs will be able to attract less charge from its counter ion and will be more electrophilic and acidic. The density of acidic sites in MPOs is much higher than the one of the relative MOs and the total acidity grows in the order La < Zr < Al, following the growing Lewis acidity of the metal cation. All three MPOs are characterized by a maximum of desorption around 215-220 °C and a shoulder around 300 °C. Zr/P/O TPD profile shows also a third shoulder at 450 °C.

catalyst	Total basicity [μmol/m^2 CO_2]	Maximum of CO_2 desorption [°C]	Total acidity [μmol/m^2 NH_3]	Maximum of NH_3 desorption [°C]
SiO_2	0	/	0.2	205
γ-Al_2O_3	0.7	135	4.2	275
ZrO_2	4.7	135	5.3	220
La_2O_3	7.0	445	0.2	170
$AlPO_4$	0	/	36.4	215
Zr/P/O	0	/	13.0	225
$LaPO_4$	0	/	11.4	215

Table 4: total acidity and total basicity of catalysts.

4.2.2 Catalytic tests

4.2.2.1 Catalytic activity of AlPO$_4$

The homo-ketonization of PA was investigated over all catalysts with a feed molar composition of 6 % PA in N$_2$ as carrier and a time factor (W/F) equal to 0.8 s*/mL, which were found to be a good compromise to carry out a catalytic screening of catalysts possessing much different activities. In the following Graphs the results of PA ketonization will be reported in terms of moles. The reasons behind this choice is that in most cases ketonization was the only reaction occurring, and a good correlation between PA conversion and CO$_2$ and 3-P yields was achieved calculating yields as follows:

$$Y_{(3-P \, or \, CO2)} \, [\%] = \frac{2 \cdot (mol^{OUT})}{(mol_{PA}^{IN} - mol_{PA}^{OUT})} \cdot 100$$

Only 3-P yield, however, has been taken into consideration for the calculation of the molar balance because otherwise, in case of 100 % conversion and 100 % of selectivity of ketonization, the YS/X calculated considering also CO$_2$ would have been equal to 200 % (CO$_2$ being formed only as a co-product of the target reaction). Graph 1 shows the results of a typical catalytic test over AlPO$_4$ catalyst as a function of the time on stream and at the temperature of 325 °C.
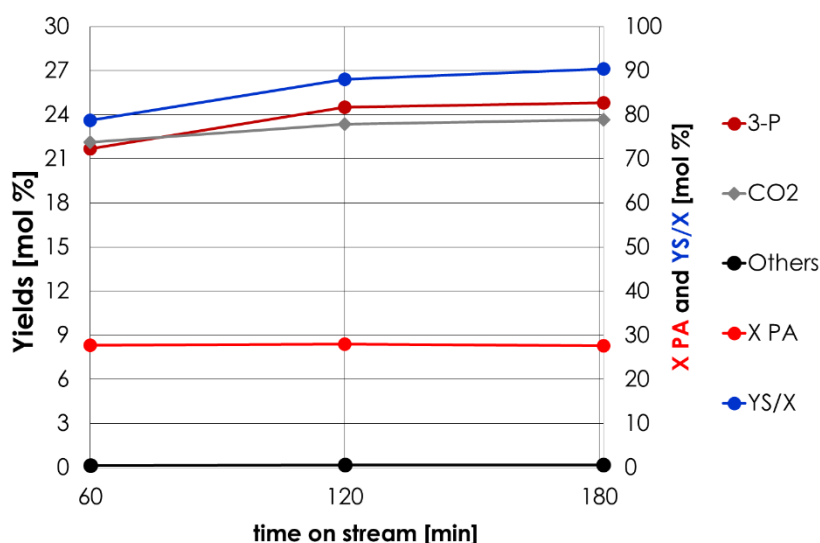
*Graph 1: Typical experiment. Gas-phase ketonization of PA as a function of time on stream: catalyst = AlPO$_4$; temperature = 325°C; PA/N$_2$ feed composition [mol %] = 6/94; W/F = 0.8 s*g/mL. Others includes unknown compounds. Yields calculated in terms of moles.*

Conversion of PA (X PA) and molar balance (YS/X) are reported on the right y-axis, while the yields in the various products are reported on the left y-axis. Unknown products are grouped in "Others". During the first hour of reaction the yields in 3-P and CO$_2$ were lower than the ones obtained after longer time on streams. This is a behavior common to all investigated catalysts and has been attributed to a partial, initial deactivation of the most active and less abundant sites on catalyst surface at the beginning of the reaction, due to the deposition of carbonaceous materials formed by consecutive reactions of the desired product. Starting from the second hour of reaction conversion and yields stabilized indicating that the system reached a steady state of stable catalytic activity and better molar balances were obtained. The values of X PA and yields reported in all the following Graphs (except for Graph 1) have always been calculated as a mean value of the points

were the system reached such steady state. At 325 °C PA ketonization is the only reaction occurring over $AlPO_4$. However, at this temperature, the catalyst is poorly active and about 24 % yield in 3-P and CO_2 were achieved. The results of PA ketonization over $AlPO_4$ as a function of reaction temperature are shown in Graph 2 in the form of histogram; in this case, X PA and YS/X are reported on the left y-axis together with product yields.
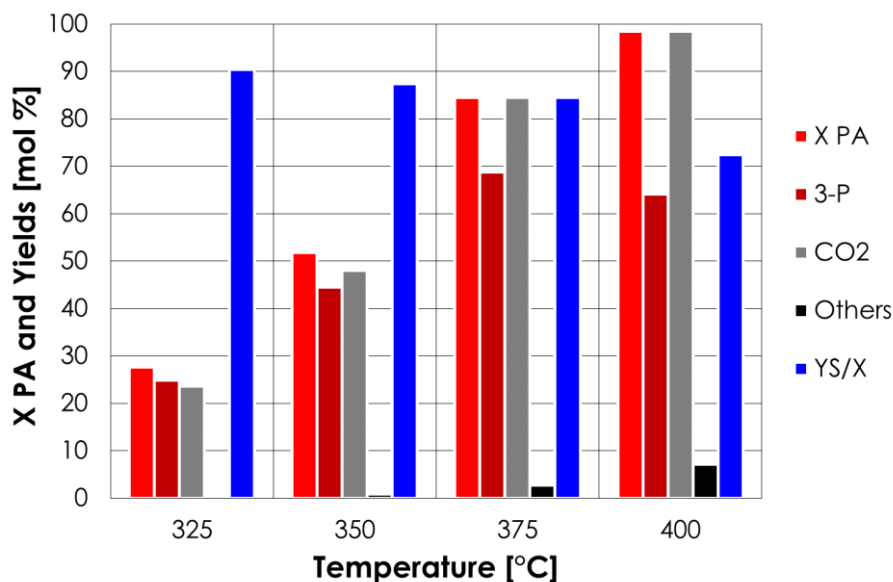
Graph 2: Gas-phase ketonization of PA as a function of reaction temperature: catalyst = $AlPO_4$; PA/N_2 feed composition [mol %] = 6/94; W/F = 0.8 s*g/mL. Others includes unknown compounds. Yields calculated in terms of moles.

PA conversion increase from about 30 % to a value near to 100 % in the temperature range 325-400 °C. Ketonization of PA is the only reaction occurring the temperature range 325-350 °C and the formation of unknown products from side reaction is negligible. This fact is confirmed by the good correlation between the yields in 3-P and CO_2. In the temperature range 375-400 °C instead, the yield of 3-P became lower PA conversion, and, at the same time, the CO_2 yields remained equal to X PA. These results suggest that ketonization, in the temperature range 375-400 °C, is the only reaction occurring on PA, but the resulting 3-P undergoes consecutive reactions that reduce its yields. In fact, ethane and ethylene were not found among reaction products, while the formation of unknown products with higher retention time in respect to 3-P (probably resulting from aldolic reactions) increased. A secondary argument in favor of this hypothesis is that, if side reactions such as decarboxylation of PA to ethane and CO_2 occurred, the use of the stoichiometric factor "2" for the calculation of CO_2 yield would have been incorrect. In that case, a part of CO_2 would have been produced in a 1:1 molar ratio in respect to PA, and its yield calculated with the stoichiometric factor for ketonization would have led to values of CO_2 yield higher than PA conversion.
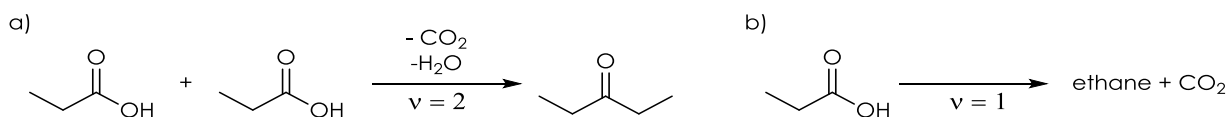
Scheme 25: a) ketonization (ν = 2); b) decarboxylation (ν = 1).

For these reasons, the increasingly low molar balances obtained at 375 and 400 °C have been attributed to the occurrence of consecutive side reaction on 3-P (e.g. aldol condensation) that produced heavy products (oligomers). A large part of these products condensed on the relatively cold reactor walls below the catalytic bed forming noticeable yellow- brown solid deposits. The unknown products grouped in "Others" are probably the lighter fraction of the aldol condensation products of 3-P. Graph 3 shows the results of the

Carboxylic acids ketonization

homo-ketonization of PA, of AA and the cross ketonization of an equimolar mixture of PA and AA over $AlPO_4$ at the temperature of 350 °C. Cross ketonization has been carried out with a feed molar composition PA/AA/N_2 equal to 3/3/94; both X PA and X AA will be reported, but yields were expressed in respect to both reagents, as follows:

$$Y \, [\%] = \frac{2 \cdot (mol^{OUT})}{(mol_{PA}^{IN} + mol_{AA}^{IN})} \cdot 100$$

The homo-ketonization of AA yielded acetone as the main product, together with minor amounts of unknown compounds.
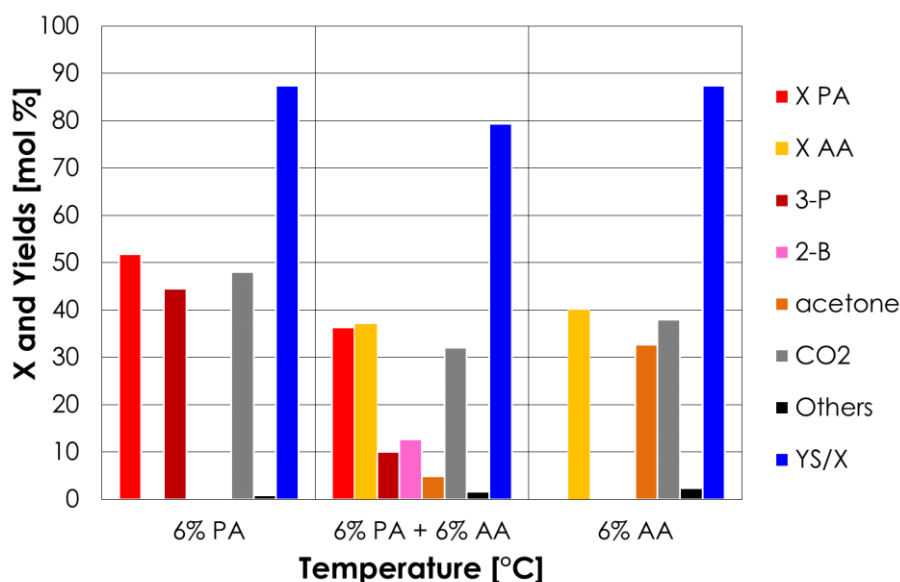
Graph 3: Gas-phase homo- and cross-ketonization of PA and AA: catalyst = AlPO₄; temperature = 350 °C; W/F = 0.8 s*g/mL. Others includes unknown compounds. Yields calculated in terms of moles.

A good correlation between the yield of acetone and CO_2 was obtained also in this case: the only reaction occurring on AA is ketonization, and acetone seems to be more prone to decomposition than 3-P over $AlPO_4$, because the yields in "Others" is higher in respect to the one obtained during PA ketonization at 350 °C. Surprisingly, AA conversion was lower than PA conversion in the same conditions: this fact is in contrast with the literature that agrees on the higher reactivity of acids with a higher number of α-protons and less steric hindrance on the α-carbon. However, it is worth noticing that most literature regarding ketonization focus on MOs and, at the best of our knowledge, no examples of ketonization over MPOs have ever been reported. The cross-ketonization of PA and AA yielded the asymmetric product 2-butanone (2-B, 12.7 %) as the main product, followed by 3-P (Y = 10.1 %) and acetone (Y = 4.8 %). Even in this case CO_2 (Y = 32 %) is helpful in determining that ketonization is the main reaction occurring on AA (SY$_{3-P+2-B+acetone}$ = 27.6 %). The conversion of both acids is during cross-ketonization is lower than the one of PA alone and the one of AA alone during homo-ketonization; the same happens for the "Others" yields in the three case. PA/AA mixture cross-ketonization was investigated also as a function of the reaction temperature. These results are shown in Graph 4 and Table 5. The cross-ketonization of PA/AA mixture over $AlPO_4$ show some similarities with the one of PA alone. In this case an increase in reaction temperature leads to an increase in "Others" yield and is detrimental for molar balances. Moreover, the yield in CO_2 is almost equal to the conversion at all temperatures, while the sum of yields of ketones at 400 °C is significantly lower than total conversion indicating that also in this case ketonization is the only reaction that occurs on the acids and the worsening of the molar balance is attributable to consecutive aldol reactions occurring on ketones, mainly at 400 °C. 2-B is the major product at all temperature, followed by 3-P and acetone. Detailed value of yields and conversion are reported in Table

6. Scheme 26 depicts the proposed reaction scheme for PA/AA mixture ketonization over AlPO₄.
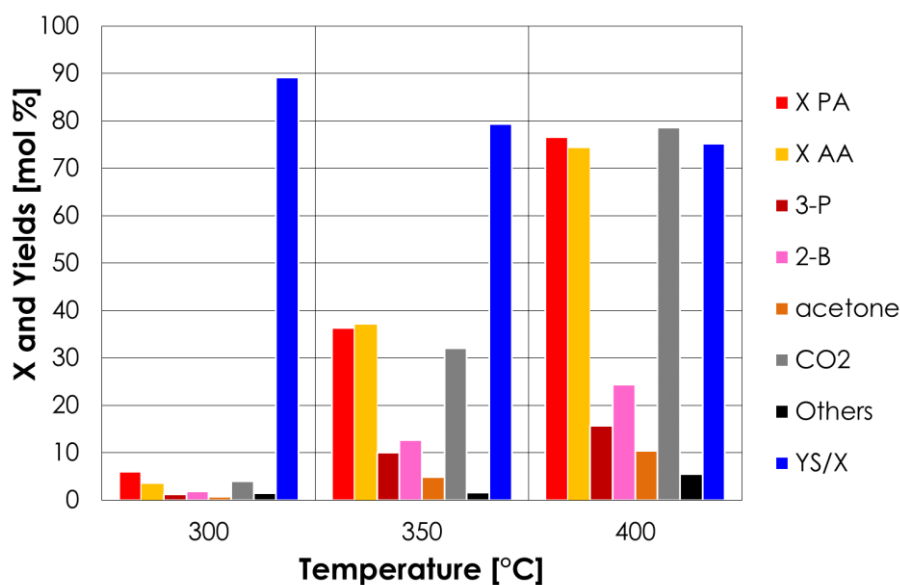
Graph 4: Gas-phase cross-ketonization between PA and AA as a function of reaction temperature: catalyst = AlPO₄; PA/AA/N₂ feed composition [mol %] = 3/3/94; W/F = 0.8 s*g/mL. Others includes unknown compounds. Yields calculated in terms of moles.

compound	Yield (300 °C)	Yield (350 °C)	Yield (400 °C)
Y (2-B)	1.8	12.7	24.4
Y (3-P)	1.2	10.1	15.6
Y acetone	0.8	4.8	10.4
Y (2-B+3-P+acetone)	3.8	27.6	50.4
Y (CO₂)	4.0	32.0	78.6
X tot (PA + AA)	5.9	36.8	77.5

Table 5: Yields of the three ketones, sum of yields of the three ketones, CO₂ yields and total conversion at 300, 350 and 350 °C for the AA/PA mixture cross-ketonization over AlPO₄.
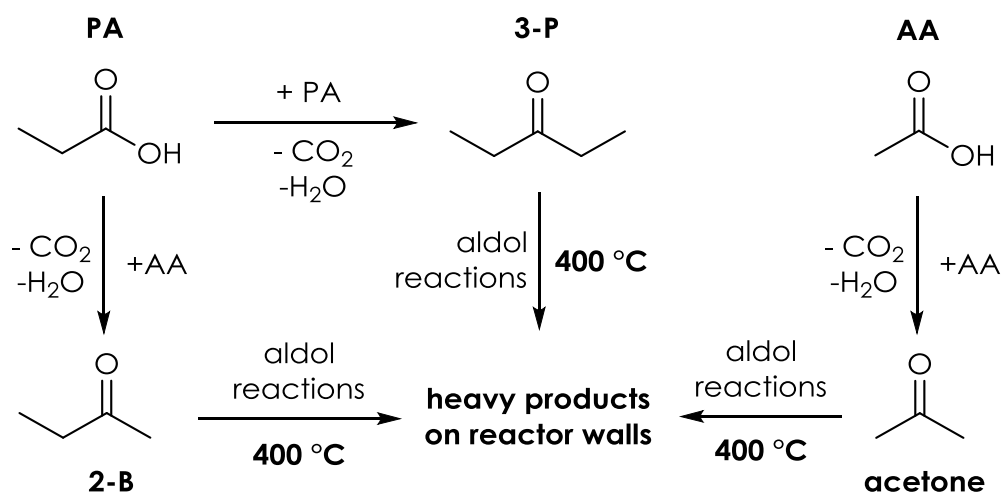
Scheme 26: proposed reaction scheme for PA/AA cross- ketonization over AlPO₄.

4.2.2.2 Catalytic activity of Zr/P/O

Graph 5 show the results of PA homo-ketonization over Zr/P/O in the temperature range 350-425 °C.
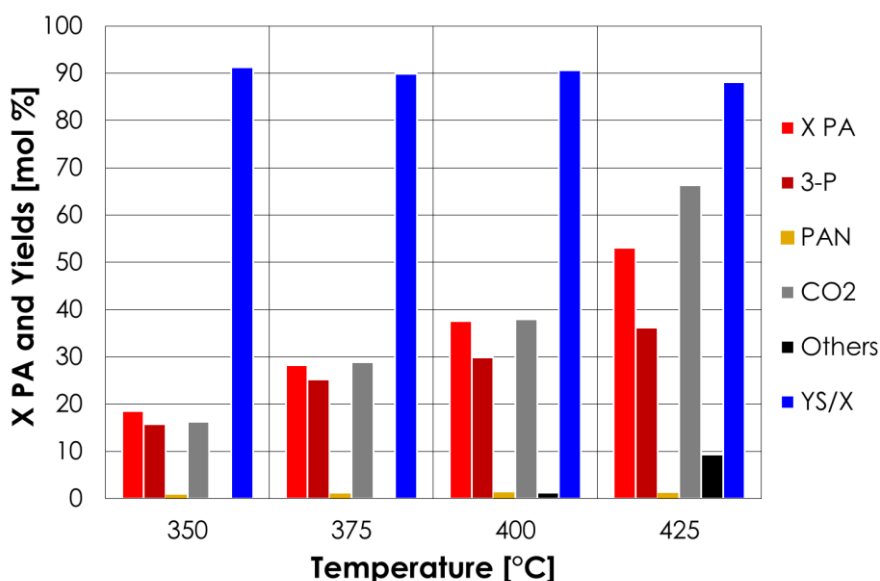
Graph 5: Gas-phase ketonization of PA as a function of reaction temperature: catalyst = Zr/P/O; PA/N₂ feed composition [mol %] = 6/94; W/F = 0.8 s*g/mL. Others includes unknown compounds and minor amounts of ethylene and CO. Yields calculated in terms of moles.

In order to compare properly the activity of $AlPO_4$ and Zr/P/O towards ketonization, the conversion of PA obtained over the two catalysts in the same reaction conditions has been normalized with their specific surface area (126 and 49 m^2/g respectively). The resulting values of "specific conversion of PA" (X PA/SSA, conversion per square meter of catalyst) are reported in Table 6.

catalyst	X PA/SSA [m^{-2}] 350 °C	X PA/SSA 375 °C [m^{-2}]	X PA/SSA 400 °C [m^{-2}]
$AlPO_4$	0.41	0.67	0.78
Zr/P/O	0.38	0.58	0.77

Table 6: X PA conversion normalized by the SSA of catalysts.

These results indicate that $AlPO_4$ is more active than Zr/P/O. Moreover, X PA over Zr/P/O is only slightly above 50 % at 425 °C. In the low temperature range 350-375 °C, the course of reaction over Zr/P/O is like the one over $AlPO_4$: ketonization was the only reaction and only a small fraction of 3-P underwent consecutive reactions on catalyst surface. However, starting from 400 °C a new product, propionic anhydride (PAN, Y = 1.6 %) began to form, together with CO and ethylene (in "Others" in Graph 6), and their yield increased at 425 °C (Y PAN = 5.4 %). The formation of CO, ethylene and PAN can be explained considering a parallel reaction of PA dehydration to methyl ketene, as depicted in Scheme 27:
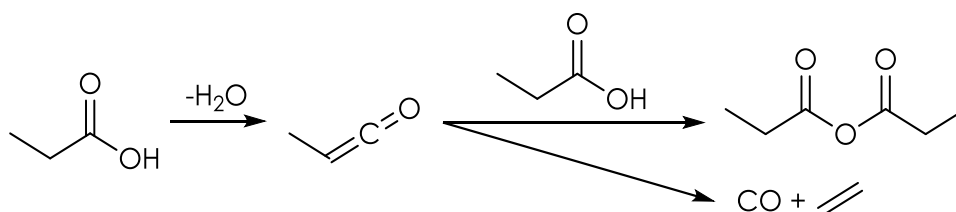
Scheme 27: dehydration of PA to methyl ketene followed by coupling with PA to produce PAN or thermal decomposition of the methyl ketene into CO and ethylene.

Moreover, at 425 °C the yields in CO_2 calculated with the stoichiometric factor "2" became higher than X PA, indicating that a significant fraction of this product was not produced by ketonization, but, more likely, following PA decarboxylation. In fact, if CO_2 was formed by means of PAN decarboxylation, the stoichiometric coefficient "2" should have been correct, because this product is ultimately formed by the coupling of two PA molecules.

4.2.2.3 Catalytic activity of LaPO₄

PA ketonization over LaPO₄ was investigated in the temperature range 350-400 °C and results are reported in Graph 6. At 350 °C and 400 °C PA conversions over LaPO₄ were roughly half of those obtained over Zr/P/O. Taking into account that the SSA of LaPO₄ is 85 m^2/g (almost 2 times the one of Zr/P/O, 49 m^2/g) it can be concluded that this is the less active catalyst among MPOs. The course of reaction over LaPO₄ is similar to the one over Zr/P/O in terms of product distribution.
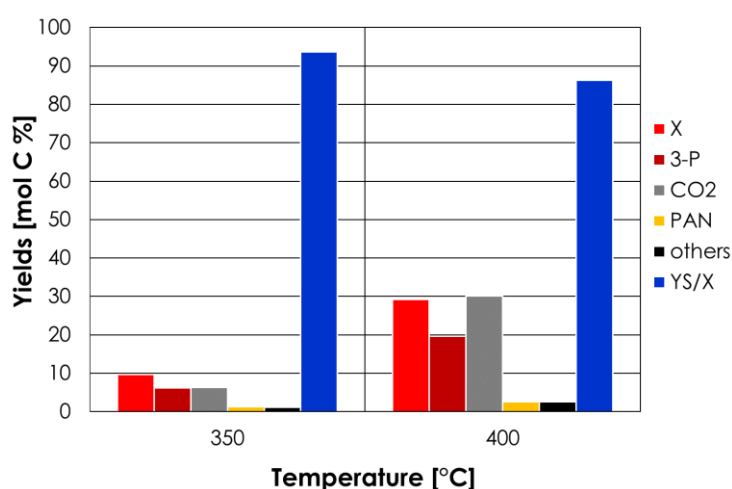
Graph 6: Gas-phase ketonization of PA as a function of reaction temperature: catalyst = LaPO₄; PA/N₂ feed composition [mol %] = 6/94; W/F = 0.8 s*g/mL. Others includes CO, ethylene and unknown compounds. Yields calculated in terms of moles of carbon.

To sum up, the activity of MPOs towards ketonization increase with the total acidity of catalysts measured by NH₃-TPD (Table 4, Chapter 4.2.1.4) and follows the order AlPO₄ > Zr/P/O > LaPO₄. Ketonization is the main reaction occurring on PA over all MPOs and the major amounts of side products derive from aldol condensation reaction occurring on 3-P, which were impossible to quantify: their amount had to be estimated from the loss in the molar balance. At high temperature a small fraction of PA is dehydrated to methyl ketene over Zr/P/O and LaPO₄, which then decompose into CO and ethylene or react with PA to produce PAN. The selectivity toward PAN follows the order: LaPO₄ > Zr/P/O > AlPO₄.

Compound (temperature)	X PA	Y PAN	S PAN
AlPO₄ (350 °C)	51.8	0	0
Zr/P/O (350°C)	18.5	0.9	4.9
LaPO₄ (350°C)	9.7	1.3	13.4
AlPO₄ (400°C)	98.5	0	0
Zr/P/O (400°C)	37.6	1.3	3.5
LaPO₄ (400°C)	29.2	2.5	8.6

Table 7: trends in PA conversion and PAN selectivity over different metal phosphate catalyst between 350 and 400°C.

Carboxylic acids ketonization

Scheme 28 depicts the proposed reaction scheme for PA ketonization over MPOs.
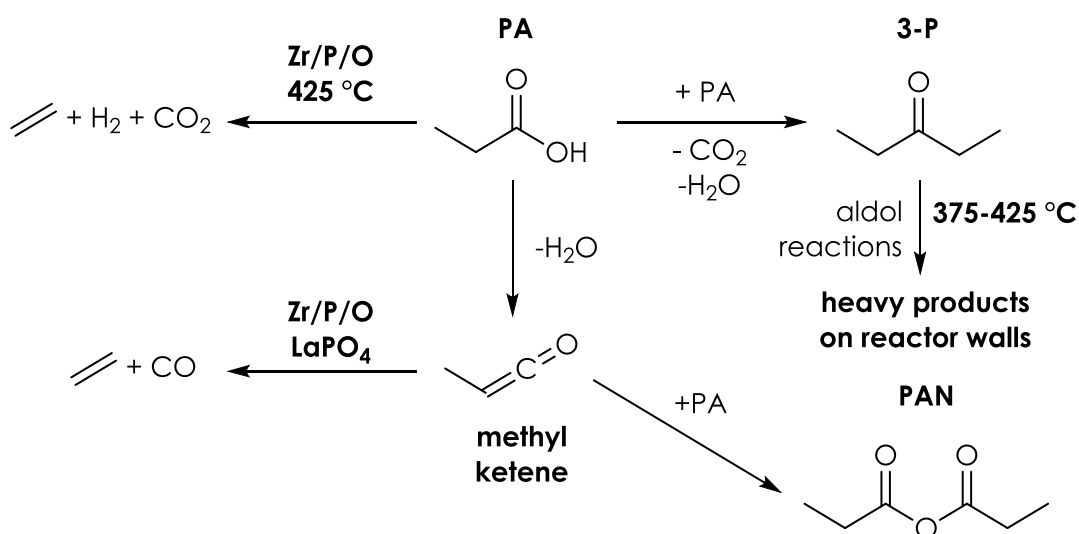
Scheme 28: proposed reaction scheme for PA ketonization over MPOs.

From a mechanistic point of view, results obtained over MPOs demonstrates that the presence of basic sites on catalyst surface is not mandatory in order to achieve the abstraction of an α-hydrogen from a carboxylic acid and obtain a nucleophilic active species capable to couple with an adjacent adsorbed carboxylate. In fact, CO_2-TPD characterization (Figure 28, Chapter 4.2.1.4) of MPOs suggests that they do not possess any basicity. In other words, the α-proton of carboxylic acids over such catalysts is not directly abstracted, but more likely loosen following the keto-enol tautomerization equilibrium between a carboxylate ion and 1-hydroxy enolate ion proposed by Pham et al [53] and depicted in Scheme 19, Chapter 4.1.4.2.1. The order of activity of MPOs ($AlPO_4$ > Zr/P/O > $LaPO_4$) suggests that a higher acidity is beneficial, but at present time it is unclear if this effect is related to a stabilization of the 1-hydroxyenolate anion form or if a strong interaction with an acidic site activates the carboxylate increasing its electrophilicity. Moreover, it is still unclear the role of Brønsted acidic sites, which are likely to be present on M/P/O surface during reaction due to the co-production of water by ketonization. In analogy with the mechanism of AA adsorption over Brønsted Si-OH groups of SiO_2 [82] discussed in Chapter 4.1.4.2.1, they might play a role in the acid chemisorption over metal phosphates (Scheme 29).
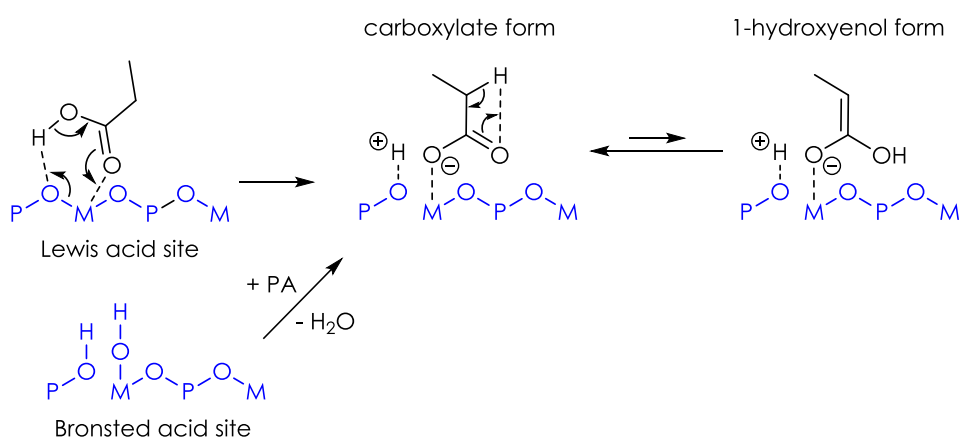
Scheme 29: keto-enolic tautomerism between carboxylate anion and 1-hydroxyenolate anion over MPOs surface adapted from the one on MOs depicted in Scheme 19.

Finally, the literature lacks information regarding the adsorption of carboxylic acids over MPOs.

4.2.2.4 Comparison between MPOs and the respective MOs

The catalytic activity of MPOs for PA ketonization was compared to the one of the respective MOs at the temperature of 350 °C, W/F = 0.8 s*g/mL and feed molar composition PA/N_2 = 6/94. These results are reported in Graph 7 and detailed values of X PA and Y 3-P are compiled in Table 8.
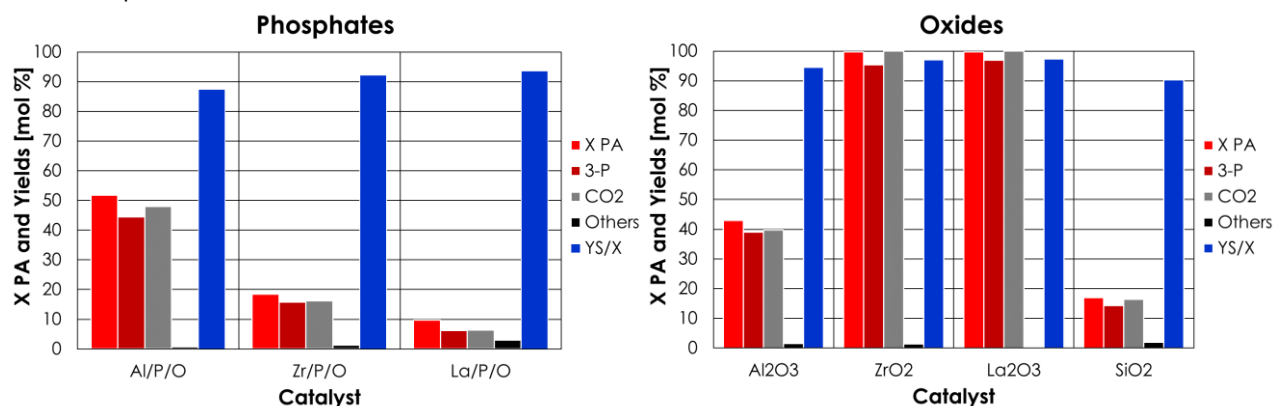
*Graph 7: Gas-phase ketonization of PA over MPOs and MOs: temperature = 350 °C; PA/N_2 feed composition [mol %] = 6/94; W/F = 0.8 s*g/mL. Others includes unknown compounds. Yields calculated in terms of moles.*

catalyst	X PA [%]	Y 3-P [%]	X PA/SSA [m^{-2}]	Y 3-P/SSA [m^{-2}]
γ-Al_2O_3	42.9	39.0	0.27	0.25
$AlPO_4$	51.8	44.5	0.41	0.35
Zr/P/O	18.5	16.7	0.38	0.34
$LaPO_4$	9.7	6.2	0.11	0.07
SiO_2	16.9	14.3	0.031	0.026

Table 8: comparison between the catalytic activity of MOs and phosphates: X PA and Y of 3-P as they are and normalized by catalysts SSA.

ZrO_2 and La_2O_3 proved to be much more active in respect to the relative phosphates and afforded quantitative PA conversion and 3-P yields of 95 and 97 % respectively; for this reason, values of X PA/SSA and Y 3-P/SSA for these catalysts may be incorrect and are not reported in Table 8. SiO_2, which possess (in principle) only weakly Brønsted acidity and the highest SSA among all catalysts investigated (544 m^2/g), was the least active catalyst. However, it is known that calcination of SiO_2 at high temperatures induce the condensation of vicinal silanol groups, resulting in the formation of strained Si-O-Si bonds that can act as Lewis sites. Therefore, since SiO_2 was calcined at a relatively high temperature (650 °C), the fact that 3-P was obtained over this catalyst is not a definitive evidence that Brønsted acidic sites can catalyze PA ketonization. On the other hand, surface carboxylates may be formed also over silanol groups, as explained in Chapter 4.1.4.2.1. Interestingly, γ-Al_2O_3 was the only metal oxide less active than the relative phosphate, even possessing a higher SSA in respect to $AlPO_4$ (159 and 126 m^2/g respectively); the comparison of X PA/SSA shows that γ-Al_2O_3 was even less active than Zr/P/O (Table 8). Both $LaPO_4$ and Zr/P/O were instead much less active than the relative oxides (even possessing higher specific surface areas). This fact suggests that the high catalytic activity of La_2O_3 and ZrO_2 is related to the presence of basic sites on their surface with significant concentration and strength. Such basic sites are capable to abstract directly the α-proton of PA. Such basicity is entirely suppressed by the presence of phosphorus in $LaPO_4$ and Zr/P/O (as demonstrated by means of CO_2-TPD characterization, Figure 27 and 38, Chapter 4.2.1.4) and this is why Zr and La phosphates

Carboxylic acids ketonization

are much less active than the respective oxides. The catalytic activity of γ-Al$_2$O$_3$ instead seems to depend strongly on its acidity. In fact, if its weakly basic lattice O^{2-} anions possessed enough strength to abstract directly the α-proton of PA, they would have led to a synergistic effect with Al^{3+} Lewis acidic sites and the activity of this catalyst would have been higher compared to the corresponding phosphate (AlPO$_4$), which do not possess any basicity and possess a lower SSA. It is worth noticing that is unlikely that the P^{5+} cations in MPOs could act as Lewis acidic sites because they are tightly bounded to oxygen in the phosphate group and the P-O bond have a mostly a covalent character. Therefore, Lewis acidic sites in MPOs are likely to be constituted by Al^{3+}, Zr^{4+} and La^{3+} cations, while Brønsted acidic sites are constituted by both M-OH and P-OH groups. If the catalytic activity of γ-Al$_2$O$_3$, AlPO$_4$, Zr/P/O and LaPO$_4$ depends only on their acidity, as the results of the catalytic screening suggests, the higher activity of AlPO$_4$ and Zr/P/O in respect to γ-Al$_2$O$_3$ could be rationalized with the effects of the introduction of phosphorus discussed in Chapter 4.2.1.4. Metal cations are Lewis acids that attract electronic density from their counter ions in ionic solids. Being oxygen in the form of O^{2-} anion (in MOs) more electron rich than oxygen in the form of PO$_4^{3-}$ (in MPOs), the same metal cation in MPOs will be more electron poor, and its electrophilic and Lewis acidic character will be enhanced. Moreover, the presence of phosphorus introduces P-OH Brønsted acidic sites stronger than the ones (Al-OH) of γ-Al$_2$O$_3$. The results of the catalysts screening showed also that, in contrast with the literature, highly basic La$_2$O$_3$ seems to be more active than amphoteric ZrO$_2$. However, over both catalysts quantitative X PA was achieved; in order to properly compare their activities, the ketonization of PA was investigated again in the same conditions but reducing the W/F to 0.2 s*g/mL, in order to achieve lower PA conversions. The results of these catalytic tests are reported in Graph 8 and Table 9.
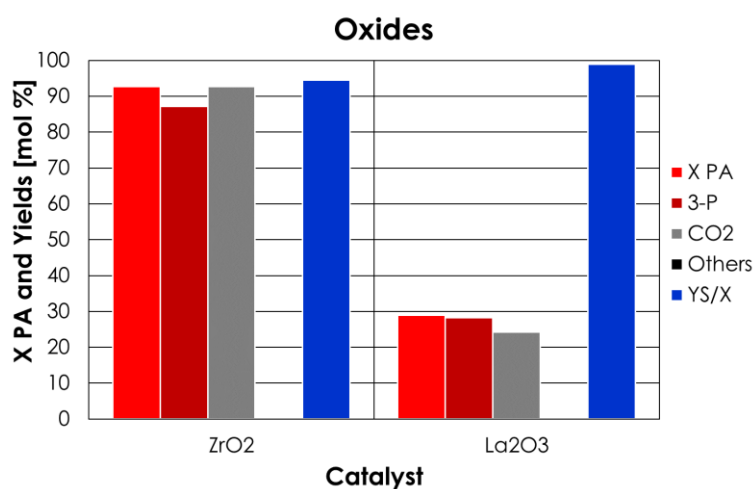
*Graph 8: Gas-phase ketonization of PA over ZrO$_2$ and La$_2$O$_3$: temperature = 350 °C; PA/N$_2$ feed composition [mol %] = 6/94; W/F = 0.2 s*g/mL. Others includes unknown compounds. Yields calculated in terms of moles.*

catalyst	X PA [%]	Y 3-P [%]	X PA/SSA [m^{-2}]	Y 3-P/SSA [m^{-2}]
ZrO$_2$	92.6	87.2	2.57	2.42
La$_2$O3	29.0	28.3	1.11	1.10

Table 9: comparison between the catalytic activity of ZrO$_2$ and La$_2$O$_3$: X PA and Y of 3-P as they are and normalized by catalysts SSA.

Data shown indicate clearly that ZrO$_2$ is more active than La$_2$O$_3$, in agreement with the literature which claims that amphoteric catalysts are usually more active than purely basic and purely acidic oxides. On the other hand, La$_2$O$_3$ seems to be slightly more selective than ZrO$_2$. This may be because the abstraction of a α-proton from ketones is required in order to

activate them for consecutive aldolic reactions; perhaps the lower selectivity of ZrO_2 can be explained with is higher activity for both ketonization and aldolic reactions, resulting from the cooperative effect of acid-base pairs during α-proton abstraction.

4.2.3 Catalysts characterization after reaction

Catalyst after reaction were characterized by means of XRD in order to detect crystal structure changes. Moreover, attenuated total reflectance spectroscopy (ATR) and thermogravimetric analysis (TGA) were used to investigate carbon deposition over catalysts surface.
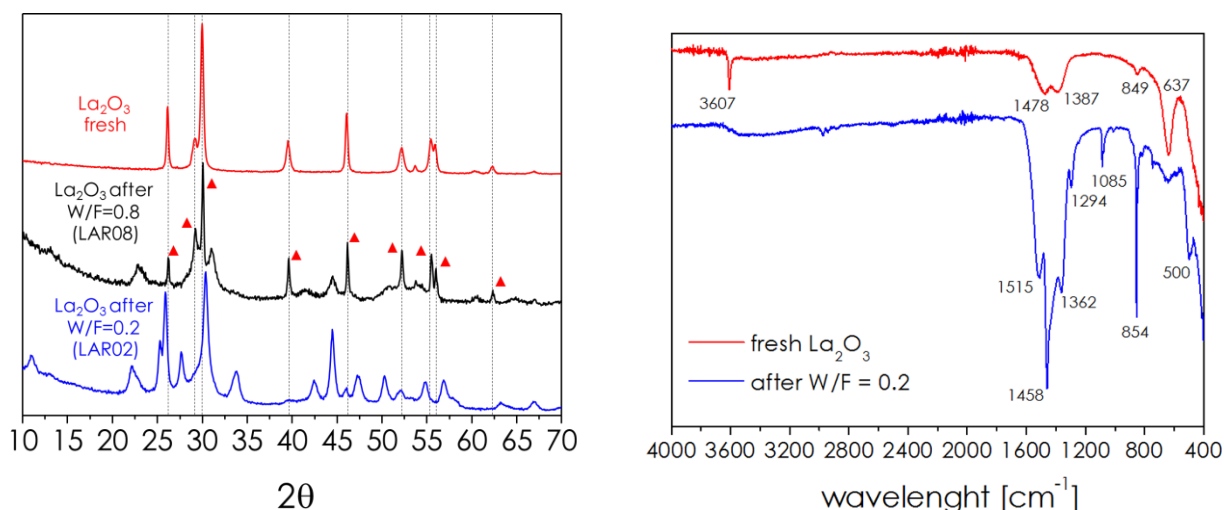
Figure 29: XRD patterns (left) and ATR spectra (right) of: fresh La_2O_3 = red; of La_2O_3 after reaction with PA (W/F = 0.8 s*g/mL) = black; La_2O3 after reaction of PA (W/F = 0.2 s*g/mL) = blue.

Detailed data for MOs will not be reported, because XRD diffraction patterns and ATR analysis did not evidence any change in their crystal structure; TGA analyses evidenced negligible carbon deposition (molar balance equal or higher to 95 % were obtained over all metal oxide). In the case of MPOs, XRD and ATR analysis did not evidence any change in their crystal structure nor carbon deposition. Weight losses measured by thermogravimetric analysis justified a minimal fraction of the deficits on molar balances obtained over MPOs, suggesting that these deficits indeed depended on the condensation of heavy product on the relatively cooler reactor walls below the catalytic bed. The only exception was La_2O_3, which was deeply modified during the reaction with PA. Figure 28 depicts the results of the XRD and ATR analysis carried out over La_2O_3 before and after reaction. In order to avoid confusion, La_2O_3 after reaction at W/F = 0.8 s*g/mL and La_2O_3 after reaction at W/F = 0.2 s*g/mL will be called from now on LAR08 and LAR02 respectively in the text (AR = after reaction, the number refers to the W/F value). The significant changes in the XRD pattern of La_2O_3 after reaction with PA represent a strong evidence of the bulk-type ketonization mechanism that occurs over this catalyst, in agreement with the literature [62]. The XRD pattern of LAR08 (in black in Figure 29) retain several reflection of the parent La_2O_3 (red triangles). The one of LAR02 (in blue in Figure 29) is instead less similar, suggesting that in this case the catalyst underwent a deeper chemical modification. This is because depending on how a lower W/F is achieved, it implies a larger volumetric flow of reagent in respect to the same mass of catalyst or, alternatively, the interaction of a lower mass of catalyst with the same volumetric flow of reagent. The comparison of the reflexes of LAR08 and LAR02 with the International Crystal Structures Database (ICSD) gave a good match with a $La_2O_3/La_2O_2CO_3$ mixture and $La_2O_2CO_3$ alone respectively, and the FT-IR spectra of La_2O_3 and of LAR02 matches those reported in the literature for the oxide and oxycarbonate species [92, 93, 94]. These results are in agreement with the mechanism of ketonization

Carboxylic acids ketonization

reported in the literature for rare earth oxides [62] and depicted in Scheme 15c, Chapter 4.1.4.1. The results of TGA analysis on LAR02 is shown in Figure 30.
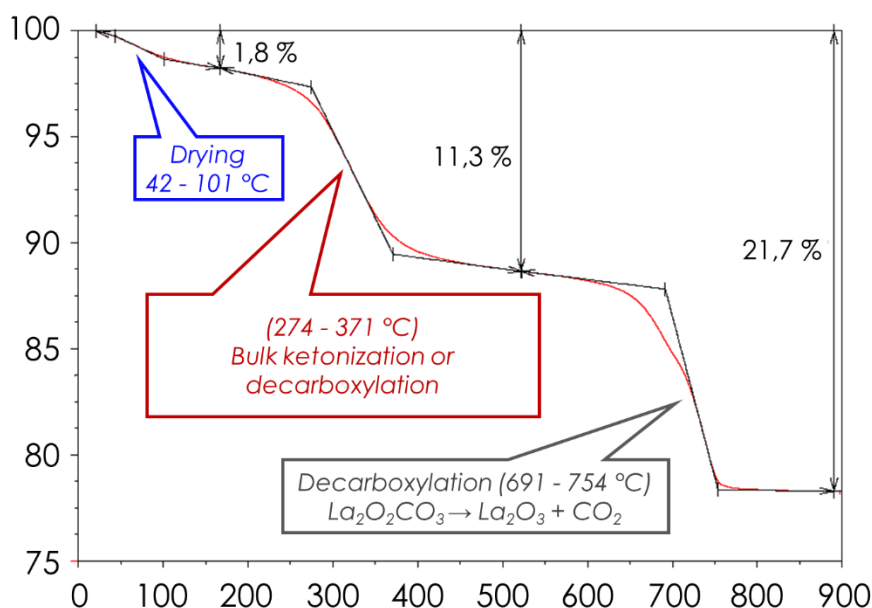
Figure 30: TGA profile up to 900 °C in air of LAR02.

The first weight loss between 40 and 100 °C is related to water desorption (drying). The second weight loss between 274 and 371 °C indicates that the sample cannot consist of pure $La_2O_2CO_3$, which decompose at much higher temperatures [95, 94], while third weight loss between 691 and 754 °C is located were $La_2O_2CO_3$ decarboxylation to La_2O_3 is expected to occur. These results can be rationalized supposing that LAR02 consists of a different phase from $La_2O_2CO_3$ such as $La_2O(CO_3)_2$ (in contrast with XRD results), or a mixture of crystalline $La_2O_2CO_3$ and amorphous or poorly crystalline oxypropionate salt of Lanthanum. A good agreement between the experimental (11.7 %) and theoretical (11.9 %) weight loss for the decarboxylation of $La_2O_2CO_3$ to La_2O_3 and CO_2 was obtained assuming that the only phase present on the third plateau (754-900 °C) is La_2O_3, after the subtraction of the contribute for water loss. Similarly, a good agreement between the theoretical (10.6 %) and experimental (9.7 %) weight loss for the decarboxylation of $La_2O(CO_3)_2$ to $La_2O_2CO_3$ and CO_2 was obtained assuming that the only phase present on the second plateau (371-691 °C) was $La_2O_2CO_3$. However, the possibility that the weight loss between 274 and 371 °C was due to the bulk ketonization of an oxypropionate salt of lanthanum cannot be ruled out. In fact, this weight loss occurs exactly in the temperature range in which also ketonization occur. As an example, if LAR02 consisted of $La_2O_2(OOC-CH_2CH_3)_2$ rather than $La_2O(CO_3)_2$, a theoretical weight loss of 18.9 % was calculated. Therefore, the experimental weight loss of 9.7 % would have been produced by the decomposition of a mixture containing 71.5 wt. % of $La_2O_2(OOC-CH_2CH_3)_2$ and 28.5 wt. % $La_2O_2CO_3$. The thermal behavior of LAR02 was investigated also by means of programmed temperature XRD in the temperature range 30-750 °C, collecting diffraction powder patterns in air every 50 °C. The results of this characterization are reported in Figure 31. Hexagonal $La_2O_2CO_3$ is thermally stable and no change in its diffraction pattern occur up to 400 °C; however, above this temperature a reorganization of its crystal structure leads to the segregation of a tetragonal $La_2O_2CO_3$ phase. In the temperature range 400-600 °C, LAR02 consists of a mixture of hexagonal and tetragonal $La_2O_2CO_3$, but still no decarboxylation occurs. Finally, above 600 °C the reflexes of the tetragonal phase suddenly disappear in favor of the ones of a hexagonal La_2O_3 phase, which coexist with hexagonal $La_2O_2CO_3$ and develops completely at 750 °C. At this temperature, the hexagonal $La_2O_2CO_3$ is completely disappeared. The temperature range of $La_2O_2CO_3$

decomposition obtained by thermal XRD characterization overlaps well with the one obtained by means of TGA.
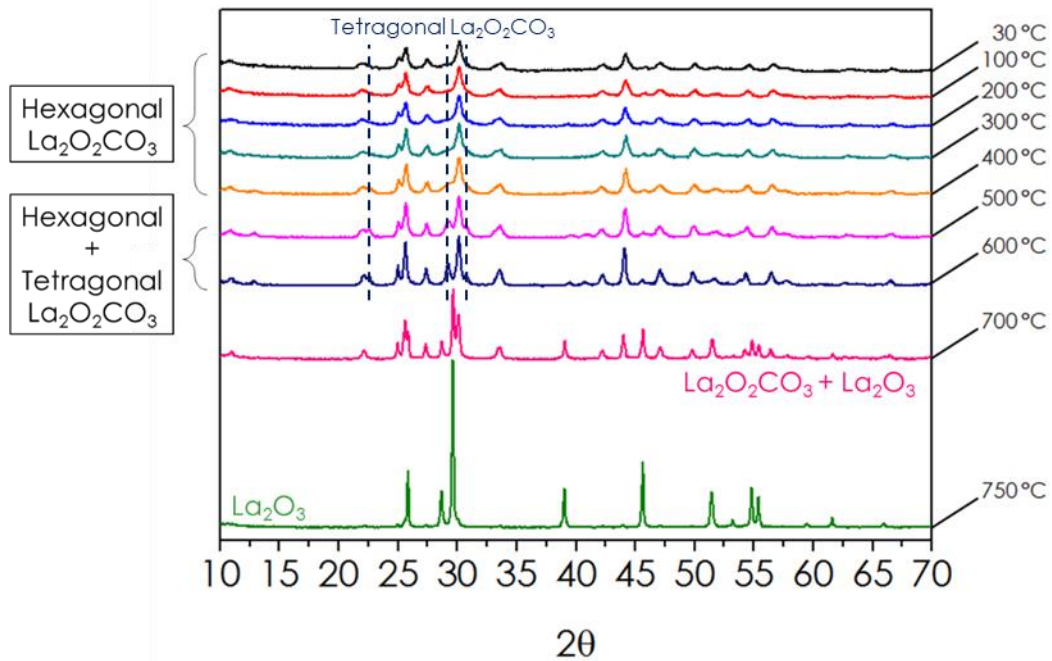
*Figure 31: Temperature programmed XRD patterns of La_2O_3 catalyst after reaction with PA at W/F=0.2 s*g/mL.*

In conclusion, the weight loss between 274 and 371 °C detected with TGA, which coincides with the temperature at which PA ketonization occur, together with the thermal stability of $La_2O_2CO_3$ up to 600 °C demonstrated by means of thermal XRD and TGA, allowed speculating the catalytic cycle for PA bulk ketonization over La_2O_3 reported in Scheme 30.
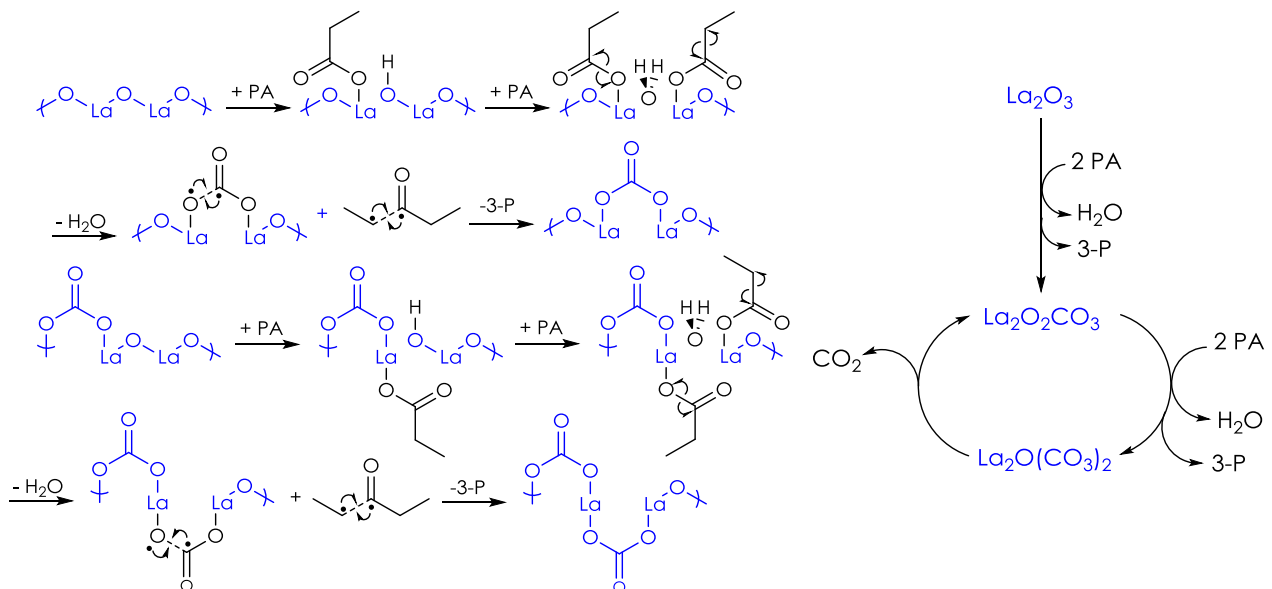
Scheme 30: proposed catalytic cycle for PA ketonization over La_2O_3.

4.3 Conclusions

The ketonization of PA was investigated over several catalytic systems consisting of metal oxides of Al, Zr, La and Si and metal phosphates of Al, Zr and La in order to investigate how acid-base properties of catalysts influence the reaction. Results shown and discussed in this Chapter indicate that ketonization of PA occurs to a certain extent over all catalytic systems investigated. The catalytic performances (from the most active ketonization catalyst to the least active) can be reassumed as follows: ZrO_2 > La_2O_3 > $AlPO_4$ > $Zr/P/O$ > γ-Al_2O_3 > $LaPO_4$ > SiO_2. Amphoteric (ZrO_2) and strongly basic (La_2O_3) catalysts are the most active in agreement with the literature and both do not show any sign of deactivation in the short period (6-8 hours of time on stream).

Three main side reactions reduce the yield of the desired product (3-P) and all of them are favored by an increase of reaction temperature: 1) the consecutive aldolic condensation of 3-P, over all catalysts; 2) the formation of PAN via a ketene intermediate over MPOs (the selectivity towards the anhydride increase with a decrease in cation acidity); 3) the direct decarboxylation of PA into ethylene, H_2 and CO_2 at temperatures higher than 400 °C.

In agreement with the literature, over La_2O_3, PA ketonization occur via a bulk mechanism, as demonstrated by means of ATR, XRD and TGA characterizations of the catalyst after reaction, which consist mainly of $La_2O_2CO_3$. The thermal stability of such oxycarbonate compound of Lanthanum up to 700 °C indicates that it is very likely to be the real catalytic specie of La during PA ketonization.

From a mechanistic point of view, results obtained over MPOs and SiO_2 indicates that the presence of basic sites capable to activate PA towards ketonization by means of direct α-hydrogens abstraction is not mandatory. In fact, oxygen atoms in these catalysts possess negligible basicity, as predicted based on the low ionic character of the Si-O and P-O bonds in SiO_2 and MPOs and as demonstrated by means of CO_2-TPD characterization. It has been therefore proposed that α-hydrogens of PA over acidic catalysts is removed because of a keto-enolic tautomerism between surface carboxylate and 1-hydroxy-enolate ions. Since the activity of MPOs is proportional to the Lewis acidity of the metal cation, such tautomerism is likely to be favored by stronger acidic sites; the lower activity of γ-Al_2O_3 in respect to $AlPO_4$, the latter being more acidic than the former, is in agreement with the aforementioned conclusion. The high catalytic activity of La_2O_3 depends on the high strength of its basic sites, capable to abstract directly the α-hydrogens of PA. Amphoteric ZrO_2 is the most active catalyst because of the presence of balanced basic and acidic sites on its surface, which give rise to a cooperative effect during α-hydrogens abstraction.

5 MP/MeOH mixture reaction over ketonization catalysts

5.1 Aim of this Chapter

As described in Chapter 4.3.1 and 4.3.1.1, bio oils from lignocellulosic materials pyrolysis are complex mixtures containing, among other products, carboxylic acids, esters, aldehydes, alcohols and ketones. Esters may undergo ketonization as well as acids, therefore the investigation of their ketonization possesses scientific and industrial relevance too. Moreover, esters can be formed over ketonization catalysts during the catalytic upgrading of bio oils due to the presence of aldehydes, which can react to produce esters via a Tishchenko reaction, and because of the presence of alcohols, which can produce esters via transesterification of acids. Therefore, in order to improve the quality of such mixtures, the ketonization of esters and the parallel reactions of esters with other components of the mixture (e.g. alcohols) over ketonization catalysts needs to be investigated. The same is true for the consecutive reactions of the newly formed ketones and the other components of the mixture. The aim of this Chapter was the study of the reaction of a MP/MeOH mixture over the catalytic systems investigated for PA ketonization in Chapter 4, which was carried out in order to assess the complex reaction scheme arising from several possible reaction pathways:

1. MP propionate ketonization to 3-P.

2. MP hydrolysis to PA and MeOH.

3. MeOH dehydrogenation to FAL.

4. Hydroxy-methylation/dehydration with FAL of compounds containing acidic α-hydrogens.

5. Retro-Tishchenko reaction of esters that produce aldehydes.

6. H-transfer hydrogenolysis of esters to the respective aldehydes with MeOH or FAL as H-donors.

7. H-transfer hydrogenation of C=O double bonds in aldehydes with MeOH or FAL as H-donors.

8. H-transfer hydrogenation of C=C double bonds in compounds formed by the reaction of FAL with molecules containing acidic α-hydrogens.

Such study represents also a preliminary step towards the synthesis of MMA which will be discussed in Chapter 6, for two reasons. The former is related to the choice of the most favorable reactant for MMA synthesis. In fact, both bio-based MP and bio-based PA could be used for MMA synthesis, but the choice of MP is more favorable because it already contains a methoxy group and its use reduce the number of step required to obtain the desired product. However, the different reactivity of acids and esters towards the parasitic ketonization should also be considered to justify the choice of MP or PA as reactant for MMA synthesis. In order to do so, the homo-ketonization of PA and MP was compared over ZrO_2, the most active catalyst among those investigated in Chapter 4. Finally, the catalyst screening for the reaction of MP/MeOH mixture presented in this Chapter was aimed at identifying the catalyst showing the best compromise between:

1. High MeOH dehydrogenation activity to FAL.

2. High activity for the coupling of FAL with MP.

3. Low activity for ketonization and other detrimental side reactions.

5.2 Introduction

5.2.1 Carboxylic esters ketonization

The ketonic decarboxylation of esters has been intensively investigated over several MOs such as CeO_2 [96], ZrO_2 [97], Ce/Zr/O [98], Mg/Al/O mixed oxides and Al_2O_3 [99]. Since carboxylic esters moiety contains both an acidic and an alcoholic residue, the chain length and branching of the alcoholic residue represent an additional factor influencing the reaction. As an example, Glinski et al [100] investigated the ketonization of ethyl propionate and the one of C_1-C_4 heptanoates [97], and reported that the reactivity of an ester increase with the alcoholic residue chain length and branching, probably because sterically hindered alcoholic residues are better leaving groups. Gaertner et al [98] arrived at the same conclusion comparing the ketonization 1-pentyl hexanoate and 2-pentyl hexanoate over Ce/Zr/O. In another work, the same authors demonstrated that the ketonization of esters proceed slower than the one of the respective acids [90], because their adsorption on catalyst surface is less thermodynamically favorable [98]. They investigated also the ketonization of pentanoic acid in the presence of 1-pentanol and 2-pentanol. Their results indicate that at low temperature, the esterification competes with ketonization of pentanoic acid and both esters and 5-nonanone were present in the reaction mixture. At higher temperatures instead, the esters undergone ketonization too, therefore the reaction mixture consisted of a mixture of ketones. Several authors investigated the adsorption of carboxylic esters on MOs surface using methyl acetate, ethyl acetate and methyl stearate as molecular probe. Bayman et al [101] investigated the adsorption of deuterated and not deuterated ethyl acetate on Al_2O_3 and found that the resulting inelastic tunneling spectrum resemble the one of the respective acid but the feature relative to methoxide species are absent. In other words, they claim that only acetate ions bond the surface (scheme 31, left side). Other authors [102] reported that over Al_2O_3 methyl stearate dissociate into surface stearates and methoxides species, detected by means of infrared analyses. In this paper, it is unclear if adsorption occurs on Lewis or Brønsted sites, because the spectral region of the O-H stretching is not shown. However, another work on Al_2O_3 [81] clearly shows that in the adsorption of acids (PA and AA) results in a negative band in that region, therefore it is likely that the participation of surface hydroxyl groups is involved in the formation of carboxylates and methoxides (Scheme 31, right side).
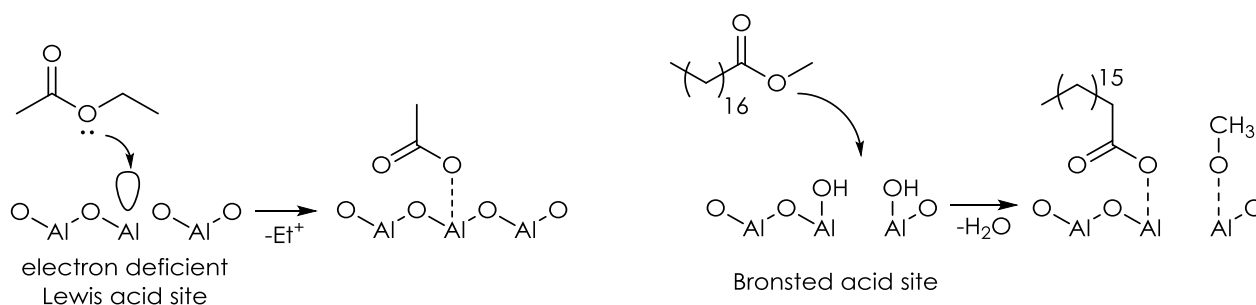
Scheme 31: adsorption of ethyl acetate and methyl stearate on Al_2O_3, in the case of chemisorption on Lewis sites (left) or Brønsted sites (right).

Several authors *[103, 104, 105]* proposed that ethyl acetate adsorbs over basic MgO following the abstraction of the acidic α-proton, basing their claims on DFT calculations, MS

spectroscopy and *in situ* XPS experimental results (Figure 32). However, a route involving ester hydrolysis thanks to basic hydroxyl groups nucleophilicity was also considered *[106]*.
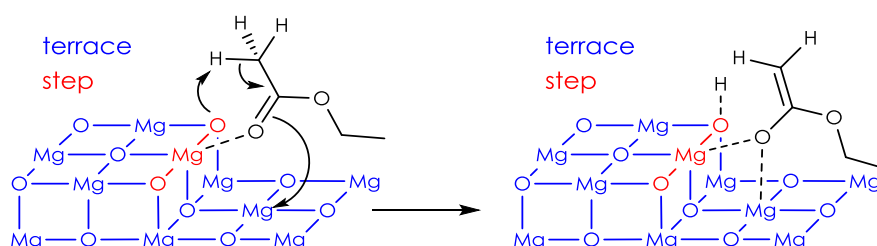
Figure 32: model of ethyl acetate adsorption/interaction over MgO surface.

Tamura et al [107] investigated the adsorption of methyl acetate on CeO_2 and analyzed the resulting surface species by means of *in situ* FT-IR, concluding that this ester is chemisorbed via dissociative chemisorption producing surface methoxy groups and acetates with a chelating bidentate configuration as depicted in Figure 33.
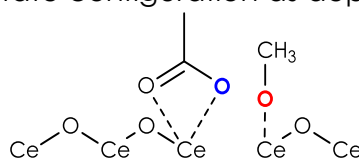
Figure 33: methyl acetate adsorption over CeO_2 as proposed by Tamura et al.

It is worth noticing that the authors do not mention any hydroxyl group participation or if a change in oxidation state Ce^{4+} follows the chemisorption. In other words, it is not clear if the catalyst provides one of the two oxygen in blue and red in Figure 33, or if water is released upon chemisorption. Since CeO_2 is a basic oxide just like MgO, it might be asked why the adsorption of esters on their surface is so different. A possible answer relates to the reducibility of CeO_2: electrophilic anionic holes can act as strong Lewis acids and might cleave the esteric bond, while such kind of Lewis acidic sites are absent on MgO surface. Natal-Santiago et al [108] stated that methyl acetate do not dissociate on SiO_2 surface but its interaction consists of H-bonding between 1, 2 or 3 silanol groups, justifying their claims with FT-IR analyses and DFT calculations (Figure 34).
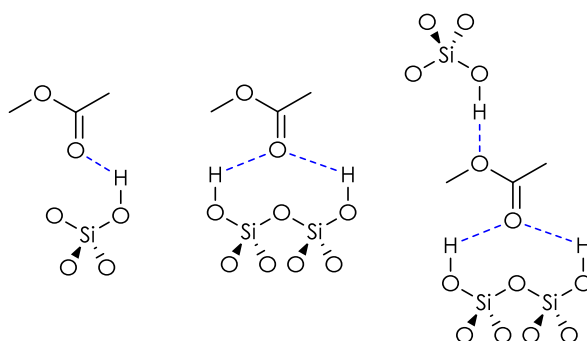
Figure 34: the three mode of adsorption of methyl acetate over SiO_2 as proposed by Natal-Santiago et al.

The picture resulting from these studies suggests that carboxylic esters dissociate on metal oxide surfaces producing surface carboxylates and methoxides residues, as it happens for carboxylic acids (which dissociate producing carboxylates and hydroxyl groups), except for SiO_2 and MgO. Given the chemical similarity between the acids and esters and their similar behavior on MOs surfaces, esters ketonization would be expected to resemble somehow that of acids. Gaertner et al [109] proposed that if enough water and acidic sites are present on Ce/Zr/O surface the preferred reaction pathway involves the hydrolysis of the ester and subsequent ketonization of the resulting acid with an ester or another acid, as depicted in Scheme 32, pathways a, for the ketonization of ethyl acetate. In both cases the enolic fragment derives from the acid, while the carboxylic fragment may derive from an

acid (pathway a2) or an ester (pathway a1). In the former case the reaction products will be acetone, CO_2 and 2 molecules of EtOH, while in the latter they will be acetone and CO_2 only, because the water consumed to hydrolyze the ethyl acetate is balanced by the one evolved during the β-keto acid decomposition. Regardless the nature of the carboxylic fragment, the resulting intermediate will be a β-keto acid. Wrzyszcz et al [110] proposed that in the absence of water in the reaction environment, the α-proton abstraction could occur directly on the ester as proposed by other authors in the case of MgO [103, 104, 105]. In this case, the nucleophilic species that will constitutes the enolic fragment in the final ketone will be a 1-alkoxy enolate anion (1-ethoxy enolate in the case of ethyl acetate) and the coupling with another ester will results in the formation of an intermediate β-keto ester, as depicted in Scheme 32, pathways b.
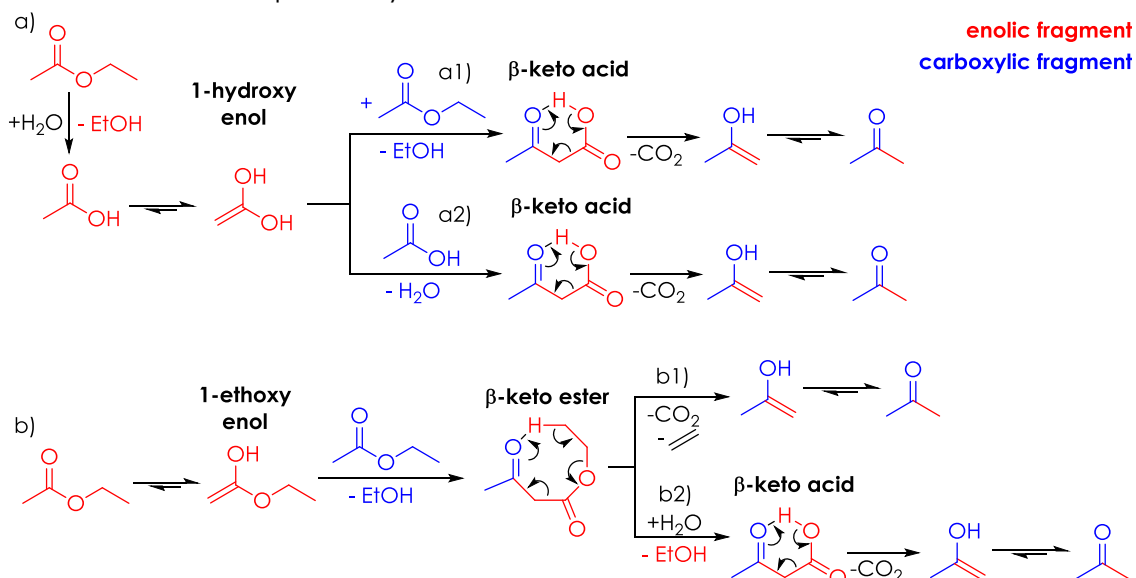
Scheme 32: ketonization of esters: a) via hydrolysis of the ester and acid ketonization (β-keto acid); b) via β-keto ester.

In the literature is reported that the β-keto ester intermediate, once formed, may undergo a monomolecular decomposition (pathway b1 in Scheme 32) or may be hydrolyzed by water (pathway b2). An argument in favor of the former mechanism is that the formation of olefins has been reported by some authors [111]. Regarding the second mechanism instead, if water was present in the reaction environment one would expect the direct hydrolysis of the ester and ketonization of the resulting acid to be the preferred pathway (Scheme 32a).
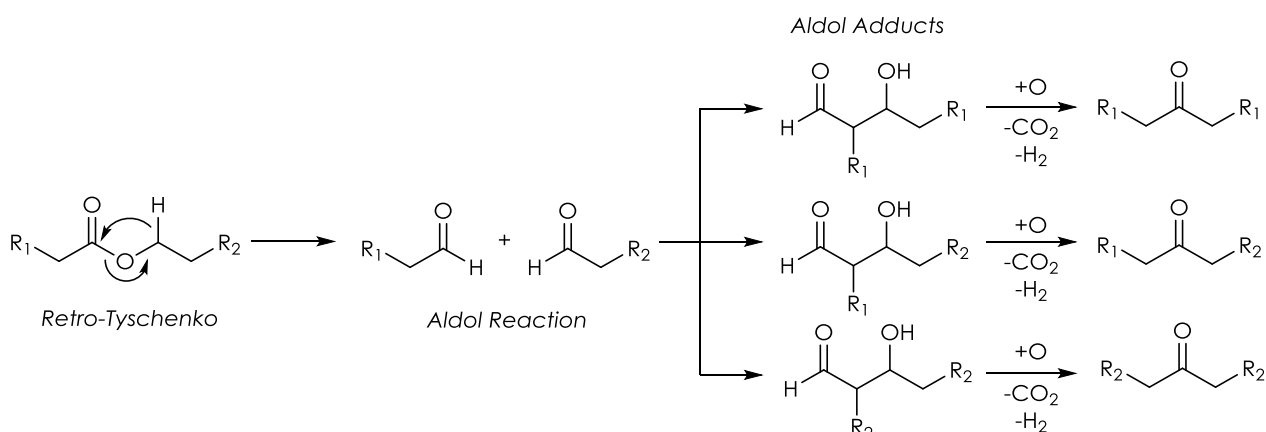
Scheme 33: ketonization of esters via retro Tishchenko, aldol addition and decarbonylation of the resulting aldol.

The last mechanism was proposed by Hendren et al [85] and is depicted in Scheme 33: according to the authors, at high temperatures esters undergoes a retro-Tishchenko reaction over CeO_2 based catalysts and the resulting aldehydes condensate to produce an aldol intermediate, which then decompose into a ketone, CO_2 and H_2 thanks to a lattice oxygen from catalyst surface. This mechanism differs from the others proposed until now for two main reason: 1) it yields a mixture of symmetric and asymmetric ketones when an asymmetric ester is used as reactant and 2) feeding water has a positive effect on the reaction rate, probably because it re-oxides catalyst surface replenishing the oxygens consumed during the oxidative decarboxylation of the aldol. One might argue, however, that the co-fed water can hydrolyze the ester producing a more reactive acid which ketonize following another mechanism. Another research group, investigating the effect of water on the direct ketonization of aldehydes (and not esters), proposed a different mechanism, which involves the oxidation of aldehydes and not the aldol adduct. Actually this mechanism excludes the participation of the aldol adduct as intermediate: aldehydes are oxidized by water over CeO_2 [112] and ZrO_2 [113] surfaces to the respective carboxylic acid, which then undergo classical ketonization. As a proof of the participation of the lattice oxygen of CeO_2 they adduced the fact that its catalytic activity rapidly dropped to zero without water co-feeding due to Ce^{4+} reduction to Ce^{3+}, and obtained a remarkably good correlation between the proposed stoichiometry (Scheme 34) and the composition of their reaction mixtures.
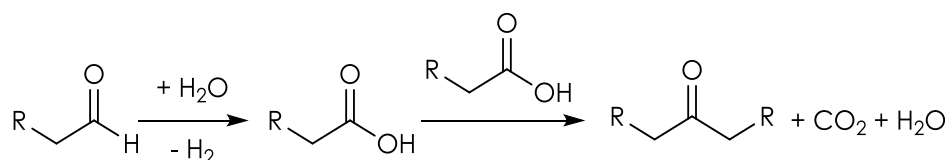
Scheme 34: ketonization of aldehydes via oxidation to the respective acids.

One final pathway deserves to be discussed in order to complete the picture of carboxylic esters ketonization and concerns the ketonization of primary alcohols. Wrzyszcz [110] investigating the ketonization of decanol over γ-Fe_2O_3, obtained results (Figure 35) that completely challenge the literature cited so far.
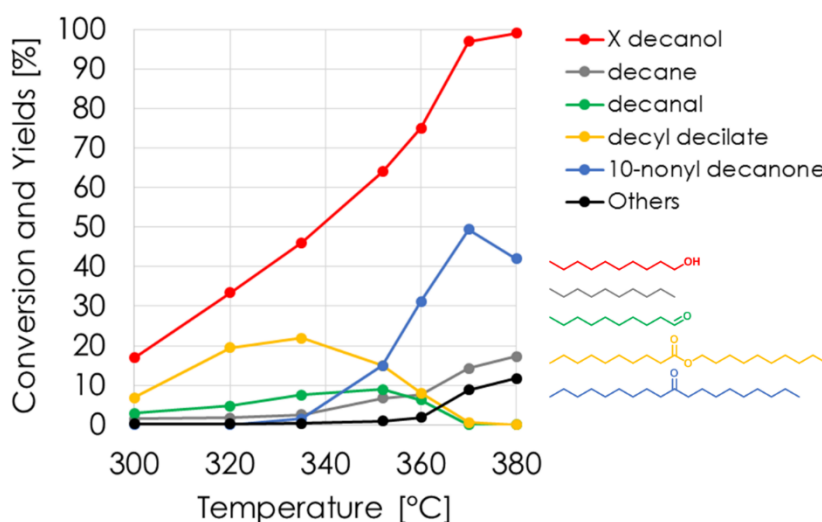
Figure 35: results of decanol ketonization over γ-Fe_2O_3 adapted from ref [110].

This trend overturns the reaction pathway proposed by Hendren et al: in fact, in the one proposed by Wrzyszcz firstly decanol is dehydrogenated to decanal; then, the aldehydes reacts with itself to produce the ester decyl decilate, which finally ketonize via the β-keto ester intermediate. These results suggest that the outcome of Tishchenko reactions over MOs might depends strongly on the composition of the feed. Aldehydes-rich feed might

ketonization via the pathway proposed by Wrzyszcz or Orozco [112, 113], while with esters rich feed the inverse Tishchenko reaction may be favored, as proposed by Hendren.

5.3 Experimental

5.3.1 Catalysts synthesis and characterization

5.3.1.1 MgO

Magnesium oxide (MgO) was synthesized according to a co-precipitation technique. A solution of $Mg(NO_3)_2*6H_2O$ (1 mol/L) in deionized water was added dropwise under vigorous stirring to a solution of $Na_2CO_3*10H_2O$ (1 mol/L) maintained at a temperature between 50 and 60 °C. Prior to start the addition of the metal nitrates the pH of the carbonate solution was adjusted with concentrated HNO_3 to the value of 10, and maintained between 9.0 and 10.1 during the precipitation with concentrated aqueous NaOH. The pH was monitored by means of an Amel Instrument 380 pH-meter, calibrated with two buffers at pH 7 and 13. The resulting magnesium hydroxide suspension was aged under stirring for 45 minutes, filtered by means of a Büchner funnel and washed with distilled water (330 mL/g of catalyst) to remove residual nitrates and carbonates ions. After drying (110°C overnight), the hydroxide precursor was crushed and calcined in static air at 500 °C (5°C/min)

5.3.1.2 Other catalysts

Other catalyst used were γ-Al_2O_3, ZrO_2, La_2O_3, $AlPO_4$, Zr/P/O and $LaPO_4$. Detailed informations on their synthesis can be found in Chapters 4.1.3.1, 4.1.3.2, 4.1.3.3 and 4.1.3.4.

5.3.1.3 Catalysts Characterization

The XRD pattern and N_2 adsorption/desorption isotherms for MgO are reported in Figure 36: it consists of a pure periclase phase and it shows a type IV isotherm (mesoporous, SSA=181 m^2/g).
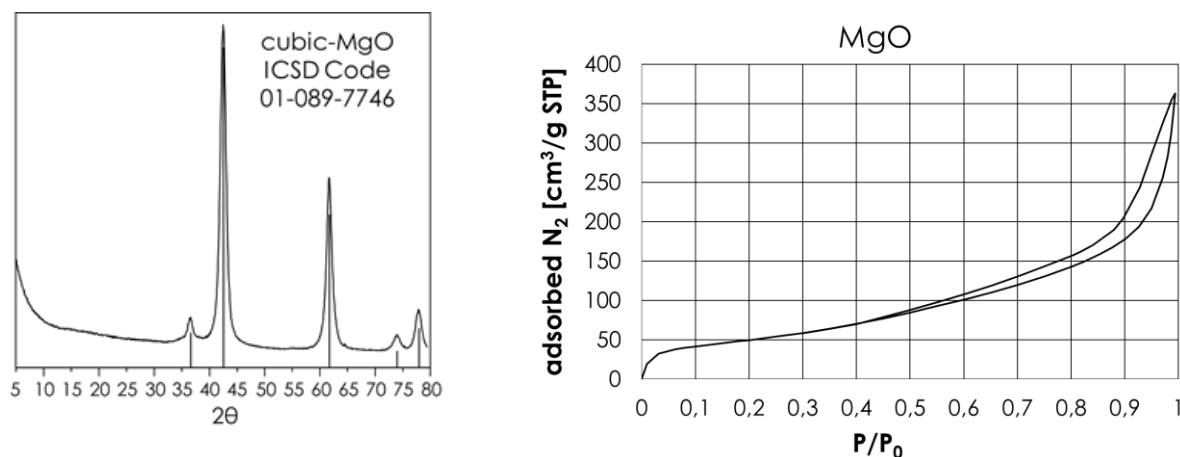
Figure 36: XRD powder pattern and N_2 adsorption/desorption isotherms of MgO.
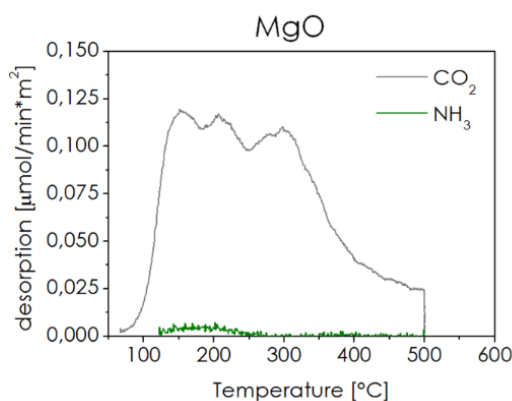
Figure 37: CO_2 and NH_3 temperature programmed desorption profiles of MgO.

MgO is a well-known basic material and the CO_2 and NH_3-TPD characterization reported in Figure 37 confirms this claim: the CO_2 desorption profile presents three maxima centered on 155, 210 and 295 °C; CO_2 however keeps desorbing up to 500 °C. These results indicate that this catalyst possess weak, medium strength and strong basic sites. Mg^{2+} is an electropositive cation possessing little Lewis acidity and its oxide desorbs negligible amounts of NH_3, with the maximum of desorption centered around 170 °C. A more detailed discussion on MgO crystal structure and acid-base properties can be found in Chapter 6.3.1.2.

5.3.2 Catalytic tests

5.3.2.1 Catalytic activity of ZrO_2

As a preliminary study, the homo-ketonization of 6% MP in N_2 was investigated over monoclinic ZrO_2 at 400 °C and W/F = 0.8 and W/F = 0.2 s*g/mL in the absence of MeOH (Graph 9). The products of the reaction were 3-P, 2-methyl-3-pentenone (M-3Pe), 2-methyl-3-pentanone (M-3Pa), small amounts of MMA, methyl isobutyrate (MIB), 2-methyl-propanol (2MP), isobutylene (IB), 2,4-dimethyl-3-pentenone (DM-3Pe), 2,4-dimethyl-3-pentanone (DM-3Pa) and unknown compounds. The yields of MMA, MIB, 2MP and IB are reported together (green bar).
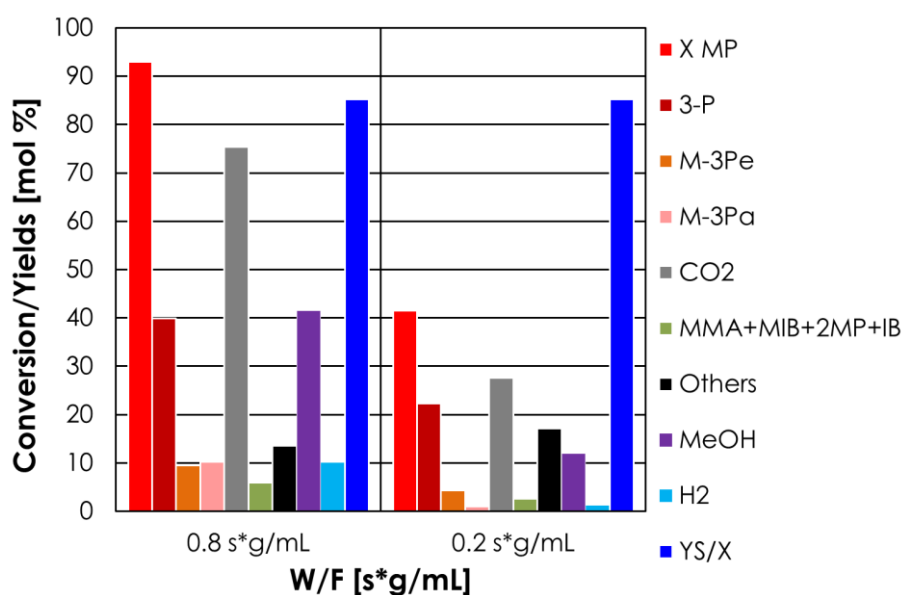
Graph 9: Gas-phase ketonization of MP as a function of W/F: catalyst = ZrO_2; temperature 400 °C; MP/N_2 feed composition [mol %] = 6/94. Others includes unknown compounds, PA, MAA, IBA, DM-3Pa and DM-3Pe. Yields calculated in terms of moles.

MP/MeOH mixture reaction over ketonization catalysts

Scheme 35: MP ketonization via 1-methoxy enolate and β-keto ester hydrolysis with water.
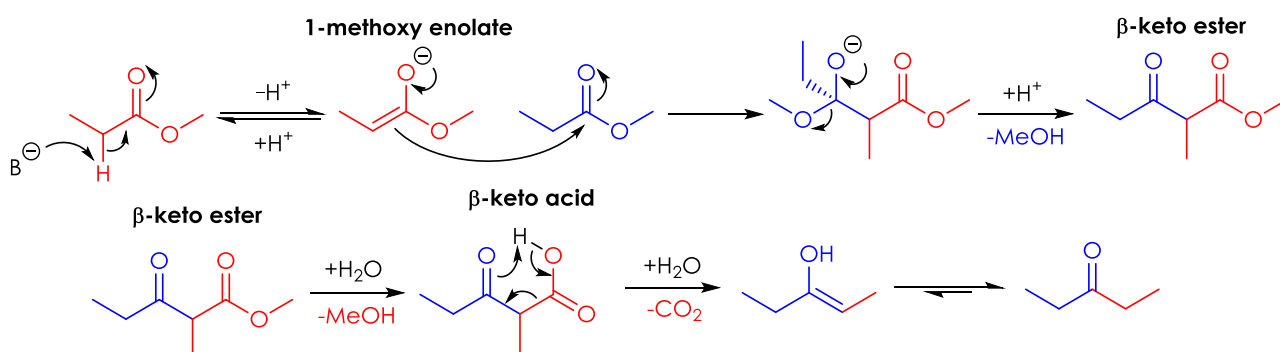
In agreement with the literature, MP proved to be less reactive than PA. In fact, even if its catalytic ketonization (Scheme 35) was investigated at a higher temperature than the one used for PA (400 °C instead of 350 °C), lower conversions were obtained. Moreover, the reaction of MP over ZrO_2 was less selective towards 3-P than the one of PA due to the occurrence of several parasitic reactions. MP ketonization is expected to occur according to Scheme 53, because the monomolecular decomposition of the β-keto ester require the presence of a β-hydrogen on its alcoholic residue; in other words, alkyl β-keto esters can decompose producing an olefin only if their alkyl chain contains at least 2 carbon atoms. To avoid confusion, refer to Figure 38:
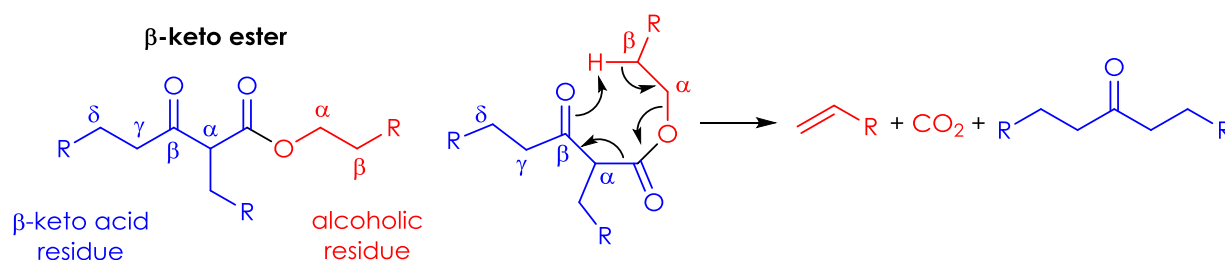
Figure 38: generic b-ketoester monomolecular decomposition to CO_2, ketone and olefin.

The MeOH co-produced by MP ketonization undergoes partial dehydrogenation over surface basic sites and the so obtained FAL reacts with compounds containing α-hydrogens, as depicted in Scheme 36:
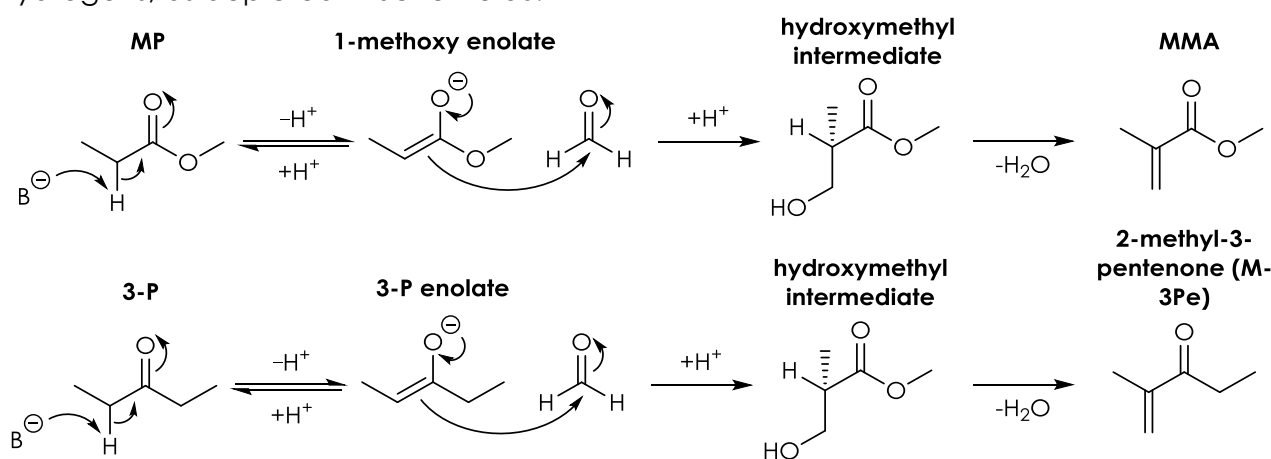
Scheme 36: hydroxy methylation/dehydration with FAL of compounds containing a-hydrogens.

It is worth noticing that 3-P possess a higher number of acidic α-protons in respect to MP. Moreover, MP α-protons are less easily abstracted from basic sites than the ones of 3-P because they are less acidic: the presence of the esteric group makes the negative charge delocalization in the enolate less efficient, as depicted in Scheme 37.

75
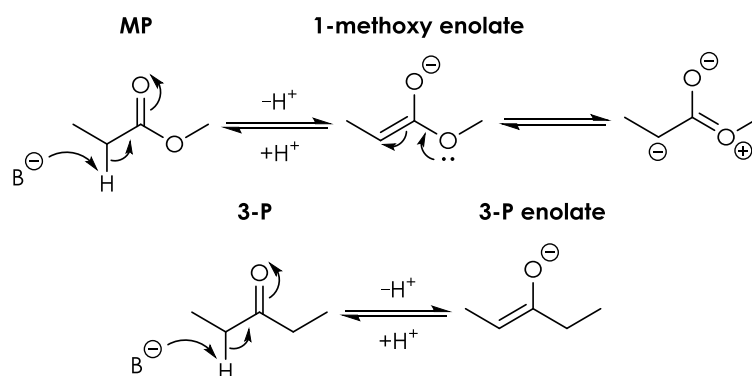
Scheme 37: electronic effects in enolate anion produced by the deprotonation of MP and 3-P.

The higher yields in products of 3-P hydroxy-methylation/dehydration with FAL in respect to those from the same reactions occurring on MP can be explained with the higher rate of proton abstraction from 3-P. A likely explanation for the formation of unsaturated compounds such as M-3Pa, MIB and 2MP, is the occurrence of H-transfer hydrogenation reactions with both MeOH and FAL as the H-donor. An argument in favor of the participation of FAL to H-transfer hydrogenations is related to the yield in H_2, which were systematically lower than the one in MeOH. Unluckily, FAL was not detectable with the analytical system in use. The largely accepted mechanism for the H-transfer hydrogenation of C=O double bonds with an alcohol over metal oxide catalysts is commonly referred to as the Meerwein−Ponndorf−Verley mechanism (MPV) [114]. When an alcohol acts as the H-donor, the α-H is transferred from the α-C of the alcohol to the carbonyl carbon in a concerted step via a six-membered-ring intermediate, without the formation of a metal hydride; this is why the MPV mechanism is also called the direct hydrogen transfer pathway. The MPV mechanism reaction in the liquid phase is catalyzed by aluminum alkoxides [115], but a strong parallel can be drawn for heterogeneous catalysts: Lewis acid site and a neighboring base site can catalyze H-transfer reactions following the MPV mechanism depicted in Scheme 38 [116].
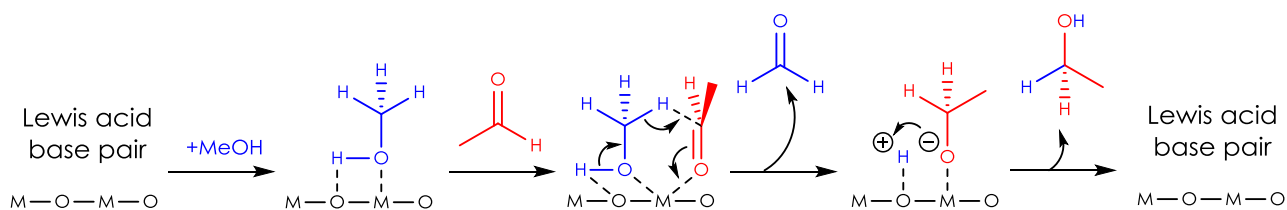
Scheme 38: heterogeneous MPV mechanism of acetaldehyde hydrogenation with MeOH involving the adsorption of two molecules on the same Lewis acid site adapted from the one proposed by Gilkey et al [116].

This mechanism has a general value and slight difference can exist between the reaction over basic and acidic catalysts. As an example, basic catalyst directly abstracts the alcoholic proton from MeOH. The strong bond between the basic site and the proton allows the chemisorption of the methoxide anion on the neighboring weak acidic metal cation. On acidic catalysts instead, a strong interaction between the alcoholic oxygen and an electron-deficient Lewis site weaken the O-H bond of alcohol allowing proton abstraction by a weak basic site. As in the case of ketonization, a synergistic effect of Lewis acid-base pairs in these reaction can be expected and amphoteric catalyst are generally considered more active [116]. The formation of a six membered ring transition state has been proposed for Al_2O_3 and ZrO_2. Over some catalysts, the formation of such intermediate, which require the adsorption of two molecules on the same Lewis acid site, could be unfavored. However, H-transfer may occur as well following the alternative mechanism depicted in Scheme 39. This mechanism has been proposed, for example, for catalysts possessing very weak Lewis sites such as MgO.

MP/MeOH mixture reaction over ketonization catalysts
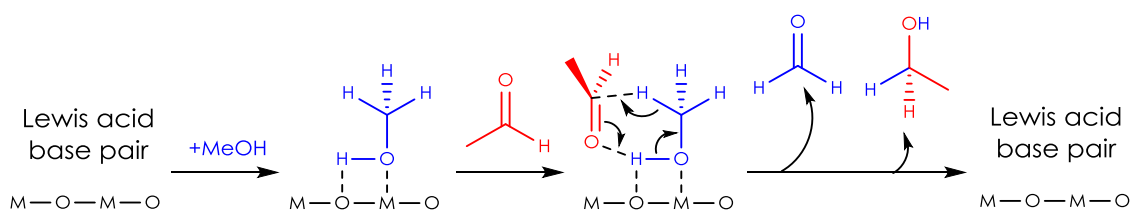
Scheme 39: heterogeneous MPV mechanism of acetaldehyde hydrogenation with MeOH that does not involve the adsorption of two molecules on the same Lewis acid site; adapted from the one proposed by Gilkey et al [116].

H-transfer hydrogenation has been reported to be effective for C=O [117] and C=C [118] double bonds hydrogenation and for C-O bonds hydrogenolysis [119]. Therefore, the formation of M-3Pa and MIB can be explained with the H-transfer hydrogenation of the C=C double bonds of M-3Pe and MMA with MeOH or FAL as H-donors (Scheme 40, reactions a and b respectively).
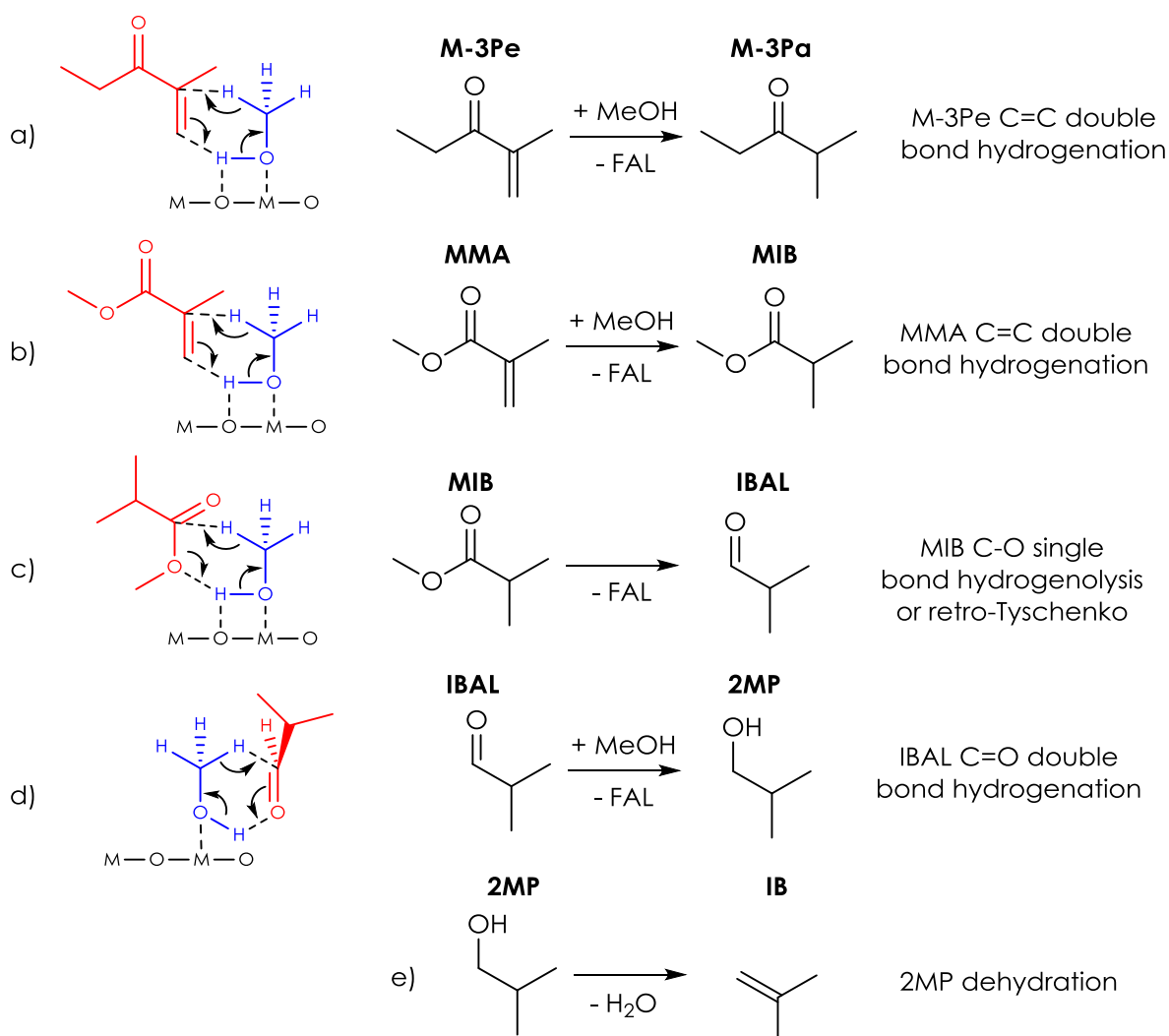
Scheme 40: proposed intermediates for H-transfer hydrogenation reactions occurring over ZrO$_2$ with MeOH as H-donor and 2MP dehydration to IB.

The formation of 2-methyl propanol (2MP) can be explained considering a H-transfer hydrogenolysis or a retro-Tishchenko of MIB to isobutyraldehyde (IBAL) (Scheme 40, reaction c), followed by the H-transfer hydrogenation of the C=O double bond of the latter (Scheme 40, reaction d). IBAL, however, was not found among reaction products perhaps because is too reactive and completely consumed reacting with MeOH or FAL. Finally, IB forms via dehydration of 2MP, which easily occur at high temperatures (Scheme 40, reaction e). The

intermediates for these reactions are reported in Scheme 40, in analogy with the general mechanism reported in Scheme 38 and 39. The deficit on molar balances in the catalytic test at W/F = 0.8 s*mL/g is probably due to parasitic aldol reactions of ketones that led to heavy products condensation on the inner wall of the reactor. In fact, dark brown spots attributable to organic heavy molecules where found below the catalytic bed, which is relatively colder than the reaction zone. These reactions, just like ketonization, require the abstraction of a α-proton, therefore their occurrence over ZrO_2, which is the most active catalyst for ketonization, is not surprising. The higher yield in CO_2 in respect to the one of ketones in the same experiment are attributable to MeOH/FAL consecutive oxidation and decomposition. Moreover, the evidence that MP ketonization produce MeOH implicates that the conversion of the latter in catalytic tests carried out feeding a MP/MeOH mixture may be incorrect or even become negative. In fact, if only ketonization occurs and the MeOH entering the reactor does not react, the outgoing flow will contain more MeOH than the ingoing one. For this reason, MeOH conversion has been monitored during catalytic tests but its conversion will not be shown in the following Graphs. The results of the catalytic tests carried out feeding a MeOH/MP/N_2 mixture (molar fractions = 12/6/82) over ZrO_2 as a function of reaction temperature are shown in Graph 10. Ketonization was the main reaction in the temperature range investigated (300-400 °C) and as expected, as a result of the dilution of MP into MeOH the sum of yields of ketones at 400 °C (40.1 %) is lower than the one obtained feeding MP alone (60.7 %).
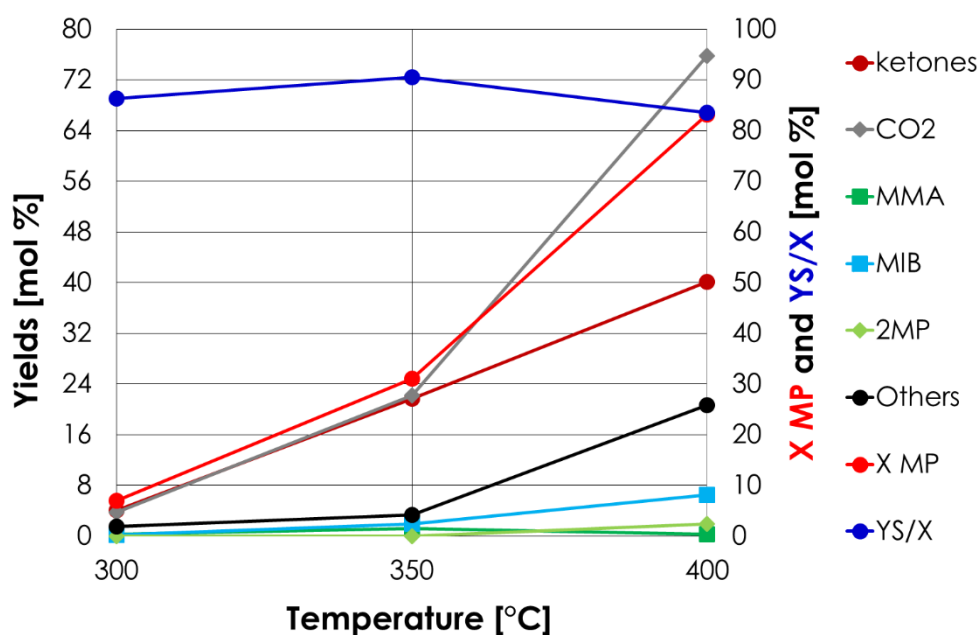
Graph 10: Gas-phase ketonization of MP in presence of MeOH as a function of reaction temperature: catalyst = ZrO_2; MP/MeOH/N_2 feed composition [mol %] = 6/12/82; W/F = 0.8 s*g/mL. Others includes unknown compounds, PA, MAA, IBA, ethylene, propylene, IB. Yields calculated in terms of moles.

The opposite happens for products of MP hydroxy-methylation/dehydration: their yield at 400 °C (8.8 %) is slightly higher than the one obtained feeding MP alone in the same conditions (6.0 %). However, in this case the degree of reduction of these products is lower: MIB is the main product (6.5 %) followed by 2MP (1.9 %). When MP was fed alone in the same conditions, IB was the main product (3.1 %), followed by MIB (2.1 %). One would expect that the higher excess of MeOH would have led to a higher degree of reduction; instead, this is not the case, perhaps because the adsorption of MP alone and its subsequent dissociation over catalyst surface leads to the formation of carboxylate anions and reactive methoxy species in close vicinity. The trend that emerges from results in Graph 10 is that ZrO_2 do not possess a strong dehydrogenating activity towards MeOH; in fact, even at 400 °C and in excess of MeOH (MeOH/MP feed molar ratio = 2) the hydroxy-methylation/dehydration of

MP/MeOH mixture reaction over ketonization catalysts

MP do not compete with ketonization, which is much faster. The yield in CO_2 follows closely the one of ketones until 350 °C. Above this temperature CO_2 yield (75.8 %) almost double the one of ketones (40.1 %) and the molar balance become worse. These results suggest that ketones undergo aldol reaction extensively at temperature higher than 350 °C, forming heavy products on reactor walls, but a contribution from MeOH/FAL decomposition cannot be ruled out. The distribution of ketones obtained in the same catalytic test is reported in Graph 11. 3-P is the main product in all the temperature range investigated. At 350 °C M-3Pe is obtained in yields comparable to the ones of MMA and MIB at the same temperature (1.7 %, 1.2 % and 1.9 % respectively). This fact is not in contrast with the higher reactivity of 3-P in respect to MP towards hydroxy-methylation and dehydration. In fact, at 350 °C X MP was 31.1 %, which means that MP was more than two times more concentrated than 3-P in the reaction environment. Raising reaction temperature up to 400, X MP reached 83.1 % and the yields in MMA dropped to zero, while the one of MIB built up to 6.5 %. In the same conditions, the yields in M-3Pe and M-3Pa were 6.5 % and 7.1 % respectively. The distribution of ketones obtained over ZrO_2 substantially confirm the pathway for the formation methylated pentanones and pentenones previously proposed: at first M-3Pe is formed by hydroxy-methylation and dehydration of 3-P with FAL at 350 °C. Raising reaction temperature to 400 °C M-3Pe reduction via H-transfer hydrogenation mechanism became favored leading to the formation of M-3Pa.
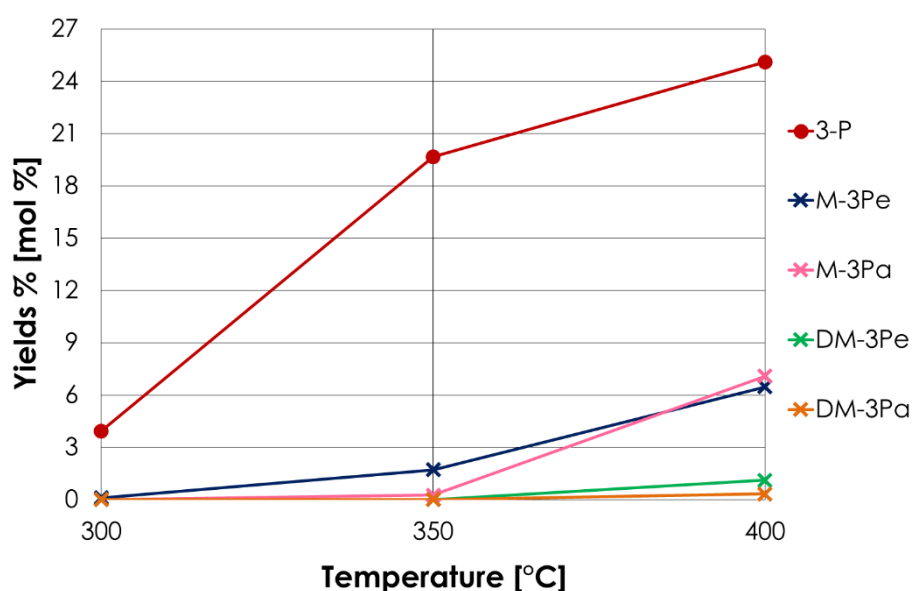
Graph 11: Ketones distribution in the gas-phase ketonization of MP in presence of MeOH as a function of reaction temperature: catalyst = ZrO_2; MP/MeOH/N_2 feed composition [mol %] = 6/12/82; W/F = 0.8 s*g/mL. Yields calculated in terms of moles.

In order to confirm the mechanism proposed for IB formation (e.g. dehydration of 2MP) and clarify all the possible pathways that could led to 2,4-dimethyl-3-pentanone (DM-3Pa), 2% 2-methyl propanol (2MP) in N_2 was fed alone over ZrO_2 in the reaction conditions previously investigated. In this way, we wanted to confirm the dehydration pathway toward IB and rule out (or confirm) the ketonization pathway of alcohols proposed by Wrzyszcz [110] and cited at the end of Chapter 5.2.1. The results of this catalytic test are shown in Graph 12. At the lower temperature, the stream exiting the reactor consisted of IB (10.4 %), IBAL (7.22 %), isobutyl isobutyrate (IBIB, 12.4 %), DM-3Pa (8.5 %) and unknown products. Raising reaction temperature IBAL and IBIB disappeared, leaving IB and DM-3Pa the only products of the reaction, together with unknown compounds. These results substantially confirm the pathway proposed by Wrzyszcz, depicted in Scheme 41 for 2MP. Two equivalents of IBAL, formed by means of 2MP dehydrogenation, undergo a Tishchenko reaction to produce IBIB, which then couples with another equivalent of IBIB to produce DM-3Pa. IBIB ketonization

co-produce CO_2 and two equivalents of 2MP, while IB is entirely produced by means of 2MP dehydration and not via monomolecular decomposition of the β-keto ester.
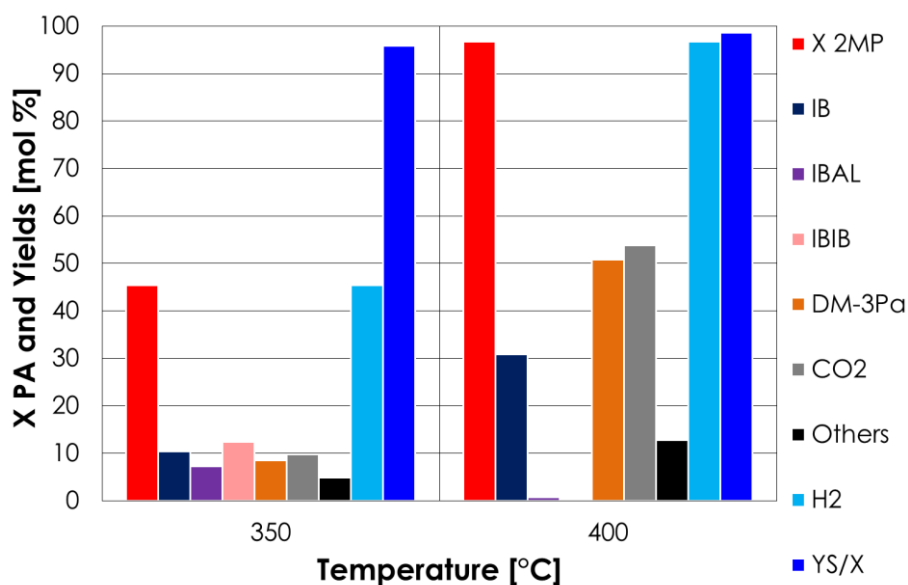
Graph 12: Gas-phase reaction of 2MP as a function of reaction temperature: catalyst = ZrO_2; MP/MeOH/N_2 feed composition [mol %] = 2/98; W/F = 0.8 s*g/mL. Others includes unknown compounds, PA, MAA, IBA, ethylene, propylene, IB. Yields calculated in terms of moles.
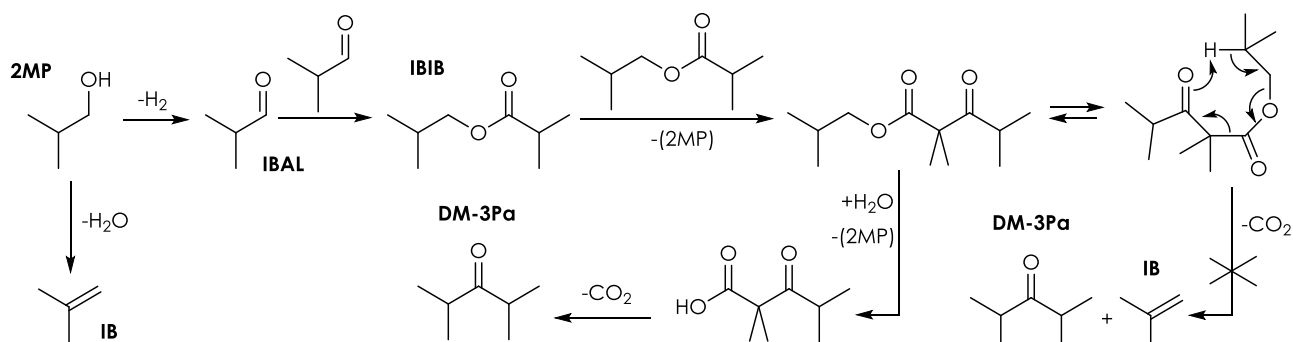
Scheme 41: proposed reaction scheme for 2MP ketonization over ZrO_2.

This fact resulted clearly from molar balances because under the hypothesis that IB forms in equal amounts together with CO_2 and DM-3Pa, the maximum obtainable number of molecules of DM-Pa would have been lower. Results obtained showed that under that hypothesis, the YS/X would be higher than 100 %. Another argument against the monomolecular decomposition of the β-keto ester is related to yield of IB, which should be equal or higher to the one of DM-3Pa, and instead is lower. Scheme 42 (next page) shows the stoichiometry of the reactions involved and the stoichiometric factors employed for calculations. The results of the last catalytic tests demonstrate that ketones may form following a completely different pathway from the one proposed before and highlight a high degree of complexity of the overall reaction scheme that can occur over catalyst surface. In fact, DM-3Pa is not the only ketone that might be formed by alcohols: as an example, 3-P may be formed from PrOH obtained by consecutive hydrogenolysis and H-transfer hydrogenation of MP. However, even if these results prove that two different pathways may lead to the same product, they also indicate a useful strategy to determine the presence of a contribution of alcohol ketonization. If a ketone forms via alcohols ketonization, the presence of a symmetric ester deriving from the Tishchenko reaction (e.g. propyl propionate, PP, in the case of PrOH) should be detected.
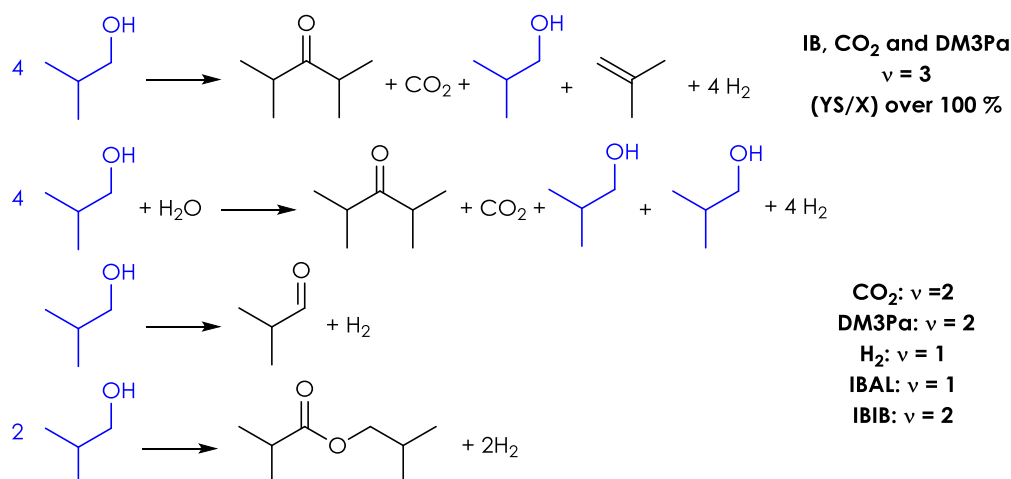
Scheme 42: stoichiometry of the reactions involved in 2-MP ketonization.

5.3.2.2 Catalytic activity of La_2O_3

Graph 13 shows the results obtained feeding the MeOH/MP mixture over La_2O_3 in the temperature range 350-450 °C.
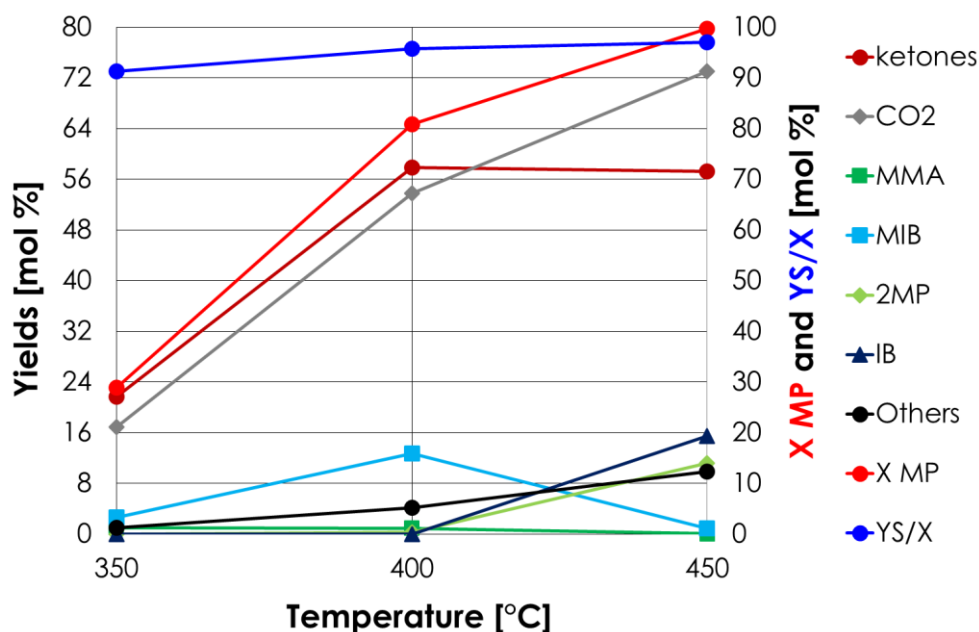
*Graph 13: Gas-phase ketonization of MP in presence of MeOH as a function of reaction temperature: catalyst = La_2O_3; MP/MeOH/N_2 feed composition [mol %] = 6/12/82; W/F = 0.8 s*g/mL. Others includes unknown compounds, PA, MAA, IBA, ethylene, propylene. Yields calculated in terms of moles.*

MP conversion over this catalyst is almost the same obtained over ZrO_2 at the same temperature and ketonization was the main reaction as well. However, La_2O_3 is more selective than ZrO_2 as demonstrated by the higher sum of yields of ketones at 400 °C and the better molar balances. This comparison suggests that the presence of both acidic and basic sites on ZrO_2 surface may favor consecutive aldol reactions occurring on ketones more than the presence of basic or acidic sites only. The trend of CO_2 yield is peculiar: it is lower on the respect of the ketones formed between 350 and 400°C, while at 450 °C it rapidly increases, reaching 73%. These results have been interpreted as follows: at low temperature, a small fraction of the CO_2 produced by MP ketonization remain adsorbed on catalyst surface or react with La_2O_3 due to its very strong basicity. At 450 °C instead, the

contribution of MeOH/FAL consecutive oxidation and decomposition becomes relevant for the overall CO_2 yield. La_2O_3 is also more selective than ZrO_2 for MP hydroxy-methylation/dehydration, even if MMA is never obtained in significant yields due to immediate consecutive H-transfer hydrogenations of its C=C double bond. MIB yield reached 12.7 % at 400 °C; at 450 °C its yield drops to zero because is quickly reduced to 2MP (11.2 %) which simultaneously dehydrates to IB. To sum up, La_2O_3 dehydrogenating properties toward MeOH are superior in respect to that of ZrO_2 but it remains a very good ketonization catalyst. Very high temperatures are required to obtain significant yields in products of hydroxy-methylation (sum of yields of MMA, MIB, 2MP and IB at 450 °C is 27.7 %) and ketonization remains the faster reaction. Moreover, the most valuable products (MMA and MIB) are converted into less valuable C4 molecules by consecutive H-transfer parasitic hydrogenations. The distribution of ketones obtained in the same catalytic test is shown in Graph 14. 3-P is the main product in all the temperature range investigated, but its yield presents a maximum at 400 °C and the drops from 45.2 % to 28.9 %, while the yields in methylated pentanones and pentenones grows linearly with temperature. The comparison between the distribution of ketones (Graph 14) and the sum of their yields (Graph 13) indicates that the total amount of ketones does not change from 400 to 450 °C, but only their degree of methylation. This result suggests that at high conversions it becomes increasingly difficult for MP molecules to encounter each other on catalyst surface and the rate of ketonization drops. This fact favors the hydroxy-methylation of both MP and 3-P.
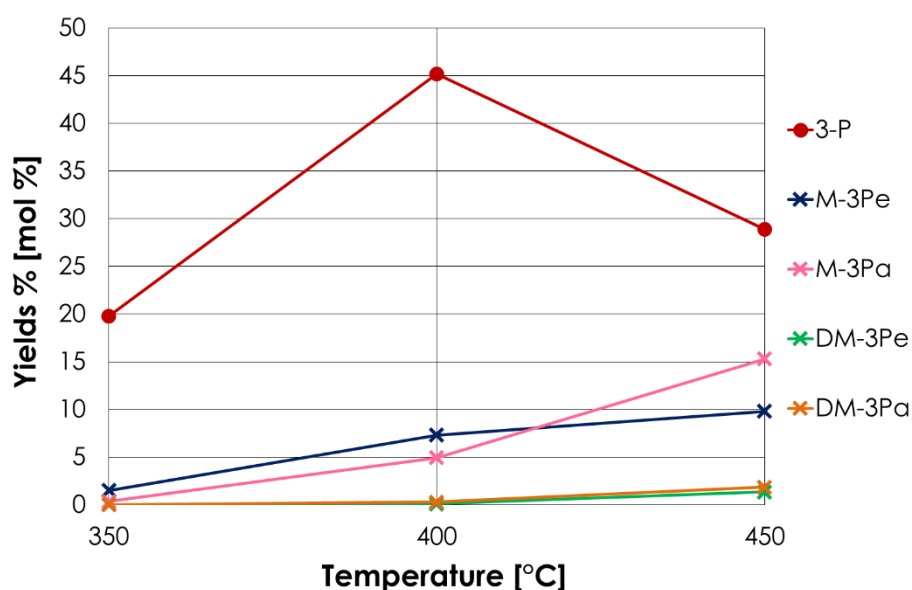
Graph 14: Ketones distribution in the gas-phase ketonization of MP in presence of MeOH as a function of reaction temperature: catalyst = La_2O_3; MP/MeOH/N_2 feed composition [mol %] = 6/12/82; W/F = 0.8 s*g/mL.. Yields calculated in terms of moles.

5.3.2.3 Catalytic activity of MgO

Graph 15 shows the results of the target reaction over MgO as a function of temperature. Between 350 and 400 °C, the only products detected over MgO were ketones, as it were for ZrO_2 and the yield in CO_2 follow closely the one of ketones. The hydroxy-methylation of MP starts to occur at 450 °C as can be deduced from the formation of MIB and 2MP and the trend of CO_2 yield, which become higher than the one in ketones. As it happened for La_2O_3, molar balance at this temperature is good, therefore it has been concluded that ketones aldol condensation is limited, and the surplus of CO_2 is attributable to MeOH/FAL decomposition. Since extensive ketones aldol condensation at high temperature occurred

MP/MeOH mixture reaction over ketonization catalysts

over ZrO_2 (amphoteric) to a significantly higher extent in respect to both MgO and La_2O_3 (basic), a participation of both basic and acidic sites in order to promote the condensation is very likely to occur.
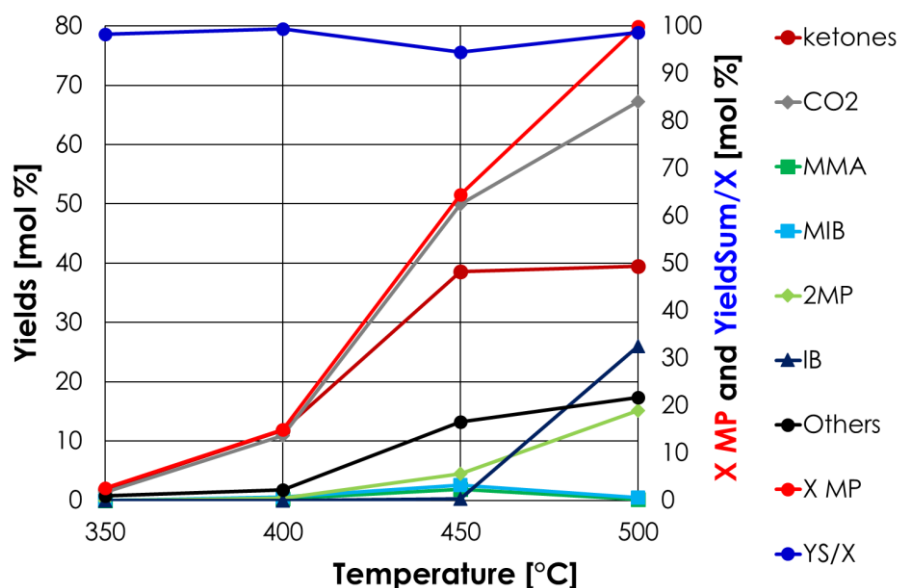
*Graph 15: Gas-phase ketonization of MP in presence of MeOH as a function of reaction temperature: catalyst = MgO; MP/MeOH/N_2 feed composition [mol %] = 6/12/82; W/F = 0.8 s*g/mL. Others includes unknown compounds, PA, MAA, IBA, ethylene, propylene. Yields calculated in terms of moles.*

Over MgO very higher temperatures (500 °) are required to achieve significant amount of C_4 products, which, however, are the less valuable IB (26.0 %) and 2MP (15.1 %). The remarkably high yield in IB is attributable to the very high reaction temperature and not to a peculiar activity of MgO. This catalyst is significantly less active than ZrO_2 and La_2O_3 for both ketonization and hydroxy-methylation/dehydration at the same temperature. A comparison of the ketonization and hydroxy-methylation/dehydration of MP performances for the three catalysts is given in Table 10 and 11.

T	catalyst	X PA [%]	Y 3-P [%]	Y M-3Pe [%]	Y M-3Pa [%]	Tot [%]
	ZrO_2	31.1	19.7	1.7	0.3	21.6
350	La_2O_3	28.9	19.8	1.5	0.4	21.7
	MgO	2.6	1.8	0.1	0	1.9
	ZrO_2	83.1	25.1	6.5	7.1	40.1
400	La_2O_3	80.8	45.1	7.3	4.9	57.8
	MgO	14.9	10.0	1.3	0.4	11.8

Table 10: comparison of ketones distribution over ZrO_2, La_2O_3 and MgO.

T	catalyst	Y MMA [%]	Y MIB [%]	Y 2MP [%]	Y IB [%]	Tot [%]
	ZrO_2	1.2	1.8	0	0	3.0
350	La_2O_3	1.1	2.6	0	0	3.7
	MgO	0	0	0	0	0
	ZrO_2	0.3	6.5	1.9	0.1	8.8
400	La_2O_3	0.9	12.7	0.3	0	13.9
	MgO	0.3	0.6	0.4	0	1.3

Table 11: comparison of C4 products distribution over ZrO_2, La_2O_3 and MgO.

The lower activity of MgO for ketonization may be explained as follows: results of carboxylic acids adsorption over TiO_2 [76] and CeO_2 [77, 78] cited in Chapter 4.1.4.2.1 indicated that the active reticular planes on these catalysts are those capable to bond two carboxylates ions on the same metal cation. The similarities between ZrO_2 and TiO_2 (which belong to the same group) and between La_2O_3 and CeO_2 (which possess a similar ionic radii, 1.17, 1.01 and 1.15 Å for La^{3+}, Ce^{4+} and Ce^{3+} respectively), suggests that these MOs might possess similar ability to coordinate two carboxylates moiety on the same metal cation. In MgO instead, Mg^{2+} possess a much lower ionic radius (0.86 Å), therefore it is unlikely that weakly acidic five-coordinated Mg^{2+} cations in terraces may be capable to bond two carboxylate anions. Similar considerations have been exposed in Chapter 5.3.2.1 regarding the formation of a cyclic six-membered transition state following the adsorption of an alcohol and an aldehyde on a single Mg^{2+} cation for H-transfer reactions [116] (see Scheme 39). Nonetheless, a certain catalytic activity of MgO may arise from the presence of a small fraction of coordinatively unsaturated Mg^{2+} cations on defects such as steps (four coordinated Mg^{2+}, as depicted in Figure 32, Chapter 5.2.1 and figure 46, Chapter 6.3.1.3), or even on kinks (three coordinated Mg^{2+}). Graph 16 shows the distribution of ketones over MgO. The reaction pathway proposed to explain the formation of methyl-pentanones and methyl-pentenones emerges clearly. At 350 °C the only product is 3-P; its yield grows until 450 °C, then it drops to lower values because it is consumed by consecutive reactions. M-3Pe starts to form due to 3-P hydroxy-methylation/dehydration at 400 °C and its yield grows until 450 °C (where a maximum is reached) to finally drop due to consecutive reduction/hydroxy-alkylation reactions. M-3Pa starts to form at 450 °C and its yield becomes higher than the one of 3-P at 500 °C. At the same temperature, M-3Pa undergoes a second hydroxy-methylation/dehydration to produce DM-3Pe, which is reduced immediately to DM-3Pa. 3-P and M-3Pe trends are typical of intermediate products consumed by consecutive reactions.
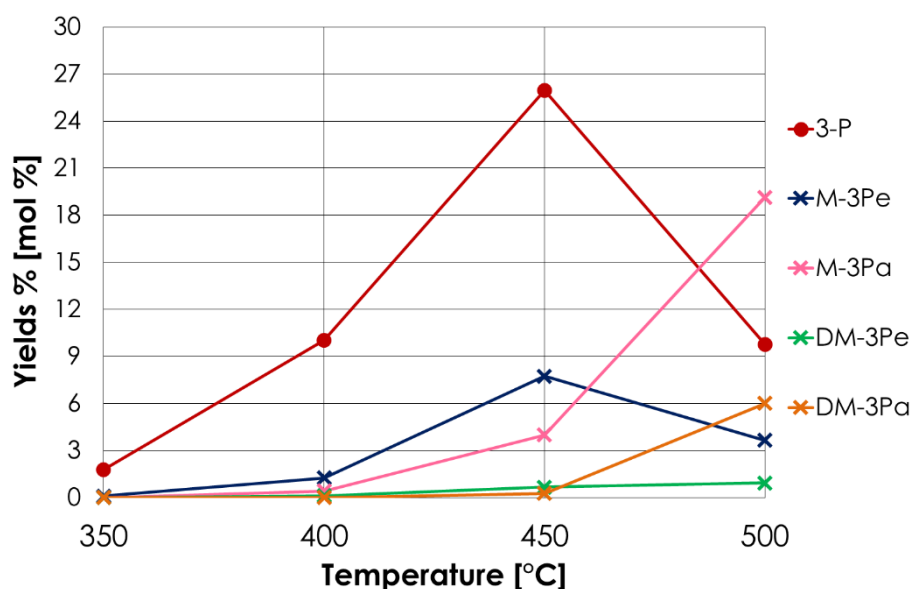
Graph 16: Ketones distribution in the gas-phase ketonization of MP in presence of MeOH as a function of reaction temperature: catalyst = MgO; MP/MeOH/N_2 feed composition [mol %] = 6/12/82; W/F = 0.8 s*g/mL. Yields calculated in terms of moles.

Results obtained over ZrO_2, La_2O_3 and MgO allowed drawing and proposing a reaction scheme for the reaction of the MeOH/MP mixture over these oxides. Such pathway are depicted in Scheme 43 in red (ester ketonization and consecutive reaction on ketones), green (MP hydroxy-methylation/dehydration and consecutive reactions on MMA) and blue (2MP ketonization via dehydrogenation to IBAL, homo-coupling of IBAL via Tishchenko reaction to IBIB and ketonization of the latter).
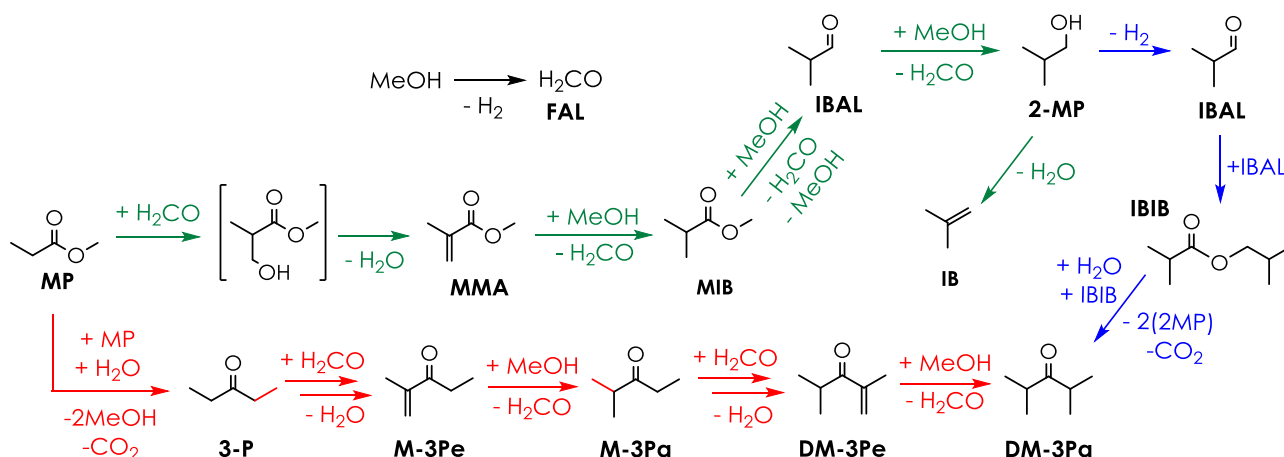
Scheme 43: proposed reaction scheme over MgO, ZrO₂ and La₂O₃: the three main reaction pathways are MP ketonization and consecutive hydroxy-methylation and H-transfers (in red), MP hydroxy-methylation to MMA and consecutive H-transfers (in green), and 2-MP ketonization via Tishchenko and IBIB ketonization (in blue [110]).

5.3.2.4 Catalytic activity of γ-Al₂O₃ and MPOs

The results of catalytic tests obtained over γ-Al₂O₃ deviated significantly from those obtained over the other three MOs and will be reported together with those obtained over MPOs due to the close similarities between the compositions of the reaction mixtures obtained over these acidic catalysts. Results of the reaction of the 2:1 MeOH/MP mixture over γ-Al₂O₃ are reported in Graph 17.
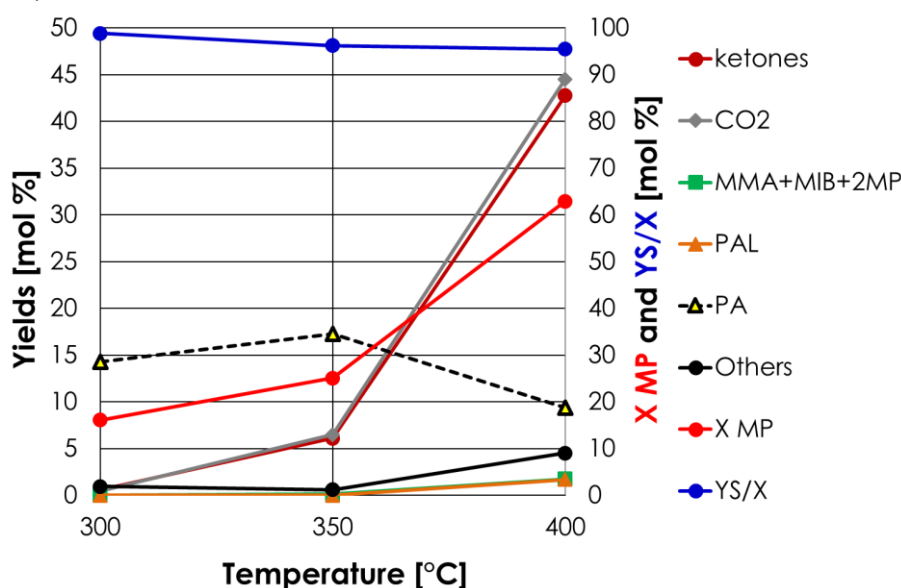
Graph 17: Gas-phase ketonization of MP in presence of MeOH as a function of reaction temperature: catalyst = γ-Al₂O₃; MP/MeOH/N₂ feed composition [mol %] = 6/12/82; W/F = 0.8 s*g/mL. Others includes unknown compounds, MAA, IBA, ethylene, propylene. Yields calculated in terms of moles.

The reaction was investigated in the temperature range 300-350 °C. MP conversion did not change greatly from 300 to 350 °C (16.1 and 25.1 % respectively). In agreement with the literature [87], γ-Al₂O₃ proved to be more active than MgO for ketonization, but less active than La₂O₃ and ZrO₂. Interestingly, at 300 °C MP conversion was higher than the one obtained over ZrO₂, because on the former catalyst the main reaction was MP hydrolysis to PA instead of MP ketonization; MP hydrolysis was preponderant also at 350 °C. The proposed surface mechanism for MP hydrolysis to PA is shown in Scheme 44. This reaction requires the presence of water in the reaction environment and is likely to occur due to the absorption

of MP on surface hydroxyl groups, which result in the formation of adsorbed methoxides and carboxylates anion. Even if calcined γ-Al_2O_3 is a strong Lewis acid, it can chemisorb water leading to the formation of Brønsted acidic sites on its surface; moreover, this catalyst is well known for its dehydrating properties towards MeOH. Therefore, it is likely that the excess of MeOH in the feed mixture led to the formation of dimethyl ether (DME) and the co-produced water remained strongly bonded to catalyst surface fostering the formation of Brønsted acidic Al-OH groups, responsible for MP hydrolysis. Unluckily, DME could not be quantified with the analytical system in use, but its formation was verified by means of offline GC-MS analyses. The presence of MeOH in excess somehow hindered both MP hydrolysis and PA ketonization, because of the competing inverse reaction, the esterification of PA with MeOH, pushed back the equilibrium of hydrolysis. Therefore, X MP is limited at low temperature, PA was produced in low yields between 300 and 350 °C, and small amounts of ketones were obtained at 350 °C only. At 400 °C instead, a substantial increase in MP conversion was observed and ketones became the main reaction products (44.2 % yield). This result might be explained with the tendency of vicinal hydroxyl groups to condensate in response to an increase of temperature. The result of this condensation is the production of water and a Lewis acidic site. The water produced via MeOH hydrolysis bonds more strongly γ-Al_2O_3 surface at low temperature (e.g. 300 and 350 °C), forming more stable surface hydroxyls groups. At 400 °C instead, these surface hydroxyl groups have a shorter life and condense more quickly, restoring Lewis acid sites. Therefore, it seems that the higher ratio between Lewis/Brønsted sites at 400 °C is responsible for higher activity towards MP ketonization over γ-Al_2O_3.
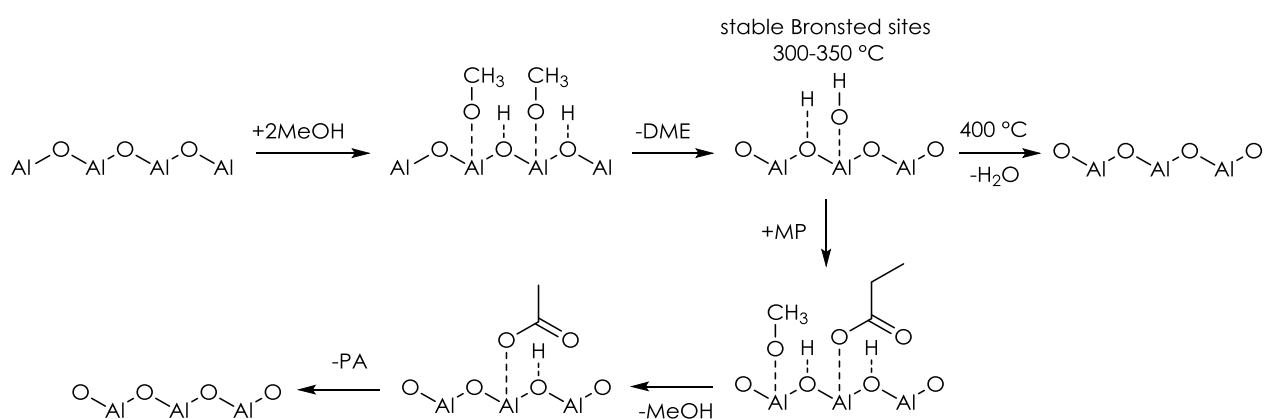
Scheme 44: proposed mechanism for MP hydrolysis to PA and MeOH.
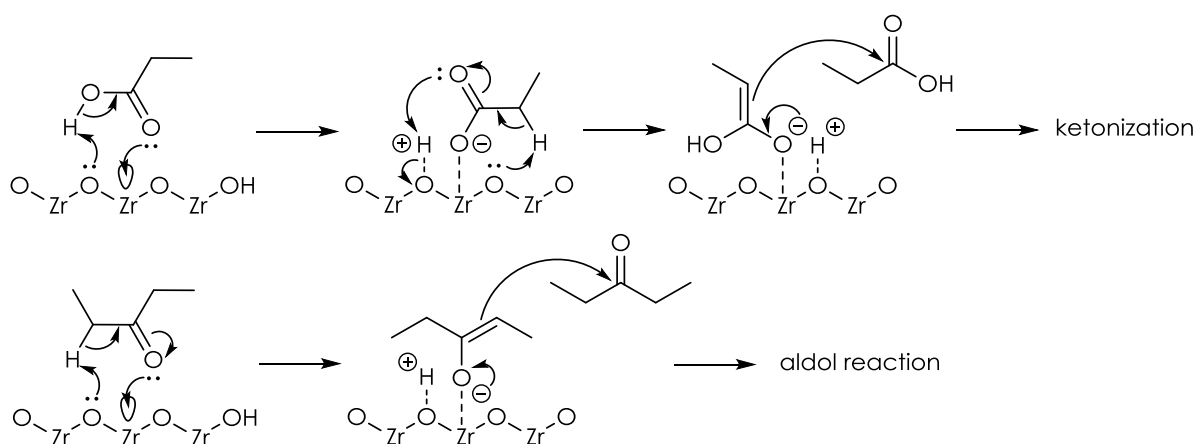
Scheme 45: cooperative α-proton abstraction over Lewis acid-base pairs of ZrO_2: the analogy between PA and 3-P activation for ketonization and aldol reactions respectively.

In fact, one of the requirements for α-proton abstraction is the presence of a neighboring "free" basic site that can "accept" the proton. It is likely that the lower Lewis/Brønsted sites

ratio at 300 and 350 °C significantly reduce the amount of such basic sites, minimizing ketonization rate. Such effect during PA ketonization over γ-Al$_2$O$_3$ (Graph 7, Chapter 4.2.2.4) was much less significant because only the water coproduced by ketonization could form surface hydroxyls groups. The trend of CO$_2$ yield closely follows the one of ketones and the molar balances were always higher than 90 %, therefore significant oligomerization via aldol reactions of ketones over this acidic catalyst has been ruled out. This result represents the last missing piece of information required to propose that aldol condensations, in analogy with ketonization, are more favored on amphoteric oxide (ZrO$_2$) than on oxide displaying mainly acidic (γ-Al$_2$O$_3$) or basic (MgO, La$_2$O$_3$) properties, because the α-proton abstraction rate is higher over catalysts where a cooperative effect between acidic and basic site occur, as depicted in Scheme 45. The yield sum of ketones over γ-Al$_2$O$_3$ at 400 °C is higher than the one obtained over ZrO$_2$ at the same temperature (44.5 and 40.1 % respectively). This result is only apparently in disagreement with the higher activity of ZrO$_2$ for ketonization, because on this catalyst a significant fraction of ketones underwent aldol reactions and was lost. Ketones distribution over γ-Al$_2$O$_3$ is reported in Graph 18. As expected, γ-Al$_2$O$_3$ was the least active catalyst towards MeOH dehydrogenation, due to the very weak basicity of its basic sites. 3-P was the main product of ketonization at all temperature investigated, and very small amounts of M-3Pa only were obtained at 400 °C. The direct formation of this compound without the intermediate M-3Pe may be explained in two ways. The former involves the reaction pathway previously proposed under the assumption that M-3Pe is quantitatively hydrogenated to M3-Pa. The latter involves a nucleophilic attack of the 3-P enolate ion on one of the methyl group of DME, as depicted in Scheme 46.
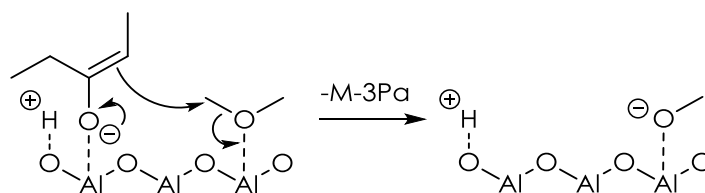
Scheme 46: methylation with DME over γ-Al$_2$O$_3$.

Since γ-Al$_2$O$_3$ possess very low dehydrogenating activity and is known to catalyze the reaction depicted in Scheme 46 [120], the second pathway seems to be the most likely cause of ketone alkylation.
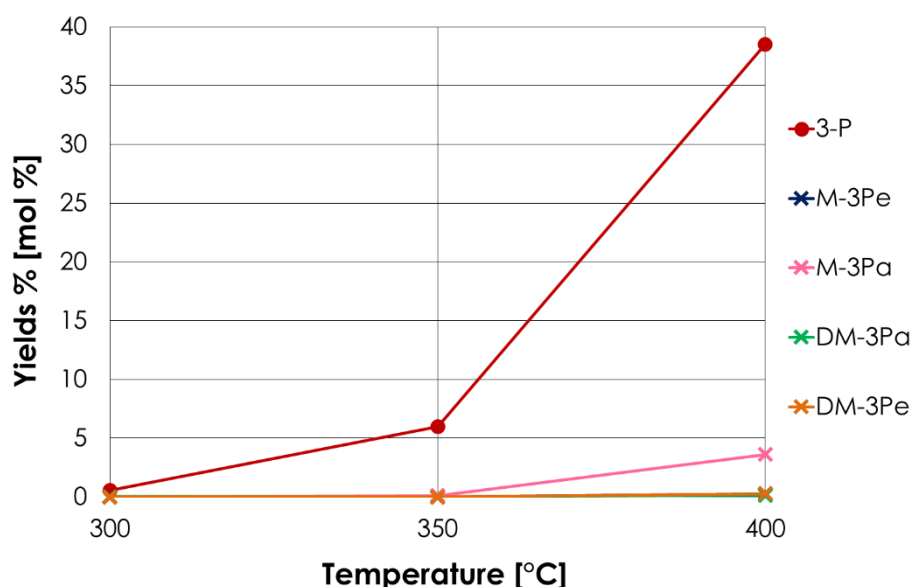
Graph 18: Ketones distribution in the gas-phase ketonization of MP in presence of MeOH as a function of reaction temperature: catalyst = γ-Al$_2$O$_3$; MP/MeOH/N$_2$ feed composition [mol %] = 6/12/82; W/F = 0.8 s*g/mL. Yields calculated in terms of moles.

As anticipated at the beginning of this Chapter, the course of reaction over acidic catalysts was quite homogenous and the main difference between different catalysts depended on their activity and not in the occurrence of different reaction pathways. It will be shown, however, that MPOs are less active than γ-Al_2O_3 for MP ketonization, in contrast with results obtained when PA ketonization was investigated. The results of the reaction of the MeOH/MP mixture over $AlPO_4$ are reported in Graph 19.
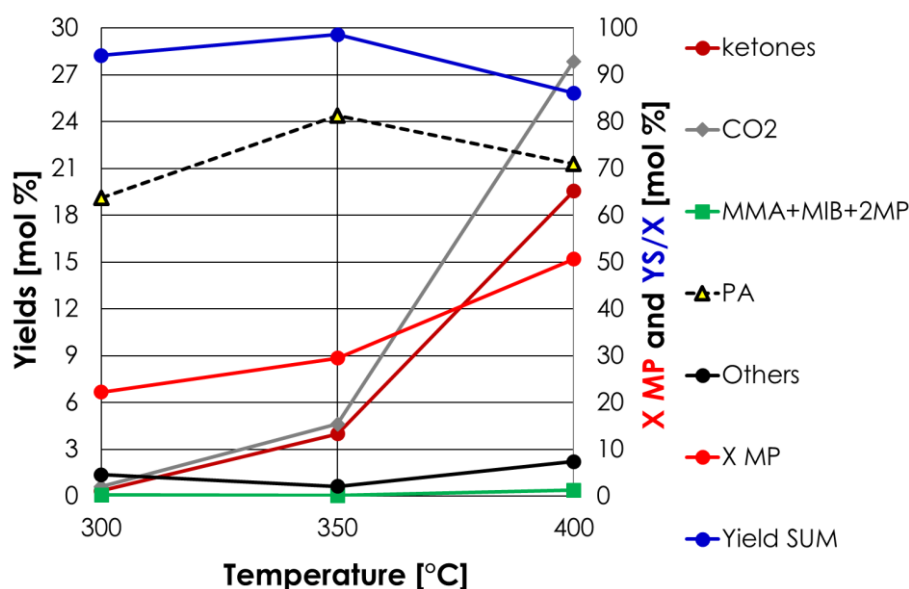
Graph 19: Gas-phase ketonization of MP in presence of MeOH as a function of reaction temperature: catalyst = AlPO₄; MP/MeOH/N₂ feed composition [mol %] = 6/12/82; W/F = 0.8 s*g/mL. Others includes unknown compounds, MAA, IBA, ethylene, propylene. Yields calculated in terms of moles.
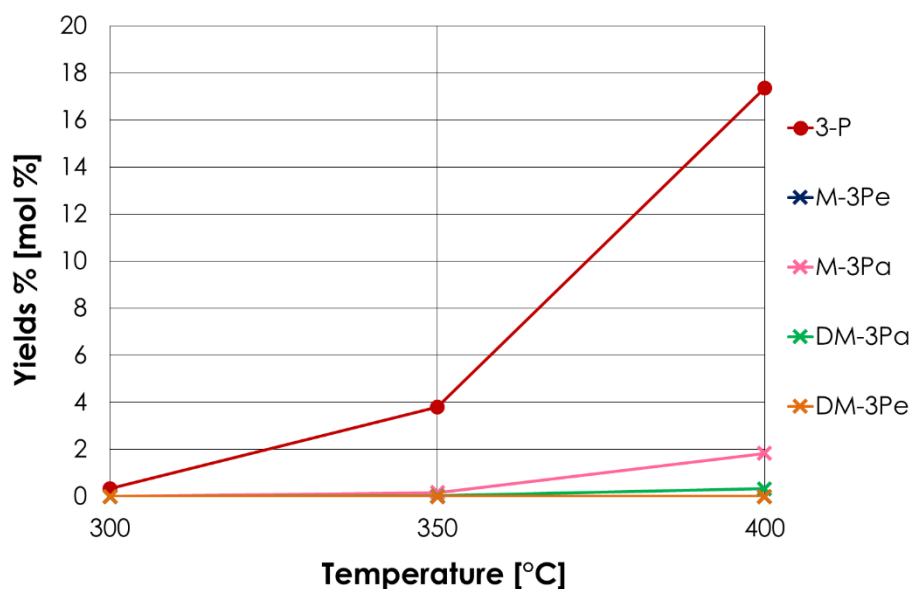
Graph 20: Ketones distribution in the gas-phase ketonization of MP in presence of MeOH as a function of reaction temperature: catalyst = AlPO₄; MP/MeOH/N₂ feed composition [mol %] = 6/12/82; W/F = 0.8 s*g/mL. Yields calculated in terms of moles.

In this case PA was the main product in all the temperature range investigated and the increase in X MP conversion between 350 and 400 °C was much less significant than the one obtained over γ-Al_2O_3. MP hydrolysis over $AlPO_4$ afforded higher yields of PA and lower yields of ketones at all temperatures in respect to the relative oxide. $AlPO_4$ structural/chemical features and catalytic results suggests that on this catalyst the ratio between Lewis and Brønsted sites is lower than the one of γ-Al_2O_3. Therefore, the trend

emerged during catalytic tests of PA ketonization (e.g. $AlPO_4$ more active than γ-Al_2O_3) is overturned when MeOH is fed together with MP. MeOH dehydration to DME led to the formation of water in the form of Brønsted acidic sites over catalyst surface and the large excess of protons from water dissociation occupied most of the weak basic sites required to accept MP α-hydrogen. Unlike Brønsted sites of γ-Al_2O_3, those formed on $AlPO_4$ seems to be more stable at 400 °C due to the higher electronegativity and hydrophilicity of P^{5+} anions. A higher electrophilicity is expected also by electron poor Al^{3+} anions bonded to PO_4^{3-} anions. Moreover, Brønsted acidic groups are likely to be stronger and present in higher number in $AlPO_4$ in respect to γ-Al_2O_3 due to the presence of P-OH groups too. Ketones distribution for the same catalytic test is reported in Graph 20. Such distribution resembles the one obtained over γ-Al_2O_3: the main product is 3-P and negligible amounts of M-3Pa are obtained only at the highest temperature investigated (400 °C). To sum up, the effect of the introduction of phosphorus consists in enhancing the acidity of the catalyst; this fact leads to higher activity in MeOH dehydration to DME and higher affinity of catalyst surface for the coproduced water, which results in the formation of stronger Brønsted acidic sites, stable at higher temperatures. The presence of stronger Brønsted acidic sites enhance MP hydrolysis to PA and their higher thermal stability reduce the probability of α-proton abstraction from MP and 3-P, thus reducing the yields in 3-P and M-3Pa. Over $AlPO_4$, the reaction pathway leading to M-3Pa is expected to be the same occurring on γ-Al_2O_3, via nucleophilic attack on DME and not FAL, which is not formed because catalysts possess negligible basicity. Graph 21 show the results obtained when the 2:1 MeOH/MP mixture was fed over Zr/P/O catalyst. This catalyst, in respect to $AlPO_4$ yielded less PA at 300 °C but raising reaction temperature up to 350 and then at 400 °C, its performance in this regard became like those of $AlPO_4$. From the point of view of ketonization, it is less active than $AlPO_4$ as it were for PA ketonization. The yield in CO_2 follow closely the one of ketones until 350 °C, while above this temperature more CO_2 than ketones is obtained. This catalyst yielded negligible amounts of methylated pentanones, therefore the yield of ketones in Graph 21 can be assumed equal to the one of 3-P.
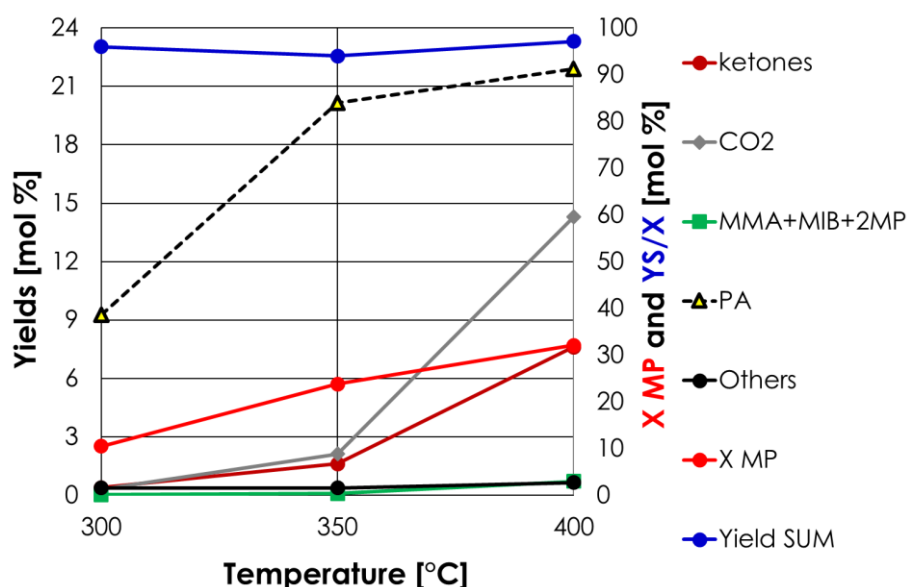
Graph 21: Gas-phase ketonization of MP in presence of MeOH as a function of reaction temperature: catalyst = Zr/P/O; MP/MeOH/N₂ feed composition [mol %] = 6/12/82; W/F = 0.8 s*g/mL. Others includes unknown compounds, MAA, IBA, ethylene, propylene. Yields calculated in terms of moles.

Results obtained over $LaPO_4$ are shown in Graph 22. Since this catalyst was the least active among phosphates, its catalytic activity was investigated between 350 and 450 °C. It can be said that in presence of MeOH the activity of MPOs for the ketonization of MP follows the same order of PA ketonization in the absence of MeOH, e.g. $AlPO_4$ > Zr/P/O > $LaPO_4$. In this

case, the yield of ketones was lower than 1 % in all the temperature range investigated and the yield of PA from MP hydrolysis increase linearly with temperature. PA yields are much lower too, in respect to the other MPOs and γ-Al_2O_3. The yield in CO_2, lower than 2 % between 350 and 400 °C, increased up to 69.9 % at 450 °C, together with the yield in other gaseous products such as ethylene and propylene. The two latter compounds have been considered for the calculation of molar balance because they may derive from PA or MP decarboxylation at high temperature. In conclusion, the reaction scheme for the MeOH/MP mixture over acidic catalysts (γ-Al_2O_3 and MPOs) was different from the preferred one over the other MOs investigated and depicted in Scheme 43, Chapter 5.3.2.3.
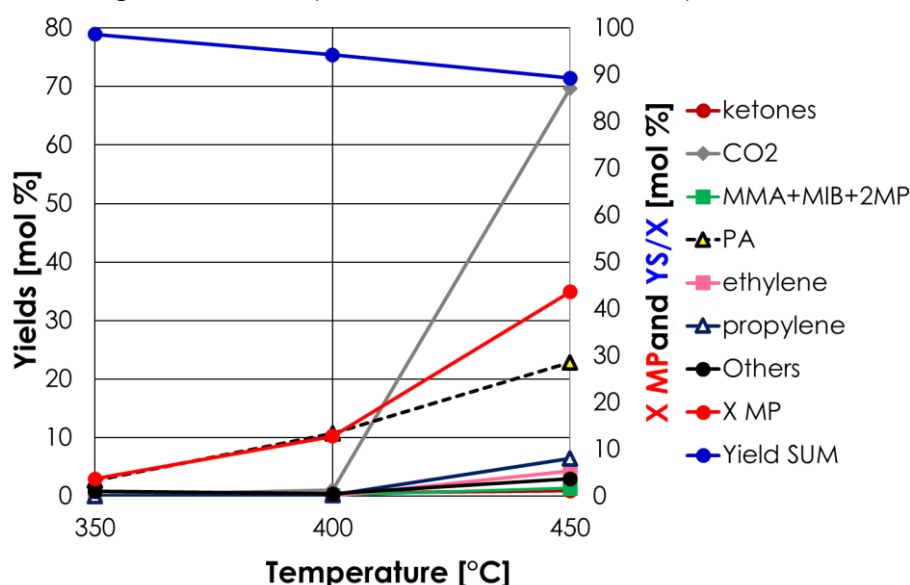
Graph 22: Gas-phase ketonization of MP in presence of MeOH as a function of reaction temperature: catalyst = LaPO$_4$; MP/MeOH/N$_2$ feed composition [mol %] = 6/12/82; W/F = 0.8 s*g/mL. Others includes unknown compounds, MAA, IBA, ethylene, propylene. Yields calculated in terms of moles.

Two main reaction pathways were discovered, being MP hydrolysis to PA the preferred one over most catalysts. Over γ-Al_2O_3 ketonization competes with MP hydrolysis and become the preferred pathway at 400 °C. When reaction temperature was risen to 400 °C over $AlPO_4$, ketonization competed with MP hydrolysis and the reaction mixture was composed by a mixture roughly 50:50 of PA and ketones. Over Zr/P/O and LaPO$_4$ instead, ketonization was always significantly slower than hydrolysis and on the latter catalyst, negligible yields of ketones were obtained. Methylation of ketones occurred to a limited extent and it has been proposed that DME, rather than FAL, is the real alkylating agent. The proposed reaction scheme over acidic catalysts is shown in Scheme 47.
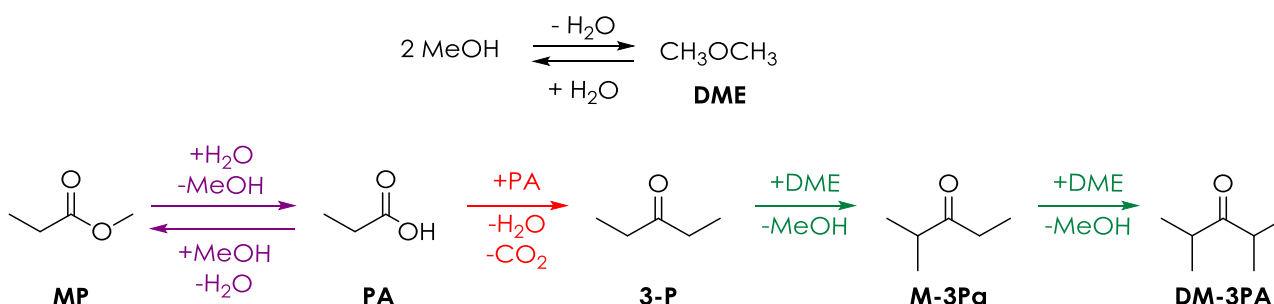
Scheme 47: proposed reaction pathways the reaction of MeOH/MP mixture over acidic catalysts; purple: MP hydrolysis to PA; red: PA ketonization; green: ketones methylation with DME as the alkylating species.

5.3.3 Catalysts characterization after reaction

All catalysts were characterized by means of TGA and XRD after reaction. In all cases, no significant differences were found in their XRD pattern (except for La_2O_3) and the weight loss upon thermogravimetric analysis was very low. Therefore, significant carbon deposition and changes in their crystal structure have been ruled out. Table 12 compile the mass loss measured by means of TGA: for all catalyst two contribution were present, the former due to water evaporation (drying) and the latter due to decomposition in air of small amounts of carbon deposits.

catalyst	Total weight loss [%]	Carbon weight loss [%]
ZrO_2	1.5	1.0
La_2O_3	4.1	2.2
MgO	6.3	3.9
γ-Al_2O_3	4.7	3.6
$AlPO_4$	3.7	1.4
$Zr/P/O$	2.5	1.8
$LaPO_4$	2.1	1.2

Table 12: catalysts weight loss upon thermogravimetric analysis in air.

Since after PA ketonization the chemical composition and diffraction pattern of La_2O_3 underwent a dramatic change, the XRD powder pattern for the same catalyst after reaction with the MeOH/MP mixture will be shown for comparison (Figure 39, left side). Even if the main reaction of MP over La_2O_3 was ketonization (Graph 13, Chapter 5.3.2.2), in this case the only difference between the two XRD patterns consists in a broadening of the reflexes in the one after reaction, without the appearance of peaks attributable to the $La_2O_2CO_3$ phase formed after PA ketonization.
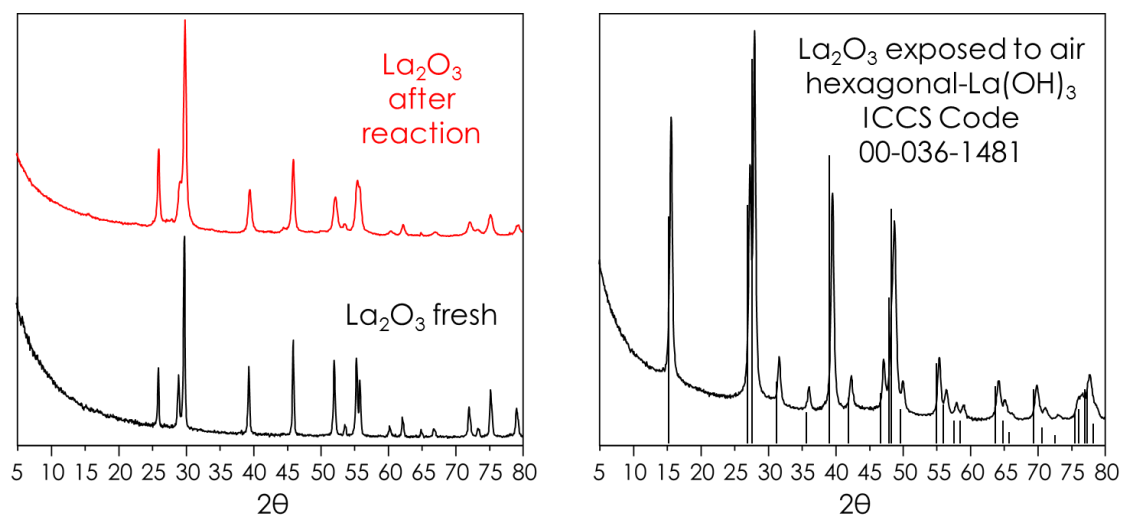
Figure 39: XRD Powder pattern of La_2O_3 before and after reaction with the MeOH/MP mixture.

This result suggests that over La_2O_3 the formation of 3-P from MP occurs preferably via a surface mechanism involving a β-keto ester intermediate. This finding, however, do not exclude that a minor fraction of MP could undergo a hydrolysis over La_2O_3 surface, leading to the formation of PA that reacts with the catalyst to form 3-P and $La_2O_2CO_3$ via the bulk-type mechanism. A minor contribution of PA ketonization via the bulk-type mechanism could explain the loss of definition due to peak broadening of the XRD pattern of La_2O_3 after

reaction with MP. One might argue that MP hydrolysis requires water, which could not form over basic La_2O_3 via MeOH dehydration as it happened in the case of acidic catalysts (e.g. MPOs and γ-Al_2O_3). In this regard, the strong hydrophilicity of La_2O_3 is well documented and it is known to convert into $La(OH)_3$ upon exposure to atmospheric moisture at room temperature [121]. This behavior has been confirmed by means of XRD analysis over a portion of the fresh catalyst let in contact with air for a couple of days (Figure 39, right side). Moreover, the presence of hydroxyl groups on the surface of fresh La_2O_3 was proved by means of ATR spectroscopy (Figure 29, Chapter 4.2.3). Fresh La_2O_3 ATR spectrum is characterized by the presence of a narrow band centered at 3607 cm^{-1}. Therefore, a certain amount of basic hydroxyl groups exists on La_2O_3 surface and are likely to be responsible for MP hydrolysis. Once PA is formed, its reaction with the catalyst produce a lanthanum salt and a molecule of water (Scheme 30, Chapter 4.2.3), which can react with the catalyst and regenerate basic hydroxyl groups. Scheme 48 depicts the mechanism proposed for α-proton abstraction and MP hydrolysis over the surface of La_2O_3.
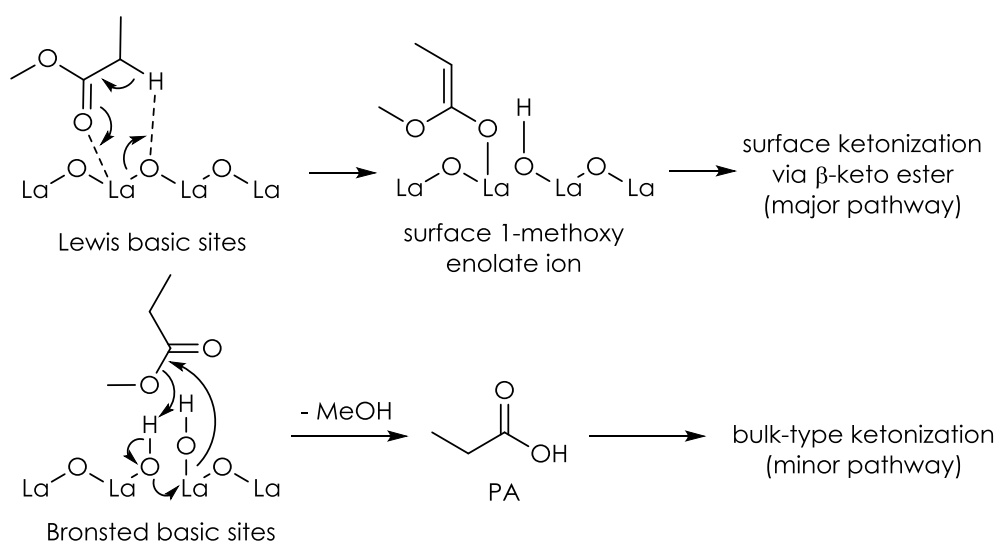
Scheme 48: proposed surface mechanisms for a) MP α-hydrogen abstraction and b) MP hydrolysis over La_2O_3.

5.4 Conclusions

The reaction of a 2:1 mixture of MeOH and MP was investigated over metal oxides of Al, Zr, La and Mg and over metal phosphates of Al, Zr and La. Even in the presence of an excess of MeOH in respect to MP the main reaction over metal oxides is ketonization and the activity order of metal oxides towards ketonization follows the order Zr $\approx$ La > Al > Mg. ZrO_2 and La_2O_3 were the best ketonization catalyst, in agreement with results obtained over PA in Chapter 4.

The temperature required for MeOH dehydrogenation was significantly higher than the one required for ketonization. As a consequence, the hydroxy-methylation/dehydration of α-H containing compounds with FAL became fast only at high temperature and the one of ketones was favored in respect to the one of MP; therefore, the preferred products rising reaction temperature were methylated pentenones instead of MMA. An increase in reaction temperature led also to H-transfer hydrogenations of the newly formed C=C double bonds of methyl-pentenones and MMA with MeOH or FAL as H-donors.

Acidic catalysts (γ-Al_2O_3, $AlPO_4$, Zr/P/O and $LaPO_4$) do not possess significant dehydrogenating activity towards MeOH, which is instead dehydrated to dimethyl ether

MP/MeOH mixture reaction over ketonization catalysts

(DME). Over these catalysts the main reaction at low temperature is MP hydrolysis to PA, being the required water supplied by MeOH dehydration; rising reaction temperature up to 400 °C small amounts of 3-P are obtained but, except for γ-Al_2O_3, MP hydrolysis to PA remained the major reaction. Moreover, over these catalysts it likely that the real methylating agent is DME instead of FAL.

The homo-ketonization of MP and 2-methyl propanol (2-MP) where investigated over the best ketonization catalyst (ZrO_2). Results obtained feeding MP indicate that esters are less reactive than their respective acids in agreement with literature. Results obtained feeding 2-MP showed that ZrO_2 is capable to yield ketones as products also when the feed is constituted by alcohols possessing α-hydrogens. In the case of 2-MP, ketonization is very likely to occur via a first dehydrogenation to isobutyraldehyde followed by a Tishchenko reaction that produce the symmetric ester isobutyl isobutyrate, which finally ketonize.

From the point of view bio oil upgrading, results shown and discussed in this Chapter and in the previous one indicates that ZrO_2 catalyze both carboxylic acids and esters ketonization and that the presence of alcohols in the feed, far from being a problem, can lead to three favorable reactions:

1) Ketonization of alcohols.
2) Alkylation of ketones to more branched molecules with higher octane number.
3) H-transfer hydrogenation of double bonds that enhances the calorific power.

From the point of view of MMA synthesis instead, none of the catalyst investigated yielded satisfying amounts of the desired product due to extensive ketonization of MP and H-transfer hydrogenation of MMA over metal oxides (ZrO_2, La_2O_3, MgO) and the lack of dehydrogenating power of acidic catalysts (MPOs and Al_2O_3). Parasitic ketonization is much faster than MeOH dehydrogenation and hydroxy-methylation/dehydration of MP at low temperatures. At higher temperatures the desired reactions compete with ketonization, but also H-transfer hydrogenations become favored consuming the so obtained MMA. Starting from these results a strategy to enhance the MMA yield by modifying reaction conditions and the catalyst design has been developed and will be the argument of the next Chapter.

6 MMA synthesis from MP and MeOH

6.1 Aim of this Chapter

The aim of the work presented in this Chapter was the design of a catalyst for MMA synthesis starting from MeOH and MP as reactants. At the end of Chapter 5 it was concluded that no one of the catalyst investigated so far was capable to produce satisfying amounts of MMA:

1. ZrO_2 (amphoteric) and La_2O_3 (strongly basic) are the best catalyst for MP ketonization, which occur extensively at low temperatures. High ketonization activity is detrimental for MMA synthesis because competes with the desired reaction consuming the reagent MP.

2. La_2O_3 and MgO (both basic, the former being a stronger base) are the most effective catalyst for MeOH dehydrogenation; dehydrogenating features are of the utmost importance in order to obtain the FAL required for MMA hydroxy-methylation.

3. Acidic catalysts (MPOs and γ-Al_2O_3) are poor ketonization catalysts but possess negligible dehydrogenating power. Moreover, they lack the required basicity and α-proton abstraction rate is extremely low.

It was decided that, among the materials investigated, MgO displayed the best balance between a good dehydrogenating activity, a scarce ketonization activity and the ability to activate MP by means of α-proton abstraction. Still, it was not an effective catalyst for MMA production. In fact, high temperatures are required to achieve extensive MeOH dehydrogenation and in these conditions the parallel reaction of ketonization and the consecutive reaction of H-transfer are favored and consume the reagent and the desired product respectively. However, results obtained during this catalyst screening have allowed to outline the most favorable reaction conditions and the most desirable properties for a MgO-based catalyst. In order to minimize H-transfer reactions, relatively low reaction temperature is needed. In the same conditions, both ketonization and dehydrogenation activity of MgO are low. Therefore, the formulation of the MgO-catalyst needs to be aimed at strongly enhancing its dehydrogenating activity at low temperature, for example introducing redox elements in its structure, in order to obtain larger amounts of FAL from MeOH. The excess of FAL in respect to MP can be further enhanced by increasing the molar MeOH-to-MP feed ratio. Moreover, an increase of this reaction parameter would result in a dilution of MP, which would make more difficult for two ester molecules to encounter each other and undergo ketonization over catalyst surface.

6.2 Introduction

6.2.1 MMA industrial production

Methacrylic acid (MAA) is a colorless, moderately volatile, corrosive liquid with a strongly acrid odor. Its chemistry depends on the presence, in its moiety, of both a carboxylic group (which could lead to decarboxylation, esterification, reaction with amines to produce amides) and a C=C double bond (reactive in the addition reactions, e.g. of hydrogen cyanide, hydrogen halides, hydrogen sulfide, mercaptans, alkyl amines, alcohols, phenols, or phosphines leads to β-substituted α-methyl propionates, Diels-Alder reactions with dienes, polymerizations). Its methyl ester, MMA, with a global production of 2.7Mt/y is a chemical compound halfway between commodities and specialties. It finds direct application in the

formulation of road mark paints and glues, but its main use is by far as monomer for poly(methyl methacrylate) manufacture (PMMA, 1.6 Mt/y). This high-performance plastic material has many applications as cheap and robust alternative to glass in automotive, construction and technology industries. Given MMA monomer relevance, several processes have been developed up to commercial level for its production. The first was the process via acetone cyanohydrin (ACH) [122], developed by DuPont and ICI, which is still in use in some countries and is depicted in Scheme 49.
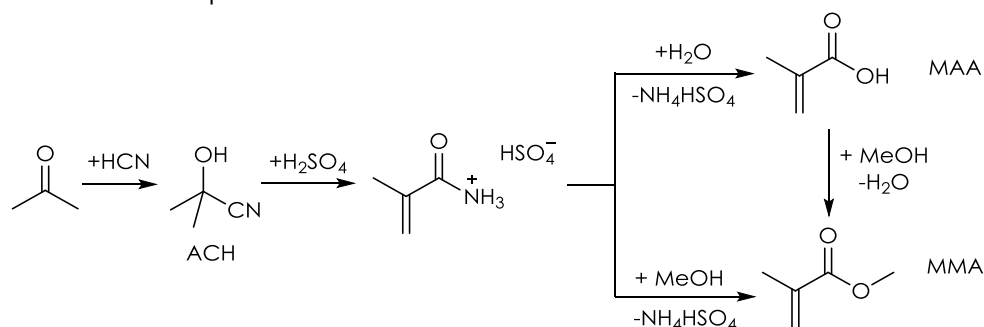
Scheme 49: MAA and MMA production via acetone cyanohydrin (ACH Process).

In this process, dry acetone is reacted with hydrocyanic acid to produce the intermediate acetone cyanohydrin over a basic catalyst. This intermediate is then reacted with excess sulfuric acid to produce a methacrylamide acid sulphate: the reaction involves the formation of a α-sulfatoamide intermediate that can be hydrolyzed to α-hydroxy-isobutyl amide in the presence of water (Scheme 50). To minimize the formation of this byproduct, all reagent must be anhydrous, and a brief thermal cracking step is required to convert α-hydroxy-isobutyl amide into the desired methacrylamide acid sulphate before the following stage of the process. If insufficient sulfuric acid is used, the reaction mixture becomes a slurry or solid which is impossible to cool and pump, therefore the acid acts as both stoichiometric reagent and solvent. In the second stage of the process, the methacrylamide acid sulphate is hydrolyzed with water or MeOH in order to obtain respectively MAA or MMA, and ammonium bisulfate as by-product.
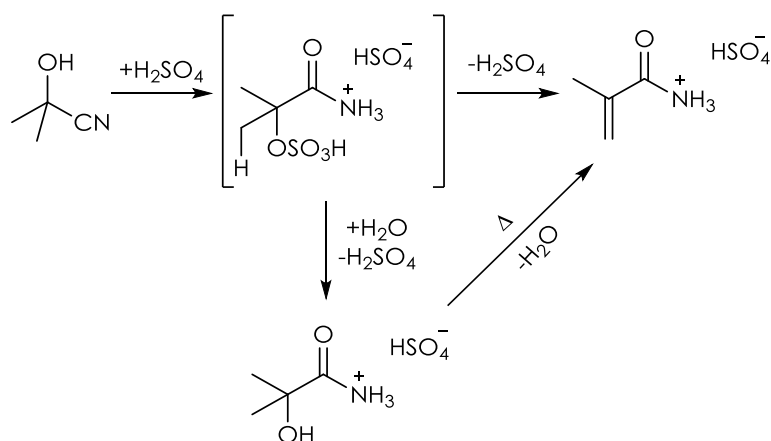
Scheme 50: α-hydroxy isobutylamide by-product formation from the sulfatoamide intermediate in the presence of water.

From the economic point of view, this process has the advantage to use hydrocyanic acid and acetone, which are cheap by-product of other industrial processes (namely, acrylonitrile manufacture and phenol manufacture respectively), but is not sustainable and suffers from several drawbacks:

1. Corrosion issues related to the use of sulfuric acid and energy intensive work up operation for its regeneration and recycle.

2. Hazard associated with transporting hydrogen cyanide, which is not always generated at the methacrylate plant site.

3. Ammonium bisulfate (1.6 Kg for each Kg of MMA) must be disposed of, either reacting it with NH₃ to produce fertilizer or by incineration.

Mitsubishi Gas Chemical modified the ACH process [123] in order to avoid the use of sulfuric acid and the formation of inorganic wastes. In this process, acetone cyanohydrin is hydrolyzed with water over a MnO₂ catalyst producing α-hydroxy-isobutyl amide, which is further reacted with methyl formate to obtain a α-hydroxy isobutyrate methyl ester intermediate and formamide (Scheme 51).
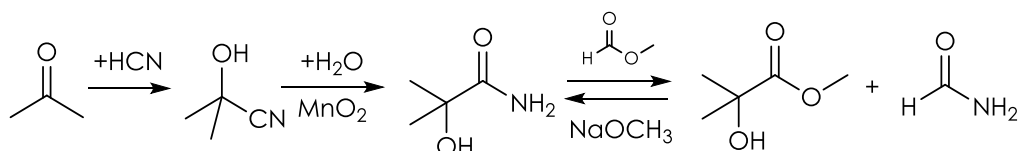
Scheme 51: first step of the modified ACH process.

The former is then dehydrated to MMA, while the latter is decomposed into water and hydrocyanic acid, which is recycled for the synthesis of acetone cyanohydrin, leading to a higher atom economy in respect to the conventional ACH process (Scheme 52).

Scheme 52: second step of the modified ACH process.

Safety concerns related to the use hydrocyanic acid led several companies to develop processes starting from different feedstock such as isobutylene (IB) and ethylene. In general, these processes are characterized by higher atom economies and higher safety, even if they suffer from the typical limitation of oxidative processes (e.g. risk of explosion). Nippon Shokubai Kagaku Kogyo Co [123] commercialized a process that involves the two-step oxidation of IB (or isobutanol, which readily dehydrates to IB under reaction conditions) to produce MAA, with methacrolein (MAL) as the intermediate (Scheme 53).
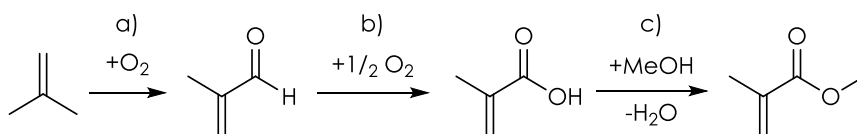
Scheme 53: MMA from C₄ feedstock: IB oxidation process via MAL: a) oxidation of IB to MAL, b) oxidation of MAL to MAA, c) esterification of MAA with MeOH.

The first-stage catalysts for the oxidation of IB to MAL are based on complex mixed-metal oxides (MOs) of Molybdenum, Bismuth, and Iron, while the MAL oxidation step is carried out using phosphomolybdic acid-based catalyst, usually with Copper, Vanadium, and a heavy alkali metal additive. Further improvements (Halcon [122] and Asahi Chemical [123]) led to the shift to IB to cheaper isobutane as feed (thanks to the development of a first dehydrogenation step), and to the integration of MAL oxidation with MAA esterification in order to obtain MMA directly (Scheme 54).
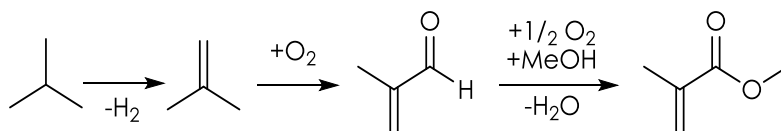
Scheme 54: modifications proposed for the C₄ route for MMA production.

MMA synthesis from MP and MeOH

BASF developed a three-step process starting from cheaper C_1-C_2 feedstocks. In the first reactor, ethylene is hydro-formylated with syngas (CO/H_2=1) to produce propionaldehyde (PAL), which is then reacted with formaldehyde (FAL) in the second reactor; the resulting MAL intermediate is finally oxidized to MAA in the third reactor (Scheme 55).
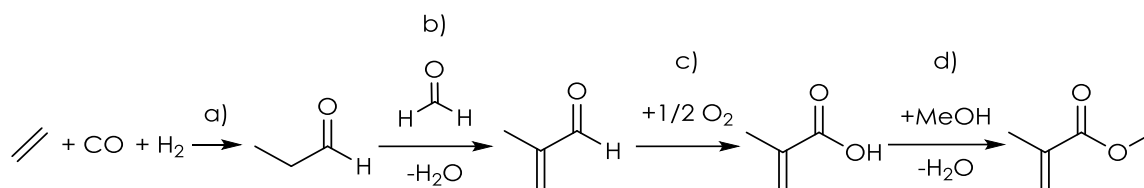
Scheme 55: BASF process a) hydroformylation of ethylene, b) hydroxy-methylation/dehydration of PAL with FAL to produce MAL c) oxidation of MAL to MAA, d) esterification of MAA to MMA.

The state of art in the sustainable MMA production is the Lucite alpha-process (Scheme 56). In this process ethylene is formylated with CO in the presence of MeOH to produce methyl propionate (MP) in a single step with a palladium biphosphine catalyst, which ensure selectivities near to 100 %. The reaction is carried out in continuously stirred reactor, in mild condition of pressure and temperature. Then, MP hydroxy-methylation with anhydrous FAL takes place in a fixed bed gas-phase reactor at 300-400 °C, over a catalyst consisting in Cs_2O supported on SiO_2; the resulting hydroxy-methylated intermediate immediately dehydrates to MMA over the same catalytic bed. The presence of water in the feed influences negatively catalyst activity; therefore, pure FAL is needed. It is produced in a dedicated reactor by means of oxidative dehydrogenation of MeOH (forming water as a co-product); then it is dehydrated by means of distillation prior to be send to the hydroxy-methylation/dehydration reactor.
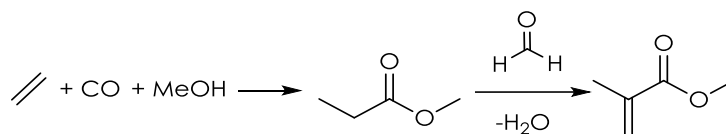
Scheme 56: Lucite alpha-Process.

The overall process is extremely selective, and the theoretical atom economy can be considered close to 100%, being water the only co-product. However, during real industrial operations small amounts of heavy by-products deposit over Cs_2O/SiO_2 catalyst during time leading to its deactivation. In order to ensure a continuous production, two reactors, which alternates operativity and catalyst regeneration by means of heavy product combustion, are needed, and this fact leads to slightly lower atom economy and to increased GHGs emissions. Even if the Lucite alpha process represents a huge step forward in terms of sustainability in respect to the ACH process, it still depends on non-renewable feedstocks (CO, ethylene, H_2 and MeOH) and requires a pure stream of gaseous FAL as reactant, which is a well-known toxic and carcinogenic compound. Therefore, in order to further enhance the sustainability of MMA industrial synthesis, two main hurdles still need to be overcome: the former is the production of MP from renewable resources (e.g. glycerol from biodiesel production), which will be discussed in Chapter 6.2.2 and following, while the latter is the substitution of carcinogenic FAL with a safer reactant (e.g. MeOH), which will be discussed in Chapter 6.2.3 and following.

6.2.2 Sustainable MMA production from renewables

6.2.2.1 Triglycerides

Triglycerides are esters derived from glycerol (GLY) and three fatty acids; they are the main constituents of body fat in animals and vegetable oils. Two kind of triglycerides can be

distinguished: saturated triglycerides contains saturated fatty acid residues (e.g. stearic acid) and having a higher melting point are more likely to be solid at room temperature. Unsaturated triglycerides contain unsaturated fatty acid residues (e.g. oleic acid) and having a lower melting point are more likely to be liquid at room temperature.
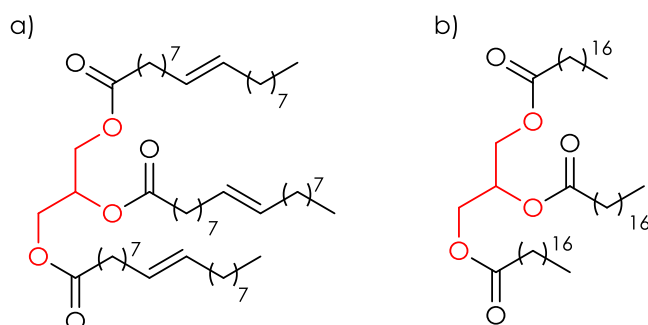
Figure 40: examples of triglycerides: a) glyceryl trioleate (vegetable oil); b) glyceryl tristearate (animal fat).

Pure animal fats are traditionally produced from tissue fats obtained from livestock. The rendering process consist of finely chopping fat materials, boiling it and then separating the water from the fats by centrifuge. The process yields stable and edible products such as lard and tallow. Vegetable oils too are constituted by triglycerides mixtures but usually are liquid at room temperature and are obtained crushing seeds or other parts of oil-rich plants. Chemical extraction with solvent is possible but is generally avoided as far the production of edible oil is concerned. Rendered animal fats and vegetable oils are considered not sustainable for bio diesel production; nonetheless, 1st generation biodiesel is obtained from edible oil such as palm oil. The chemical upgrading into fuels of cheap exhausted oils and waste animal fats from food industry and tannery is instead a more sustainable route to produce 2nd generation biodiesel, together with the use of vegetable oils from non-edible oily crops, which do not compete with food because are grown on marginal lands not suitable for agriculture. Another sustainable source of triglyceride for biodiesel production that is gaining growing attention is constituted by microalgae cultures; microalgae are eukaryotic or prokaryotic unicellular organism that can grow rapidly and are capable to survive in harsh environment. They are diffused in both marine and terrestrial environments and their exploitation lead to several advantages in respect to conventional forestry feedstocks: they show much higher growth rates and higher productivity, have a 30 % weight content of oil and requiring much less area for culture do not compete with agriculture [124].

6.2.2.2 Bio diesel production

Biodiesel production started in the late 1990s and knew an explosive growth in the last two decades thanks to governmental incentives all over the world (e.g. in 1994 the European Parliament accorded a 90 % tax exemption for bio diesel producers). World production grew steadily by 32 % per year between 2000 and 2005, reaching 4.5 Mt/y [125]. In 2017, the share of 1st generation bio diesel was 95 % of the world production. In countries where abundant fertile lands and water resources are easily accessible, first generation bio diesel such as soybean and sunflower bio diesels seems to be economically sustainable. However, 1st generation bio diesel is taking place at the expense of the shrinkage of the land area dedicated to food crops cultivation. Moreover, palm oil culture for bio diesel production is among the main responsible from deforestation in South America and Southeast Asia [126]. For these reasons, 2nd generation biodiesel needs to be developed as fast as possible in order to meet both production, societal and environmental demands. Bio diesel production

technology is rather simple: it consists in the transesterification of triglycerides with alcohols in the presence of a catalyst (Scheme 57).
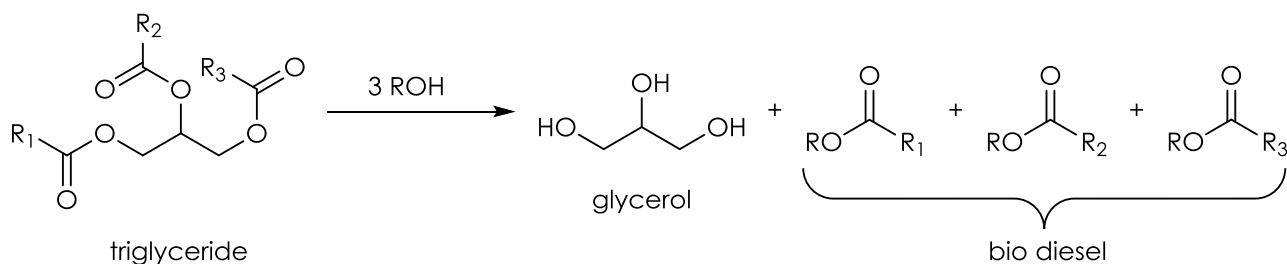
Scheme 57: bio diesel production via transesterification of triglycerides with alcohols.

The alcohols used in the transesterification process include MeOH, EtOH, PrOH, BuOH, and amyl alcohol. Among these alcohols, MeOH and EtOH are the most used. Catalyst can be divided into two main categories:

1. Basic catalyst: NaOH [127] and KOH [128] are the most used homogeneous catalysts due to their low cost and high activity. However, undesired saponification reaction may occur with emulsion formation, which makes separation more difficult. Moreover, homogeneous catalysts removal after reaction via water washing produces large amounts of wastewater. Heterogeneous catalysts ensure an easier product purification but requires harsher conditions and often suffer from mass transfer limitations. Typical heterogeneous catalysts are CaO [129], CaTiO$_3$, CaZrO$_3$ [130], KOH/Al$_2$O$_3$ [131], NaOH/Al$_2$O$_3$ [127] and K$_2$CO$_3$ supported on silica/alumina [132]. The reaction mechanism involves the abstraction of the alcoholic proton from the alcohol by a homogeneous OH$^-$ ion or a basic site on catalyst surface with the formation of a strong nucleophilic alkoxy ion, which then substitutes the glyceryl residue bonded to the fatty acid.

2. Acidic catalysts: concentrated H$_2$SO$_4$ is the most common; its use avoid saponification and emulsions formation, but leads to corrosion issues, difficult recycle the need for neutralization of acidic waste. Acidic heterogeneous catalysts ensure the same advantages compared to heterogeneous basic catalysts but suffers from the same drawbacks. Typical materials are sulfated zirconia [133], vanadyl phosphates [134] and amberlyst-15 [135]. The reaction mechanism involves the protonation of the carbonyl oxygen of the esteric group or its interaction with a Lewis acidic site on catalyst surface, which enhances the electrophilicity of the carbonyl carbon atom allowing a nucleophilic attack by a molecule of alcohol (weaker nucleophile in respect to alkoxy species).

Bio diesel production coproduce roughly 100 Kg of GLY for each ton of biodiesel (10 wt. %). It is easily separated from biodiesel in the form of a non-miscible mixture of MeOH, GLY and water. Such mixture is usually centrifuged to remove fats and fatty acids and immediately concentrated up to about 80-90 % in a multistage flash evaporator in order to avoid fermentation to 1,3-propandiol. Then, this crude GLY is treated with active carbon for bleaching and NaOH to remove residual fats by means of saponification. Each treatment is followed by filtration. The last two work up operation consist in the desalination by means of ion exclusion chromatography with a cationic, strongly acidic resin and distillation under vacuum (10-15 kPa) in order to avoid thermal decomposition of high-boiling GLY. The final product possesses a purity of 99.5 %. Crude GLY is also much cheaper than high purity GLY obtained from fossil resources: by 2014, high-grade GLY price reached 900 $/t whereas crude GLY (80 % pure) reached about 250 $/t.

6.2.2.3 Renewable bio glycerol as a platform molecule

GLY (1,2,3-propanetriol) is a tasteless and colorless viscous liquid. It is a hygroscopic high boiling (290 °C) compound possessing solvent properties similar to these of water and simple aliphatic alcohols due to the presence of three hydroxy group in its moiety. It is completely miscible with water, alcohols, phenols, diols and amines, while is immiscible with hydrocarbons, long chain alcohols, fatty oils and halogenated solvents. The two terminal primary hydroxyl groups are slightly more reactive than the secondary one. GLY undergoes dehydration reactions in acidic medium forming hydroxy acetone or 3-hydroxy propionaldehyde depending on which hydroxy group is removed; it is oxidized to glyceric acid by dilute nitric acid and to tartronic acid by concentrated nitric acid. The most relevant applications of GLY as it is, without chemical derivatization, are in food industry as sweetener, humectant for tobaccos and food preserver. It is also a main component in the formulation of pharmaceuticals, cosmetics, electronic cigarette liquids and antifreeze mixtures. It is the starting material, after chemical derivatization, for the manufacture of nitroglycerin (an important drug for the treatment of angina pectoris, and the active component in dynamite), alkyd resins (by reaction with phthalic or maleic anhydrides), polyurethanes foams (via reaction with isocyanates) and fuel additive (glycerin tert-butyl ether). Technical esters of GLY with fatty acids are used for biodegradable loss lubrication in the automotive, food, agriculture and forest industry. For decades GLY have had only two major industrial application as reactant, namely the synthesis of nitroglycerine and in alkyd resins production. Pure GLY, however, was used in the formulation of pharmaceuticals and cosmetics, and sold at high price (2500-4000 $/t) to their manufacturer. As a consequence of the exponential growth of biodiesel production since 2003, the GLY market experienced such a significant oversupply that in the late 2010 its price dropped to 0; in other words, it became a waste without any value, which only uses were as low calorific power fuel and as feedstock feeding. Such unprecedented low prices created new markets in developing countries, where GLY had not been used yet because of its high price. By 2014, high-grade GLY price reached 900 $/t whereas crude GLY (80 % pure) reached about 250 $/t. Prior to the boom of bio diesel production, when a fourth of GLY demand was met by the synthetic route from propylene via allyl chloride and epichlorohydrin and the remaining part by saponification, the price of GLY suffered from volatility due to fluctuations in its demand. At present time, however, its price keep suffering from fluctuations due to its supply, which depends on politics and oil price; in other words, GLY supply is completely independent from its market demand. This situation makes the synthesis of chemicals from GLY economically viable only if the final product is valuable enough not to suffer from GLY price fluctuations. Anyway, GLY is a renewable and reactive platform molecule: its transformation into other chemicals consumes less than 20 % of its supply, which, however, is expected to grow steadily in the next years. Therefore, it represents one of the most valuable raw material for 2nd generation biorefinery and is currently under investigation for the synthesis of relevant building blocks such as acrolein, a key intermediate in the synthesis of acrylic acid (Scheme 58). It is well known that heating GLY leads to its decomposition into acrolein and water, with the formation of by-products. In order to achieve a better control over the reaction, an acidic catalyst is required. The first patent regarding a heterogeneous catalyst (Lithium and Copper phosphates) was published in 1933 [136]; later on, in 1936, a process catalyzed by aqueous sulfuric acid was patented too [137], but the lack of cheap GLY hindered the development of such a process until the last two decades. In more recent years, huge efforts in the development of active and selective heterogeneous catalysts for acrolein synthesis were made and several examples are reported in Table13.
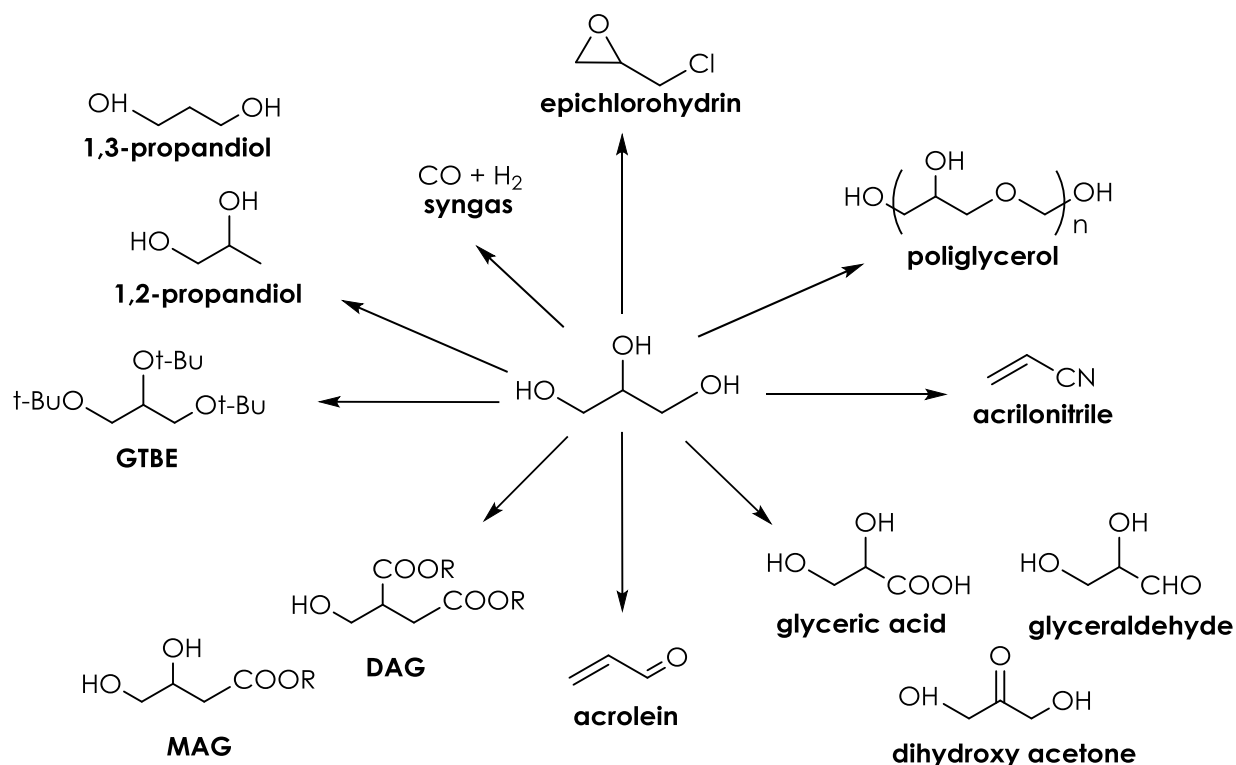
Figure 41: valuable products obtainable from GLY.

catalyst	conditions	phase	X GLY [%]	Y acrolein [%]	ref
H_3PO_4/Al_2O_3	300 °C	heterogeneous	100	75	[138]
$(VO)_2P_2O_7$	320 °C	heterogeneous	100	70.1	[139]
30 wt. % WO_3/ZrO_2	315 °C	heterogeneous	100	70	[140]
Zr/Nb/O	300 °C	heterogeneous	100	72	[141]
Zr/P/O	315 °C	heterogeneous	100	71	[142]

Table 13: heterogeneous catalysts for GLY conversion to acrolein.
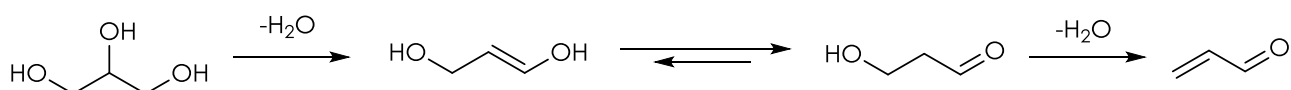
Scheme 58: GLY dehydration to acrolein via 3-hydroxypropionaldehyde.

The literature is not limited to the investigation of metal oxide catalysts, but also zeolites and heteropolyacids are currently being evaluated; moreover, this process is extensively studied also in the liquid phase with homogeneous catalysts. Further details can be found in these reviews [143, 144]. The efforts spent in the research aimed at valorizing GLY as starting material for the synthesis of valuable C_3 intermediates have also led to the successful development of several processes up to commercial level. Epichlorohydrin is the most

important starting material to produce epoxy resins. Before the boom of bio diesel production, one fourth of GLY global supply derived from the hydrolysis of epichlorohydrin with NaOH or Na_2CO_3. This process produces high-purity GLY for advanced application. Epichlorohydrin is synthesized from non-renewable propylene by means of a three step process: 1) chlorination of propylene to propylene chloride, 2) oxidation of propylene chloride with hypochloric acid to yield a mixture of dichlorohydrins and 3) hydrolysis with $Ca(OH)_2$ to yield epichlorohydrin (Scheme 59a). The large availability of biobased GLY, however, at present days makes environmentally beneficial and economically viable the production of epichlorohydrin from renewable GLY. A two-step GLY-to-epichlorohydrin process [145] (GTE) has been developed successfully up to commercial level and involves 1) GLY hydrochlorination with HCl at high temperature and pressure with a carboxylic acid catalyst to yield a mixture of dichlorohydrins and 2) the conversion of the intermediate mixture into epichlorohydrin (Scheme 59b).

a)

b)
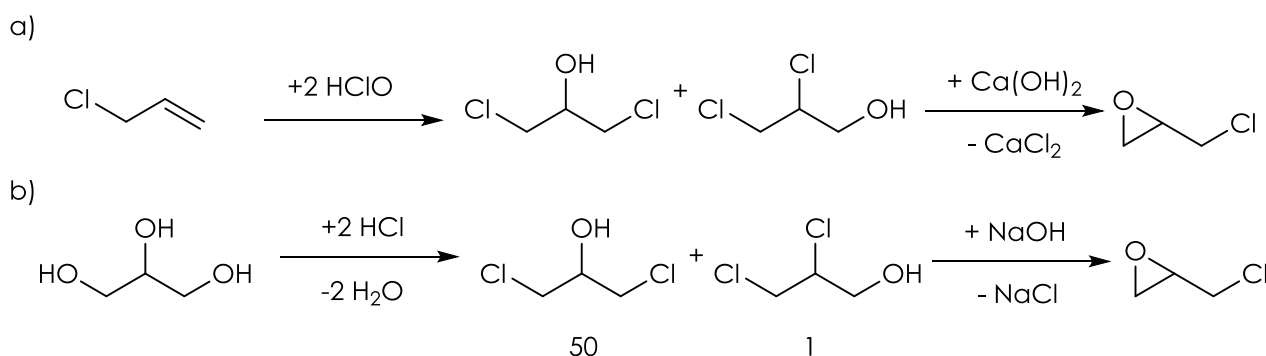
Scheme 59: a) fossil-based process for epichlorohydrin synthesis and b) Glycerin to epichlorohydrin (GTE) process.

1,3-propanediol (0.045 Mt/y [146]) is an important monomer in polyesters (e.g. SORONA, DuPont), polyurethanes, and polyethers manufacture. It is synthesized from non-renewable feedstock by means of two processes, the main difference between them being the first reaction step: 1) hydration of acrolein to 3-hydroxypropionaldehyde, followed by selective hydrogenation to 1,3-propanediol [147] or 2) Hydroformylation of ethylene oxide to 3-hydroxypropionaldehyde and hydrogenation [148]. It industrially synthesized from renewable GLY in a two-step process: 1) starch glucose fermentation to GLY with recombinant *E. Coli* and 2) GLY fermentation to 1,3-propanediol with *Klebsiella*. This process has been commercialized by DuPont [149] to produce the 1,3-propanediol monomer for its SORONA polyester (the other monomer being terephthalic acid). 1,2-propanediol (1,2-PDO) (2.6 Mt/y in 2017) is a relevant chemical intermediate that is industrially produced via hydration of fossil-based propylene oxide with water [150]. Renewable biobased GLY selective hydrogenation represent a promising alternative route to obtain this valuable chemical. Dilute GLY (30 % weight aqueous solution) react selectively with H_2 in the presence of catalysts such as Ni Raney, Cu Raney and supported Ru, Pt or Pd. Copper chromite catalysts, however, where found more active and selective, and capable to process crude GLY (80 % weight aqueous solution) [151]. The reaction proceeds in two steps: at first, GLY is dehydrated to hydroxy acetone, which is then reacted with molecular H_2 to obtain 1,2PDO (Scheme 60). When the reaction is carried out using crude GLY (80 % weight aqueous solution) at 20 bars of H_2 pressure and 200 °C for 24 h, 65 % conversion and about 90 % selectivity were achieved. A continuous process for its production has been commercialized by BASF and Oleon in Belgium [152].
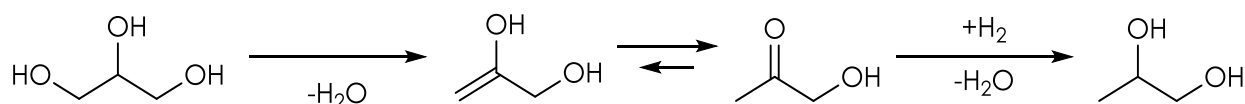
Scheme 60: GLY hydrogenation to 1,2-PDO via hydroxy acetone.

The availability of bio-based 1,2-PDO opens new synthetic routes for more valuable chemicals; in particular, it is a promising starting material for the multi-step synthesis of bio-based methacrylic acid (MAA) and methyl methacrylate (MMA) via the synthetic pathway depicted in Scheme 61 [153]:
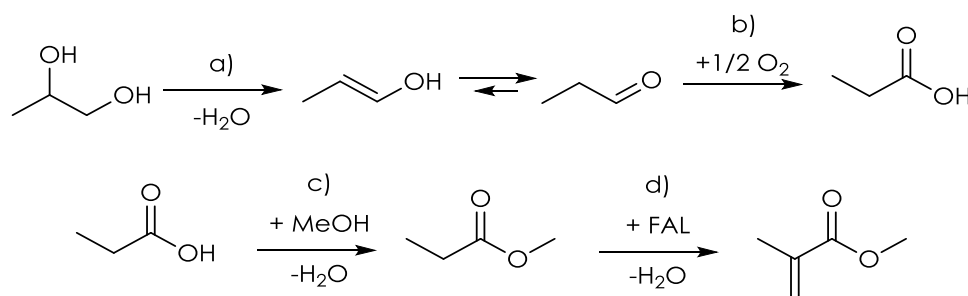
Scheme 61: synthetic route for bio-based MMA via a) 1,2-propandiol dehydration to PAL, b) PAL oxidation to PA, c) esterification of PA to MP with MeOH; d) hydroxy-methylation/dehydration of MP to MMA with FAL.

6.2.3 Safer MMA production avoiding the use of FAL

From the safety point of view, a relevant drawback of the Lucite Alpha-Process lays in the need for a pure stream of pure, anhydrous FAL, because water vapor dramatically reduces catalyst activity. Its direct use should be avoided because it is considered extremely harmful for human health due to its carcinogenicity and toxicity; moreover, pure FAL represent a serious threat in case of accident, makes the routine operation more expensive due to safety measures and requires a dedicated reactor for MeOH oxidation and columns for water removal. This requirement may be overcome if FAL was produced by means of non-oxidative MeOH dehydrogenation in the same fixed bed reactor where hydroxy-methylation/dehydration of MP takes place (Scheme 62). This "one-pot" strategy would allow forming this reactant *in situ,* without water as co-product, and then consumes it immediately, avoiding the need for an ingoing stream of pure FAL. This strategy would allow obtaining FAL in a closed environment and under strictly controlled conditions, reducing the risks connected to its use and enhancing process safety. Moreover, the FAL concentration in the outlet stream would be minimal because it reacts/decompose extensively in reaction conditions.
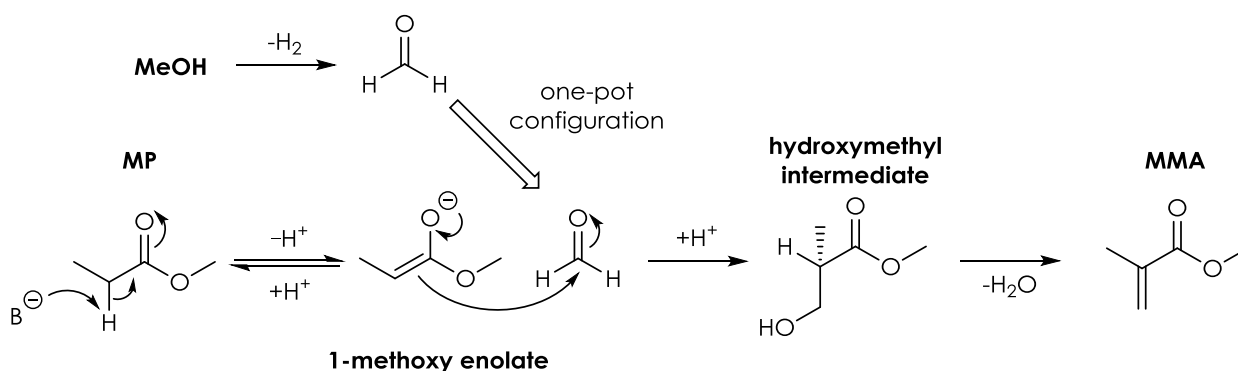
Scheme 62: One pot synthesis of MMA from MP and MeOH.

6.2.3.1 MeOH dehydrogenation to FAL

FAL is industrially produced from methanol by three processes [154]. The former involves the reaction of MeOH with a mixture of air and steam over Ag crystals at 680-720 °C and

atmospheric pressure (BASF process, X MeOH = 97 - 98 %). The feed contains MeOH in excess in respect to air to lie outside the upper explosive limits of the gas mixture. The second process involves the partial oxidation and dehydrogenation of MeOH with a mixture of air and steam over Ag crystals or Ag gauzes at lower temperature (600 – 650 °C, X MeOH = 77 - 87 %), which avoid the occurrence of parasitic reactions. The unreacted MeOH is distilled and recycled. Both processes yield an aqueous solution containing 50-55 wt. % FAL, 1-1.5 % MeOH and minor amounts of formic acid (FA). Silver catalysts promote MeOH dehydration to FAL and H_2 ($\Delta_R H$ = +84 kJ/mol), MeOH partial oxidation to FAL and H_2O ($\Delta_R H$ = -159 kJ/mol) and H_2 oxidation to H_2O ($\Delta_R H$ = - 243 kJ/mol) [154]. The two exothermic reactions produce the heat required for the endothermic dehydrogenation of MeOH and the temperature inside the adiabatic reactor is controlled by the amount of air fed. The last industrial process involves the oxidation of MeOH with excess air over a V_2O_5 or a Mo/Fe/O mixed metal oxide, at atmospheric pressure and 300-400 °C. Both V/O and Mo/Fe/O based catalysts performances are improved by modification with small amounts of other metals (e.g. Cu, Cr, Co, P) and by dispersion over an inert support. In contrast to the silver processes [155], in metal oxides processes the FAL is entirely produced via partial oxidation of MeOH and the main byproducts are CO and DME (the latter formed due to catalysts acidity), together with minor amounts of CO_2 and FA. The reaction mechanism for Ag-based catalysts involves the dissociative adsorption of MeOH, O_2 and H_2 over the metal surface: metallic silver do not undergo oxidation in operative condition and the reaction is confined to catalyst surface [156]. Metal oxide catalyst instead promotes MeOH oxidation via a Mars-Van Krevelen mechanism, and the catalytic cycle involves MeOH oxidation by a lattice oxygen [154]. The catalyst during this process is reduced, and the co-fed air is needed in order to re-oxidize the metal oxide and restore catalytic its activity. The literature about the direct synthesis of MMA from MeOH and MP (which will be discussed in more detail in the next Chapter) lacks of information regarding the catalytic activity for the target reaction over single metal oxides possessing redox properties (e.g. CuO, Fe_2O_3, Cr_2O_3, Ga_2O_3, MnO_2, V_2O_5, Co_2O_3, ZnO, MoO_3, WO_3, CeO_2). Some of these oxides have been reported to be better catalyst for ketonization in respect to MgO (CeO_2, MnO_2, V_2O_5, Fe_2O_3, and Co_2O_3) [100]. Some others (WO_3 and MoO_3), even if not active for ketonization [87], display only acidic features [153, 157], and their ability to catalyze hydroxy-methylation was expected to be scarce, after results obtained in Chapter 5.3.2.4 over other acidic catalysts (Al_2O_3 and MPOs). For others, a rapid deactivation due to reduction to the inactive metallic form in the absence of oxygen by organic reactants has been reported (CuO, AgO, ZnO) [87, 158]. In the present work, however, it has been preferred to avoid oxygen co-feeding because it could have led to extensive coproduction of water, which could compete with MeOH and MP for active sites and generate surface hydroxyl groups. These hydroxyl groups are likely to be responsible for MP hydrolysis to PA, which is more reactive for ketonization than MP. These considerations reduced the possible candidates to promote the dehydrogenative activity of MgO to Ga^{3+} and Cr^{3+}. Both are reported to be scarcely active for ketonization [87]. Moreover, the introduction of such elements into Mg-based oxides is known to boost the dehydrogenating activity towards MeOH in respect to pure MgO [159, 160, 161], allowing to obtain FAL at lower temperature. The introduction of such guest cations into MgO structure reduces catalyst basicity and generates some acidic sites, but an overall basic character is maintained in the resulting mixed metal oxide [159]. Both Mg/Ga/O and Mg/Cr/O systems has been investigated for phenol (PhOH) methylation with MeOH; this reaction (which is known to proceed via *in situ* dehydrogenation of MeOH to FAL, hydroxy-methylation of the aromatic ring of PhOH and finally H-transfer reduction of the so-obtained salicylic alcohol to methyl phenol) shares some feature with the target reaction. In particular, Mg/Ga/O mixed metal oxides displayed outstanding activity for the production of 2,4,6-trimethyl phenol, and superior performance in respect to Mg/Cr/O mixed oxides. For this reason, Ga^{3+} has been chosen as dehydrogenating promoter for MgO.

6.2.3.2 State of art of the MP hydroxy-methylation with FAL and MeOH

Several authors investigated the gas-phase hydroxy-methylation between MP (or PA) and FAL, the latter fed either as an aqueous solution or as trioxane. Catalyst reported to be active can be divided into four main categories:

1. Alkali metals (Li, Na, K or Cs) supported on SiO_2 [162, 163, 164, 165]

2. V/P binary oxides [$(VO_2)P_2O_7$] [166];

3. M/V/P ternary oxides [167] with a third metal "M" selected among Zr, Ti or Sb; M/Si/P ternary oxides [168] with a third metal M selected among W, Mo, Al, Zr, Ti, Zn, Sn, Fe, V [169, 170].

4. V, Nb, Ta or W supported on SiO_2 [170, 171].

The generally accepted mechanism [164, 166, 170] involves the activation of PA or MP by means of the abstraction of an acidic α-proton by a basic site (O^{2-} anions in metal oxides) and the formation of a nucleophilic carbanion or enolate ion adsorbed on catalyst surface, which then reacts with FAL (this mechanism is depicted in Scheme 62, Chapter 6.2.3). It has also been pointed out that the presence of Brønsted acidic sites on catalyst surface may enhances FAL electrophilicity activating it toward nucleophilic attack. Two experimental evidences corroborate this mechanism:

1. The activity order of alkali ions supported on SiO_2 is proportional to their basicity [165] (Cs > K > Na > Li).

2. All catalysts listed above possess the Brønsted acidity required to activate FAL due to the presence of either Si-OH groups (in SiO_2 supported catalysts) or P-OH groups (in phosphorus-containing catalysts).

However, the abstraction of the α-proton from MP (or PA) by those catalysts possessing negligible or low basicity remains difficult to explain, as pointed out by Ai [166]. In Chapter 4.2.2.3, in analogy with the hypothesis formulated by another author [84], a possible explanation has been proposed. A strong interaction between a Lewis acidic sites of a metal oxide or a metal phosphate may favor the enolization of an adsorbed carboxylate anion, by either stabilizing the 1-hydroxy-enolate form or increasing the electrophilicity of the carboxylate form, thus loosening the bond between the α-carbon and the α-hydrogen and speeding the enolization (Scheme 19, Chapter 4.1.4.2.1 and Scheme 29, Chapter 4.2.2.3). The scientific literature regarding the hydroxy-methylation of MP with MeOH as the source of FAL is very scarce. At the best of our knowledge, besides patents, only two paper exists. Ai [172] investigated a catalyst consisting in Ag, Cs and Zr supported on SiO_2 with atomic ratio between the elements equal to 4/10/22/1000 respectively. Cs and Ag provide respectively the basicity required for MP activation and the redox activity for MeOH dehydrogenation, while Zr acts as a promoter. The author pointed out the following findings:

1. The catalytic activity dropped during time-on-stream due to the reduction of silver oxide to metallic Ag.

2. Oxygen co-feeding after catalyst deactivation restored almost completely catalyst activity because, as explained in the previous Chapter, Ag is able to catalyze both the oxidative and non-oxidative dehydrogenation of MeOH.

3. At the beginning of the reaction, the sole product was methyl isobutyrate (MIB), which after a few hours of time on stream disappeared favoring the formation of MMA.

Apart from pointing out the formation of MIB, the author did not mention other by-products. On the other hand, Ueda [173] investigated several MgO-based catalyst impregnated with different other elements (Al^{3+}, Fe^{3+}, Cr^{3+}, Ni^{2+}, Cu^{2+} or Mn^{2+}), using MeOH as source FAL for the synthesis of MMA from MP, the synthesis of acrylonitrile from acetonitrile and the synthesis of vinyl methyl ketone from acetone. The best catalyst for MMA synthesis was the MgO impregnated with Mn^{2+}: in the same reaction conditions, the presence of Mn^{2+} up to 5 wt. % boosted both MP conversion (from 5 to 10 %) and MMA selectivity (from 8 to 60 %) compared to pure MgO; further Mn^{2+} loading did not affect conversion and selectivities. Three main side products were reported, in agreement with our results obtained so far: methyl isobutyrate (MIB) (in agreement with Ai [172]), 3-pentanone (3-P) and 2-methyl-3-pentenone (M-3Pe), the latter produced by the condensation between 3-P and FAL (in agreement with Bailey et al [165]). In conclusion, both authors recognized the need of the simultaneous presence of basic and redox features in the design of a catalyst for the target reaction.

6.3 Experimental

6.3.1 Catalysts synthesis and characterization

6.3.1.1 Commercial catalysts

β-Ga_2O_3 99.99 % was purchased from Alfa Aesar and calcined in static air prior to use at 450 °C for 3 hours with heating rate of 5 °C/min.

6.3.1.2 Mg/Ga/O mixed metal oxides

Two Magnesium/Gallium mixed oxides with Mg/Ga atomic ratio equal to 10 and 20 (Mg/Ga/O-10 and Mg/Ga/O-20) were synthesized by co-precipitation, adapting a technique used to synthesize hydrotalcites. $Mg(NO_3)_2*6H_2O$ and $Ga(NO_3)_3*2H_2O$ were dissolved in deionized water in order to obtain a Mg^{2+} = 1M and Ga^{3+} = 0.1 M solution for Mg/Ga/O-10 and a Mg^{2+} = 1M and Ga^{3+} = 0.05 M solution for Mg/Ga/O-20. These solutions were slowly added dropwise under vigorous stirring to a solution of $Na_2CO_3*10H_2O$ (1 mol/L) maintained at a temperature between 50 and 60 °C. Prior to start the addition of the metal nitrates the pH of the carbonate solution was adjusted with concentrated HNO_3 to the optimal value of 8.5 and maintained between 8.4 and 8.6 during the precipitation with concentrated aqueous NaOH. The optimal pH for the synthesis of Mg/Ga mixed oxide is lower than the one used for the synthesis of MgO because Gallium is amphoteric in nature and its hydroxide becomes soluble at pH higher than 9. The pH was monitored by means of an Amel Instrument 380 pH-meter, calibrated with two buffers at pH 7 and 13. The resulting magnesium and gallium hydroxides suspension was aged under stirring for 45 minutes, filtered by means of a Büchner funnel and washed with distilled water (330 mL every g of catalyst) to remove residual nitrates and carbonates ions. After drying (110°C overnight), the hydroxide precursors of Mg/Ga/O-10 and Mg/Ga/O-20 were crushed and calcined in static air at 450 °C for 4 hours with heating rate of 5°C/min. A physical mixture of MgO (see Chapter 4.2.2.1) and commercial β-Ga_2O_3 with Mg/Ga ratio equal to 10 was also prepared by mixing the powder of the two pure oxide in a mortar. The resulting solid mixture was calcined in the same way of mixed metal oxides.

6.3.1.3 Mg/Ga/O mixed metal oxides characterization

The XRD powder pattern of β-Ga_2O_3, the physical mixture MgO/β-Ga_2O_3, MgO, Mg/Ga/O-20 and Mg/Ga/O-10 are reported in Figure 42 (left side). Commercial β-Ga_2O_3 was highly crystalline and its pattern was characterized by the typical reflections of the most stable monoclinic β-phase (Figure 42, right side). Synthetic MgO, Mg/Ga-10 and Mg/Ga-20 patterns presents the typical reflections of the periclase structure $2θ = 37$ (111), 43 (200), 63 (220), 75 (311), and 79 (222) degree, with no impurities of any polymorph of Ga_2O_3 nor the spinel-phase $MgGa_2O_4$.
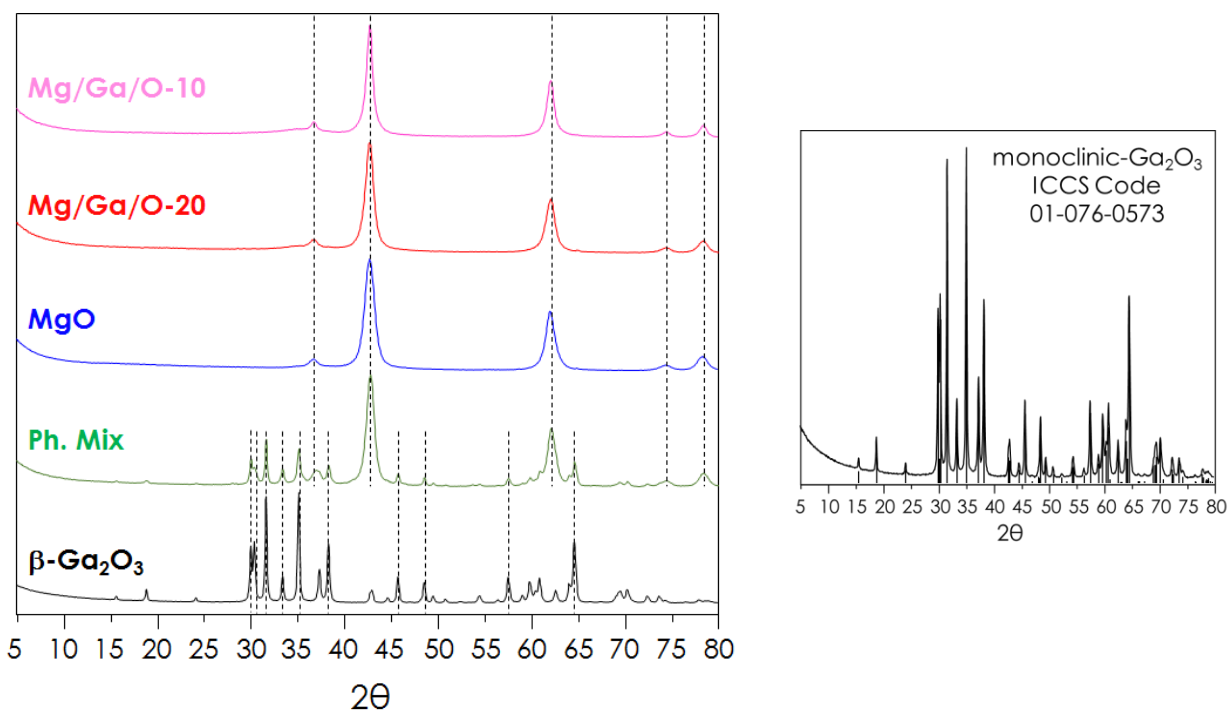
Figure 42: XRD powder patterns of β-Ga_2O_3 (black), the physical mixture MgO/β-Ga_2O_3 (green), MgO (blue), Mg/Ga/O-20 (red) and Mg/Ga/O-10 (magenta) (left side); reference pattern of β-Ga_2O_3 (right side).

The low crystallinity of MgO made not possible to detect any important shift of reflections due to the substitution of Mg^{2+} with Ga^{3+} in the periclase lattice of mixed oxides. In fact, the substitution of Mg^{2+} (0.72 Å) with a cation of greater charge and different size (Ga^{3+}, 0.62 Å) should have led to an alteration of the unit cell and to cationic vacancies which reduce crystallinity [174]. This was not the case for synthesized mixed oxides, probably also because of the high Mg/Ga ratios used. The XRD pattern of Mg/Ga-mix is completely different from those of the two mixed oxides and arises from combination of the patterns of MgO (broad reflections) and β-Ga_2O_3 (sharp reflections). These results suggest that Ga^{3+} was effectively incorporated in the cubic structure of MgO leading to the formation of two real mixed oxides. Commercial β-Ga_2O_3 possessed a low specific surface area due to its high crystallinity, while all Mg-containing catalysts possess specific surface areas higher than 100 m^2/g. Table 14 compile the results of BET analyses and values of Mg-to-Ga ratio of mixed oxides measure by means of SEM-EDS. Multipoint N_2 adsorption/desorption isotherms for β-Ga_2O_3 and Mg/Ga/O-10 are shown in Figure 43, the one for Mg/Ga/O-20 is shown in Figure 44.

catalyst	BET-SSA [m²/g]	Pore mean diameter [nm]	Mg/Ga ratio
MgO	181	3	∞
Mg/Ga/O-20	118	4-6	21.4
Mg/Ga/O-10	132	14	9.8
β-Ga₂O₃	14	4-7	/

Table 14:catalysts specific surface area, pore mean diameter (porosimetry) and Mg/Ga ratio (SEM-EDS).
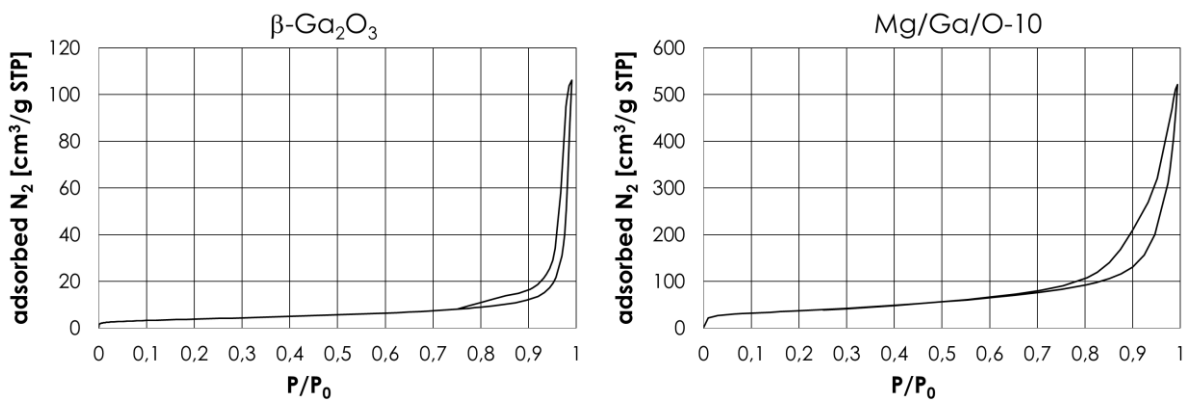
Figure 43: N₂ adsorption/desorption isotherms of β-Ga₂O₃ (left side) and Mg/Ga/O-10 (right side).
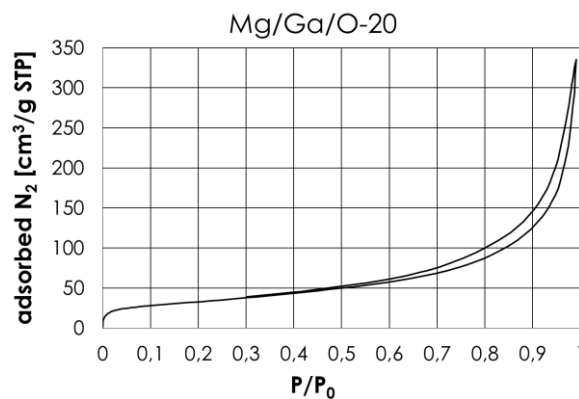
Figure 44: N₂ adsorption/desorption isotherms of Mg/Ga/O-20.
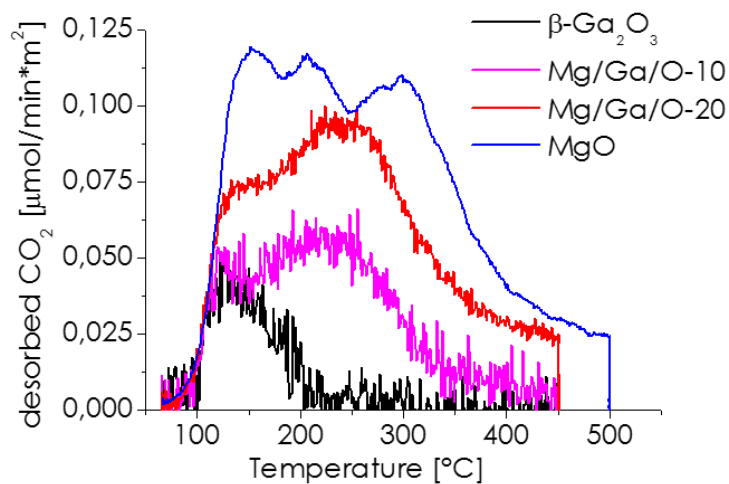
Figure 45: CO₂ temperature programmed desorption profiles of β-Ga₂O₃ (black), MgO (blue), Mg/Ga/O-20 (red) and Mg/Ga/O-10 (magenta).

Figure 45 depicts the CO_2 and NH_3-TPD profiles for β-Ga_2O_3, MgO, Mg/Ga/O-20 and Mg/Ga/O-10. The CO_2-TPD profile of MgO suggest the presence of basic sites with different strength and shows three maxima of desorption around 155 , 210 and 295 °C; above this temperature CO_2 keeps desorbing until 500 °C and then stops after 1h of isotherm, in agreement with the recent literature [175]. As expected, MgO possesses the highest density and strength of basic sites among all materials investigated. These sites consist of coordinatively unsaturated O^{2-} anions bound to the highly electropositive Mg^{2+} cations. Their strength is expected to increase with their degree of unsaturation: five coordinated O^{2-} anions in terraces > 4 coordinated O^{2-} anions on steps > 3 coordinated O^{2-} anions in kinks > cationic vacancies in terraces. The latter consists in negatively charged "holes" on catalysts surface formed by 5 different O^2 anions and resulting from the absence of a Mg^{2+} cation, as can be seen in Figure 46. Lewis acidity of Mg^{2+} cations increase in the same order.
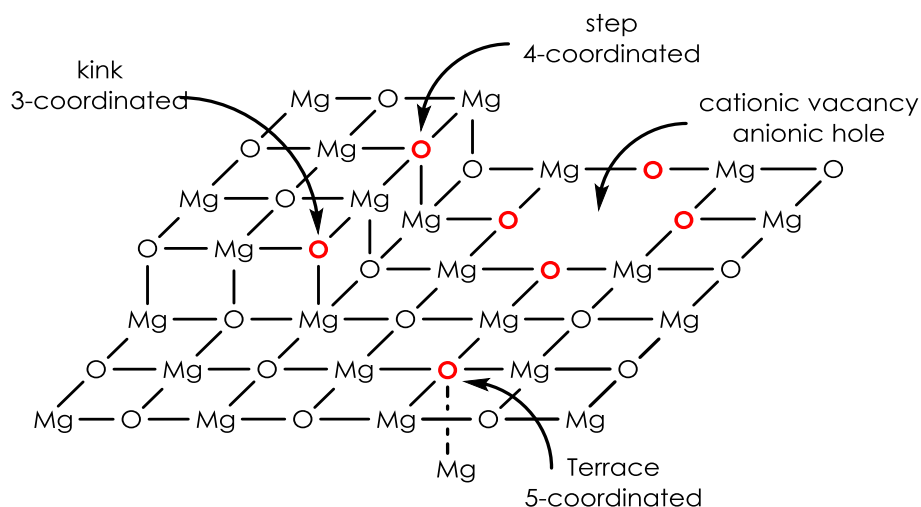
Figure 46: model of MgO surface.

According to literature [176], in MgO-based mixed systems containing a highly electronegative guest cation such as Ga^{3+}, the density of basic sites and their strength decrease compared to the one of pure MgO, due to the higher covalent character of the bond between O^{2-} anions and the highly electronegative cations. This behavior of mixed systems is noticeable in the TPD profiles of Mg/Ga-20 and Mg/Ga-10, where the strength and density decrease with an increase in the Ga^{3+} content. Mg/Ga-20 shows two maxima at 140 and 245 °C; CO_2 evolution continues up to calcination temperature and stops during the final isotherm. Mg/Ga-10 CO_2-TPD shows a very similar profile with a lower density of basic sites and two maxima at 135 °C and 220 °C. Even in this case, small amounts of CO_2 continue to desorb up to the calcination temperature, which means that this catalyst possesses a small fraction of strong basic sites. Interestingly, the density of medium strength basic sites in these two materials is higher than both weak and strong sites. β-Ga_2O_3 possess a density of weak basic sites very similar to that of Mg/Ga-10, but differs from this one because no medium strength or high strength basic sites are present: CO_2 desorption stops completely at 210 °C. NH_3-TPD profiles for β-Ga_2O_3, Mg/Ga-20, Mg/Ga-10 and MgO are shown in Figure 47. MgO desorbs a negligible amount of NH_3 around 187 °C; as expected this catalyst is the one with the lowest density and strength of acidic sites. Mg/Ga-20 behaves in a similar way: the desorbed amount of NH_3 is very low; the maximum of desorption is around 205 °C. Mg/Ga-10 shows a relatively high density of weak acidic sites with a maximum of desorption at 210 °C. All Mg-containing samples possess only weak acidic sites regardless their density, and NH_3 desorption completes at around 300 °C. As expected, β-Ga_2O_3 shows the highest density and strength of acidic sites. In this case, NH_3 keeps desorbing up to the calcination temperature and stops only during the final isothermal step. The unit cell of monoclinic β-Ga_2O_3 contains 8 Ga^{3+} cations: half of them

assumes a distorted octahedral coordination, the other half is in a distorted tetrahedral coordination; therefore, two distinct Ga-O bond length of 2.00 and 1.83 Å are present [177].
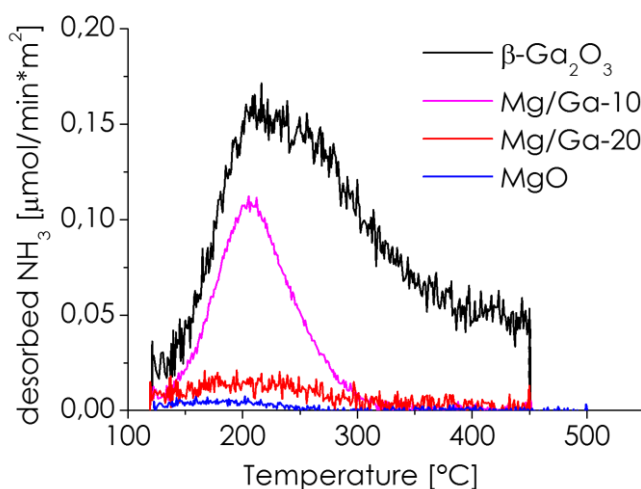
Figure 47: *NH$_3$ temperature programmed desorption profiles of β-Ga$_2$O$_3$ (black), MgO (blue), Mg/Ga/O-20 (red) and Mg/Ga/O-10 (magenta).*

In general, tetrahedral cations are considered stronger acidic sites than octahedral cations due to their lower coordination number; therefore, it is likely that strong acidic sites present only in β-Ga$_2$O$_3$ are related to the presence of tetrahedral Ga^{3+} ions, which seem to be absent in the mixed oxides. In the periclase lattice Mg^{2+} cations occupy only octahedral cavities but the guest Ga^{3+} cations in principle may occupy both octahedral and tetrahedral cavities because the crystal field theory predicts that neither the octahedral nor tetrahedral coordination are energetically preferred for metals possessing a d^{10} electronic configuration in spinels, which have a cubic crystal just like periclase. Therefore, even if the NH$_3$-TPD results suggest the absence of tetrahedral Ga^{3+} in mixed oxides, their presence cannot be ruled out. Concluding, in mixed Ga/Mg mixed oxides, the introduction of Ga^{3+} into the periclase structure of MgO leads to an increase of the density of weak acidic sites. The temperature of maximum NH$_3$ desorption increases with an increase of Ga content (MgO: 187 °C, Mg/Ga-20: 205 °C, Mg/Ga-10: 210 °C, β-Ga$_2$O$_3$: 220°C), suggesting that not only the density but also the strength of weak acid sites is affected by the Ga content.

catalyst	Total basicity [μmol/m^2 CO$_2$]	Total acidity [μmol/m^2 NH$_3$]
MgO	3.5	0.09
M/Ga/O-20	2.5	0.4
M/Ga/O-10	1.3	1.1
β-Ga$_2$O$_3$	0.4	3.9

Table 15: *total acidity and total basicity of catalysts.*

6.3.2 Catalytic tests

6.3.2.1 Catalytic activity of MgO and β-Ga$_2$O$_3$

Results obtained feeding a MP/MeOH/N$_2$=6/12/82 mixture over MgO (W/F = 0.8 s*g/mL) as a function of reaction temperature (Graph 15, Chapter 5.3.2.3) indicated that MgO is not a good catalyst for MMA synthesis, because this compound was obtained in negligible yields. However, since ketonization requires the encounter of two MP molecules on catalyst surface to occur, it has been decided to investigate the possibility to reduce MP

concentration in the feed. In order to do so, the molar fraction of MP in the feed was decreased from 6 % to 1 %, while simultaneously increasing the MeOH/MP feed molar ratio from 2 to 5 (molar fraction of MeOH = 5 %). This way ketonization should be unfavored, while at the same time a higher excess of FAL available for MP hydroxy-methylation should be obtained from MeOH *in situ* dehydrogenation. Finally, in the attempt to reduce the extent of consecutive H-transfer hydrogenations, W/F was reduced from 0.8 to 0.5 s*g/mL. Results of the catalytic activity of MgO, in these optimized reaction conditions and in the temperature range 350-450 °C, are shown in Graph 23. Despite the precautions taken to favor the desired reaction, MMA yield remained low in all the temperature range investigated (0.1 %, 1.3 % and 0.3 % at 350, 400 and 450 °C respectively). However, the overall reaction scheme proved to be sensitive to the different reaction conditions because different products were formed. Propionaldehyde (PAL) was the main product at 300 and 350 °C (4.8 % and 16.0 % yield respectively); this compound may be formed by either H-transfer hydrogenolysis of MP or retro-Tishchenko, being the latter pathway the most likely because H-transfer hydrogenolysis have been proved to be generally favored by higher temperatures.
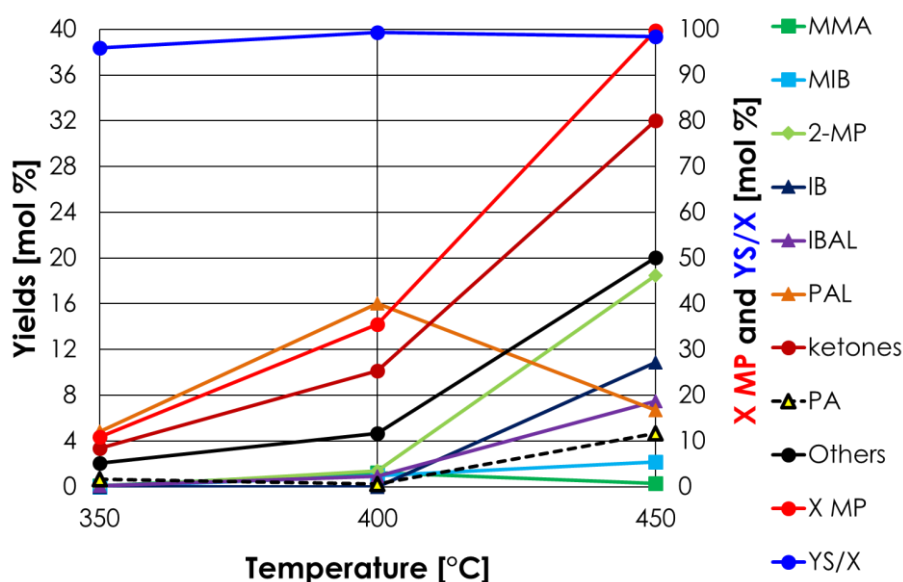
*Graph 23: Gas-phase reaction of MP and MeOH as a function of reaction temperature: catalyst = MgO; MP/MeOH/N$_2$ feed composition [mol %] = 1/5/94; W/F = 0.5 s*g/mL. Others includes unknown compounds, PA, MAA, IBA, MAL, PrOH. Yields calculated in terms of moles.*

These results suggest that a larger excess of MeOH indeed minimizes the occurrence of the undesired ketonization but might also favor undesired reactions on MP. Ketones were formed at all temperatures but became the main products only at 450 °C (sum of yields = 32.0 %). It is worth noticing that at 450 °C the sum of yields of products of hydroxy-methylation (MMA, methacrylic acid (MAA), isobutyric acid (IBA), methacrolein (MAL), MIB, IBAL, 2MP and IB) was higher (42.5 %) than the one of ketones. This is another argument in favor of the hypothesis that the higher excess of MeOH, and the resulting higher excess of FAL, indeed reduces the occurrence of the parallel reaction of ketonization. However, even if in this reaction conditions (T = 450 °C, W/F = 0.5 s*g/mL and MeOH/MP = 5) hydroxy-methylation competes with ketonization, the obtained MMA is immediately reduced, by consecutive reactions, to less valuable C$_4$ products: MIB (Y = 2.2 %), IBAL (Y = 7.5 %), 2-MP (Y = 18.5 %), and IB (Y = 10.9 %). Results shown here and in Chapter 5.3.2.3 indicates that MgO is not an effective catalyst for the target reaction. In fact, depending on the MeOH excess in respect to MP, at low temperature (350-400 °C) the main products are ketones or PAL, while at high temperature, even if MeOH is effectively converted to FAL and MP hydroxy-methylation competes with ketonization, ketones are the main products and MMA is not obtained due to consecutive H-transfer hydrogenations. The presence of significant

amounts of PAL in the reaction environment at all temperature complicates the reaction scheme because this compound might react with FAL to produce MAL. MAL was found in very small amount and is reported together with "others". This reaction is likely to occur because PAL α-hydrogens are more acidic in respect to the ones of MP and their abstraction is expected to proceed faster. The higher acidity of PAL α-hydrogens depends on the better delocalization of the excess negative charge in the resulting PAL enolate ion in respect to the MP enolate anion, as explained in Chapter 5.3.2.1, Scheme 37. Moreover, in principle PAL may lead to the formation of propyl propionate (PP) via Tishchenko reaction, which can further react to produce 3-P, following the ketonization pathway of alcohols. The presence of PP in reaction mixtures is, however, uncertain. A very small peak with compatible retention time in GC-FID chromatograms was present only at 450 °C and, at this temperature, a very large number of unknown compounds have been observed as well. The uncertainty characterizes the possible presence of IBIB from the Tishchenko condensation of IBAL. In conclusion, the results obtained over MgO indicates that three main reactions reduces the yield in MMA: the former two are parallel in respect to the desired reaction (MP ketonization and MP H-transfer hydrogenation) while the latter is consecutive (H-transfer hydrogenation of MMA) as depicted in Scheme 40 at the end of Chapter 5.3.2.1. The results of the catalytic tests over β-Ga_2O_3 as a function of temperature are shown in Graph 24.
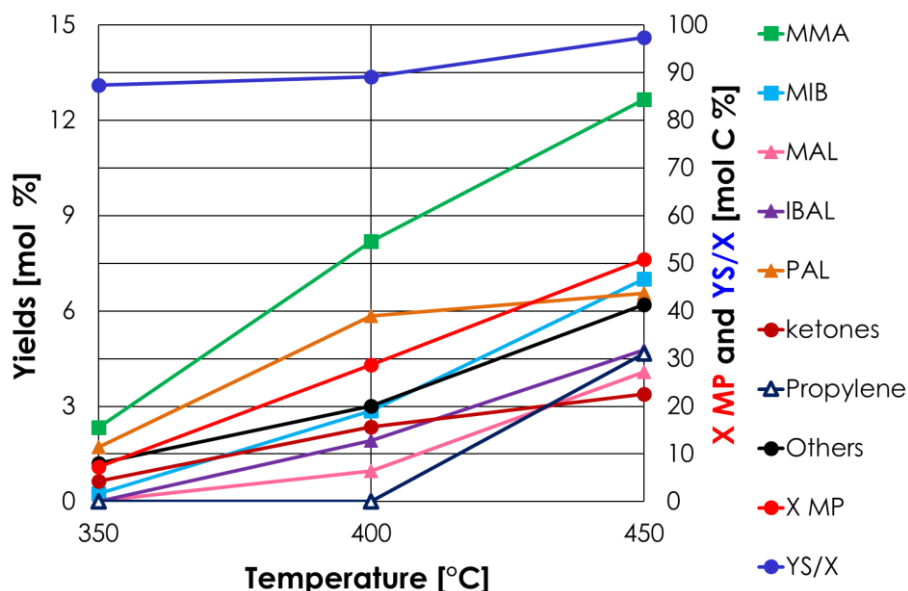
Graph 24: Gas-phase reaction of MP and MeOH as a function of reaction temperature: catalyst = β-Ga_2O_3; MP/MeOH/N_2 feed composition [mol %] = 1/5/94; W/F = 0.5 s*g/mL. Others includes unknown compounds, PA, MAA, IBA, 2MP, PrOH. Yields calculated in terms of moles.

Over this catalyst, MP conversion increased from 7.3 % to 50.9 % in the temperature range between 350 and 450 °C. Considering the significant difference between the specific surface area of MgO and β-Ga_2O_3, 181 and 14 m^2/g respectively, this result indicates that the latter catalyst is far more active than the former, probably due to the enhanced methanol dehydrogenation activity toward FAL. Values of X MP normalized by SSA of catalyst MgO and β-Ga_2O_3 are shown in Table 16.

catalyst	X MP/SSA [m^{-2}] 350 °C	X MP/SSA 400 °C [m^{-2}]
MgO	0.06	0.20
β-Ga_2O_3	0.52	2.05
Ratio X MP/SSA (Ga/Mg)	8.7	10.3

Table 16: X MP normalized by SSA of catalysts at 350 and 400 °C

MMA synthesis from MP and MeOH

MMA was the main product of the reaction in all the temperature range investigated (2.3 %, 8.2 % and 12.7 % yield at 350, 400 and 450 °C respectively). These results can be explained by considering the strong dehydrogenating activity of β-Ga₂O₃, which leads to the production of larger amounts of FAL at lower temperatures compared to MgO. Ketonization, far from being the main reaction as it was for MgO, yielded only 3.4 % ketones at 450 °C and the major by-products were those deriving from the consecutive H-transfer reactions occurring on both MMA (with formation of MAL, IBAL, and MIB) and MP (with formation of PAL), together with propylene. The latter is probably formed due to parasitic reaction occurring on C4 products at high temperature, which cause the loss of a carbon atom in the form of CO_2. Consecutive H-transfer becomes more preferred on both MgO and β-Ga₂O₃ when the reaction temperature is increased. However, surprisingly, β-Ga₂O₃ was less active than MgO for both ketonization and H-transfer, even if both reactions more easily occur on amphoteric catalysts than on those displaying only basic features. This result suggest that the strength of basic sites may be more important than the one of acidic sites for ketonization and H-transfer reactions. This hypothesis would explain why activity for ketonization and H-transfer follows the order ZrO₂ > La₂O₃ > MgO > β-Ga₂O₃: ZrO₂ possess balanced strong acid and basic sites, the following two are extremely basic, being La₂O₃ the stronger base, while β-Ga₂O₃, even being amphoteric, possess only weak basicity. Even if no evidences of deactivation were found at 350 and 400 °C, during the catalytic test at 450 °C a consistent decrease in MP conversion and product yields was evident. A catalyst stability test was performed carrying out the reaction over β-Ga₂O₃ for a prolonged time on stream (18 hours); after that, the catalyst was calcined in air at 450 °C for 3 hours and the catalyst stability test was repeated (13 hours). The results of this short-term deactivation-reactivation test are shown in Graph 25 as function the time on stream, while the results previously reported in Graph 24 for the catalytic test at 450 °C consist of the mean values of X MP and yields over 6 hours of time on stream. In order to facilitate the interpretation of Graph 25, the products resulting from the hydroxy-methylation and dehydration of MP and the consecutive H-transfer hydrogenation or hydrogenolysis of MMA were grouped together in the category "H-transfer MMA" (purple line, MIB + MAL + IBAL + 2-MP + MAA + IBA). PAL and PrOH deriving from H-transfer reaction occurring on MP were grouped together in the category "H-transfer MP" (orange line).
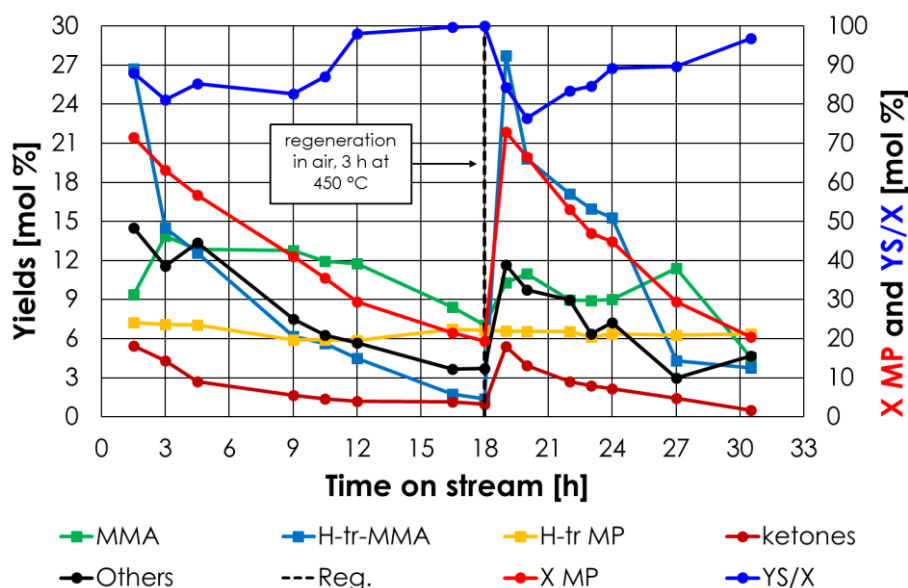
Graph 25: Gas-phase reaction of MP and MeOH as a function of time on stream: catalyst = β-Ga₂O₃; temperature = 450 °C; MP/MeOH/N₂ feed composition [mol %] = 1/5/94; W/F = 0.5 s*g/mL. Others includes unknown compounds, PA, MAA, IBA, 2MP, PrOH. Yields calculated in terms of moles.

During 18-hour time-on-stream MP conversion dropped from 71.6 % down to 19.7 %. At the beginning of the reaction (1.5 hours of time on stream) H-transfer reduction of MMA (purple line) was the main side reaction (MIB= 13.1 %, IBAL= 7.1 %, MAL= 5.9 %); at the same time MMA yield was 9.4 %, higher than those of H-transfer MP products (orange line) and ketones (dark red line). However, during the next 9 hours MMA yield stabilized at around 12 % while those of H-transfer MMA products and ketones dropped down to values well below 5 %. Finally, starting from the 12th hour of reaction, also MMA yield started to decrease down to 7 % after 18 hours of reaction. The reasons behind the deactivation of β-Ga$_2$O$_3$ will be discussed in Chapter 6.3.3. During the 13-hour time-on-stream regeneration test, MP conversion dropped from 72.9 % down to 20.5 %: these results indicate that calcination restores the initial catalyst activity but not its stability, in fact, after calcination, it deactivated to the same degree in a shorter time (13 hours instead of 18 hours). Moreover, after calcination the yields towards MMA was slightly reduced (9.9 %) while the one towards MMA H-transfer products (purple line) increased. No significant difference was found before and after regeneration regarding the yields in ketones and MP H-transfer hydrogenation products. In conclusion, catalytic results obtained over MgO and β-Ga$_2$O$_3$ indicate that the former catalyst is not effective for the target reaction, while the latter proved to be more active and selective for the one-pot reaction between MP and MeOH. Being β-Ga$_2$O$_3$ a commercial reference material with low SSA, there is plenty of room for optimization, for example investigating the activity of different polymorphs. However, such line of research was not covered, because besides the fast deactivation of β-Ga$_2$O$_3$, another significant drawback of every Ga-based catalyst is the very high cost of Ga. Even if not rare (it is about 10 time more abundant than Sn, which is not considered a rare metal [178]), it does not form Ga-rich ores and the only economically viable production processes are its extraction from sulphidic zinc ores, coal and bauxite, the latter being the more relevant. In these ores, Ga is found in trace amounts. Therefore, being a by-product of Al production (bauxite), its supply is constrained by Al demand. On top of that, it is considered a technology critical element, because it finds application in several strategic high-tech products [179]. Therefore, a Ga-containing catalyst to be used for large-scale production should be formulated reducing as much as possible the Ga content. In order to achieve this goal, we evaluated Ga^{3+} as a dehydrogenation promoter in MgO-based mixed oxides. In fact, the incorporation of redox elements into MgO-based mixed oxides is known to boost their dehydrogenating features and sensibly reduces the temperature needed in order to obtain a satisfying amount of FAL [180, 181]. As an example, Mg/Ga/O mixed oxides have been reported to display an excellent activity towards phenol methylation to 1,4,6-trimethylphenol with MeOH via FAL as the real methylating agent [161]. Moreover, oxides containing Ga^{3+} have been reported to be active even for the dehydrogenation molecules of less reactive than MeOH, such as ethane [182] and propane [183]. As a proof of concept, two mixed MOs containing a small fraction of Ga^{3+} in respect to Mg^{2+} ions were synthesized (Mg/Ga/O-10 and Mg/Ga/O-20, where the numbers represent the atomic Mg/Ga ratio) and their catalytic performance were compared to the ones of the pure oxides and a physical mixture of MgO and β-Ga$_2$O$_3$ with Mg/Ga atomic ratio equal to 10.

6.3.2.2 Catalytic activity of Mg/Ga/O mixed MOs

The comparison between the catalytic performance of MgO, Mg/Ga-20, Mg/Ga-10, the physical mixture of pure oxides with Mg/Ga= 10 and pure β-Ga$_2$O$_3$ at 400 °C is shown in Graph 26. As in the case of Graph 25, in order to achieve an easier interpretation, the products resulting from the hydroxy-methylation and dehydration of MP and the consecutive H-transfer hydrogenation or hydrogenolysis of MMA were grouped together in the category "H-transfer MMA" (purple bars, MIB + MAL + IBAL + 2-MP + MAA + IBA). PAL and PrOH deriving from H-transfer reaction occurring on MP were grouped together in the

category "H-transfer MP" (orange bars). Moreover, in this case the YieldSum (YS) was reported instead of the molar balance (YS/X), in order to keep the same Y scale. Remarkably, apart from β-Ga$_2$O$_3$ at 450 °C (Graph 25, previous Chapter) all the other catalysts did not show any deactivation during time on stream. The comparison between MgO and mixed MOs (Table 17) shows that both Mg/Ga-20 and Mg/Ga-10 yielded a lower amount of H-transfer MP products and ketones, and a higher amount of H-transfer MMA products compared to pure MgO. These results suggest that the incorporation of Ga^{3+} enhances the dehydrogenating properties of the catalyst leading to a higher excess of FAL, and, as a consequence, MP and ketones hydroxy-methylation occur to a greater extent. In fact, if we compare the sum of yields to MMA, H-transfer MMA products and methylated ketones (Y Hydr. Meth. in Table 17), which represent the overall yield of hydroxy-methylation, obtained over MgO, Mg/Ga-20 and Mg/Ga-10, it appears proportional to the Ga^{3+} content and not to catalyst basicity. In fact, it could be said that it is inversely proportional to catalysts basicity. Therefore, even if basic sites are required to activate MP, and the more basic the site is, the easier would be the α-proton abstraction, the higher activity of Mg/Ga mixed oxides depends on their higher dehydrogenating activity, which is related to the Ga^{3+} content, and not their basicity.
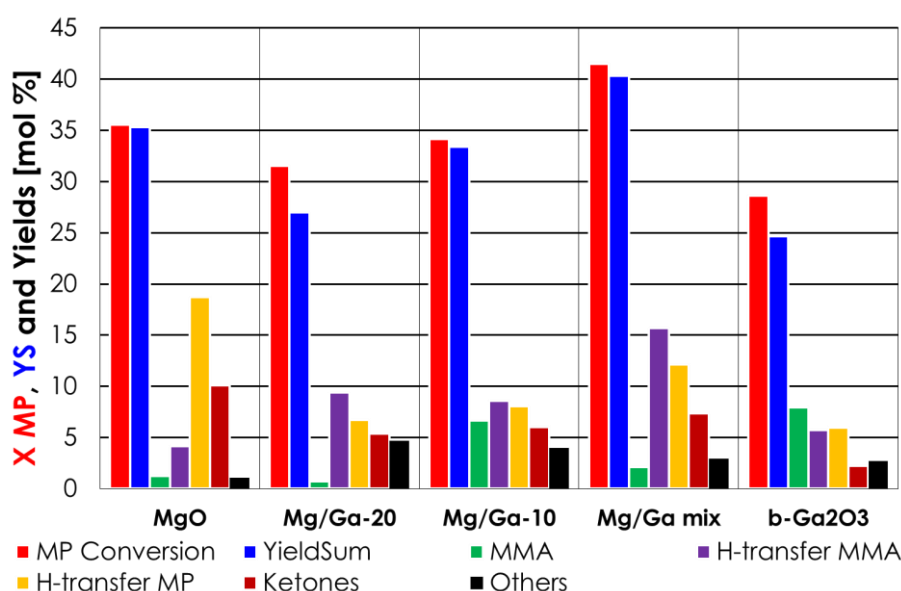
Graph 26: Gas-phase reaction of MP and MeOH over pure oxides, mixed MOs and the physical mixture of pure oxides; temperature = 400 °C; MP/MeOH/N$_2$ feed composition [mol %] = 1/5/94; W/F = 0.5 s*g/mL. Others includes PA and unknown compound. Yields calculated in terms of moles.

catalyst	Y MMA [%]	Y H-tr. MMA [%]	Y Hydr. Meth. [%]	Y H-tr. MP [%]	Y ketones [%]
MgO	1.3	4.1	8.5	18.7	10.1
M/Ga/O-20	1.4	9.4	12.7	6.7	5.4
M/Ga/O-10	6.6	8.6	17.8	8.1	6.0
β-Ga$_2$O$_3$	8.0	5.8	15.3	6.8	2.2
Mg/Ga-mix	2.1	15.7	20.4	12.1	7.4

Table 17: comparison between the performance of pure oxides, mixed MOs and the physical mixture of pure oxide

Moreover, the incorporation of Ga^{3+}, which reduces both the density and strength of basic sites (Figure 45, Chapter 6.3.1.3), seems to have a positive effect on the selectivity to MMA

because H-transfer hydrogenation on both MP and MMA occurs to a lower extent. The behavior of the physical mixture of the two oxides (catalyst Mg/Ga-mix in Graph 26 and Table 17) confirms what was said above. This catalyst should possess a basicity comparable to that of MgO and a redox power comparable to that of Mg/Ga-10. Therefore, the higher yield in H-transfer MMA products (purple bar) in respect to all other catalyst can be explained with its higher activity for both hydroxy-methylation and H-transfer hydrogenations, related to the presence of pure β-Ga_2O_3 and MgO respectively. The lower yield in MMA (green bar) in respect to β-Ga_2O_3 and mixed MOs depends on its higher basicity, which favors consecutive the H-transfer hydrogenations MMA. The yield in H-transfer MP products (orange bar) over this catalyst is higher than the one obtained over the two mixed oxides (due to its higher basicity), but lower than the one over MgO, because on the latter hydroxy-methylation occurs to a much lower extent and H-transfer hydrogenations occurs preferably on MP because MMA is produced in small amounts. Finally, ketonization activity is intermediate between the one of MgO and the ones of mixed MOs and β-Ga_2O_3. To sum up, a higher basicity makes a catalyst more active for α-proton abstraction and hydroxy-methylation, but also for H-transfer, and therefore MMA is obtained with low yields because of its consecutive transformation. Conversely, a catalyst possessing a low density of weak basic sites, such as Mg/Ga-10 and β-Ga_2O_3, activate less MP but is more selective. In conclusion, an active and selective catalyst should possess high dehydrogenating activity in order to afford a large excess of FAL at low temperature as the preliminary requirement; then, in order to avoid ketonization and H-transfer side reactions, the catalyst should possess a moderate basicity. Starting from this early conclusion, we decided to study thoroughly how some key reaction parameter affect catalytic performance over Mg/Ga/O-10. This material has been chosen because the catalysts screening depicted in Graph 26 showed that it is capable to produce MMA in yield similar to β-Ga_2O_3, even if it is slightly less selective. Experiments conducted so far have shown that one of the most important parameters is the amount of FAL generated by *in situ* MeOH dehydrogenation, which should be obviously affected by temperature and molar feed ratio. Graph 27 shows the results of the catalytic performance of Mg/Ga-10 as a function of the molar ratio between MeOH and MP at 400°C and W/F = 0.5 s*g/mL. In these experiments, the inlet molar fraction of MP was maintained constant and equal to 1 %, while MeOH content was varied between 2 and 10 %.
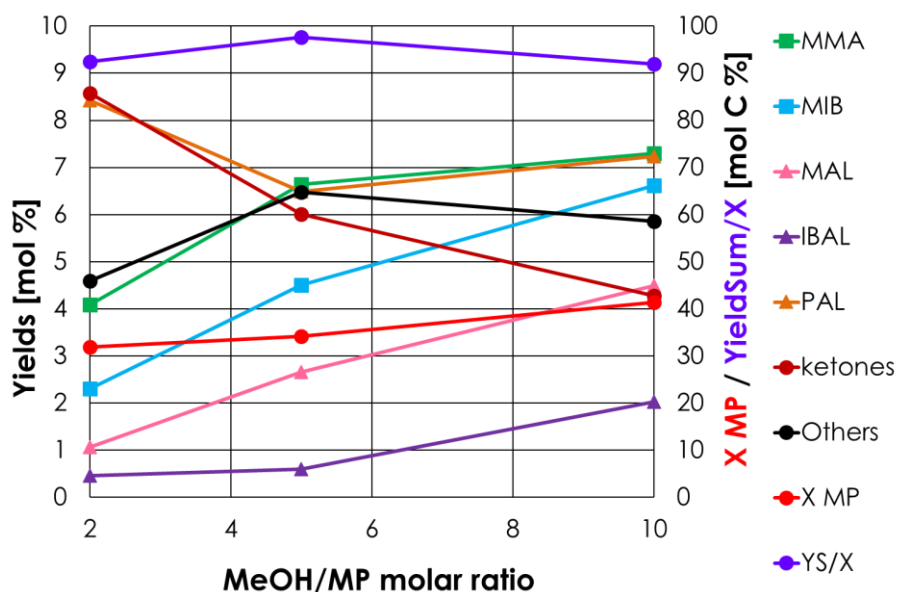
*Graph 27: Gas-phase reaction of MP and MeOH as a function of the molar ratio MeOH/MP; catalyst: Mg/Ga/O-10; temperature = 400 °C; W/F = 0.5 s*g/mL. Others includes PA, 2MP, PrOH, MAA, IBA and unknown compounds. Yields calculated in terms of moles.*

MMA synthesis from MP and MeOH

As expected, a higher MeOH/MP excess made more difficult for two MP molecules to encounter each other on catalyst surface and react to produce ketones. An increase of MeOH/MP molar ratio from 5 to 10 led to a reduction of the overall yield of ketones from 6.0 to 4.7 %. On the other hand, a decrease in MeOH/MP molar feed ratio led to an increase in the yield of ketones up to 8.6 %. Regarding the effect of MeOH/MP molar feed ratio on the rate of hydroxy-methylation and H-transfer hydrogenations, it was, as easily predictable, exactly opposite. The yield of MMA increased from 4.1 to 6.6 % raising the excess of MeOH in respect to MP from 2 to 5 and reached 7.3 % with MeOH/MP = 10. If the overall yield of hydroxy-methylated products including ketones is considered, it increases from 10.9 % to 17.8 % with an increase of MeOH/MP from 2 to 5 and reached 24.5 % when the MeOH/MP molar ratio was 10. Therefore, the fraction of MMA in respect to the sum of hydroxy-methylated products became lower by increasing MeOH/MP molar ratio because a larger excess of MeOH and FAL favored parasitic H-transfer hydrogenations. At first sight, the same cannot be said for PAL. Previously it has been proposed that this compound can be formed via MP H-transfer hydrogenation or via a retro-Tishchenko reaction of MP. In both cases, one would expect PAL yield to be lower in the presence of a lower excess of MeOH, because H-transfer reaction are favored by larger excess of MeOH/FAL and the retro-Tishchenko would have competed with more ketonization. Instead, its yield decreased with an increase in MeOH/MP from 2 to 5. This result strongly suggest that in the presence of more FAL it is consumed to produce MAL. Raising MeOH/MP ratio from 5 to 10 PAL yield became slightly higher, therefore it can be concluded that higher excess of MeOH favor also MP H-transfer hydrogenolysis or retro-Tishchenko to PAL (the latter thanks to less competition from ketonization). Starting from this result, it has been decided to investigate the possibility to enhance MMA selectivity by reducing the W/F (and therefore reduce the occurrence of consecutive H-transfer hydrogenations) while feeding an excess of MeOH in respect to MP equal to 10, in order to ensure that a large excess of FAL was present. Moreover, this set of catalytic tests was aimed at the investigation of the reaction scheme; therefore, also a higher contact time has been investigated. Graph 28 shows the effect of W/F (time factor) on product distribution at 400 °C. Figure 48 depicts the particular of the results obtained with very low W/F in order to facilitate their interpretation.
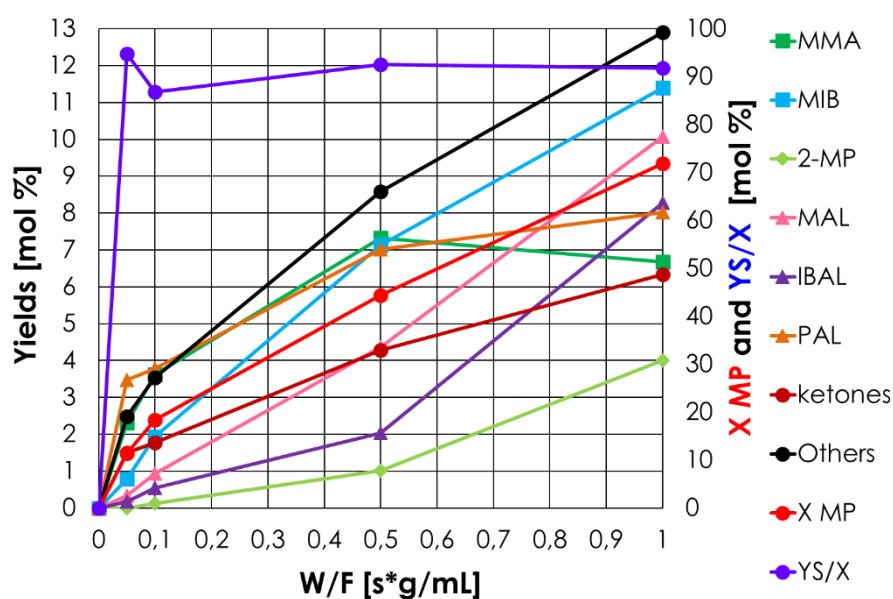
Graph 28: Gas-phase reaction of MP and MeOH as a function of the W/F; catalyst: Mg/Ga/O-10; temperature = 400 °C; MP/MeOH/N_2 feed composition [mol %] = 1/10/89; Others includes PA, PrOH, MAA, IBA and unknown compounds. Yields calculated in terms of moles.
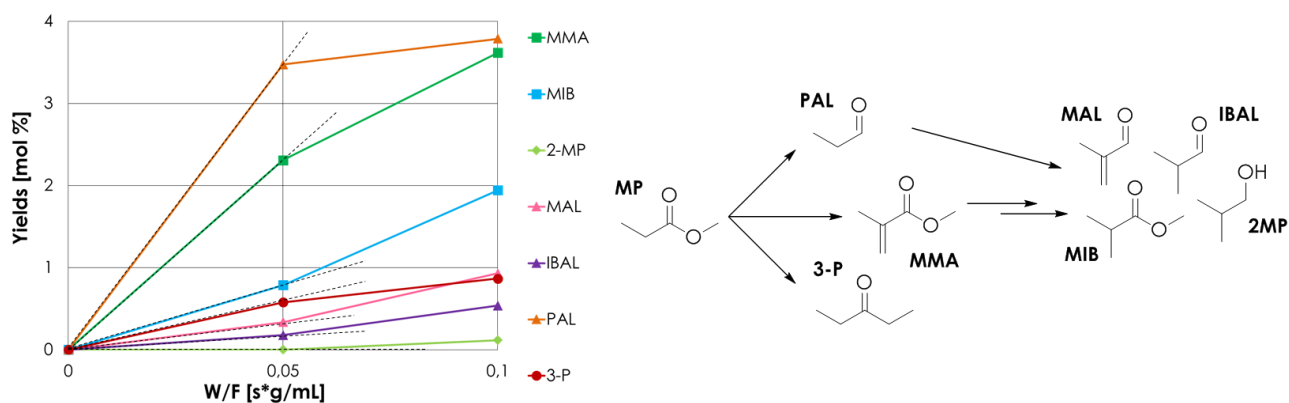
Figure 48: particular of the region of Graph 28 comprised between W/F=0 s*g/mL and W/F=0.1 s*g/mL.

As expected, MMA, PAL and 3-P are formed by parallel reactions occurring on MP because their yield trends show a downward concavity, with a positive slope for W/F tending to zero (refer to Figure 48). Actually, MMA cannot be considered a primary product, because it forms via the dehydration of a hydroxy-methylated intermediate. However, the dehydration of this intermediate is so fast that, in order to appreciate its effect on the concavity of the yield trend of MMA, much lower contact time are needed. A similar consideration can be made for 3-P, which is formed by the decarboxylation of the β-keto ester (the real primary product). MIB, MAL, IBAL and 2-MP yield trends instead exhibit an upward concavity and their slope tends to 0 for W/F tending to 0, meaning that they are formed by consecutive reactions (Figure 48). Moreover, MMA yield shows a maximum at 0.5 s*g/mL and then slightly drops at 1.0 s*g/mL meaning that this product is consumed by consecutive reaction. The final set of catalytic tests consisted in the study of the effect of reaction temperature over Mg/Ga/O-10 in the range between 350 and 425 °C. MeOH/MP molar ratio was equal to 10 and W/F equal to 1 s*g/mL. These reaction conditions have been chosen in the attempt to maximize MMA yield in respect to H-transfer and ketonization by product by reducing reaction temperature while maintaining a large excess of MeOH. To facilitate the interpretation of Graph 29, IBAL yield is reported on the right-y-axis together with X MP and the molar balance YS/X.
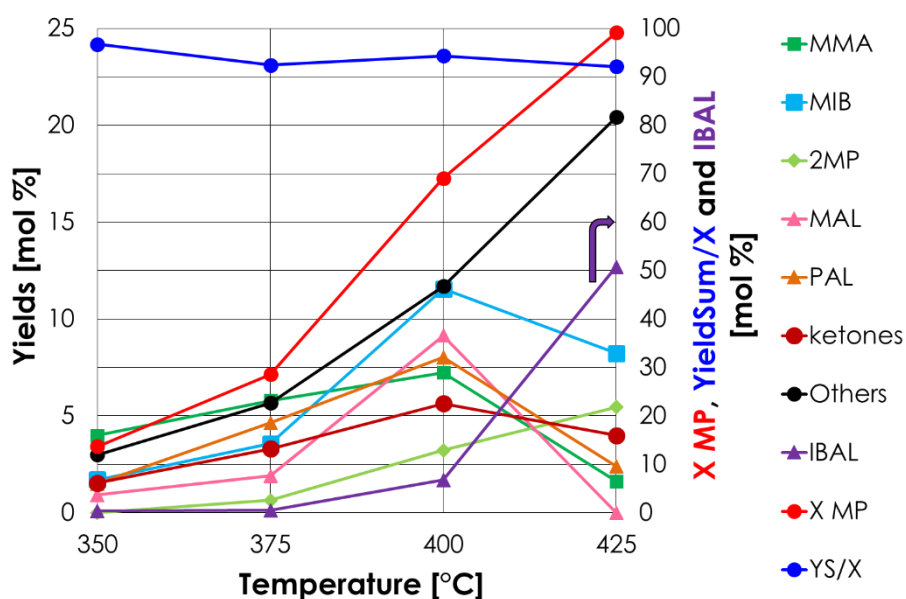
Graph 29: Gas-phase reaction of MP and MeOH as a function of reaction temperature; catalyst: Mg/Ga/O-10; temperature = 400 °C; MP/MeOH/N$_2$ feed composition [mol %] = 1/10/89; W/F = 0.5 s*g/mL. Others includes PA, PrOH, MAA, IBA and unknown compounds. Yields calculated in terms of moles.

MMA synthesis from MP and MeOH

Under these conditions, ketones formation was minimized (highest yield 5.6 % at 400°C), thanks to the high MeOH/MP inlet feed ratio, and MMA was the main product between 350 and 375°C, formed together with lower amounts of MIB, PAL and MAL. As expected, the occurrence of both hydroxy-methylation and parasitic H-transfer reactions increased raising reaction temperature: at 400 °C the yield of MMA and PAL reached their maximum value (7.2 % and 8.0 %, respectively) but MIB and MAL became the main products (11.7 % and 9.1 % yield, respectively), together with IBAL (6.7 %). A further increase of temperature up to 425 °C led to a drop of MMA, PAL, MIB and MAL yields, while IBAL yield increased up to 50.8 %. These results are in good agreement with our proposed reaction scheme: MAL forms from both MMA hydrogenolysis and PAL hydroxy-methylation; both reactions are preferred at higher temperatures but the latter occurs extensively only at 425 °C; in the same conditions, the MAL produced is immediately reduced to IBAL. Even if MMA was obtained in very low yields at 450 °C, 50.8 % IBAL yield plus 8.2 % MIB yield represents an interesting result because IBA and similar molecules can be used as reactant for MMA synthesis via catalytic oxidation [184, 185]. MIB forms from MMA hydrogenation and becomes unstable at above 400°C, with IBAL being formed by its hydrogenolysis. In other words, IBAL is the final product for the three side-reaction pathways: 1) MMA → MAL → IBAL, 2) MMA → MIB → IBAL and 3) PAL → MAL → IBAL. The activity of Mg/Ga-10 in H-transfer as a function of temperature is somewhat intermediate between that of MgO and β-Ga$_2$O$_3$ and can be explained by considering the modulation of catalyst surface properties due to the introduction of Ga^{3+} into MgO. Ga^{3+} ions enhance the dehydrogenating features and reduce the overall basicity in respect to MgO, promoting MeOH dehydrogenation and MMA selective formation at 350-375 °C. Above 400 °C, Mg/Ga-10 becomes much less selective and H-transfer parasitic reactions become preferred forming mainly IBAL. Conversely, with MgO IBAL reacts further to produce 2-MP and IB (Graph 23, Chapter 6.3.2.1). On the other hand, β-Ga$_2$O$_3$, which possess weak basic sites only, proved to be able to afford MMA as the main product at temperatures as high as 450°C. These results confirm our hypothesis that the presence of strong and medium-strength basic sites vigorously promote H-transfer parasitic reactions even in the absence of strong acidic sites on catalyst surface, while the opposite (e.g. high activity for H-transfer in presence of strong acidic sites and weak basic sites) do not.
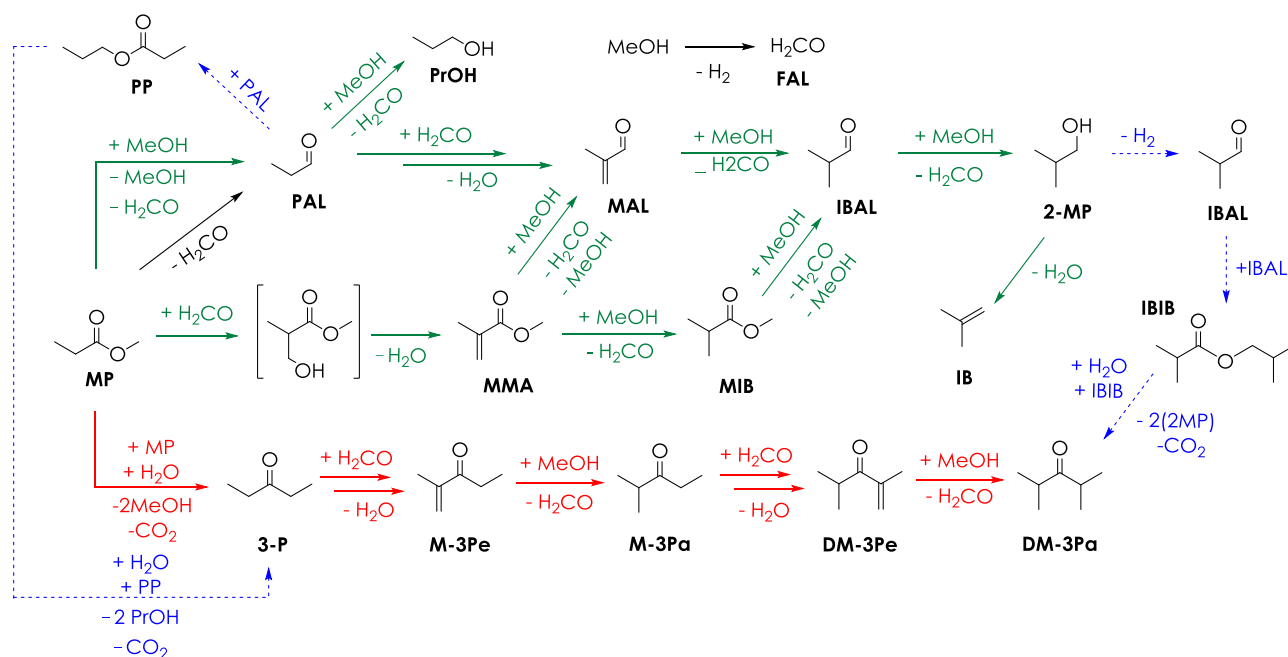
Scheme 63: proposed complete reaction scheme over MgO, β-Ga$_2$O$_3$ and Mg/Ga mixed oxides: the main reaction pathways are MP ketonization and consecutive hydroxy-methylation and H-transfers (in red), MP hydroxy-methylation to MMA and consecutive H-transfers (in green); alcohol condensation by means of Tishchenko and subsequent ketonization of the so obtained esters (in blue) is possible but unconfirmed.

Scheme 63 shows the proposed reaction scheme over MgO, β-Ga₂O₃ and Mg/Ga mixed metal oxides, while Table 18 compile the best catalytic results obtained with our Mg/Ga/O-10 and b-Ga2O3 and ones for the other catalytic systems reported in the literature.

Cat.	X MP [%]	S MMA [%]	Temp. [°C]	W/F [s*g/mL]	MeOH/MP/N₂ (mol %)	Productivity [h⁻¹]
β-Ga₂O₃	50.9	25.0	450	0.5	5/1/94	0.014
Ref [184]	14.9	75.7	360	3.8	13.3/20/66.7	0.32
Ref [185]	2.5	65	400	0.33	1.3/13/85.7	0.0037

Table 18: comparison between the catalytic performances of MgO and β-Ga₂O₃ and those of the other catalytic systems reported in literature. Productivity is calculated as gram/hour of produced MMA divided by grams of catalyst.

6.3.3 Catalysts characterization after reaction

All catalysts were characterized by means of TGA, XRD, XPS and ATR spectroscopy after reaction. In the case of MgO and mixed MOs, no significant differences either in their XRD pattern and in their ATR spectra were found before and after reaction; moreover, the weight loss upon thermogravimetric analysis was negligible. Therefore, carbon deposition and changes in their crystal structure have been ruled out and those data will not be shown. In order to determine the reason behind β-Ga_2O_3 deactivation, the portion of catalyst used during the short-term 18 hours deactivation test (Graph 25, Chapter 4.3.4.1) was subjected to a deeper characterization before regeneration, and N_2 porosimetry after reaction was carried out too. The main results of these analyses are summarized in Table 19.

β-Ga_2O_3	BET-SSA [m²/g]	Crystal Phase	Mass Loss [%]	Surface Carbon [mol %]
fresh	14	β	/	12.6*
spent	6	β	1.1	52.3

*Table 19: characterization of β-Ga_2O_3 before and after reaction; BET-SSA (N2-porosimetry), crystal phase (XRD), Mass loss (TGA), Surface Carbon (semi-quantitative analysis, XPS). *adventitious carbon.*

The mass loss measured by means of TGA was very low, and do not justify the loss in the molar balance observed during the short-term deactivation test. Brown solid organic deposits were found on the inner walls of the reactor below the catalytic bed; therefore, it is likely that some heavy reaction products were lost this way. However, XPS semiquantitative elemental analysis evidenced a much higher amount of carbon on β-Ga_2O_3 surface after reaction in respect to the fresh.
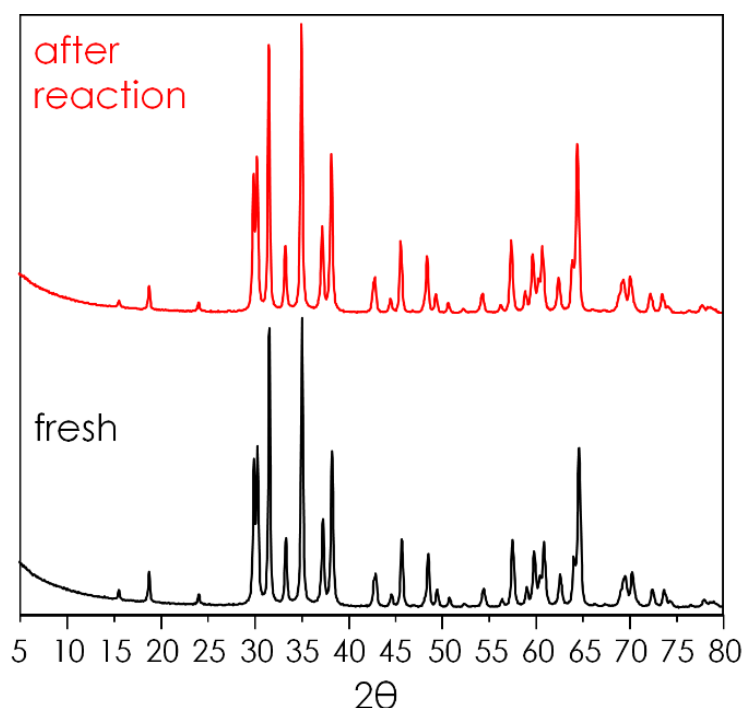
Figure 49: XRD pattern of β-Ga_2O_3 before and after reaction.

X-ray photoelectron spectroscopy (XPS) was used in order to investigate in-depth catalyst surface features. Figure 50 shows the XPS spectra for the C 1s, O 1s and Ga $2p_{3/2}$ core levels of the fresh (GC = β-Ga_2O_3 calcined) and spent (GS = β-Ga_2O_3 spent) material. The spectrum relative to the C 1s energy core level for GC (Figure 50, left side) shows two peaks,

related to the presence of adventitious graphitic carbon (284.8 eV) and carbonate groups (289.2 eV) [186]. The carbonatation of β-Ga$_2$O$_3$ surface is another evidence of the existence of basic sites on its surface. The presence of adventitious carbon on catalyst surface depends on the electrostatic attraction between the surface of the material and the atmospheric dust and is an unavoidable impurity. The same spectrum for GS is characterized by the absence of the signal related to carbonate groups (which are decomposed during catalyst heating up to reaction temperature) and a much more intense signal for graphitic carbon (atomic percentage of superficial C on GS = 52.3%, against 12.6% on GC).
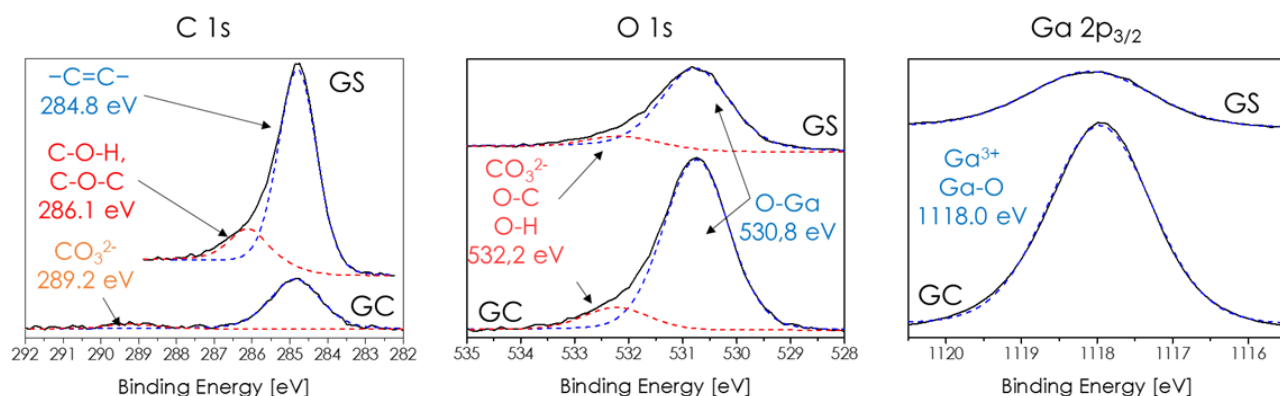
Figure 50: XPS spectra of β-Ga$_2$O$_3$ fresh (GC) and after 18 hours of reaction (GS): the investigated core levels were C 1s, O 1s and Ga 2p$_{3/2}$.

This fact, together with the presence of a third signal centered at 286.1 eV and attributable to the presence of carbon bound to oxygen (e.g. etheric and alcoholic groups [186]), has been interpreted as a confirmation of carbonaceous material deposition over catalysts surface. Since the catalyst after reaction was exposed to air for a long time before XPS analysis, the absence of carbonates in GS suggests that CO$_2$ did not re-adsorb, perhaps because carbon deposits shield the metal oxide surface. The XPS spectra for the O 1s core level of GC and GS are characterized by two signals centered at 530.8 eV and 532.2 eV (Figure 50, center). The former was attributed to O^{2-} bonded to Ga^{3+} [187], while the latter results either by the presence of carbonates (in GC) or organic molecules containing C-O bonds (in GS) [188]. The XPS spectra for the core level Ga 2p$_{3/2}$ (Figure 50, right side) of both GC and GS is characterized by one signal attributable to Ga^{3+} (1118.0-1118.1 eV) [189], therefore it can be concluded surface Ga^{3+} were not reduced under reaction conditions and catalyst deactivation did not depend on the formation of superficial Ga(0) species (ref 1116.7 eV) [189]. The experimental Ga/O surface atomic ratio for fresh β-Ga$_2$O$_3$, calculated by XPS, was 0.664 and this is in good agreement with the theoretical "bulk" value of 0.666. In the case of the spent catalyst, instead, the Ga/O atomic ratio (0.420) was lower than the theoretical one, due to the presence of carbon residues. It is uncertain if this result depends on the fact that the carbon on catalysts surface was oxidized to a certain degree (signal O 1s relative to O-C and O-H bonds) or if this finding may suggest that carbon deposits preferentially over Ga^{3+}. In this regard, β-Ga$_2$O$_3$ was the only catalyst that underwent deactivation among Ga-based catalysts, and NH$_3$-TPD characterization (Figure 47, Chapter 6.3.1.3) showed that it is the one possessing the stronger acidic sites: NH$_3$ desorption from β-Ga$_2$O$_3$ continued up to 450 °C, while it completely stopped at 310 °C in the case of all the others. Either way, it is likely that the reason behind β-Ga$_2$O$_3$ deactivation is due to the deposition of carbon on its surface, which reduced drastically the surface area available for the reaction. Figure 51 shows the results of XPS analysis of MgO. The spectrum relative to the energy level C 1s (Figure 51, left side) for fresh MgO (M) shows two signals related to the presence of adventitious graphitic carbon (284.9 eV) and carbonate groups (289.9 eV), plus a third signal centered at 282 eV. Unless this signal is due to an electronic transition of an element different from carbon that did not occurred to us, it is typical of carbides, perhaps

formed during the calcination of the material, which was synthesized by precipitation with sodium carbonate.
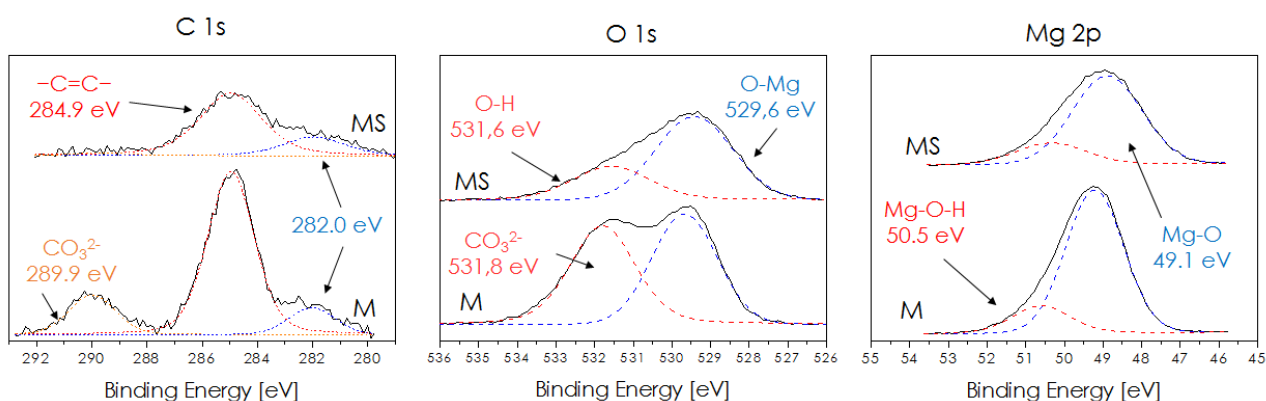
Figure 51: XPS spectra of MgO fresh (G) and after reaction (MS): the investigated core levels were C 1s, O 1s and Mg 2p.
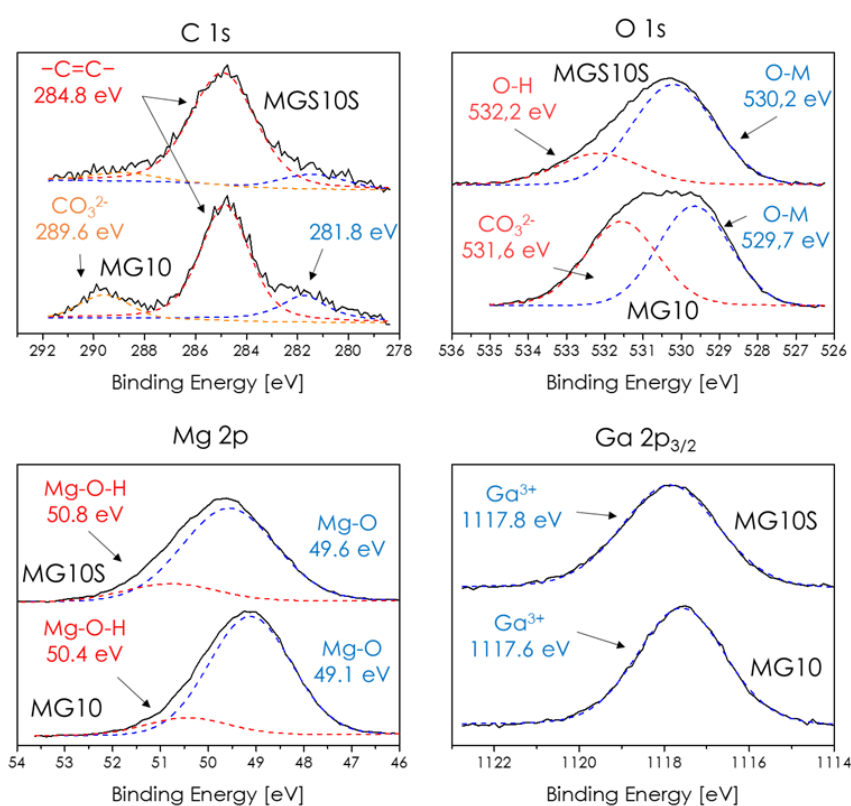
Figure 52: XPS spectra of Mg/Ga/O-10 fresh (MG10) and after reaction (M10S): the investigated core levels were C 1s, O 1s, Mg 2p and Ga 2p$_{3/2}$.

In the spectra of MgO after reaction (MS) the signal relative to carbonates (289.9 eV) almost disappear. The spectrum of the O 1s core level (Figure 51, center) of fresh MgO (M) is characterized by the presence of two signals with similar intensities centered on 529.6 and 531.6 eV, attributable respectively to the oxygen bound to Mg^{2+} and to that of a carbonate or hydroxyl groups. In the spectrum of MgO after reaction (MS) the signal at 531.6 eV becomes much weaker, therefore it is likely due to carbonates to a certain extent. These results indicate that both β-Ga_2O_3 and MgO are less carbonated after reaction. The semi-quantitative determination of the surface carbon indicates that in the case of MgO there is no deposition of carbon residues on the catalyst. Instead, the carbon percentage on catalyst surface was less after reaction (C = 15.1 % in M, C = 11.7 % in MS), perhaps due to decarbonatation. Finally, the spectrum relative to the Mg 2p core energy level (Figure 51, right side) shows an asymmetric signal both in the case of M and in that of MS. These two

123

contributions are probably related to Mg^{2+} linked to O^{2-} (49.1 eV) and Mg^{2+} linked to HO^-. Electronic spectra of Mg/Ga/O-10 (MG10) are shown in Figure 52. The C 1s core energy level spectrum for MG10 is similar to that of MgO and is characterized by the presence of signals at 289.6 eV (carbonate), 284.8 eV (C graphitic adventitious carbon) and 281.8 eV (carbides). It is worth noting that this catalyst was synthesized modifying slightly the precipitation technique with carbonates used for M, while GC was a commercial reference material and carbides are absent. After reaction Mg/Ga/O-10 (MG10S) is less carbonated than the fresh, as can be seen from the decrease in the signals of the carbonate groups in C 1s and O 1s spectra (289.6 and 531.6 eV respectively). The semiquantitative determination of surface carbon indicates that there is no significant deposition of carbon residues on the surface even in this case (C in MG10 = 14.7 %; C in MG10S = 17 %).

7 General conclusions and future trends

The three year of my PhD work the investigations of which are collected in the present thesis were dedicated at the study of catalytic reactions for the upgrading of carboxylic acids and their esters, obtainable from renewable resources, to molecule of higher value, such as bio fuels and bio chemicals. Two main topics had been addressed: the study of ketonization of carboxylic acids, esters and alcohols, and the synthesis of methyl methacrylate starting from methyl propionate and methanol. The former line of research was more focused on the valorization of lignocellulosics materials, which are the most abundant biomass resource, and on the improvement of the current knowledges regarding the catalytic upgrading of bio oils via the formation of new carbon-carbon bonds between light molecules, especially acids and esters. Their ketonization enhance the quality of bio oils and reduce the hydrogen consumption and the loss of precious renewable carbon upon further upgrading by means of hydrogenation. However, during the study of the behavior of esters and alcohols mixtures over ketonization catalysts, it was found that this reaction, and more in general other aldolic-type reactions too, are useful tools also for the upgrading of alcohols, and aldehydes. The latter topic, although falling within the scope of the exploitation of molecules obtainable also from renewable sources (e.g. methyl propionate from bio-based glycerol and methanol from bio-gas), was more focused on the enhancement of the safety of methyl methacrylate synthesis, because its main goal was the substitution of the harmful formaldehyde currently used in its industrial production with the less dangerous methanol. Addressing these two topics, it has been given more importance to scientific research rather than process optimization. This mean that the main goal was the investigation and the comprehension of the chemical and physico/chemical reasons that lead to a certain catalytic behavior. In fact, the research on innovative chemical processes and catalysis needs to focus on the deep understanding of the interaction between the reactants, the catalyst and the reaction environment. Only once the chemistry at the basis of a definite chemical process is disclosed, the research aimed at process and catalyst optimization becomes fruitful. The research work did during these three years of PhD course was carried out taking in mind this principle.

The main results exposed in this PhD thesis can be summarized as follows:

- Propionic acid ketonization was investigated with the aim to obtain a better understanding of the effect that physico/chemical properties have on catalytic activity. Therefore, several catalyst possessing different acid base properties were investigated (Al, Zr, La and Si oxides and Al, Zr and La phosphates). It was found that ketonization occurs to a certain extent over all catalyst. From the mechanistic point of view, this is a significant result, because the abstraction of a α-proton is required to activate the reactant, and catalytic results and characterizations over metal phosphates and SiO_2 shows that the presence of basic sites is not a mandatory requirement. Therefore, it has been proposed that the nucleophilic enolate anion, which represents the activated form of the carboxylate anion, may form via a keto-enol tautomerism. Catalytic results showed that strong acidity is beneficial in this regard, either by stabilizing the enol form or loosening the bond between the α-

carbon and the α-hydrogen. However, deeper investigation is needed in order to better understand this phenomenon.

- Methyl propionate reaction with methanol over the same catalyst object of study for PA ketonization was investigated in order to determine the complex reaction scheme arising from their interaction over ketonization catalysts, and as preliminary study prior to undertake the investigation of MMA synthesis. Results showed that the reaction scheme is very complex. Ketonization is favored at low temperature over catalysts displaying basic and amphoteric character following a surface mechanism via β-keto acid or β-keto ester. Raising reaction temperature, methanol dehydrogenation and hydroxy-methylation with formaldehyde of α-hydrogen-containing compounds (esters, aldehydes, ketones) become more favored and at temperature as high as 450-500 °C competes with ketonization. However, at the same temperature, H-transfer hydrogenations and hydrogenolysis become favored too and unsaturated compounds are immediately consumed. ZrO_2 is the most active catalyst for ketonization, closely followed by La_2O_3, which, however, is more selective because less active for consecutive aldol reactions of 3-pentanone. Remarkably, the mechanism of ketonization over La_2O_3 has been found to be different in the case of PA (bulk-ketonization) and MP (surface ketonization via β-keto ester). ZrO_2 proved to be capable to lead to ketones formation also from alcohols: this pathway involves dehydrogenation to the respective aldehyde, Tishchenko condensation of two aldehydes to the respective symmetric ester and ketonization of two esters. MgO is the least active catalyst for ketonization among catalyst displaying significant basicity. In contrast with the trend mentioned above, the favored reaction over acidic catalysts is methyl propionate hydrolysis. It has been proposed that the water resulting from the acid catalyzed dehydration of methanol to dimethyl ether leads to the formation of hydroxyl groups and a significant increase of the ratio between Brønsted acidic sites and Lewis acidic sites. This results in a drop of the α-proton abstraction rate because the protons from water dissociation occupy most of the weak basic sites on catalyst surface. Ketonization became faster than MP hydrolysis only in the case of Al_2O_3.

- Results obtained during the first two year of PhD constituted the basis on which a promising catalytic system for synthesis one-pot of MMA from MP and formaldehyde produced *in situ* by means of methanol dehydrogenation was designed and investigated. Moreover, the previous work was also the basis on which reaction conditions were optimized. In order to avoid the parasitic reaction of ketonization and H-transfer favored at high temperatures, the least active catalyst for ketonization among those displaying significant basic features (MgO) was promoted with Ga^{3+} in small amounts due to its cost, in the attempt to enhance its dehydrogenating activity at lower temperatures. This way, a larger excess of formaldehyde produced by *in situ* methanol dehydrogenation was expected. The catalytic activity of MgO, Ga_2O_3 and two mixed metal oxides were compared, and it was found that Ga_2O_3 is the most active and selective catalyst towards MMA synthesis. The comparison showed that MMA yield increase with an increase in the Ga content and not catalyst basicity. Instead, the more basic catalysts proved to be less selective, due to the occurrence of more H-transfer reactions. Moreover, the higher basicity and the lower excess of formaldehyde favored ketonization. These results indicate that an effective catalyst should possess a high dehydrogenating power at low temperature and mild basicity, as it happens for Ga_2O_3 and Mg/Ga/O-10. However, the presence of strong acidic

sites is detrimental for catalyst stability under reaction condition, and the most acidic catalyst, Ga_2O_3, deactivated after several hours of reaction due to deposition of carbonaceous materials over its surface. Remarkably, no sign of deactivation was detected over Mg/Ga/O-10, therefore this catalyst was used to further investigate the reaction scheme. As expected, it was found that H-transfer and hydroxy-methylation are favored by an increase in temperature, in contact time and in the molar feed ratio between MeOH and MP, while low MeOH/MP molar ratio makes more easy for MP molecule to encounter each other on catalyst surface, thus favoring ketonization. The comparison between the most active and selective catalyst, Ga_2O_3, and literature benchmarks for MMA synthesis from MP and MeOH, however, showed that more work is needed in order to enhance catalyst selectivity. Despite this result, Ga_2O_3 and Ga-based oxides are innovative catalysts for this reaction and their activity is reported here for the first time.

Given the number of applications of PMMA in the sectors of signs & displays, construction, automotive and electronics, MMA production and market will probably maintain their relevance and keep growing around the globe during the next years. Despite the availability of a modern and selective process for MMA production (Lucite Process), older and less sustainable synthetic pathways such as the ACH and isobutylene processes are still in use in some regions of the world, and the production of this monomer still heavily depends on fossil feedstock. It is therefore advisable to continue to strive to develop a process for its production starting from renewables such as glycerol and to seek to improve process safety by avoiding the direct use of dangerous compounds such as formaldehyde and hydrocyanic acid.

The pyrolysis of lignocellulosics possesses the potential to become one of the pillars of the future biorefinery thanks to large availability of lignocellulosic materials and its ability to process different feedstock. It is however mandatory to overcome the issues related to bio oil upgrading before a large-scale biofuel production from woods could be achievable. Ketonization of carboxylic acids, esters, aldehydes and alcohols and other coupling reactions such as aldol condensation are expected to play an important role in the future processes of bio oil upgrading, enhancing the quality of the bio oil itself and reducing the loss of precious renewable carbon during the subsequent hydrodeoxygenation process. It is therefore advisable to carry on this line of research with the aim of developing robust catalysts capable of converting into valuable biofuels mixtures as complex as bio oil.

8 References

[1]   M. Appl, "Ammonia, 1. Introduction," *Ullmann's Encyclopedia of Industrial Chemistry,* vol. 3, pp. 107-137, 2012.

[2]   J. W. Erisman, M. A. Sutton, J. Galloway, Z. Klimont and W. Winiwarter, "How a century of ammonia synthesis changed the world," *Nature Geoscience,* vol. 1, pp. 636-639, 2008.

[3]   R. F. Barron, "Cryogenic Technology," *Ullmann's Encyclopedia of Industrial Chemistry,* vol. 10, pp. 481-526, 2012.

[4]   R. Reimert, F. Marschner, H. J. Renner, W. Boll, E. Supp, M. Brejc, W. Liebner and G. Schaub, "Gas Production, 2. Processes," *Ullmann's Encyclopedia of Industrial Chemistry,* vol. 16, pp. 423-482, 2012.

[5]   P. Haussinger, R. Lohmuller and A. M. Watson, "Hydrogen, 2. Production," *Ullmann's Encyclopedia of Industrial Chemistry,* vol. 18, pp. 249-307, 2012.

[6]   M. Appl, "Ammonia, 2. Production Processes," *Ullmann's Encyclopedia of Industrial Chemistry,* vol. 3, pp. 139-225, 2012.

[7]   V. Smil, "Nitrogen cycle and world food production," *World Agriculture,* vol. 2, pp. 9-13, 2011.

[8]   A. R. Douglass, P. A. Newman and S. Solomon, "The antaric ozone hole: an update," *Physics Today,* vol. 67, pp. 42-48, 2014.

[9]   O. Edenhofer, R. Pichs-Madruga, Y. Sokona, J. C. Minx, E. Farahani, S. Kadner, K. Seyboth, A. Adler, I. Baum, S. Brunner, P. Eickemeier, B. Kriemann, J. Savolainen, S. Schlomer, C. Von Stechow and T. Zwickel, "Climate Change 2014: Mitigation of Climate Change. Working Group III Contribution to the Fifth Assessment Report of the Intergovernmental Panel on Climate Change," p. 1454, 2014.

[10]   T. F. Stocker, D. Qin, G. K. Plattner, M. Tignor, S. K. Allen, J. Boschung, A. Nauels, Y. Xia, V. Bex and P.M. Midgley, "IPCC, 2013: Climate Change 2013: The Physical Science Basis. Contribution of Working Group I to the Fifth Assessment Report of the Intergovernmental Panel on Climate Change," p. 1585, 2013.

[11]   P. T. Anastas and J. C. Warner, "Green Chemistry: Theory and Practice," p. 135, 1998.

[12]   R. A. Sheldon, "Metrics of Green Chemistry and Sustainability: Past, Present, and Future," *ACS Sustainable Chemistry & Engineering,* vol. 6, pp. 62-48, 2018.

[13]   M. Yinon, R. Phillips and R. Milo, "The biomass distribution on Earth," *Proceedings of the National Academy of Science of the United States of America,* vol. 115, pp. 6506-6511, 2018.

[14]   B. Groombridge and M. D. Jenkins, "World Atlas of Biodiversity: Earth's Living Resources in the 21st Century," p. 340, 2002.

[15]   C. B. Fields, M. J. Behrenfeld, J. T. Randerson and P. Falkowski, "Primary production of the biosphere: integrating terrestrial and oceanic components," *Science,* vol. 281, pp. 237-240, 1998.

[16]   V. Smil, "Harvesting the Biosphere," *The World Financial Review,* pp. 46-49, 2016.

[17]   J. F. Bastin, Y. Finegold, C. Garcia , D. Mollicone, M. Rezende, D. Routh, C. M. Zohner and T. W. Crowther, "The global tree restoration potential," *Science,* vol. 365, pp. 76-79, 2019.

[18]   D.Graham-Rowe, "Agriculture: Beyond food versus fuel," *Nature,* vol. 474, pp. S6-S8, 2011.

[19]   K. Azad, M. Rasul, M. M. K. Khan and S. Sharma, "A review on socio-economic aspects of sustainable biofuels," *International Journal of Global Warming,* vol. 10, pp. 32-54, 2016.

[20]   F. Cherubini, "The biorefinery concept: Using biomass instead of oil for producing energy and chemicals," *Energy Conversion and Management 5,* vol. 51, pp. 1412-1421, 2010.

[21]   R. A. Lee and J. M. Lavoie, "From first- to third-generation biofuels: Challenges of producing a commodity from a biomass of increasing complexity," *Animal Frontiers,* vol. 3, pp. 6-11, 2013.

[22]   S. D. Stefanidis, K. G. Kalogiannis, E. F. Iliopoulou, C. M. Michailof, P. A. Pilavachi and A. A. Lappas, "A study of lignocellulosic biomass pyrolysis via the pyrolysis of cellulose, hemicellulose and lignin," *Journal of Analytical and Applied Pyrolysis,* vol. 105, pp. 143-150, 2014.

References

[23] S. H. Mood, A. H. Golfeshan, M. Tabatabaei, G. S. Jouzani, G. H. Najafi, M. Gholami and M. Ardjmand, "Lignocellulosic biomass to bioethanol, a comprehensive review with afocus on pretreatment," *Renewable and Sustainable Energy Reviews,* vol. 27, pp. 77-93, 2013.

[24] L. J. Gibson, "The hierarchical structure and mechanics of plant materials," *Journal of the Royal Society Interface,* vol. 9, p. 2749–2766, 2012.

[25] F. M. Girio, C. Fonseca, F. Carvalheiro, L. C. Duarte, S. Marques and R. Bogel-Lukasik, "Hemicelluloses for fuel ethanol: A review," *Bioresource Technology,* vol. 101, pp. 4775-4800, 2010.

[26] A. Ebringerova, Z. Hromadkova and T. Heinze, "Hemicellulose," *Advances in Polymer Science,* vol. 186, p. 1–67, 2005.

[27] J. Zakzeski, P. C. A. Bruijnincx, A. L. Jongerius and B. M. Weckhuysen, "The Catalytic Valorization of Lignin for the Production of Renewable Chemicals," *Chemical Reviews,* vol. 110, p. 3552–3599, 2010.

[28] M. J. C. Van der Stelt, H. Gerhauser, J. H. A. Kiel and K. J. Ptasinski, "Biomass upgrading by torrefaction for the production of biofuels: A review," *biomass and bioenergy,* vol. 35, pp. 3748-3762, 2011.

[29] L. J. R. Nunes, J. C. O. Matias and J. P. S. Catalao, "A review on torrefied biomass pellets as a sustainable alternative to coal in power generation," *Renewable and Sustainable Energy Reviews,* vol. 40, pp. 153-160, 2014.

[30] J. S. Tumuluru, S. Sokhansanj, J. R. Hess, C. T. Wright and R. D. Boardman, "A review on biomass torrefaction process and product properties for energy applications," *Industrial Biotechnology,* vol. 7, pp. 384-401, 2011.

[31] A. V. Bridgewater, "Review of fast pyrolysis of biomass and product upgrading," *Biomass and Bioenergy,* vol. 38, pp. 68-94, 2012.

[32] D. A. Laird, R. C. Brown, J. E. Amonette and J. Lehmann, "Review of the pyrolysis platform for coproducing bio-oil and biochar," *Biofuels, Bioproducts & Biorefinery,* vol. 3, pp. 547-562, 2009.

[33] B. J. Alvarez-Chavez, S. Godbout, J. H. Palacios-Rios, E. Le Roux and V. Raghavan, "Physical, chemical, thermal and biological pre-treatment technologies in fast pyrolysis to maximize bio-oil quality: A critical review," *Biomass and Bioenergy,* vol. 128, p. 105333, 2019.

[34] F. X. Collard and J. Blin, "A review on pyrolysis of biomass constituents: Mechanisms and composition of the products obtained from the conversion of cellulose, hemicelluloses and lignin," *Renewable and Sustainable Energy Reviews,* vol. 38, pp. 594-608, 2014.

[35] S. Czernik and V. Brisgewater, "Overview of Applications of Biomass Fast Pyrolysis Oil," *Energy & Fuels,* vol. 18, pp. 590-598, 2004.

[36] D. Mohan, C. H. Pittman and P. H. Steele, "Pyrolysis of Wood/Biomass for Bio-Oil: A Critical Review," *Energy & Fuels,* vol. 20, pp. 848-889, 2006.

[37] S. Xiu and A. Shahbazi, "Bio-oil productionandupgradingresearch:Areview," *Renewable andSustainableEnergyReviews,* vol. 16, p. 4406–4414, 2012.

[38] B. S. Kang, K. H. Lee, H. J. Park, Y. K. Park and J. S. Kim, "Fast pyrolysis of radiata pine in a bench scale plant with a fluidized bed: Influence of a char separation system and reaction conditions on the production of bio-oil," *Journal of Analytical and Applied Pyrolysis,* vol. 76, pp. 32-37, 2006.

[39] A. Javaid, T. Ryan, G. Berg, X. Pan, T. Vispute, S. R. Bhatia, G. W. Huber and D. M. Ford, "Removal of char particles from fast pyrolysis bio-oil by microfiltration," *Journal of Membrane Science,* vol. 363, pp. 120-127, 2010.

[40] J. Peng, P. Chen, H. Lou and X. Zheng, "Upgrading of Bio-oil over Aluminum Silicate in Supercritical Ethanol," *Energy Fuels,* vol. 22, pp. 3489-3492, 2008.

[41] Q. Zhang, J. Chang, T. Wang and Y. Xu, "Upgrading Bio-oil over Different Solid Catalysts," *Energy & Fuels,* vol. 20, pp. 2717-2720, 2006.

[42] X. Jiang and N. Ellis, "Upgrading Bio-oil through Emulsification with Biodiesel: Mixture Production," *Energy Fuels,* vol. 24, pp. 1358-1364, 2010.

[43] W. Baldauf, U. Balfanz and M. Rupp, "Upgrading of Flash Pyrolysis Oil and Utilization inRefineries," *Biomass and Bioenergy,* vol. 7, pp. 237-244, 1994.

[44] Y. E. Sheu, R. G. Anthony and E. J. Soltes, "Kinetic studies of upgrading pine pyrolytic oil by hydrotreatment," *Fuel Processing Technology,* vol. 19, pp. 31-50, 1988.

[45] D. C. Elliott, T. R. Hart, G. G. Neuenschwander, L. J. Rotness and A. H. Zacher, "Catalytic hydroprocessing of biomass fast pyrolysis bio-oil to produce hydrocarbon products," *Environmental Progress & Sustainable Energy,* vol. 28, p. 441–449, 2009.

[46] R. H. Venderbosch, A.R. Ardiyanti, J.Wildschut, A. Oasmaa and H. J. Heeres, "Stabilization of biomass-derived pyrolysis oils," *Chemical Technology and Biotechnology,* vol. 85, p. 674–686, 2010.

[47] J. D. Adjaye and N. N. Bakhshi, "Production of hydrocarbons by catalytic upgrading of a fast pyrolysis bio-oil. Part I: Conversion over various catalysts," *Fuel Processing Technology,* vol. 45, pp. 161-183, 1995.

[48] S. P. R. Katikaneni, J. D. Adjaye and N. N. Bakhshi, "Performance of aluminophosphate molecular sieve catalysts for the production of hydrocarbons from wood-derived and vegetable oils," *Energy Fuels,* vol. 9, p. 1065–1078, 1995.

[49] P. M. Mortensen, J. D. Grunwaldt, P. A. Jensen, K. G. Knudsen and A. D. Jensen, "A review of catalytic upgrading of bio-oil to engine fuels," *Applied Catalysis A: General,* vol. 407, pp. 1-19, 2011.

[50] S. Luo and J. L. Falconer, "Acetone and Acetaldehyde Oligomerization on TiO2 Surfaces," *Journal of Catalysis,* vol. 185, p. 393–407, 1999.

[51] A. Chieregato, J. Velasquez Ochoa, C. Bandinelli, G. Fornasari, F. Cavani and M. Mella, "On the Chemistry of Ethanol on Basic Oxides: Revising Mechanisms and Intermediates in the Lebedev and Guerbet reactions," *ChemSusChem,* vol. 8, pp. 377-388, 2015.

[52] D. Gabriels, W. Y. Hernandez, B. Sels, P. Van Der Voort and A. Verberckmoes, "Review of catalytic systems and thermodynamics for the Guerbet condensation reaction and challenges for biomass valorization," *Catalysis Science & Technology,* vol. 5, pp. 3876-3902, 2015.

[53] T. N. Pham, T. Sooknoi, S. P. Crossley and D. E. Resasco, "Ketonization of Carboxylic Acids: Mechanisms, Catalysts, and Applications in Bio-oil Upgrading," *ACS Catalysis,* vol. 3, pp. 2456-2473, 2013.

[54] I. Sadaba, M. Ojeda, R. Mariscal, J. L. G. Fierro and M. Lopez Granado, "Catalytic and structural properties of co-precipitated Mg–Zr mixed oxides for furfural valorization via aqueous aldol condensation with acetone," *Applied Catalysis B: Environmental,* vol. 101, p. 638–648, 2011.

[55] N. Ballarini, F. Cavani, L. Maselli, S. Passeri and S. Rovinetti, "Mechanistic studies of the role of formaldehyde in the gas-phase methylation of phenol," *Journal of Catalysis,* vol. 256, pp. 215-225, 2019.

[56] J. Lecomte, A. Finiels, P. Geneste and C. Moreau, "Selective hydroxymethylation of furfuryl alcohol with aqueous formaldehyde in the presence of dealuminated mordenites," *Applied Catalysis A: General,* vol. 27, pp. 235-241, 1998.

[57] C. Friedel, *C. Ann.,* vol. 108, p. 125, 1858.

[58] E. R. Squibb, "Improvement in the manufacture of acetone," *Journal of the American Chemical Society,* vol. 3, pp. 187-201, 1895.

[59] R. Piria, *Annales de Chimie et de Physique,* vol. 48, p. 113, 1856.

[60] O. Neunhoeffer and P. Paschke, *Berichte der Deutschen Chemischen Gesellschaft,* vol. 72B, p. 919, 1939.

[61] V. I. Yakerson , "Mechanism of thermal decomposition of salts of carboxylic acids," *Izvestiya Akademu Nauk SSSR, Otdelenie Khimikcheskikh Nauk,* vol. 6, pp. 1003-1011, 1963.

[62] Y. Yamada, M. Segawa, F. Sato, T. Kojima and S. Sato, "Catalytic performance of rare earth oxides in ketonization of acetic acid," *Journal of Molecular Catalysis A: Chemical,* vol. 346, pp. 79-86, 2011.

References

[63] R. Pestman, R. M. Koster, A. van Duijne, J. A. Z. Pieterse and V. Ponec, "Reactions of Carboxylic Acids on Oxides. 2. Bimolecular Reaction of Aliphatic Acids to Ketones," *Journal of Catalysis,* vol. 168, p. 265–272, 1997.

[64] R. A. Hites and K. Biemann, "On the Mechanism of Ketonic Decarboxylation. Pyrolysis of Calcium Decanoate," *Journal of the American Chemical Society,* vol. 94, pp. 5772-5777, 1972.

[65] Y. Sakata, C. A. van Tol-Koutstaal and V. Ponec, "Selectivity Problems in the Catalytic Deoxygenation of Benzoic Acid," *Journal of Catalysis,* vol. 169, pp. 13-21, 1997.

[66] R. Pestman, R. M. Koster, J. A. Z. Pieterse and V. Ponec, "Reactions of Carboxylic Acids on Oxides. 1. Selective Hydrogenation of Acetic Acid to Acetaldehyde," *Journal of catalysis,* vol. 168, pp. 255-264, 1997.

[67] O. Nagashima, S. Sato, R. Takahashi and T. J. Sodesawa, "Ketonization of carboxylic acids over CeO2-based composite oxides," *Journal of Molecular Catalysis A: Chemical,* vol. 227, pp. 231-239, 2005.

[68] A. V. Ignatchenko and E. I. Kozliak, "Distinguishing Enolic and Carbonyl Components in the Mechanism of Carboxylic Acid Ketonization on Monoclinic Zirconia," *ACS Catalysis,* vol. 2, pp. 1555-1562, 2012.

[69] M. Renz, "Ketonization of Carboxylic Acids by Decarboxylation: Mechanism and Scope," *European Journal of Organic Chemistry,* vol. 2005, pp. 979-988, 2005.

[70] T. N. Pham, D. Shi and D. E. Resasco, "Reaction kinetics and mechanism of ketonization of aliphatic carboxylic acids with different carbon chain lengths over Ru/TiO2 catalyst," *Journal of Catalysis,* vol. 314, p. 149–158, 2014.

[71] M. Jayamani and C. N. Pillai, "Reaction of Carboxylic Acids with Carbonyl Compounds over Alumina," *Journal of Catalysis,* vol. 87, pp. 93-97, 1984.

[72] F. Gonzales, G. Munuera and J. A. Prieto, "Mechanism of Ketonization of Acetic Acid on Anatase TiO2 Surfaces," *Journal of the Chemical Society, Faraday Transactions 1: Physical Chemistry in Condensed Phases,* vol. 74, pp. 1517-1529, 1978.

[73] A. V. Ignatchenko, "Density Functional Theory Study of Carboxylic Acids Adsorption and Enolization on Monoclinic Zirconia Surfaces," *Journal of Physical Chemistry,* vol. 115, p. 16012–16018, 2011.

[74] A. Pulido, B. Oliver-Tomas, M. Renz, M. Boronat and A. Corma, "Ketonic decarboxylation reaction mechanism: a combined experimental and DFT study.," *ChemSusChem,* vol. 6, pp. 141-151, 2013.

[75] Z. F. Pei and V. Ponec, "On the intermediates of the acetic acid reactions on oxides: an IR study," *Applied Surface Science,* vol. 103, pp. 171-182, 1996.

[76] K. S. Kim and M. A. Barteau, "Structure and composition requirements for deoxygenation, dehydration, and ketonization reactions of carboxylic acids on TiO2(001) single-crystal surfaces," *Journal of Catalysis,* vol. 125, pp. 353-375, 1995.

[77] M. A. Hasan, M. I. Zaki and L. Pasupulety, "Oxide-catalyzed conversion of acetic acid into acetone: an FTIR spectroscopic investigation," *Applied Catalysis A: General,* vol. 243, pp. 81-92, 2003.

[78] J. Stubenrauch, E. Brosha and J. M. Vohs, "Reaction of carboxylic acids on CeO2(111) and CeO2(100)," *Catalysis Today,* vol. 28, pp. 431-441, 1996.

[79] J. M. Vohs, "Site Requirements for the Adsorption and Reaction of Oxygenates," *Chemical Reviews,* vol. 113, pp. 4136-4163, 2013.

[80] C. Zu and B. E. Koel, "Adsorption and reaction of CH3COOH and CD3COOD on the MgO(100) surface: A Fourier transform infrared and temperature programmed desorption study," *Journal of Chemical Physiscs,* vol. 12, pp. 8158-8166, 1995.

[81] S. R. Tong, L. Y. Wu, M. F. Ge, W. G. Wang and Z. F. Pu, "Heterogeneous chemistry of monocarboxylic acids on a-Al2O3 at different relative humidities," *Atmospheric Chemistry and Physics,* vol. 10, p. 7561–7574, 2010.

[82] R. P. Young, "Infrared spectroscopic studies of adsorption and catalysis. Part 3. Carboxyllic acids," *Canadian Journal of Chemistry,* vol. 47, pp. 2237-2247, 1969.

[83] A. G. Thomas and K. L. Syres, "Adsorption of organic molecules on rutile TiO2 and anatase TiO2 single crystal surfaces," *Chemical Society Reviews,* vol. 41, p. 4207–4217, 2012.

[84] T. N. Pham, D. Shi, T. Sooknoi and D. E. Resasco, "Aqueous-phase ketonization of acetic acid over Ru/TiO2/carbon catalysts," *Journal of Catalysis,* vol. 295, pp. 169-178, 2012.

[85] T. S. Hendren and K. M. Dooley, "Kinetics of catalyzed acid/acid and acid/aldehyde condensation reactions to non-symmetric ketones," *Catalysis Today,* vol. 85, p. 333–351, 2003.

[86] R. Martinez, M. C. Huff and M. A. Barteau, "Ketonization of acetic acid on titania-functionalized silica monoliths," *Journal of Catalysis,* vol. 222, pp. 404-409, 2004.

[87] M. Glinski, G. Zalewski, E. Burno and A. Jerzak, "Catalytic ketonization over metal oxide catalysts. XIII. Comparative measurements of activity of oxides of 32 chemical elements in ketonization of propanoic acid," *Applied Catalysis A: General,* vol. 470, p. 278– 284, 2014.

[88] J. C. Kuriacose and R. Swaminathan, "Studies on the Ketonization of Acetic Acid on Chromia: 1. The Adsorbate-Catalyst Interaction," *Journal Of Catalysis,* vol. 14, p. 3487354, 1969.

[89] S. Rajadurai and J. C. Kuriacose, "Catalytic activity of the 1:1:1 Zn, Cr and Fe mixed oxide: Mechanistic study of the ketonization of acetic acid," *Materials Chemistry and Physics,* vol. 16, pp. 17-29, 1987.

[90] C. A. Gaertner, J. C. Serrano-Ruiz, D. J. Braden and J. A. Dumesic, "Catalytic coupling of carboxylic acids by ketonization as a processing step in biomass conversion," *Journal of Catalysis,* vol. 266, pp. 71-78, 2009.

[91] E. Mamontov, T. Egami, R. Brezny, M. Koranne and S. Tyagi, "Lattice Defects and Oxygen Storage Capacity of Nanocrystalline Ceria and Ceria-Zirconia," *The Journal of Physical Chemistry B,* vol. 107, pp. 11110-11116, 2000.

[92] Q. Mu and Y. Wang, "Synthesis, characterization, shape-preserved transformation, and optical properties of La(OH)3, La2O2CO3, and La2O3 nanorods," *Journal of Alloys and Compounds,* vol. 509, p. 396–401, 2011.

[93] R. P. Taylor and G. L. Schrader, "Lanthanum Catalysts for CH4 Oxidative Coupling: A Comparison of the Reactivity of Phases," *Industrial & Engineering Chemistry Research,* vol. 30, pp. 1016-1023, 1991.

[94] Y. Hou, W. Han, W. Xia and H. Wan, "Structure Sensitivity of La2O2CO3 Catalysts in the Oxidative Coupling," *ACS Catalysis,* vol. 5, pp. 1663-1674, 2015.

[95] R. P. Turcotte, J. O. Sawyer and L. Eyring, "On the Rare Earth Dioxymonocarbonates and Their Decomposition," *Inorganic Chemistry,* vol. 8, pp. 238-246, 1969.

[96] L. Vivier and D. Duprez, "Ceria-Based Solid Catalysts for Organic Chemistry," *ChemSusChem,* vol. 3, pp. 654-678, 2010.

[97] M. Glinski, W. Szymanski and D. Lomot, "Catalytic ketonization over oxide catalysts : X. Transformations of various alkyl heptanoates," *Applied Catalysis A General,* vol. 281, p. 107–113, 2005.

[98] C. A. Gartner, J. C. Serrano-Ruiz, D. J. Braden and J. A. Dumesic, "Catalytic Upgrading of Bio-Oils by Ketonization," *ChemSusChem,* vol. 2, pp. 1121 - 1124, 2009.

[99] T. K. Phung, A. A. Casazza, P. Perego, P. Capranica and G. Busca, "Catalytic pyrolysis of vegetable oils to biofuels: Catalyst functionalities and the role of ketonization on the oxygenate paths," *Fuel Processing Technology,* vol. 140, pp. 119-124, 2015.

[100] M. Glinski and J. Szudybill, "Catalytic ketonization over oxide catalysts, Part VI.a Cross-ketonization of aliphatic and aromatic esters," *Reaction Kinetics and Catalysis Letters,* vol. 77, p. 335–340, 2002.

[101] A. Bayman, P. K. Hansma and L. H. Gale, "Esters Dissociatively Adsorb on Alumina," *Surface Science,* vol. 125, pp. 613-623, 1983.

[102] K. Oberg, P. Persson, A. Shchukarev and B. Eliasson, "Comparison of monolayer films of stearicac id and methyl stearate on an Al2O3 surfac," *Thin Solid Films,* vol. 397, p. 102–108, 2001.

[103] D. Cornu, H. Guezmi, G. Laugel, J. M. Krafft and H. Lauron-Pernot, "On the relationship between the basicity of a surface and its ability to catalyze transesterification in liquid and

References

gas phases: the case of MgO," *Physical Chemistry Chemical Physics,* vol. 17, pp. 4168--14176, 2015.

[104] J. M . Montero, M. A. Isaacs, A. F. Lee, J. M. Lynam and K. Wilson, "The surface chemistry of nanocrystalline MgO catalysts for FAME production: an in situ XPS study of H2O, CH3OH and CH3OAc adsorption," *Surface Science,* vol. 646, pp. 170-178, 2016.

[105] G. W. Haas, D. E. Giblin and M. L. Gross, "The mechanism and thermodynamics of transesterification of acetate-ester enolates in the gas phase," *International Journal of Mass Spectrometry and Ion Processes,* vol. 172, pp. 25-46, 1998.

[106] M. Verziu, B. Cojacaru, J. Hu, R. Richards, C. Ciuculescu, P. Filip and V. I. Parvulescu, "Sunflower and rapeseed oil transesterification to biodiesel over different nanocrystalline MgO catalysts," *Green Chemistry,* vol. 10, p. 373–381, 2008.

[107] M. Tamura, S. M. A. H. Siddiki and K. Shimizu, "CeO2 as a versatile and reusable catalyst for transesterification of esters with alcohols under solvent-free conditions," *Green Chemistry,* vol. 15, pp. 1641-1646, 2013.

[108] M. A. Natal-Santiago, J. M. Hill and J. A. Dumesic, "Studies of the adsorption of acetaldehyde, methyl acetate, ethyl acetate, and methyl trifluoroacetate on silica," *Journal of Molecular Catalysis A: Chemical,* vol. 40, p. 199–214, 1999.

[109] C. A. Gaertner, J. C. Serrano Ruiz, D. J. Braden and J. A. Dumesic, "Ketonization Reactions of Carboxylic Acids and Esters over Ceria-Zirconia as Biomass-Upgrading Processes," *Industrial & Engineering Chemistry Research,* vol. 49, pp. 6027-6033, 2010.

[110] J. Wrzyszcz, H. Grabowska, R. Klimkiewicz and L. Syper, "Reactions of normal alcohols in the presence of a dehydrogenating iron catalyst," *Catalysis Letters,* vol. 54, pp. 55-58, 1998.

[111] R. Kumar, N. Enjamuri, S. Shah, A. S. Al-Fatesh, J. J. Bravo-Suarez and B. Chowdury, "Ketonization of oxygenated hydrocarbons on metal oxide based catalysts," *Catalysis Today,* vol. 302, pp. 16-49, 2018.

[112] L. M. Orozco, M. Renz and A. Corma, "Cerium oxide as catalyst for the ketonization of aldehydes: Mechanistic insights and a convenient way to alkanes without consumption of external hydrogen," *Green Chemistry,* vol. 19, pp. 1555-1569, 2017.

[113] L. M. Orozco, M. Renz and A. Corma, "Carbon-carbon bond formation and hydrogen production in the ketonization of aldehydes," *ChemSusChem,* vol. 9, pp. 2430-2442, 2016.

[114] W. Ponndorf, "Der reversible Austausch der Oxydationsstufen zwischen Aldehyden oder Ketonen einerseits und primären oder sekundären Alkoholen anderseits," *Angewandte Chemie,* vol. 39, pp. 138-143, 1926.

[115] H. Meerwein and R. Schmidt, "Ein neues Verfahren zur Reduktion von Aldehyden und Ketonen," *Justus Liebigs Annalen der Chemie,* vol. 444, pp. 221-238, 1925.

[116] M. J. Gilkey and B. Xu, "Heterogeneous Catalytic Transfer Hydrogenation as an Effective Pathway in Biomass Upgrading," *ACS Catalysis,* vol. 6, pp. 1420-1436, 2016.

[117] M. A. Armendia, V. Borau, C. Jimenez, J. M. Marinas, J. R. Ruiz and F. J. Urbano, "Liquid-phase heterogeneous catalytic transfer hydrogenation of citral on basic catalysts," *Journal of Molecular Catalysis A: Chemical,* vol. 171, pp. 153-158, 2001.

[118] N. A. Cortese and R. F. Heck, "Palladium-catalyzed reductions of .alpha.,.beta.-unsaturated carbonyl compounds, conjugated dienes, and acetylenes with trialkylammonium formates," *Journal of organic chemistry,* vol. 43, pp. 3985-3987, 1978.

[119] I. Gandarias, P. L. Arias, S. G. Fernandez, J. Requies, M. El Doukkali and M. B. Guemez, "Hydrogenolysis through catalytic transfer hydrogenation: Glycerol conversion to 1,2-propanediol," *Catalysis Today,* vol. 195, pp. 22-31, 2012.

[120] F. J. Waller and G. E. Parris, "Dimethyl ether for methyl group attachment on a carbon adjacent to an electron withdrawing group". Patent US 6,329,549 B1, 2001.

[121] B. Klingenberg and M. A. Vannice, "Influence of Pretreatment on Lanthanum Nitrate, Carbonate, and Oxide Powders," *Chemistry of Materials,* vol. 8, pp. 2755-2768, 1996.

[122] W. J. Bauer, "Methacrylic Acid and Derivatives," *Ullmann's Encyclopedia of Industrial Chemistry,* vol. 23, pp. 1-12, 2012.

[123] R. Wilczynski and J. J. Juliette, "Methacrylic Acid and Derivatives," *Kirk-Othmer Encyclopedia of Chemical Technology,* vol. 16, pp. 227-270, 2003.

[124] T. M. Mata, A. A. Martins and N. S. Caetano, "Microalgae for biodiesel production and other applications: A review," *Renewable and Sustainable Energy Reviews,* vol. 14, pp. 217-232, 2010.

[125] M. Balat, "Global Bio-fuel Processing and Production Trends," *Energy Exploration & Exploitation,* vol. 25, pp. 195-218, 2007.

[126] F. Danielsen, H. Beukema, N. D. Burgess, F. Parish, C. A. Bruhl, P. F. Donald, D. Murdiyarso, B. Phalan, L. Reijnders, M. Struebig and E. B. Fitzherbert, "Biofuel Plantations on Forested Lands: Double Jeopardy for Biodiversity and Climate," *Conservation Biology,* vol. 23, pp. 348-358, 2008.

[127] G. Arzamendi, I. Campo, E. Arguinarena, M. Sanchez, M. Montes and L. M. Gandia, "Synthesis of biodiesel with heterogeneous NaOH/alumina catalysts: Comparison with homogeneous NaOH," *Chemical Engineering Journal,* vol. 134, pp. 123-130, 2007.

[128] K. Komers, F. Skopal, R. Stloukal and J. Machek, "Kinetics and mechanism of the KOH - catalyzed methanolysis of rapeseed oil for biodiesel production," *European Journal of Lipid Science and Technology,* vol. 107, p. 728–737, 2002.

[129] M. Di Serio, M. Ledda, M. Cozzolino, G. Minutillo, R. Tesser and E. Santacesaria, "Transesterification of Soybean Oil to Biodiesel by Using Heterogeneous Basic Catalysts," *Industrial & Engineering Chemistry Research,* vol. 45, pp. 3009-3014, 2006.

[130] Z. Kesic, I. Lukic, M. Zdujic, C. Jovalekic, V. Veljkovic and D. Skala, "Assessment of CaTiO3, CaMnO3, CaZrO3 and Ca2Fe2O5 perovskites as heterogeneous base catalysts for biodiesel synthesis," *Fuel Processing Technology,* vol. 143, pp. 162-168, 2016.

[131] K. Noiroj, P. Intarapong, A. Luengnaruemitchai and S. Jai-In, "A comparative study of KOH/Al2O3 and KOH/NaY catalysts for biodiesel production via transesterification from palm oil," *Renewable Energy,* vol. 34, pp. 1145-1150, 2009.

[132] I. Lukic, J. Krstic, D. Jovanovic and D. Skala, "Alumina/silica supported K2CO3 as a catalyst for biodiesel synthesis from sunflower oil.," *Bioresource Technology,* vol. 100, p. 4690–4696, 2009.

[133] A. Patel, V. Brahmkhatri and N. Singh, "Biodiesel production by esterification of free fatty acid over sulfated zirconia," *Renewable Energy,* vol. 51, pp. 227-233, 2013.

[134] M. Di Serio, M. Cozzolino, R. Tesser, P. Patrono, F. Pinzari, B. Bonelli and E. Santacesaria, "Vanadyl phosphate catalysts in biodiesel production," *Applied Catalysis A: General,* vol. 320, pp. 1-7, 2007.

[135] J. Park, D. Kim and J. Lee, "Esterification of free fatty acids using water-tolerable Amberlyst as a heterogeneous catalyst," *Bioresource Technology,* vol. 101, pp. S62-S65, 2010.

[136] E. G. M. Schwenk and F. Aichner, "Production of acrolein". Patent US1916743A, 1933.

[137] H. Groll and G. Hearne, "Process of converting a polyhydric alcohol to a carbonyl compound". Patent US2042224A, 1936.

[138] A. Neher, T. Haas, D. Arntz, H. Klenk and W. Girke, "Process for the production of acrolein". Patent US5387720A, 1995.

[139] X. Feng, Y. Yao, Q. Su, L. Zhao, W. Jiang, W. Ji and C. Au, "Vanadium pyrophosphate oxides: The role of preparation chemistry in determining renewable acrolein production from glycerol dehydration," *Applied Catalysis B: Environmental,* vol. 164, pp. 31-39, 2015.

[140] S. Chai, B. Yan, L. Tao, Y. Liang and B. Xu, "Sustainable production of acrolein: Catalytic gas-phase dehydration of glycerol over dispersed tungsten oxides on alumina, zirconia and silica," *Catalysis Today,* vol. 234, pp. 215-222, 2014.

[141] P. Lauriol-Garbay, J. M. M. Millet, S. Loridant, V. Bellier-Baca and P. Rey, "New efficient and long-life catalyst for gas-phase glycerol dehydration to acrolein," *Journal of Catalysis,* vol. 280, pp. 68-76, 2011.

[142] H. Gan, X. Zhao, B. Song, L. Guo, R. Zhang, C. Chene, J. Chen, W. Zhu and Z. Hou, "Gas phase dehydration of glycerol to acrolein catalyzed by zirconium phosphate," *Chinese Journal of Catalysis,* vol. 35, pp. 1148-1156, 2014.

References

[143] A. Galadima and O. Muraza, "A review on glycerol valorization to acrolein over solid acid catalysts," *Journal of the Taiwan Institute of Chemical Engineers,* vol. 67, pp. 29-44, 2016.

[144] B. Katryniok, S. Paul, M. Capron and F. Dumeignil, "Towards the Sustainable Production of Acrolein by Glycerol Dehydration," *ChemSusChem,* vol. 2, p. 719 – 730, 2009.

[145] B. M. Bell, J. R. Briggs, R. M. Campbell, S. M. Chambers, P. D. Gaarenstroom, J. G. Hippler, B. D. Hook, K. Kearns, J. M Kenney, W. J. Kruper, D. G. Schreck, C. N. Theriault and C. P. Wolfe, "Glycerin as a Renewable Feedstock for Epichlorohydrin Production. The GTE Process," *Clean Soil Air Water,* vol. 36, p. 657 – 661, 2008.

[146] H. Kuhz, A. Kuenz, U. Prusse, T. Willke and K. D. Vorlop, "Products Components: Alcohols," *Advances in Biochemical Engineering/Biotechnology,* vol. 166, pp. 339-372, 2019.

[147] W. Rottig, H. Tummes, B. Cornils and J. Weber, "Process for the production of divalent alcohols". Patent US4094914A, 1978.

[148] J. F. Knifton, T. G. James, L. H. Slaugh, P. R. Weider, K. D. Allen and J. B. Powell, "One-step production of 1,3-propanediol from ethylene oxide and syngas with a cobalt-iron catalyst". Patent US7538061B2, 2009.

[149] C. E. Nakamura and G. M. Withed, "Metabolic engineering for the microbial production of 1,3-propanediol.," *Current Opinion in Biotechnology,* vol. 14, pp. 454-459, 2003.

[150] C. J. Sullivan, A. Kuenz and K. D. Vorlop, "Propanediols," *Ullmann's Encyclopedia of Industrial Chemistry,* vol. 30, pp. 233-241, 2018.

[151] M. A. Dasari, P. Kiatsimkul, W. R. Sutterlin and G. J. Suppes, "Low-pressure hydrogenolysis of glycerol to propylene glycol," *Applied Catalysis A: General,* vol. 281, p. 225–231, 2005.

[152] J. Henkelmann, M. Becker, J. Burkle, P. Wahl, G. Theis and S. Maurer, "Process for the preparation of 1,2-propanediol". Patent WO2007099161A1, 2007.

[153] C. Bandinelli, B. Lambiase, T. Tabanelli, J. De Maron, N. Dimitratos, F. Basile, P. Concepcion, J. M. Lopez Nieto and F. Cavani, "A study of the oxidehydration of 1,2-propanediol to propanoic acid with bifunctional catalysts," *Applied Catalysis A: General,* vol. 582, p. 117102, 2019.

[154] G. Reuss, W. Disteldorf, A. O. Gamer and A. Hilt, "Formaldehyde," *Ullmann's Encyclopedia of Industrial Chemistry,* vol. 15, pp. 735-768, 2012.

[155] H. R. Gerberich and G. C. Seaman, "Formaldehyde," *Kirk-Othmer Encyclopedia of Chemical Technology,* vol. 12, pp. 107-128, 2004.

[156] H. Schubert, U. Tegtmeyer, D. Herein, X. Bao, M. Muhler and R. Schlögl, "On the relation between catalytic performance and microstructure of polycrystalline silver in the partial oxidation of methanol," *Catalysis Letters,* vol. 33, p. 305–319, 1995.

[157] A. Chieregato, C. Bandinelli, P. Concepcion, M. D. Soriano, F. Puzzo, F. Basile, F. Cavani and J. M. Lopez Nieto, "Structure–Reactivity Correlations in Vanadium-Containing Catalysts for One-Pot Glycerol Oxidehydration to Acrylic Acid," *ChemSusChem,* vol. 11, pp. 234-244, 2017.

[158] N. Y. Usachev, I. M. Krukovskii and A. A. Kanaev, "The Nonoxidative Methanol Dehydrogenation to Formaldehyde (a Review)," *Petroleum Chemistry,* vol. 44, p. 79–394, 2004.

[159] V. Crocellà, G. Cerrato, G. Magnacca, C. Morterra, F. Cavani, L. Maselli and S. Passeri, "Gas-phase phenolmethylation over Mg/Me/O (Me = Al, Cr, Fe) catalysts: mechanistic implications due to different acid–base and dehydrogenating properties," *Dalton Transaction,* vol. 39, pp. 8527-8537, 2010.

[160] V. Crocellà, G. Cerrato, G. Magnacca, C. Morterra, F. Cavani, S. Cocchi, S. Passeri, D. Scagliarini, C. Flego and C. Perego, "The balance of acid, basic and redox sites in Mg/Me-mixed oxides: The effect on catalytic performance in the gas-phase alkylation of m-cresol with methanol," *Journal of Catalysis,* vol. 270, pp. 125-135, 2009.

[161] T. Tabanelli, S. Cocchi, B. Gumina, L. Izzo, M. Mella, S. Passeri, F. Cavani, C. Lucarelli, J. Schutz, W. Bonrath and T. Netscher, "Mg/Ga mixed-oxide catalysts for phenol methylation: Outstanding performance in 2,4,6-trimethylphenol synthesis with co-feeding of water," *Applied Catalysis A: General,* vol. 552, pp. 86-97, 2018.

[162] M. Ai, "Formation of methyl methacrylate by condensation of methyl propionate with formaldehyde over silica-supported cesium hydroxide catalysts," *Applied Catalysis A: General,* vol. 288, pp. 211-215, 2005.

[163] J. Tai and R. J. Davis, "Synthesis of methacrylic acid by aldol condensation of propionic acid with formaldehyde over acid–base bifunctional catalysts," *Catalysis Today,* vol. 123, pp. 42-49, 2007.

[164] B. Li, R. Yan, L. Wang, Y. Diao, Z. Li and S. Zhan, "Synthesis of Methyl Methacrylate by Aldol Condensation of Methyl Propionate with Formaldehyde Over Acid–Base Bifunctional Catalysts," *Catalysis Letters,* vol. 143, pp. 829-838, 2013.

[165] O. H. Bailey, R. A. Montag and J. S. Yoo , "Methacrylic acid synthesis: I. Condensation of propionic acid with formaldehyde over alkali metal cation on silica catalysts," *Applied Catalysis A: General,* vol. 88, pp. 163-177, 1992.

[166] M. Ai, "Vapor-Phase Aldol Condensation of Formaldehyde with Propionic Acid on Vanadium Pentoxide-Phosphorus Pentoxide," *Applied Catalysis,* vol. 36, pp. 221-230, 1988.

[167] M. Ai, "The production of methacrylic acid by the vapor-phase aldol condensation of propionic acid with formaldehyde," *Journal of atalysis,* vol. 124, pp. 293-296, 1990.

[168] M. Ai, H. Fujihashi, S. Hosoi and A. Yoshida, "Production of methacrylic acid by vapor-phase aldol condensation of propionic acid with formaldehyde over silica-supported metal phosphate catalysts," *Applied Catalysis A: General,* vol. 252, pp. 185-191, 2003.

[169] M. Ai, "The Production of Methacrylic Acid by the Vapor-Phase Aldol Condensation over V–Si–P Ternary Oxide Catalyst," *Bulletin of the Chemical Society of Japan,* vol. 63, pp. 1217-1220, 1990.

[170] J. J. Spivey, M. R. Gogate, J. R. Zoeller and R. D. Colberg, "Novel Catalysts for the Environmentally Friendly Synthesis of Methyl Methacrylate," *Industrial & Engineering Chemistry Research,* vol. 36, pp. 4600-4608, 1997.

[171] G. Albanesi and P. Moggi, "Methyl methacrylate by gas phase catalytic condensation of formaldehyde with methyl propionate," *Applied Catalysis,* vol. 6, pp. 293-306, 1983.

[172] M. Ai, "Formation of methyl methacrylate from methyl propionate and methanol," *Catalysis Today,* vol. 111, pp. 398-402, 2006.

[173] W. Weda, "Catalytic Synthesis of α, β-Unsaturated Compounds over Solid-bases Using Methanol for C=C Bond Formation," *Sekiyu Gakkaishi,* vol. 36, pp. 421-435, 1993.

[174] F. Cavani, C. Felloni, D. Scagliarini, C. Flego, A. Tubertini and C. Perego, "Preparation, characterization and reactivity in m-cresol methylation of new heterogeneous materials having basic properties," *Studies in Surface Science and Catalysis,* vol. 143, pp. 953-961, 2000.

[175] F. Wang, N. Ta and W. Shen, "MgO nanosheets, nanodisks, and nanofibers for the Meerwein–Ponndorf–Verley reaction," *Applied Catalysis A: General,* vol. 475, pp. 76-81, 2014.

[176] F. Cavani, L. Maselli, D. Scagliarini, C. Flego and C. Perego, "How basic properties of MgO-based mixed oxides affect the catalytic performance in gas-phase and liquid-phase methylation of m-cresol," *Studies in Surface Science and Catalysis,* vol. 155, pp. 167-177, 2005.

[177] S. Geller, "Crystal Structure of β-Ga2O3," *Journal of Chemical Physics,* vol. 33, pp. 676-684, 1960.

[178] R. L. Rudnick and S. Gao, "Composition of the Continental Crust," *Treatise on Geochemistry,* vol. 3, pp. 1-64, 2003.

[179] M. Frenzel, M. P. Ketris, T. Seifert and J. Gutzmer, "On the current and future availability of gallium," *Resources Policy,* vol. 47, pp. 38-50, 2016.

[180] N. Ballarini, F. Cavani, L. Maselli, S. Passeri and S. Rovinetti, "Mechanistic studies of the role of formaldehyde in the gas-phase methylation of phenol," *Journal of Catalysis,* vol. 256, pp. 215-225, 2008.

[181] N. Ballarini, F. Cavani, L. Maselli, A. Montaletti, S. Passeri, D. Scagliarini, C. Flego and C. Perego, "The transformations involving methanol in the acid- and base-catalyzed gas-phase methylation of phenol," *Journal of Catalysis,* vol. 251, pp. 423-436, 2007.

References

[182] K. Nakagawa, M. Okamura, N. Ikenaga, T. Suzuki and T. Kobayashi, "Dehydrogenation of ethane over gallium oxide in the presence of carbon dioxide," *1025-1026,* vol. 9, pp. 1025-1026, 1998.

[183] B. Zheng, W. Hua, Y. Yue and Z. Gao, "Dehydrogenation of propane to propene over different polymorphs of gallium oxide," *Journal of Catalysis,* vol. 232, pp. 143-151, 2005.

[184] S. Albonetti, F. Cavani, F. Trifirò, M. Gazzano, M. Koutyrev, F. C. Aissi, A. Aboukais and M. Guelton, "Mechanism of Thermal Decomposition of Potassium/Ammonium Salts of the 12-Molybdophosphoric Acid and Effect on the Catalytic Performance in the Isobutyric Acid Oxidehydrogenation," *Journal of Catalysis,* vol. 146, pp. 491-502, 1994.

[185] F. Cavani, A. Tanguy, F. Trifirò and M. Koutrev, "Effect of Antimony on the Chemical–Physical Features and Reactivity in Isobutyric Acid Oxidehydrogenation of Keggin-Type Heteropolycompounds," *Journal of Catalysis,* vol. 174, pp. 231-241, 1994.

[186] U. Gelius, P. F. Heden, J. Hedman, B. J. Lindberg, R. Manne, R. Nordberg, C. Nordling and K. Siegbahn, "Molecular Spectroscopy by Means of ESCA III. Carbon compounds," *Physica Scripta,* vol. 2, pp. 70-80,, 1970.

[187] V. D. Wheeler , D. I. Shahin, M. J. Tadjer and C. R. Eddy Jr, "Band Alignments of Atomic Layer Deposited ZrO2 and HfO2 High-k Dielectrics with (-201) β-Ga2O3," *ECS Journal of Solid State Science and Technology,* vol. 6, pp. 3052-3055, 2017.

[188] G. P. Lopez, D. G. Castner and B. D. Ratner, "XPS 0 1s Binding Energies for Polymers Containing Hydroxyl, Ether, Ketone and Ester Groups," *Surface and Interface Analysis,* vol. 17, pp. 267-272, 1991.

[189] D. A. Zatsepin, D. W. Boukhavlov, A. F. Zatsepin, Y. A. Kuznetsova, D. Gogova, V. Y. Shur and A. A. Esin, "Atomic structure, electronic states, and optical properties of epitaxially grown β-Ga2O3 layers," *Superlattices and Microstructures,* vol. 120, pp. 90-100, 2018.

[190] M. Zeng and Y. Li, "Recent advances in heterogeneous electrocatalysts for the hydrogen evolution reaction," *Journal of Materials Chemistry A,* vol. 3, pp. 14942-14962, 2015.

[191] A. B. Stambouli and E. Traversa, "Fuel cells, an alternative to standard sources of energy," *Renewable and Sustainable Energy Reviews,* vol. 6, pp. 297-306, 2002.

[192] D. D. Zhu, J. L. Liu and S. Z. Qiao, "Recent Advances in Inorganic Heterogeneous Electrocatalysts for Reduction of Carbon Dioxide," *Advanced Materials,* vol. 28, pp. 3423-3452, 2016.

[193] P. D. Tran, L. H. Wong, J. Barber and J. S. C. Loo, "Recent advances in hybrid photocatalysts for solar fuel production," *Energy & Environmental Science,* vol. 5, pp. 5902-5918, 2012.

[194] Q. Wiang, T. Jin, Z. Hu, L. Zhou and M. Zhou, "TiO2-NTs/SnO2-Sb anode for efficient electrocatalytic degradation of organic pollutants: Effect of TiO2-NTs architecture," *Separation and Purification Technology,* vol. 102, pp. 180-186, 2013.

[195] U. G. Akpan and B. H. Hameed, "Parameters affecting the photocatalytic degradation of dyes using TiO2-based photocatalysts: A review," *Journal of Hazardous Materials,* vol. 170, pp. 520-529, 2009.

[196] R. S. Haszeldine, "Carbon Capture and Storage: How Green Can Black Be?," *Science,* vol. 325, pp. 1647-1652, 2009.

[197] I. E. Agency, "Key World Energy Statistics," p. 74, 2016.

[198] O. Boullard, H. Leblanc and B. Besson, "Salicylic Acid," *Ullmann's Encyclopedia of Industrial Chemistry,* vol. 32, pp. 127-134, 2012.

[199] S. Van de Vyver, J. Geboers, P. A. Jacobs and B. F. Sels, "Recent Advances in the Catalytic Conversion of Cellulose," *ChemCatChem,* vol. 3, pp. 82-94, 2011.

[200] A. S. Mamman, J. M. Lee, Y. C. Kim, I. T. Hwang, N. J. Park, Y. K. Hwang, J. S. Chang and J. S. Hwang, "Furfural: Hemicellulose/xylose derived biochemical," *Biofuels, Bioproducts and Biorefining,* vol. 2, p. 438–454, 2008.

[201] M. Selva and A. Perosa, "Green chemistry metrics: a comparative evaluation of dimethyl carbonate, methyl iodide, dimethyl sulfate and methanol as methylating agents," *Green Chemistry,* vol. 10, pp. 457-464, 2008.

[202] P.Tundo and M. Selva, "The Chemistry of Dimethyl Carbonate," *Accounts of Chemical Research,* vol. 35, pp. 706-716, 2002.

[203] D. Delledonne, F. Rivetti and U. Romano, "Oxidative carbonylation of methanol to dimethyl carbonate (DMC):a new catalytic system," *Journal of Organometallic Chemistry,* vol. 488, pp. C15-C19, 1995.

[204] A. T. W. M. Hendricks and G. Zeeman, "Pretreatments to enhance the digestibility of lignocellulosic biomass," *Bioresource Technology,* vol. 100, pp. 10-18, 2009.

[205] P. Alvira, E. Tomàs-Pejò, M. Ballesteros and M. J. Negro, "Pretreatment technologies for an efficient bioethanol production process based on enzymatic hydrolysis: A review," *Bioresource Technology,* vol. 101, p. 4851–4861, 2010.

[206] B. Saake and R. Lehnen, "Lignin," *Ullmann's Encyclopedia of Industrial Chemistry,* vol. 21, pp. 21-36, 2012.

[207] M. G. Papatheofanous, E. Billa, D. P. Koullas, B. Monties and E. G. Koukios, "Two-stage acid-catalyzed fractionation of lignocellulosic biomass in aqueous ethanol systems at low temperatures," *Bioresource Technology,* vol. 54, pp. 305-310, 1995.

[208] P. Tomani, "The LignoBoost Process," *Cellulose Chemistry & Technology,* vol. 44, pp. 53-58, 2010.

[209] A. V. Bridgwater and G. V. C. Peacocke, "Fast pyrolysis processes for biomass," *Renewable and Sustainable Energy Reviews,* vol. 4, pp. 1-73, 2000.

[210] J. Quesada, L. Faba, E. Diaz, S. Bennici, A. Aurox and S. Ordonez, "Role of surface intermediates in the deactivation of MgZr mixed oxides in acetone self-condensation: A combined DRIFT and ex situ characterization approach," *Journal of Catalysis,* vol. 329, pp. 1-9, 2015.

[211] J. H. Meessen, "Urea," *Ullmann's Encyclopedia of Industrial Chemistry,* vol. 37, pp. 657-695, 2012.

[212] T. Sakakura, C. J. Choi and H. Yasuda, "Transformation of Carbon Dioxide," *Chemical Reviews,* vol. 107, p. 2365–2387, 2007.

[213] D. Graham-Rowe, "Agriculture: Beyond food versus fuel," *Nature,* vol. 474, pp. S6-S8, 2011.